UNIVERSITY OF CALIFORNIA

Los Angeles

Electron Localization and Superconductivity
in
Two Dimensional Metal Film Systems

A dissertation submitted in partial satisfaction of the
requirements of the degree Doctor of Philosophy
in Physics

by

Michael Joseph Burns

1984

©copyright by

Michael Joseph Burns

1984

The dissertation of Michael Joseph Burns is approved.

[redacted]

R. Stanley Williams

[redacted]

George Grüner

[redacted]

Raymond L. Orbach, Committee Co-Chair

[redacted]

Paul M. Chaikin, Committee Co-Chair

University of California, Los Angeles

1984

To those who won’t knuckle under.

TABLE OF CONTENTS

Section Page

LIST OF FIGURES ....

ACKNOWLEDGEMENTS ....

VITA AND PUBLICATIONS ....

ABSTRACT OF THE DISSERTATION ....

I. INTRODUCTION 1

  I.A Simple Theory of Metals 6

  I.B Ioffe-Regel Rule 14

  I.C Metal-Insulator Transitions 20

II. THEORY 25

  II.A Scaling Theory of Localization 26

  II.B Weak Localization in the Scaling Theory 38

  II.C Strong Localization 52

  II.D Electron-Electron Interactions in the Near Metallic Regime 62

  II.E Electron-Electron Interactions in The Insulating Regime 76

    1. Single Particle Excitations 76

    2. Polaronic Type Excitations 91

    3. Tightly Bound Electron-Hole Pairs 94

  II.F The Effects of External Fields 96

    1. Electric Fields in the Near Metallic Regime 96

2. Electric Fields and Hopping 99
Magnetic Fields 103
3. Magnetic Fields and
the Near Metallic Regime 105
i) Orbital Effects and Scaling 105
ii) Spin-Orbit Interactions, Zeeman Effects
and Scaling 108
iii) Orbital Effects and
the Interaction Theory 113
iv) Zeeman Splitting and
the Interaction Theory 116
v) Spin-Orbit Coupling and
the Interaction Theory 119
4. Magnetic Fields and Hopping 121
i) Shrinking Wavefunctions 121
ii) Zeeman Effect 126
II.G Thermoelectric Effects 130
1. Boltzman Transport 137
2. Thermopower of Metals 143
3. Thermopower of Semiconductors 145
4. Thermopower Definition of Metals
and Insulators 149

5. Thermopower in the Near Metallic Regime 155

i) Thermopower and the Scaling Theory 155

ii) Thermopower and the Interaction Theory 159

6. Thermopower and Hopping 163

II.H Localization, Interactions and Superconductivity 166

III. EXPERIMENTAL BACKGROUND 170

III.A Metal Based Systems 171

1. One Dimensional Wires 172

2. Two Dimensional Ultra Thin Films 173

3. Three Dimensional Granular Metal Films 175

III.B Inversion and Accumulation Layers 176

1. MOSFETs 176

2. Heterostructures 179

IV. EXPERIMENTAL TECHNIQUES AND PROCEDURES 181

IV.A Sample Preparation and Characterization 181

1. Palladium and Palladium-Gold Films on Glass and Quartz 181

2. Ultra Thin Silver Films Epitaxially Grown on (001) Germanium 190

IV.B Sample Geometry and Cryogenic Systems 193

IV.C Measurement Techniques 205
- 1. Probe Temperature Measurement 205
    - i) Diode Sensors 205
    - ii) Capacitance Sensors 209
    - iii) Resistance Sensors 210
- 2. Chordal Resistance Measurements 214
- 3. Electric Field Dependent Chordal and Dynamic Resistance 219
- 4. Thermoelectric Power (TEP) 229

V. EXPERIMENTAL RESULTS AND DISCUSSION 240

V.A Regimes of the Theories 241

V.B Palladium and Palladium-Gold Films On Glass and Quartz 243
- 1. Temperature Dependence of the Resistivity 244
- 2. Electric Field Dependence of the Resistivity ... 258
- 3. Magnetic Field Dependence of the Resistivity ... 269
- 4. Thermoelectric Power 276

V.C Ultrathin Silver Films Grown Epitaxially On Germanium (001) 306
- 1. Experimental Results 307
    - i) Temperature Dependence of the Resistivity 307
    - ii) Electric and Magnetic Field Dependence of the Resistivity 320

iii) Superconductivity 326

iv) Miscellaneous Observations 332

2. Discussion 334

VI. CONCLUSIONS 343

REFERENCES 348

LIST OF FIGURES

Figure 1-1

Illustration of the relationship between the mean free path of an electron and its wavelength for an electronic plane wave approximation to be valid.

Figure 1-2

Illustration of the relationship between the tight binding bandwidth V, and the localized state energy distribution width W, in the Anderson localization scheme.

Figure 2-1

Illustration of the relationship between the energy width of the states in a system and the spacing between states to the conductivity of the total system.

Figure 2-2

The scaling function β versus the logarithm of the dimensionless conductance $g(L)$.

Figure 2-3

Illustration of the diffusive paths in the intuitive model of the scaling theory as presented by Larkin and Khmelnitskii.

Figure 2-4

Resistivity versus thickness of a Pd film (measured in situ during the evaporation).

Figure 2-5

Plot of the relative probability per unit time of a hop as a function of hopping distance for 1,2 and 3 dimensions.

Figure 2-6

Example of variable range hopping in amorphous Germanium.

Figure 2-7

The vertex correction for impurity scattering.

Figure 2-8

The exchange diagram.

Figure 2-9

The Hartree diagram.

Figure 2-10

The ground state and first excited state in an interacting electron variable range hopping model.

Figure 2-11

The modification to the density of states by the presence of interactions in a variable range hopping model.

Figure 2-12

Example of a system consistent with variable range hopping with interactions - GaAs.

Figure 2-13

Illustration of the thermoelectric effect.

Figure 2-14

Illustrations of the Peltier effect and the Thomson effect.

Figure 2-15
Illustration of how thermopower can be used to differentiate between metallic and insulating systems.

Figure 2-16
Feynman diagrams which give net contributions to the heat current-electrical current correlation function K_1 for interacting electrons with weak impurity scattering.

Figure 4-1
Electron micrographs and electron diffraction patterns of Pd and Pd-Au films.

Figure 4-2
Resistivity versus film thickness measured in situ for a Pd film deposited on glass at room temperature.

Figure 4-3
Geometry used for electrical measurements.

Figure 4-4
Geometry used for measuring very small thermopower differences.

Figure 4-5

'Double can' system used for reaching temperatures down to 1°K.

Figure 4-6

'Double can' system used for reaching temperatures down to 0.5°K.

Figure 4-7

Diode and capacitor temperature sensor systems.

Figure 4-8

D.C. and A.C. resistance temperature sensor systems.

Figure 4-9

A.C. and D.C. chordal resistance measurement circuits.

Figure 4-10

Electric field dependent D.C. chordal resistance measurement circuit.

Figure 4-11

Illustration of how the dynamic resistance measurement circuit functions.

Figure 4-12
Two schematics of the bridge circuit used to measure dynamic resistance.

Figure 4-13
Illustration of apparatus for measuring gross behavior of the thermopower in thin films.

Figure 4-14
Thermopile sample arrangement.

Figure 4-15
Schematics for thermopower measurements.

Figure 5-1
Resistivity as a function of temperature from a wide selection of palladium and palladium-gold films used in these studies.

Figure 5-2
Resistivity change divided by the square of the resistivity as a function of temperature.

Figure 5-3

Resistivity of a Pd film as a function of temperature from 100 mK to 4.2°K.

Figure 5-4

Characteristic logarithmic slope of a random selection of low resistivity films from figure 5-1.

Figure 5-5

Dynamic resistivity of a Pd film in the near metallic regime.

Figure 5-6

J-E characteristic of a 26 KΩ/square (at 10°K) Pd film.

Figure 5-7

J-E characteristic of a 480KΩ/square (at 10°K) Pd film.

Figure 5-8

The fractional change in the magnetoresistance of Pd films on glass scales as H/T, independent of the resistivity.

Figure 5-9

Resistivity of some Pd and Pd-Au films used in the thermopower studies.

Figure 5-10

Resistivity of some Pd and Pd-Au films in the near metallic regime used in the thermopower studies.

Figure 5-11

Absolute thermopower as a function of temperature for Pd and Pd and Pd-Au films. Samples with resistances per square of less than 30KΩ show 'metallic' behavior, sample with resistivities above 30KΩ show the presence of an energy gap.

Figure 5-12

Absolute thermopower as a function of temperature for each of two Pd and Pd-Au films to 100°K.

Figure 5-13

Resistivity of thermopile components as a function of temperature.

Figure 5-14

Fractional difference in the thermopower between 3-d and 2-d films.

Figure 5-15

Resistivity of thermopile components as a function of temperature.

Figure 5-16

Fractional difference in the thermopower between 3-d and 2-d films.

Figure 5-17

The thermopower plotted versus 1/T for comparable Pd and Pd-Au films with thermopowers which diverge as T-->0.

Figure 5-18

Resistance of a sample comprising of a 2.5 monolayer thick Ag film on Ge (001) from 250-0.6°K.

Figure 5-19

Fractional change in the film (in Figure 5-18) resistivity at low temperatures.

Figure 5-20

Superconducting transition of 2.5 monolayers of Ag on Ge (001).

Figure 5-21

Temperature dependence of the resistivity of a 2.5 monolayer Ag film on Ge (001) below 25°K.

Figure 5-22

Temperature dependence of the resistance of a 3.0 monolayer Ag film on Ge (001) which has a misalignment between the Ge surface and the Ge (001) plane of 5°.

Figure 5-23

Dynamic resistance of a 2.5 monolayer Ag film on Ge (001).

Figure 5-24

The magnetoresistance of a 2.5 monolayer Ag film on Ge (001) above 2°K.

Figure 5-25

Magnetoresistance of the film in Figure 5-24 below 2°K.

Figure 5-26

The perpendicular magnetoresistance of the sample in figure 5-21, in fields up to 10 Tesla.

ACKNOWLEDGEMENTS

It has been a long and convoluted path leading to this dissertation, and looking back, it is difficult to clearly see past the last bend.

Foremost, I would like to thank Paul Chaikin for his support and guidance during the last four years. Paul's knowledge and intuition of physics is second to none. We don't always see things eye to eye, but my respect and admiration of Paul knows no bounds. Paul's sense of humor, while making him a natural target of quite a few Chaikinlab practical jokes, has on more than one occasion helped me over rough spots.

Very special thanks, for several good years, go to my Chaikinlab cohorts in crime: Bill Dozier, Mac Lindsay, Ron Lacoe, Wayne McGinnis, and Randy Simon. Not only did I learn how to do experiments (and especially how not to do them !) from some of these guys, but I'll never forget some of the trouble we all caused together (Anyone want a slightly used brick wall, or 14 gross of used balloons ? Eh ?). I hope the tradition of unorthodox behavior Paul tolerated in us will continue.

As the saying goes, 'Misery loves company.'. The late night sub-basement contingent deserves special credit and thanks : All of Chaikinlab, plus: Vince Kotsubo, Mary Lillian Ott-Rowland, Scott Hannahs, Mary Beth Kaiser, Dave Reagor and Alex Zettl. Many a night there was when most of the aforementioned would be working, and when the experiment at hand finally bit the twinky (invariably at 4 a.m.), one could turn to for friendly advice. Thanks guys!

I would also like to say thank you to Jeff Lince, Jeff Nelson and Stan Williams for trying to feed my insatiable appetite for monolayer Ag samples, and to the National Science Foundation for funding this work under grants DMR-81-15241, DMR-82-05810 and DMR-83-18060.

And to my family, I owe everything.

VITA

October 6, 1956	Born, Hollywood, California
June 1978	Bachelor of Science in Physics University of California, Los Angeles
June 1978 -Sept. 1980	Member of the Technical Staff Hughes Aircraft Company Los Angeles, California
June 1980	Master of Science in Physics University of California, Los Angeles
Sept. 1980 -Oct. 1983	Teaching Assistant, Research Assistant Department of Physics University of California, Los Angeles
October 1983 -Nov. 1984	Staff Research Physicist Department of Physics University of Pennsylvania Philadelphia

LIST OF PUBLICATIONS

'Transport Studies of Thin Palladium Films', W.C. McGinnis, M.J. Burns, G. Deutscher, G. Gruner, and P.M. Chaikin, Bull Am Phys Soc 26, 410 (1981)

'Magnetoresistance of Thin Palladium Films', W.C. McGinnis, M.J. Burns, R.W. Simon, G. Deutscher, and P. M. Chaikin, Physica 107B+C, 5 (1981)

'Minimum Metallic Conductivity and Thermopower in Thin Palladium Films', M.J. Burns, W.C. McGinnis, R.W. Simon, G. Deutscher, and P.M. Chaikin, Phys Rev Lett 47, 1620 (1981)

'Magnetothermopower of (TMTSF)$_2$Pf$_6$', M.J. Burns, P.M. Chaikin, and E.M. Engler, Bull Am Phys Soc 27, 151 (1982)

'Thermoelectric Power of Thin High Resistivity Films', M.J. Burns and P.M. Chaikin, Bull Am Phys Soc 27, 161 (1982)

'Ditetramethyltetraselenafulvalenium Forsulfonate: The Effect of a Dipolar Anion on the Solid State Physical Properties of the (TMTSF)$_x$ Phase', F. Wudl, E. Aharon-Shalom, D. Nalewajek, J.V. Waszczak, W.M. Walsh Jr., L.W. Rupp Jr., P. Chaikin, R. Lacoe, M. Burns, T.O. Poehler, M.A. Beno, and J.M. Williams, J Chem Phys 76, 5497 (1982)

'Tetrakis (Deuteriomethyl) Tetraselenafulvalene', E. Aharon-Shalom, F. Wudl, S.H. Bertz, W.M. Walsh Jr., L.W. Rupp Jr., P.M. Chaikin, M.J. Burns, K. Andres, and H. Schwenk, Mol Cryst Liq Cryst 86, 35 (1982)

'Thermoelectric Power of Two Dimensional Pd and Pd-Au Films', M.J. Burns and P.M. Chaikin, Phys Rev B27, 5924

(1983)

'Electron Localization in Very Thin Ag Films Epitaxially Grown on Ge (001)', M.J. Burns, P.M. Chaikin, J.R. Lince, J.G. Nelson and R.S. Williams, Bull Am Phys Soc 29, 387 (1984)

'Electron Localization and Superconductivity in Very Thin Epitaxially Grown Ag Films on Ge (001)', M.J. Burns, J.R. Lince, R.S. Williams, and P.M. Chaikin, Sol State Comm 51, 865 (1984)

'Magnetothermopower of $(TMTSF)_2PF_6$', Mu-Yong Choi, M.J. Burns, P.M. Chaikin, R.L. Greene and E.M. Engler (submitted to Phys Rev B)

ABSTRACT OF THE DISSERTATION

Electron Localization and Superconductivity
in
Two Dimensional Metal Film Systems

by

Michael Joseph Burns
Doctor of Philosophy in Physics
University of California, Los Angeles, 1984
Professor Paul M. Chaikin, Co-Chair
Professor Raymond L. Orbach, Co-Chair

The low temperature electrical transport properties of very thin polycrystalline palladium and palladium-gold films grown on glass or fused quartz, and also the properties of epitaxially grown silver films on germanium (001), have been investigated. These, and other two dimensional electronic systems, display a nonmetallic conductivity which has been attributed to electron localization and/or electron-electron interaction

effects. According to the various theories, some of the transport properties should display different behaviors, thus allowing one to distinguish between the two effects.

Measurements of Pd and Pd-Au film resistivities as a function of temperature, electric and magnetic field, plus the thermopower, were performed on films ranging from 18 to 30 Angstroms in thickness, having resistivities from 600 to 500000 ohms/square at 10°K. The magnetotransport properties imply the presence of strong spin-orbit coupling, although the temperature dependence of the resistivity of these films does not. All 'metallic' samples (resistivities less than 30000 ohms/square) have a material specific thermopower which tends to zero as the temperature goes to zero. Samples whose resistivities increase above 30000 ohms/square have thermopowers which diverges as the temperature approaches zero. Thus the density of states for the electronic transport is zero at the Fermi energy (i.e. an energy gap opens in the density of states at 30000 ohms/square) for high-resistivity films.

The very thin (2.5 monolayer) silver films epitaxially grown on Ge (001) consist of a monolayer coverage plus isolated three dimensional islands. Below 70°K the conductivity is dominated by the metal film and displays the temperature and electric and magnetic field dependencies characteristic of metallic weak localization in two dimensions. Below about 2°K, the resistance drops rapidly in a manner resembling an incomplete superconducting transition. The resistance is restored by application of a magnetic field of approximately 20 KGauss at 0.6°K.

"Our dear race, born without courage but very brave, born with a flickering intelligence and yet with beauty in its hands. What animal has made beauty, created it, save only we ? With all our horrors and our faults, somewhere in us there is a shining. That is the most important of all facts. *There is a shining.*"

Burning Bright by
John Steinbeck
(1902-1968)

CHAPTER I -- INTRODUCTION

There exists a group of materials whose discovery in early human history had an impact larger than any other save the discovery of fire. These materials possessed characteristics which rendered them superior to stone for tool and weapon making in several ways. These materials could be readily shaped when heated by fire. Tools composed of these materials were stronger than tools of stone or wood, and some could retain considerable strength even when heated until they glowed. These materials in pure form are shiny to look at, seem cool to touch and if honed to a fine edge, they retain that edge after repeatedly cutting lesser materials. Only a noble few of these materials could be found naturally in pure form and all but these few would , once pure, corrode with time: tools would become dull and slowly crumble away.

This 'group' of materials is known today as the metals. Nearly three quarters of the known elements are metals, which with their countless alloys vary considerably in all their properties. As the sophistication of human technology increased, other properties common to all metals came to light. The metals feel cool to touch because they transport heat very well. They all reflect visible light efficiently and can be polished smooth enough to reflect the light specularly. And they transport electrical energy better than any other materials. The properties and uses of the metals are one of the most important and studied areas of human knowledge and yet they are still not understood.

Modern atomic theory made its debut in 1807 introduced by John Dalton, who was inspired by a natural relation recently discovered by chemists: that the elements which make up a given compound are always present in the same weight proportions regardless of the origin of the compound. This 'law of definite proportion' and the resulting atomic theory had a profound impact on the development of the sciences. Together with concepts which were to follow such as valence (defined as the number of atoms of hydrogen or chlorine to which one atom of the element can combine) and equivalent weight (defined as the ratio of the atomic weight and the valence) of an element, scientists were soon able to exercise a great deal of control, and predict the outcome, of most of their chemical endeavors. For over a hundred years however, the atomic theory could not predict whether a given synthesized compound would be metallic. Compounds made exclusively of metals tended to be metals , but many compounds which contained relatively small amounts of metallic elements could display some of the properties associated with the metals.

While the structure of the atoms themselves remained elusive until the twentieth century, much was learned of the electrical nature of matter. In the 1830's , Michael Faraday's investigations of electrolysis uncovered that:

(1) For a given material, the weight of material deposited at an electrode is proportional to the amount of electricity used.

(2) If various materials are deposited by a given amount of electricity, the weight of materials deposited are proportional to the equivalent weights of these materials.

These findings indicated that for a given substance, fixed numbers of atoms react with fixed amounts of electricity. In 1874 G.J. Stoney proposed that this implied electricity in matter is composed of particles and suggested a name for these particles, the electron. In 1897 Joseph Thompson pulled electrons out of metals and observed some of their properties. As we shall see, these electrons play a very important role in determining the behavior of metals... and determining when a metal is not a metal.

A. A Simple Theory of Metals

In 1900, Paul Drude applied the kinetic theory of gases to the electrons in metals. He assumed that the electrons in a block of metal bounce around just as if they were gas atoms confined in a box, suffering collisions between themselves and occasionally a wall of the box. He assumed that only the collisions mattered. Between collisions there were no interactions between electrons. The collisions were assumed to be instantaneous and the average time between collisions was C. Last, Drude assumed that equilibrium was maintained only through collisions. From Drude's model one can calculate various properties of metals. For example, if **J** is the current density and **E** the electric field in the metal, then the electrical conductivity $\boldsymbol{\sigma}$ is defined by

$$\mathbf{J} = \sigma\mathbf{E} \tag{I.1}$$

If there are n electrons per unit volume and all move under the influence of the electric field with velocity **v**, then the current density is (with -e as the charge on one electron)

$$\mathbf{J}=-ne\mathbf{v} \tag{I.2}$$

Suppose we look at a typical electron in this electric field which just suffered a collision (so v=0). It will be accelerated by the field until its next collision after which it will be at rest again: this process will then repeat as long as the electric field is present. The force on the electron is -eE and if the average time between collisions is τ then the average velocity of the electron will be

$$v = \frac{-eE\tau}{m} \tag{I.3}$$

where m is the mass of the electron. From equations (I.1),(I.2) and (I.3) Drude calculated the conductivity of a metal to be:

$$\sigma = \frac{ne^2\tau}{m} \tag{I.4}$$

Intuitively this makes sense in that it says that the more electrons in a given volume and the longer the time between collisions for the electrons the better the metal will be at conducting electricity.

From the Drude model other properties of metals could be calculated. The specific heat of a metal (C), that is the amount of heat needed to raise the temperature of the metal a degree, is just that of a classical gas:

$$C=(3/2)K_b n \tag{I.5}$$

where K_b is Boltzman's constant. The thermal conductivity (k), can also be calculated as

$$k=\frac{v^2 C\tau}{3}=\frac{nv^2 K_b \tau}{2} \tag{I.6}$$

These two calculations also make sense qualitatively since they say that the more electrons in a given volume of metal to absorb heat, the harder it is to raise the metal's temperature. The faster the electrons can move carrying their heat, the better the metal will be at conducting that heat.

In the Drude model, magnetic fields have no effect on the conductivity in a single charge carrier model (no magnetoresistance), but it does predict the appearance of an electric field perpendicular to both the current and the magnetic field (assuming the current is also perpendicular to the magnetic field). This effect had been discovered in 1879 by E.H. Hall and now bears his name (the Hall effect):

$$E_y = \frac{H_z J_x}{nec} \qquad (I.7)$$

where H_z is the magnetic field in the z direction and c is the speed of light.

The Drude model has some problems, unfortunately. The specific heat of metals is temperature dependent and only approaches (3/2)K_bn at high temperatures, if ever. Most metals do display some magnetoresistance, which although small, is temperature and magnetic field direction dependent. Perhaps the biggest failure of the Drude model is its inability to explain why some metals have Hall effects which depend on the metallic crystal orientation , with the hall voltage sometimes even having opposite signs in different directions.

With the advent of quantum mechanics and the recognition that electrons were quantum particles (i.e., electrons display the wave-particle duality proposed by Louis-Victor de Broglie and furthermore, electrons belonged to the group of quantum particles which obeyed the Pauli exclusion principle, which says that no two particles can occupy the same state), new descriptions of electrons in metals were developed. The simplest quantum treatment of electrons in a metal is just the quantum analog of the Drude model. Treating the electrons in a sample of size L as free quantum particles which obey the free particle Schrodinger equation :

$$- \frac{\hbar^2}{2m} \vec{\nabla}^2 \psi(\vec{r}) = \epsilon_k \psi(\vec{r}) \qquad (I.8)$$

the (generally complex) wavefunctions will form standing waves:

$$\psi(\vec{r}) = A \sin([N_x \pi x]/L) \sin([N_y \pi y]/L) \sin([N_z \pi z]/L) \qquad (I.9)$$

where N_x, N_y, and N_z are positive integers. We may generalize this to an infinite sample (and hence forget about complications at the sample boundary) by using the method of periodic boundary conditions. This is equivalent to stacking an infinite number of the size L samples together. We just require the wavefunctions to be periodic in the x,y,and Z directions with a period L so that

$$\psi(x,y,z) = \psi(x+L,y,z) = \psi(x,y+L,z) = \psi(x,y,z+L) \qquad (I.10)$$

For a large system, this does not change the physics in any essential way. Wavefunctions which satisfy (I.8) and the periodicity condition are in the form of traveling plane waves

$$\psi(\vec{r}) = \psi_o \, e^{i \, \vec{k} \cdot \vec{r}} \qquad (I.11)$$

where $k_j=0: 2\pi/L: 4\pi/L:...$ with j=x,y,z and $i=\sqrt{-1}$. If one solves (I.8) using (I.11), one has

$$\varepsilon_k = \frac{\hbar^2 |k|^2}{2m} \qquad (I.12)$$

where the magnitude of the wavevector (**k**) is related to the traveling plane wave's wavelength (λ) and momentum (p) by

$$\mathbf{k}=|k|=|p/\hbar|=2\pi/\lambda \qquad (I.13)$$

Since the electrons must obey the Pauli exclusion principle the lowest energy state of a system of N free electrons has all of the states with energy N=0 up to some energy N_F (called the Fermi energy) occupied (all states with $0<k<k_F$) while all states with energies greater that N_F (and hence $k>k_F$) are unoccupied. For a given energy there are more states the higher the energy (more ways to come up with k's where $k_x^2+k_y^2+k_z^2$ is constant) so an important quantity in this description is the number of states per unit energy per volume of sample (called the density of states) which is given by (in three dimensions)

$$\mathcal{D}(\varepsilon) = \frac{\partial N}{\partial \varepsilon}\frac{1}{L^3} = \frac{\partial n}{\partial \varepsilon} = \frac{(2m\varepsilon)^{\frac{1}{2}}}{2\pi^2\hbar^3}2m \tag{I.14}$$

This quantum mechanical free electron model is a vast improvement over the classical Drude model. It predicts a specific heat which is temperature dependent and in much better agreement with experiments, particularly at low temperatures. When scattering of the electrons from state to state by various mechanisms is taken into account, it gives good agreement with experiment for the temperature dependence of the electrical and thermal conductivities.

More sophisticated quantum theories of electrons in metals do even better. We have ignored the atoms themselves and their formation of a periodic potential which the electrons can reflect from, and the anisotopic behavior sometimes associated with this periodic potential (which can explain the direction dependent Hall effect mentioned earlier). We have ignored how the electron orbitals of the individual atoms form bands of allowed states when the atoms are brought together to form the metal (called the tight binding approximation). Despite the elementary form of the description of electrons in metals presented so far, it is sufficient to set the stage for the question central to the investigations of this work: 'When does a metal stop being a metal... and why ?'

B. Ioffe-Regel Rule

The modern view of electrons in metals is of plane waves traveling through a periodic potential (the array of atoms forming a crystal lattice) extending throughout the volume of the metal, scattering off imperfections in the crystal such as impurities, defects in the crystal structure (misalignment of the atoms), grain boundaries (boundaries between one crystal and another) and thermal vibrations of the atoms (phonons). The wavevectors of the electrons range from 0 up to k_F, which means (see equation I.13) the wavelengths range from infinity (or really, the sample size) down to $B_F=2\pi/k_F$. An electron in a state k may scatter off, say an impurity, into an unoccupied state k' so that its wavelength changes from λ to λ'. As illustrated in figure 1-1, if the distance between scatterings is less than a wavelength one cannot establish the value of the electron's wavelength . This is a consequence of the uncertainty principle. For a plane wave electron of momentum p and position x, the

Figure 1-1

$\lambda < \ell$

Electron can be treated as a traveling wave in between scatterings.

$\lambda > \ell$

Electron's wavelength cannot be determined between scatterings. Electron wave approximation breaks down.

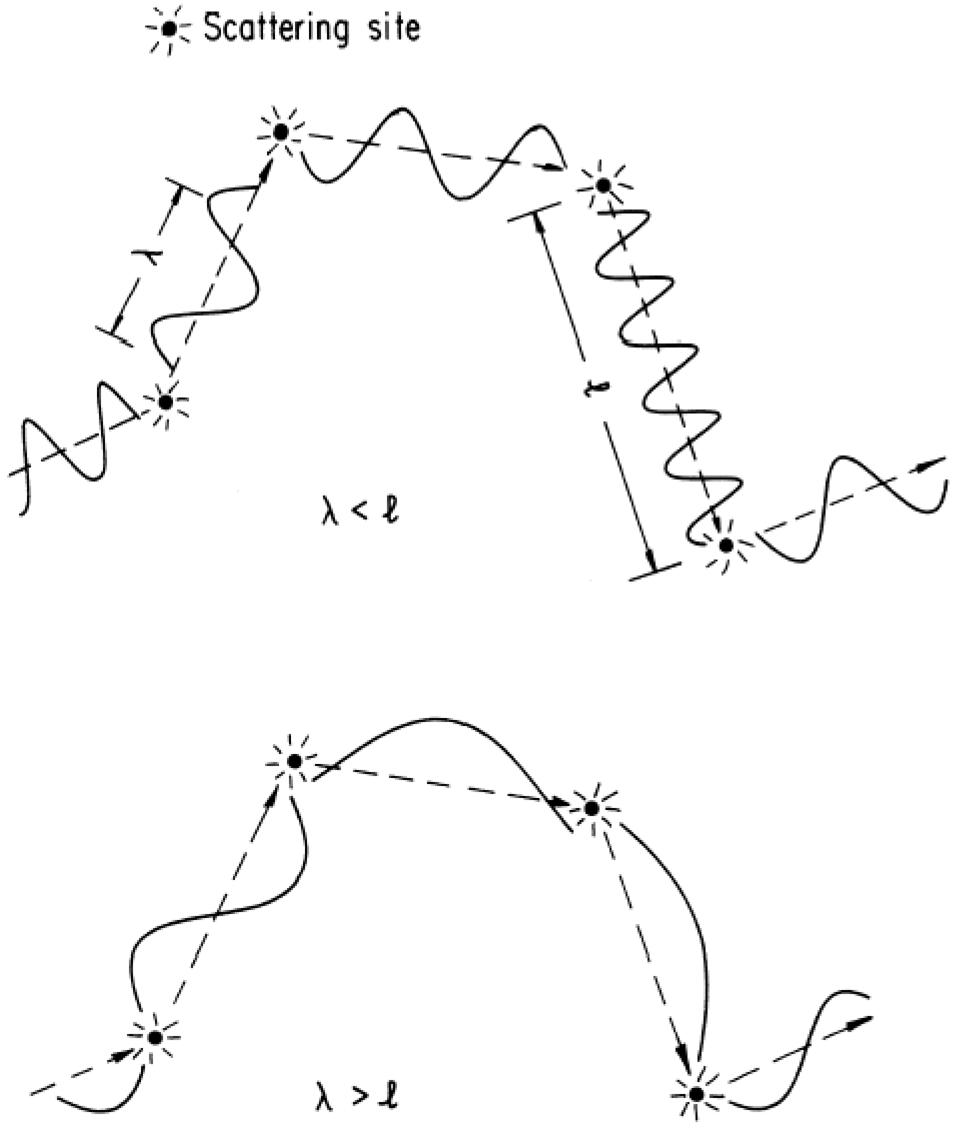
Scattering site
λ
ℓ
λ < ℓ
λ > ℓ

uncertainty principle states:

$$\Delta x \Delta p = \hbar \qquad (I.15)$$

where Δp and Δx are the uncertainty in the wavefunction's momentum and position. Combining this with equation (I.13) and noting that we only know the electron is somewhere between 0 and l away from the scatterer which caused the electron to be in its present state, $\Delta x = l$ and $\Delta p = \hbar \Delta k$. Since only states with wavevectors from k=0 up to $k=k_F$ are filled, the largest Δk can be is k_F, so :

$$\Delta k < k_F \qquad (I.16)$$

If one cannot establish the electron's wavelength and hence its wavevector k, the periodicity assumption of the wavefunction and the view of the electron as a traveling plane wave falls apart. This view was put forth in 1960 by Ioffe and Regel for impurity scattering in a metal. Their statement, known as the Ioffe-Regel rule, states that since the electrons with the shortest wavelength will have wavelengths of $\lambda_F = 2\pi/k_F$, the approximations used in the models of metallic conduction are valid only as long as (combine I.16 and I.15),

$$k_F l > 1, \qquad (I.17)$$

where l is the average distance an electron covers between scatterings, i.e. its mean free path.

Placing a bound for metallic behavior on the product of the Fermi wavevector and the mean free path sets a minimum bound on the metallic conductivity. The number of electrons per unit volume (electron density) n for a simple metal is related to the Fermi wavevector by

$$n = \frac{2^{1-d} k_F^d}{\pi^{d/2}\Gamma(\frac{d}{2}+1)} \qquad (I.18)$$

where d is the dimensionality of the metal (d=3 for the real world) and Γ is the gamma function. The scattering time for an electron with wavevector k_F is $\tau = l/v_F$ where $v_F = (\hbar k_F)/m$ (see equation I.13, p=mv). Combining this with equation I.17 gives the conductivity to be :

$$\sigma = \frac{2^{1-d} e^2 k_F^{d-2}(k_F \ell)}{\pi^{d/2}\Gamma(\frac{d}{2}+1)} \qquad (I.19)$$

For metallic conduction the Ioffe-Regel Rule requires $k_F l>1$. This implies there will be a minimum metallic conductivity when $k_F l = 1$ of

$$\sigma_{min} = \frac{2^{1-d} e^2 k_F^{d-2}}{\pi^{d/2}\Gamma(\frac{d}{2}+1)} \qquad (I.20)$$

Since k_F depends on the electron density and the electron density is specific to each material (remember Faraday's work), one can see that in 3 and 1 dimensions the minimum metallic conductivity is material specific (although in 1 dimension the minimum metallic conductance is not !). For example, copper has $k_F=1.36\text{x}10^8 \text{cm}^{-1}$ so σ_{min} = $3.3\text{x}10^4$ $(\text{ohm-cm})^{-1}$. The conductivity of a typical chunk of copper is far removed from this with $\sigma_{300k}= 6\text{x}10^5$ $(\text{ohm-cm})^{-1}$. In two dimensions the minimum metallic conductivity predicted by equation I.20 is **UNIVERSAL** :

$$\sigma_{2d}=e^2/(2\pi\hbar)=(25800 \quad \Omega/\text{Square})^{-1} \qquad (I.21)$$

and depends only upon the fact that the sample is two dimensional. The experiments presented in this thesis will be concerned with two dimensional metals with conductivites above and below this minimum metallic conductivity.

C. Metal-Insulator Transitions

One feature common only to metals is that at absolute zero (0 degrees Kelvin) all metals conduct electricity. This feature can in fact be used as a definition of metallic behavior. The ability of a metal to conduct electricity at absolute zero is a consequence of , (1) the density of states at the Fermi energy being nonzero and therefore the application of a small electric field will excite electrons to just above the Fermi energy and (2) the mobility (;) of the electrons at the Fermi energy is nonzero. The mobility is the ratio of the average drift velocity of the electron to the electric field inducing the drift, i.e.

$$\mu=v/|\mathbf{E}| \qquad (I.22)$$

Zero mobility would imply that the electron wavefunctions are localized to a given region of the material rather than extended throughout the sample volume.

The case of a material being nonmetallic due to a zero density of states at the Fermi energy is a familiar one, this being the case for a semiconductor

Figure 1-2

Starting at the bottom of the figure we see W/V << 1 where the band is composed only of extended states. As the amount of disorder is increased (W/V increases), tails of localized states form at the edges of the band separated from the extended states at the band center by a mobility edge. As the amount of disorder is increased further, the tails grow larger and as a critical value of W/V (approximately unity) is approached the mobility edges also move inward towards the band center. When W/V >> 1 the whole band is composed of localized states (top of figure).

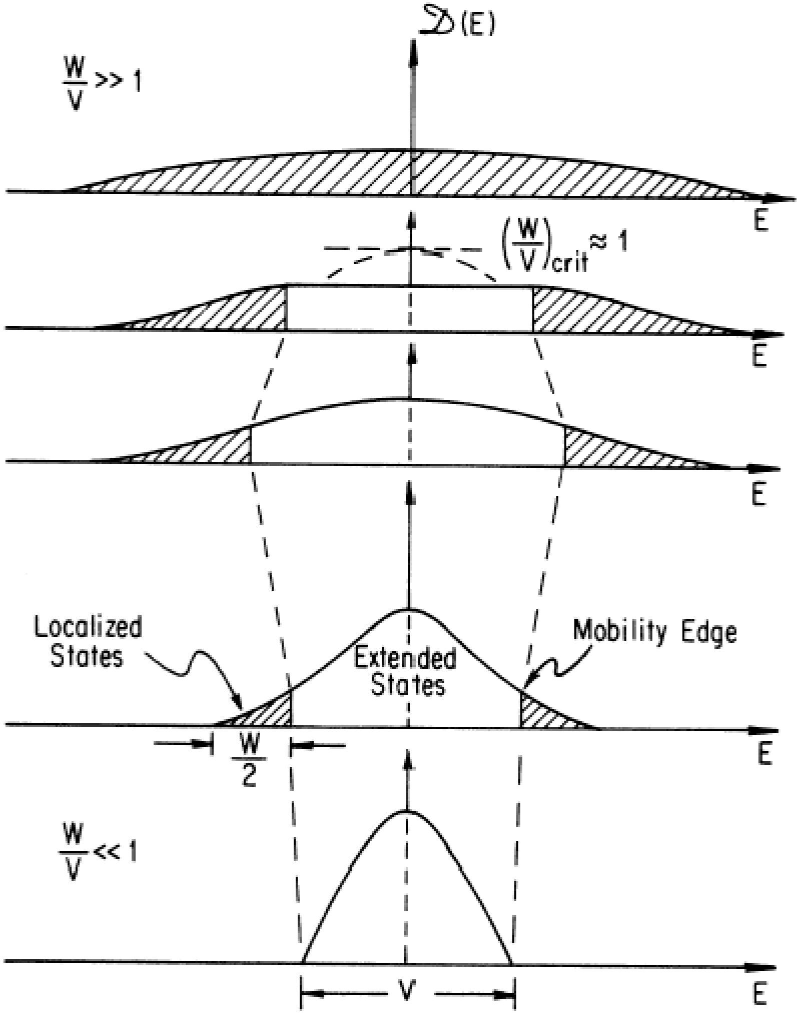

𝒟(E)
W/V >> 1
E
(W/V)crit ≈ 1
E
E
Localized States
Mobility Edge
Extended States
E
W/2
W/V << 1
V
E

such as silicon (Si) or germanium (Ge) and common insulators such as sapphire (Al_2O_3) or quartz (SiO_2). Nonmetallic behavior due to localization of the electrons, especially disorder induced localization, is less familiar to most physicists. P.W. Anderson originated the idea of disorder induced electron localization in 1958 by considering localized electrons tunneling from localized state to localized state (by disorder we mean anything which disrupts the periodicity of the lattice such as defects, impurities, etc.). Anderson's model uses a tight binding approximation (the electron states in the material are constructed by superimposing electron states of the isolated atoms) creating a tight binding band of states with a band width (V) due to the interatomic overlap and assumes the localized electron state energies are randomly distributed over an energy range W.

What Anderson found was that a band will be composed of only localized states if the energies of the localized electron states varied at random over a range greater than the width of the tight binding band. If one starts with little or no disorder in the system, $W/V \ll 1$ (see figure 1-2), one has completely metallic behavior. The first effect of disorder is to produce 'tails' of localized states at the outer edges of the tight binding bands separated from the extended metallic states in the interior of the band by 'mobility' edges. Increasing the disorder (increasing W/V) causes the localized tails to lengthen and as one approaches some critical value of disorder (and hence critical value of W/V~1), the mobility edges move inward until at $(W/V)_{crit}$ the mobility edges hit the center of the band and the whole band is then composed of localized states and no metallic behavior is observed.

It is interesting to note that the Anderson view and the Ioffe-Regel view are looking at basically the same phenomenon but from opposite vantage points. Ioffe and Regel started with extended states ($k_F l>1$) and found where they are no longer extended ($k_F l=1$), while Anderson originally started with localized states (W/V>>1) and found where the localized states became unstable (W/V=1). Both of these viewpoints involved looking at single electrons. As we shall see later, electron-electron interactions can also play an important role in transitions between metallic and nonmetallic behavior.

Taking nine Squares, each an inch every way, I had put them together so as to make one large Square, with a side of three inches, and I had hence proved to my little Grandson that- though it was impossible for us to *see* the inside of the Square- yet we might ascertain the number of square inches in a Square by simply squaring the number of inches in the side: "and thus," said I, "we know that 3^2, or 9, represents the number of square inches in a Square whose side is 3 inches long."

The little Hexagon meditated on this a while and then said to me; "But you have been teaching me to raise numbers to the third power: I suppose 3^3 must mean something in Geometry; what does it mean?" "Nothing at all," replied I, "not at least in Geometry; for Geometry has only Two Dimensions." And then I began to shew the boy how a Point by moving through a length of three inches makes a Line of three inches which may be represented by 3; and how a Line of three inches, moving parallel to itself through a length of three inches, makes a Square of three inches every way, which may be represented by 3^2.

Upon this, my Grandson, again returning to his former suggestion, took me up rather suddenly and exclaimed, "Well, then, if a Point by moving three inches, makes a line of three inches represented by 3; and if a straight Line of three inches, moving parallel to itself, makes a Square of three inches every way, represented by 3^2; it must be that a Square of three inches every way, moving somehow parallel to itself (but I don't see how) must make Something else (but I don't see what) of three inches every way- and this must be represented by 3^3."

"Go to bed," said I, a little ruffled by this interruption: "if you would talk less nonsense, you would remember more sense."

Flatland by
Edwin A. Abbott
(1838-1926)

CHAPTER II -- THEORY

A. Scaling Theory of Localization

In chapter one we were introduced to the Ioffe-Regel criteria for metallic conduction and its implication of a minimum metallic conductivity. We also saw how the Anderson model indicated that disorder could result in all electron states becoming localized. We have not however, set criteria for determining whether a given state is localized or extended.

In 1977, D.J. Thouless suggested that an electron in a sample should be considered localized if it is insensitive to changes made to the surface of the sample. Thouless develgped a model of free electrons in a d dimensional cube (called a hypercube) undergoing diffusive motion, i.e. the electrons were constantly being randomly scattered as they moved about the interior of the hypercube. The current equation (I.1) is modified in the presence of diffusion to

$$\mathbf{J} = \sigma\mathbf{E} - eD\mathbf{V}n \qquad \text{(II.1)}$$

where n is the electron density and D is the diffusion constant. The diffusion constant is defined in terms of a diffusion length L and a diffusion time τ (the time it takes to diffuse a distance L) by

$$D = L^2/\tau \qquad \text{(II.2)}$$

If one looks at the equilibrium case where there is no net motion of the electrons, J=0,

$$\sigma \mathbf{E} = eD\boldsymbol{\nabla} n \qquad \text{(II.3)}$$

The electron density may be a function of position **r** within the hypercube

$$n = n(r) = n(E_f + e\Phi(r)) \qquad \text{(II.4)}$$

where $\Phi(\mathbf{r})$ is the potential associated with the electric field **E**,

$$\mathbf{E} = -\vec{\nabla}\Phi \qquad \text{(II.5)}$$

From (II.4) and (II.5),

$$\vec{\nabla} n = \frac{\partial n}{\partial(e\Phi)} \vec{\nabla}\Phi = \frac{\partial n}{\partial E} e\vec{E} = D(\varepsilon)\, e\vec{E} \qquad \text{(II.6)}$$

(where D(ε) is the density of states, see equation I.14), which in conjunction with (II.3) gives us the Einstein relation for a quantum system of electrons:

$$\sigma = e^2 D D(\varepsilon_f) \qquad \text{(II.7)}$$

which with (II.2):

$$\sigma = \frac{e^2 L^2}{\tau} D(\varepsilon_f) \qquad \text{(II.8)}$$

Now if we apply the uncertainty principle to an electron in a hypercube of size L,

$$\Delta p \Delta x = \hbar$$

and set

$$\Delta x = L = v\tau$$

so

$$v \Delta p \tau = \hbar$$

and if we associate an energy uncertainty or width ΔE

with $v\Delta p$, then

$$\Delta E = \hbar/\tau \tag{II.9}$$

ΔE can be thought of as the energy sensitivity of the electrons to the boundary conditions, or equivalently, the energy width of the electron states. Since τ is the time for an electron to diffuse across the hypercube, a small τ implies the electron will be quick to see changes to the boundary resulting in a large energy width to the state. A large τ conversely means the electrons will notice changes to the boundary less quickly, resulting in a narrow ΔE. Combining (II.8) and (II.9) and noting that there are $N=nL^d$ electrons in a hypercube , we have :

$$\sigma = \frac{\partial E}{(\partial n/\partial E)}\frac{e^2}{\hbar^3}L^{2-d} \tag{II.10}$$

The implications of equation (II.10) are illustrated in figure (2-1). If hypercubes are placed in contact with each other then if the width of the electron states in the cubes are large ($\Delta E>>1$), and the spacing between energy levels in each cube is small ($\partial n/\partial E<<1$) then the probability of an electron in one hypercube finding a

Figure 2-1

Top: If the energy width (ΔE) of the states are broad and the spacing between states (∂n/∂E) small, the probability of a state in one hypercube overlapping a state in its neighboring hypercube is very large. Hence more electrons can slide from one hypercube to another, implying the conductivity of a conglomerate of such hypercubes is large.

Bottom: If the energy spacing (ΔE) is small and the states are far apart (∂n/∂E is large), the probability of states in neighboring hypercubes overlapping in energies is very small. Few electrons will easily slide from one hypercube to another, implying a small conductivity for a conglomerate of hypercubes.

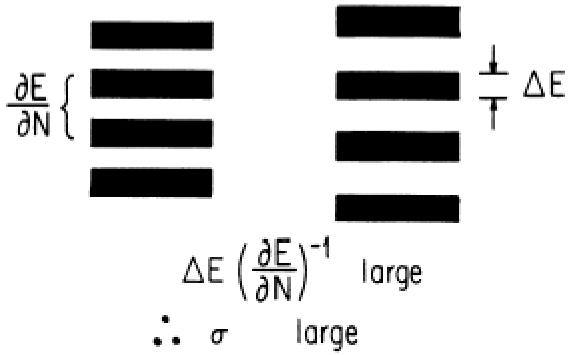
∂E/∂N
ΔE
ΔE (∂E/∂N)^-1 large
∴ σ large

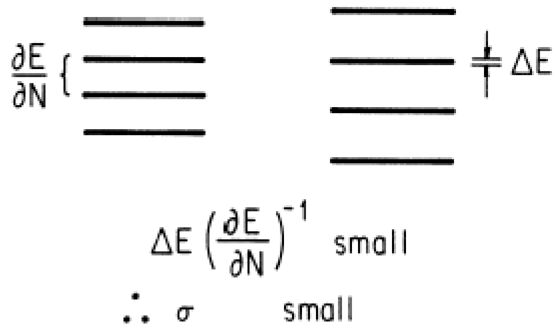
∂E/∂N
ΔE
ΔE (∂E/∂N)^-1 small
∴ σ small

state in a neighboring hypercube whose energy overlaps its own is large. Electrons will then find it easy to move from one hypercube to another, implying a large conductivity for the hypercube conglomerate. If on the other hand, the states have narrow energy widths ($\Delta E<<1$) and the spacing between energy states within the cubes is large ($\partial n/\partial E>>1$) then very few electrons will find states in neighboring hypercubes whose energies overlap their own. Very few electrons will then be able to move from hypercube to hypercube, being localized within a volume of L^d, resulting in a low conductivity for the hypercube conglomerate. The conductivity of a sample could therefore give one an indication of the degree to which the electrons within the sample are localized.

In 1979, E. Abrahams, P.W. Anderson, D.C. Liccardello and T.V. Ramakrishan, stimulated by the work of Thouless, formulated a single parameter scaling theory of localization. They started by defining a dimensionless electrical conductance, $g(L)$, for a d dimensional hypercube of side L:

$$g(L) = \sigma L^{d-2}\hbar/e^2 \qquad \text{(II.11)}$$

where σ is the d dimensional conductivity of the hypercube. Comparison with (II.10) also indicates:

$$g(L) = \Delta E/(\partial n/\partial E) \qquad \text{(II.12)}$$

The localization ideas of Thouless, by dealing with electron transport across hypercube boundaries, implies that some intrinsic scale must exist in this model (How big is a hypercube ?). Abrahams, et.al. set out to determine the consequences to the dimensionless conductance of a hypercube if its sides were changed from L to bL. They first assumed that $g(L)$ and $g(bL)$ were determined by something intrinsic to the hypercube , such as $\Delta E/(\partial n/\partial E)$, which implies $g(bL)$ depends only on b and on $g(L)$:

$$g(bL) = f(b, g(L)) \qquad \text{(II.13)}$$

The differential change in $g(L)$ can be expressed as

$$\frac{\partial g(L)}{\partial L} = \lim_{\Delta L \to 0} \frac{\Delta g}{\Delta L}$$

$$= \frac{1}{L} \lim_{\Delta L \to 0} \frac{g(bL)-g(L)}{b-1}$$

$$\frac{\partial g(L)}{\partial L} = \frac{1}{L} \lim_{b \to 1} \frac{f(b,g(L))-f(1,g(L))}{b-1}$$

which to lowest order in b becomes

$$\frac{\partial g(L)}{\partial L} = \frac{1}{L} \left. \frac{\partial f(b',g(L))}{\partial b'} \right|_{b'=1}$$

but

$$\frac{1}{f} \frac{\partial f}{\partial x} = \frac{\partial \ln f}{\partial x}$$

resulting in

$$\frac{\partial \ln g(L)}{\partial \ln L} = \frac{1}{g(L)} \left. \frac{\partial f(b',g(L))}{\partial b'} \right|_{b'=1} \equiv \beta(g(L)) \qquad \text{(II.14)}$$

In other words, the behavior of the dimensionless conductance $g(L)$ on L depends on a scaling function &(g(L)) which itself depends only on $g(L)$. This scaling function is illustrated in figure (2-2).

If the conductance of the hypercube is very small, the electrons must then be localized to some region within the hypercube with their wavefunctions tapering off from the center of this region exponentially fast,

$$\psi(r) \sim e^{-\alpha r}$$

One would then expect the conductivity of the hypercube

Figure 2-2

The scaling function β versus the logarithm of the dimensionless conductance $g(L)$.

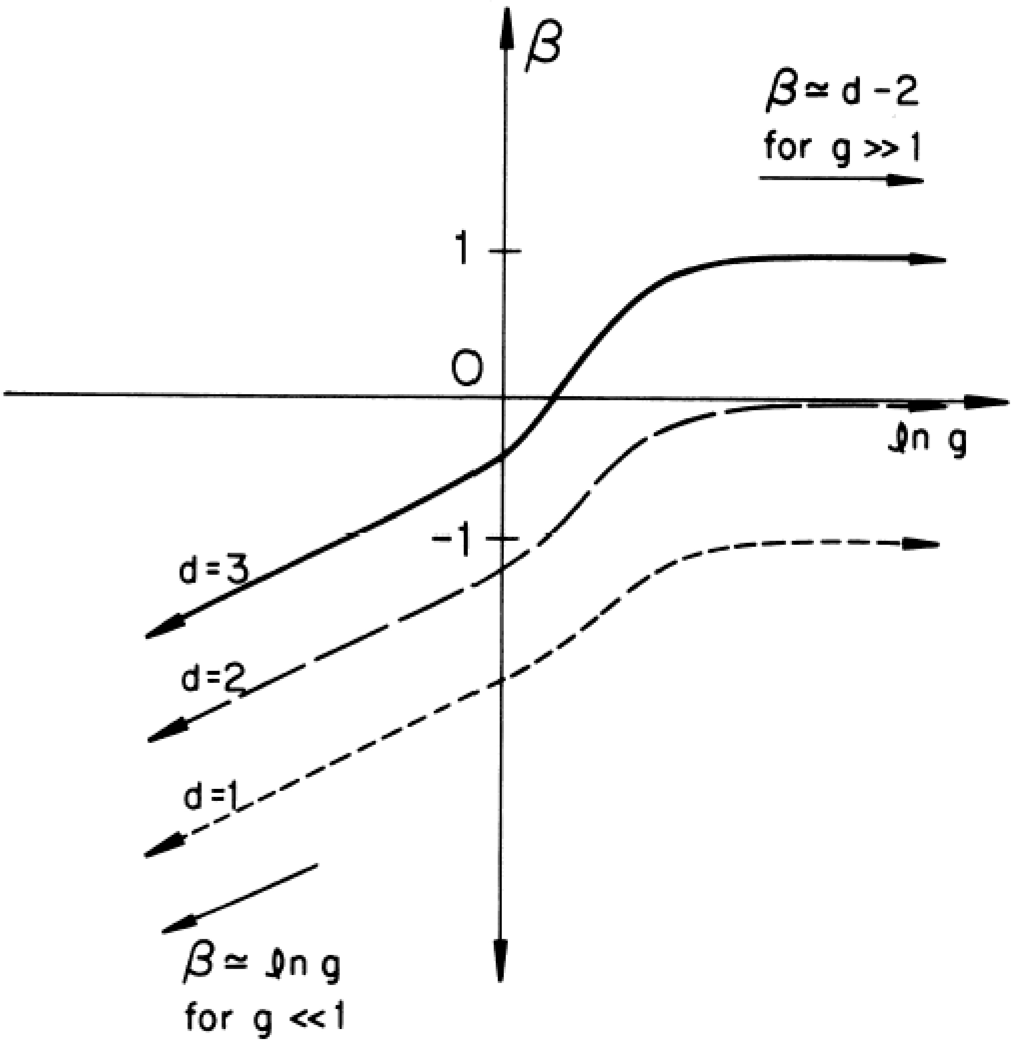

β
β ≃ d -2
for g >> 1
1
O
ln g
-1
d=3
d=2
d=1
β ≃ ln g
for g << 1

as a function of size to do likewise,

$$g(L) = g_{\circ}e^{-\alpha L} \tag{II.15}$$

implying:

$$\beta(g) = \ln(g/g_{\circ}) \tag{II.16}$$

In the opposite extreme, if the conductance of the hypercube is large so that its behavior is metallic, one would expect the traditional metallic dependence of $g(L)$ on σ and L :

$$g(L) = \sigma L^{d-2} \tag{II.17}$$

which implies:

$$\beta(g) = d-2 \tag{II.18}$$

B. Weak Localization in the Scaling Theory

Since $g(L)$ is monotonic in $\Delta E/(\partial n/\partial E)$, β should be monotonic in $g(L)$ and is illustrated in figure 2-2. Abrahams and Ramakrishnan performed a perturbation expansion of β for large $g(L)$ (and therefore weak localization) and found , to lowest order in $g(L)$:

$$\beta = (\partial \ln g \;/\; \partial \ln L) = d-2 -(a_d/g \qquad \text{(II.19)}$$

where a_d is a dimensionality dependent constant ($a_1=1/2$, $a_2=1/\pi^2$, and $a_3=3(3)^{1/2}/[2\pi^2]$). Integrating this equation,

$$\int_{g}^{g_o} \frac{\partial g'}{g'\cdot(d-2)-a_d} = \int_{L}^{L_o} \frac{dL'}{L'} \qquad \text{(II.20)}$$

gives the solutions:

$$g(L) = \begin{cases} (g_o + a_d)\dfrac{L_o}{L} - a_d & , d=1 \\ g_o - a_d \ln(L_o/L) & , d=2 \\ (g_o - a_d)\dfrac{L}{L_o} + a_d & , d=3 \end{cases} \qquad \text{(II.21)}$$

An intuitive picture for this weakly localized regime was developed by Larkin and Khmelnitskii in

Figure 2-3

a) Example of diffusive paths from $\vec{r}$ to $\vec{r}'$ each with probability amplitude A_i. For looped paths, the probability of going around the loop in each direction must be considered. The probability amplitude of going around the loop in one direction, a, is phase coherent with the amplitude for traversing the loop in the opposite direction,b : $a^*b+b^*a=2|a|^2$.

b)A path can only be localized to within a wavelength λ, and so must be treated as a d dimensional tube of cross section λ^{d-1}. The volume of space the electron sweeps out in (dt) is just $\lambda^{d-1}v(dt)$.

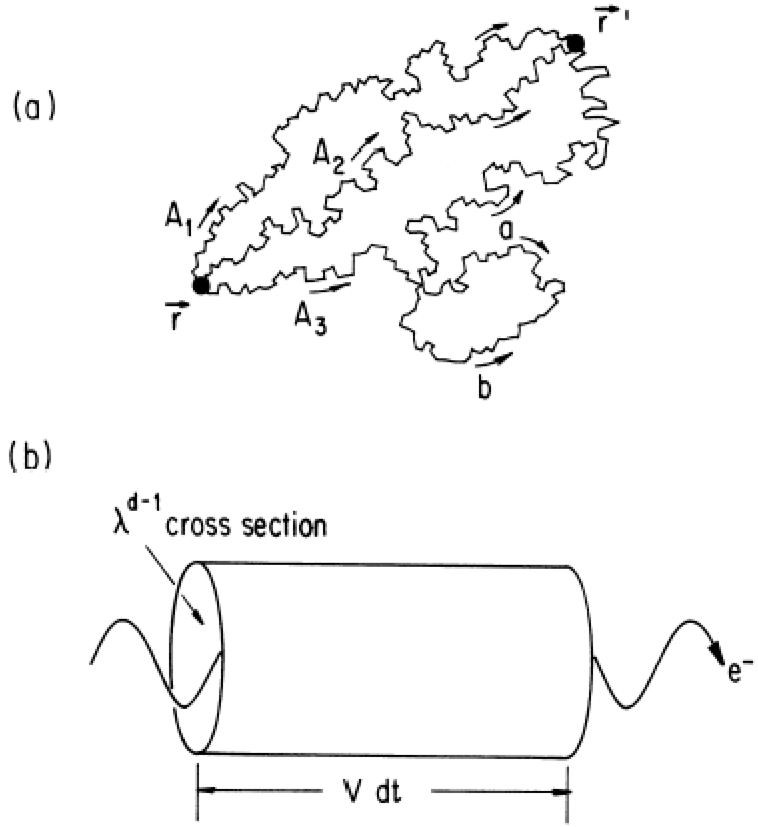
(a)
$\vec{r}\,'$
A_2
A_1
a
$\vec{r}$
A_3
b
(b)
λ^{d-1} cross section
e^-
V dt

1982. If one imagines an electron diffusing about having started at position $\vec{r}$ and suffering only elastic scatterings along the way (see figure 2-3,a), the probability P of the electron being found at position $\vec{r}'$ is just the square of the sum of the probability amplitudes (A_i) of possible paths the electron could have taken.

$$P = |A_1 + A_2 + A_3 + \ldots + A_i + \ldots|^2$$

$$P = \sum_i |A_i|^2 + \sum_{i \neq j} A_i^* A_j \qquad \text{(II.22)}$$

The first term is just the sum of the probabilities of taking each possible path. This term is all we would have if the electrons were purely classical particles (no quantum mechanical effects). The second term of (II.22) arises due to interference of the wavefunctions for the different routes the electron could take to go from $\vec{r}$ to $\vec{r}'$. Since the path lengths are very different from each other, their phases will all be different resulting in the mean value of their interference becoming zero. Paths which form loops however (see path A_3 in figure 2-3,a), can have their loops subdivided into amplitudes corresponding to the electron traversing the loop in opposite directions (path subamplitudes a and b in figure 2-3,a). These subamplitudes, being offshoots of the main amplitude A_3 must be phase coherent ($\oint \vec{p} * d\vec{r}$ is the same around the loop regardless of the direction), which implies that the mean value of the interference of the selfintersecting (looped) paths is not zero,

$$a^* b + b^* a = 2|a|^2 \tag{II.23}$$

indicating that the electron could form a standing wave about the looped path, localizing the electron to between $\vec{r}$ and $\vec{r}'$ within the sample. This model also suggests a natural scale length for the problem of electron localization, since localization in this description depends on the wavefunction preserving its phase long enough for it to interfere with itself. An inelastic scattering (which would, of course change the electrons phase) would destroy the standing wave, implying that the longest $|\vec{r}-\vec{r}'|$ can be is l_o, the inelastic scattering length. Since this model has us summing over electron states each of which represents a different electron path from $\vec{r}$ to $\vec{r}'$, the Pauli exclusion principle requires that no two paths may occupy the same space. The correction to the conductivity from this interference term is proportional to the ratio of the volume excluded from normal (nonselfintersecting) diffusively conducting paths by the selfintersecting paths to the volume which would be available if no paths were self intersecting. These paths are not infinitely thin, the uncertainty principle (I.15) implies that we can only locate a path to within a wavelength λ, requiring us to treat the path as a d dimensional tube (see figure 2-3,b). The ratio of the volume of a tube swept out in time Mt to the volume the electron could have classically diffused through during that time (see equation II.2, $(Dt)^{d/2}$) is

$$\frac{v\lambda^{d-1}\partial t}{(Dt)^{d/2}} \qquad \text{(II.24)}$$

An alternate view of equation (II.24) is this quantity is the probability of the tube intersecting itself in a time interval dt. Integrating (II.24) and remembering this scheme will work only until the electron inelastically scatters, the fractional correction to the conductivity is

$$\frac{\delta\sigma}{\sigma_0} = \int_{\tau}^{\tau_0} \frac{v\lambda^{d-1}\partial t}{(Dt)^{d/2}} \qquad \text{(II.25)}$$

which (with equation II.2) becomes:

$$\frac{\delta\sigma}{\sigma_o} = \frac{2v\lambda^{d-1}}{dD} \cdot \begin{cases} \ell_o - L & , d=1 \\ 2\ln(\ell_o/L) & , d=2 \\ \frac{1}{L} - \frac{1}{\ell_o} & , d=3 \end{cases} \qquad \text{(II.26)}$$

Expressing the total conductivity as

$$\sigma = \sigma_\circ + \delta\sigma \qquad \text{(II.27)}$$

where the conductivity correction is negative since the selfintersecting paths will hinder the ability of the electron to diffuse from $\vec{r}$ to $\vec{r}'$, this becomes

$$\sigma = \sigma_o - A_d \cdot \begin{cases} \ell_o - L & , d=1 \\ \ln(\ell_o/L) & , d=2 \\ \frac{1}{L} - \frac{1}{\ell_o} & , d=3 \end{cases} \qquad \text{(II.28)}$$

Using equations (II.11) and (II.28) to express a dimensionless conductance in terms of this conductivity, we have

$$g(L) = \frac{\hbar}{e^2}\,\sigma_o\,L^{d-2} - \frac{\hbar A_d}{e^2} \cdot \begin{cases} (\ell_o/L) - 1 & , d=1 \\ \ln(\ell_o/L) & , d=2 \\ 1 - (L/\ell_o) & , d=3 \end{cases} \qquad \text{(II.29)}$$

which, using $g_o=(\hbar/e^2)\sigma_o L^{d-2}$ and $(\hbar/e^2)A_d=a_d$, becomes

$$g(L) = \begin{cases} (g_o + a_d)\cdot(\ell_o/L) - a_d & , d=1 \\ g_o - a_d \ln(\ell_o/L) & , d=2 \\ (g_o - a_d)\cdot(L/\ell_o) + a_d & , d=3 \end{cases} \qquad \text{(II.30)}$$

Equations (II.21) and (II.30) are the same if one says that the characteristic length, L_o of Abrahams et.al. is the inelastic scattering length.

Larkin and Khmelnitskii's model gives the 'natural' maximum size of Abraham, et.al.'s hypercube (i.e., how large bL can become and equation II.13 remain valid). The scaling theory is a T=0 argument. The electrons cannot tell they are in a T≠0 world until they exchange energy with it - i.e. until they cover an inelastic scattering length (or in Larkin and Khmelnitskii's model, the electron has its phase disrupted). The inelastic scatterings setting a scale for these models has one enormous implication: if any side of a sample is

Figure 2-4

Top

The room temperature resistivity (measured in situ during the evaporation) as a function of thickness for a Pd film.

Bottom

Log-log plot of the same film as above. For thicknesses less than 100 Angstroms the film is two dimensional. As the thickness crosses above about 100 Angstroms the film resistivity goes as the inverse of the film thickness indicating a crossover to three dimensional behavior and indicating an inelastic scattering length of about 100 Angstroms at room temperature.

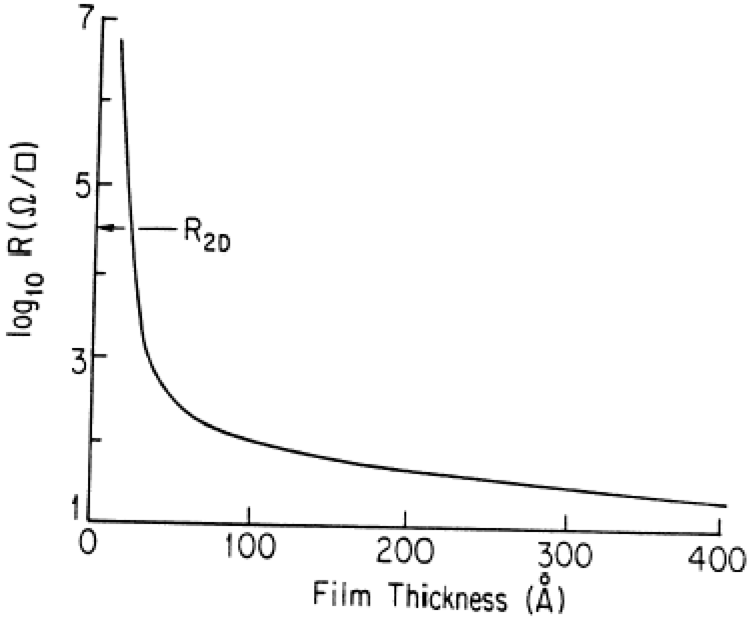
7
5
3
1
0
100
200
300
400
R_{2D}
$\log_{10} R(\Omega/\square)$
Film Thickness (Å)

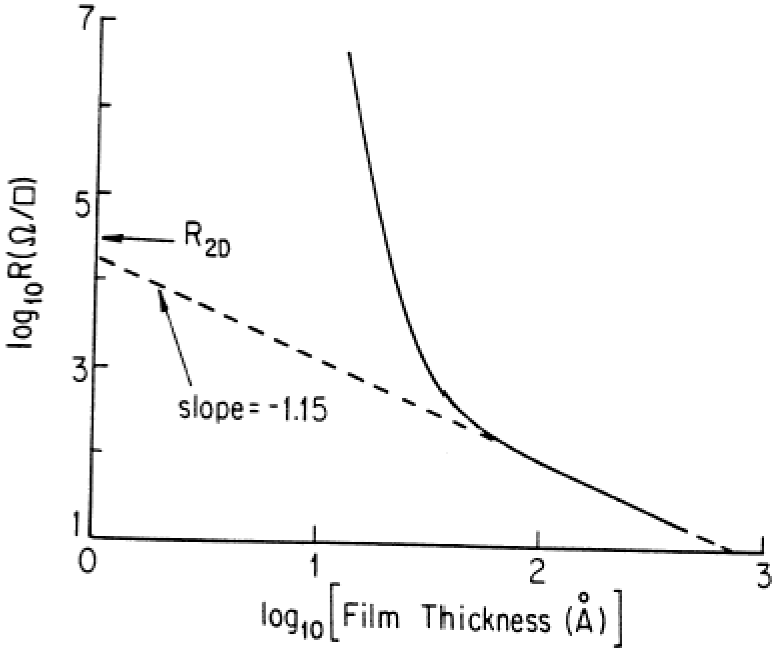
7
5
3
1
0
1
2
3
R_{2D}
slope = -1.15
$\log_{10} R(\Omega/\square)$
$\log_{10}$[Film Thickness (Å)]

thinner than the inelastic scattering length, the dimensionality of the sample in that direction is zero. For example, a film whose thickness is less than the inelastic scattering length is two dimensional (see figure 2-4). At thicknesses less than approximately 100 Angstroms the resistance per square ($R_\#$) is a very strong function of film thickness (t) implying the film's 3-d resistivity is a function of thickness ($R_\# < t^{-12}$ for the film in figure 2-4). At thicknesses greater than approximately 100 Angstroms, $R_\#$ changes as the inverse of the film thickness as one would expect for a three dimensional sample whose resistivity is determined by the electronic mean free path of the bulk material. This implies that the Pd film shown in figure 2-4 has a room temperature electronic scattering length of about 100 Angstroms.

In all of the previous discussions we have said nothing about excitation mechanisms for the electrons. The simplest effects would arise from a nonzero temperature (T), the inelastic scattering time for electron-phonon scattering depends on temperature as:

$$\tau_o \propto T^{-p} \tag{II.31}$$

In a clean metal where the electron mean free path (l_e) is much larger than the phonon wavelength (λ_{ph}) the number of phonons (N_{ph}) available to inelasically scatter electrons goes as (for $T<\Theta_D$, where Θ_D is the Debye temperature)

$$N_{ph} \propto T^{d} \qquad \text{(II.32)}$$

where d is the phonon dimensionality. If the sample is dirty (i.e. the elastic scattering length is dominated by impurity scattering) and $l_o<\lambda_{ph}$, the number of phonons available to inelastically scatter electrons is reduced by l_o/λ_{ph}, the relative probability of scattering off a phonon of wavelength λ_{ph} before scattering off impurities spaced lo apart, where for $T<\Theta_D$:

$$\lambda_{ph} \propto T^{-1} \qquad \text{(II.33)}$$

which gives us an effective number of phonons for inelastic scattering of

$$Neff = N_{ph}(l_o/\lambda_{ph}) \propto T^{d+1} \qquad \text{(II.34)}$$

Since the electron-phonon inelastic scattering time is inversely proportional to the effective number of phonons to scatter from,

$$\tau_o = \tau_{ph} \propto \begin{cases} T^{-d} & \text{, clean limit} \\ & \\ T^{-(d+1)} & \text{, dirty limit} \end{cases} \qquad \text{(II.35)}$$

which with equations (II.2),(II.11) and (II.21) gives

$$\sigma(T) = \begin{cases} \sigma_o + \dfrac{v_F \tau e^2}{2\hbar} \left(\dfrac{T'}{T}\right)^{p/2} & , d=1 \\ \sigma_o + \dfrac{e^2}{2\pi^2\hbar}\ p\ \ln(T/T') & , d=2 \\ \sigma_o - \dfrac{3\sqrt{3}e^2}{2\pi^2\hbar} \dfrac{1}{v_F\tau} \left(\dfrac{T}{T'}\right)^{p/2} & , d=3 \end{cases} \qquad \text{(II.36)}$$

where p would be

$$p = \begin{cases} d & \text{, clean limit} \\ & \\ d+1 & \text{, dirty limit} \end{cases} \qquad \text{(II.37)}$$

if the only inelastic scattering was electron-phonon scattering. In reality electron-electron inelastic scattering plays an important role and it is the total inelastic scattering time which governs the temperature dependence of the conductivity. Since the electron-electron inelastic scattering time also has the same general form as equation II.31, the total inelastic scattering time still retains this general form.

As one can see, the deviations from pure metallic behavior for a system of weakly localized electrons is small.

C. Strong Localization

In the case of strongly localized electrons (equations II.15 and II.16), the electron wavefunctions taper off as

$$\psi(r) \propto e^{-\alpha r} \qquad \text{(II.38)}$$

In 1968, Sir Nevill Mott showed that if R_o is the average distance between localized states and if $\alpha R_o<1$ or at sufficiently low temperatures, that electronic transport will take place via variable range hopping. The electrical conductivity of a variable range hopping system is determined by maximizing the distance that a localized electron (whose energy is within K_bT of the Fermi energy) can hop under the opposing conditions of the exponential decrease of its wavefunction with distance and the exponential decrease of hopping probability between nearby states with large energy differences as compared to K_bT. For a d dimensional system, the average energy (ΔE) spacing between a given state near the Fermi energy and the closest energy state to it within a hypersphere of radius r is

Figure 2-5

Plot of the relative probability per unit time of a hop $[P_{hop}(r)/P_{max}]$ as a function of hopping distance for 1,2 and 3 dimensions (see equations II.40 and II.42).

$$P_{hop}(r) = \omega_a \exp\{ -2\alpha r - \Delta E(r)/[K_b T] \}$$

The smaller ΔE the larger P_{hop}, however one may have to go very far to find a small enough ΔE, which would act to decrease P_{hop}. The electrical conductivity for a variable range hopping system is dominated by the tradeoff between these two processes.

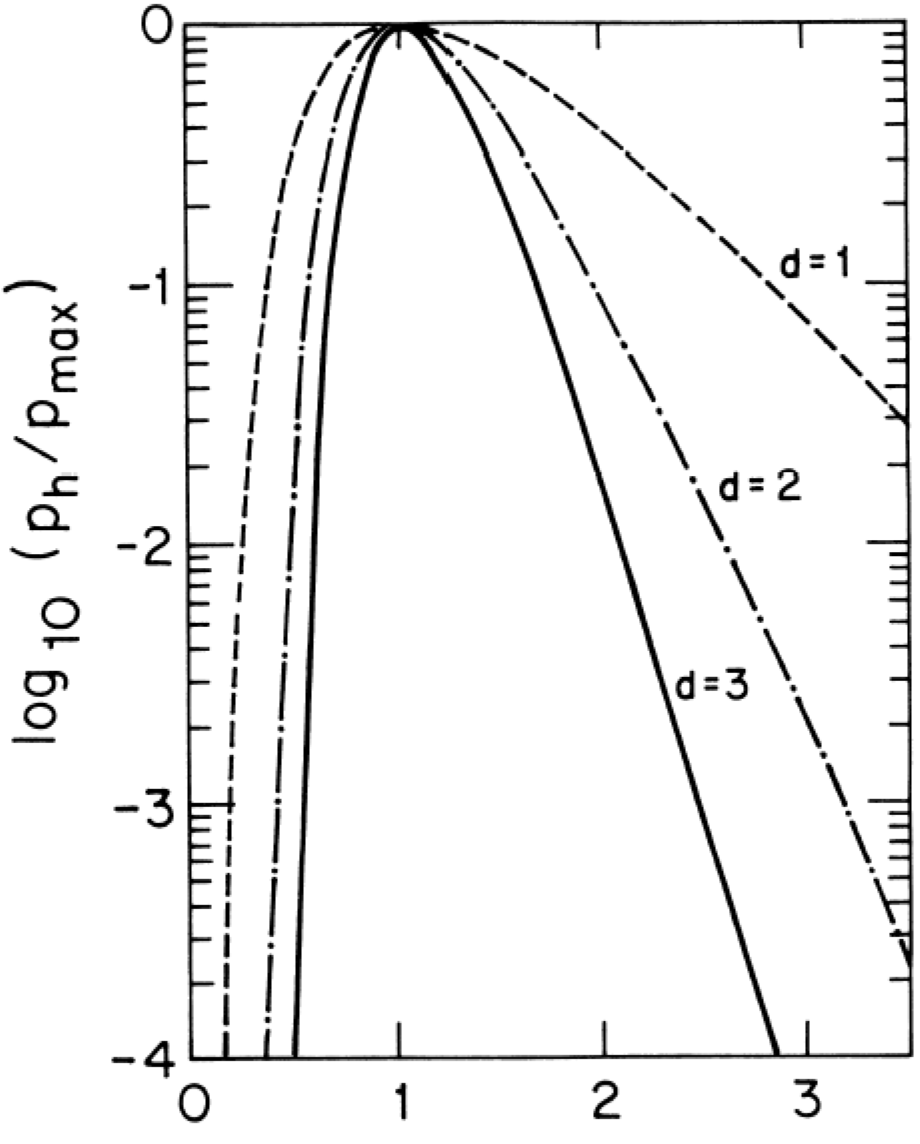
0
-1
-2
-3
-4
0
1
2
3
r / R
$\log_{10}(p_h/p_{max})$
d = 1
d = 2
d = 3

$$\Delta E(r) = \frac{\Gamma(d/2 + 1)}{\mathcal{D}(\varepsilon_F)\pi^{d/2} r^d} \qquad (II.39)$$

so the probability per unit time of a hop of distance r is

$$P_{hop}(r) = \omega_a \exp\{-2\alpha r - \Delta E(r)/[K_b T]\} \qquad (II.40)$$

where ω_a is a hopping attempt frequency which depends on details of the phonon spectrum (e.g. , the upper limit on the attempt frequency cannot be more than the frequency of the phonons which may have to supply the energy for the transition from one state to another). The maximum of equation II.40 (P_{max}) gives the optimum hopping distance,

$$R(T) = \left[\frac{d\Gamma(d/2 + 1)}{2\alpha\mathcal{D}(\varepsilon_F)\pi^{d/2} K_b T}\right]^{\frac{1}{d+1}} \qquad (II.41)$$

with,

$$P_{max}(T) = \omega_a \exp\left\{-\left[(2\alpha)^d \frac{\Gamma(d/2 + 1)}{\mathcal{D}(\varepsilon_F)\pi^{d/2} K_b T}\right]^{\frac{1}{d+1}} \cdot \left(d^{\frac{1}{d+1}} + d^{\frac{-d}{d+1}}\right)\right\} \qquad (II.42)$$

As one can see from figure 2-5, the probability of a hop per unit time is a very strong function of the hopping distance, dominated by hops of length R and probability P_{max}. We can define a diffusion constant (equation II.2) in terms of R and the time ($\tau=1/P_{max}$) it takes to cover that distance,

$$D = R2^{P}{}_{max} \tag{II.43}$$

which in conjunction with the Einstein relation (equation II.7), gives the conductivity to be

$$\sigma(T) = e^{2}\mathcal{D}(\varepsilon_{F})R^{2}\omega_{a}\ \exp\left\{-(T_{o}/T)^{\frac{1}{d+1}}\right\} \tag{II.44}$$

where

$$T_{o} = \left[(2\alpha)^{d}\quad \frac{\Gamma(d/2\ \ +1)}{\mathcal{D}(\varepsilon_{F})\pi^{d/2}K_{b}}\right] \cdot \left(d^{\frac{1}{d+1}} + d^{\frac{-d}{d+1}}\right)^{d+1} \tag{II.45}$$

An example of variable range hopping is the hopping of electrons between impurities in the impurity band of an amorphous semiconductor. In an amorphous semiconductor, the lack of long range order destroys the extended states which would exist in the conduction band of a crystalline semiconductor, leaving only the impurity states localized. Figure 2-6 shows the temperature dependence of a thick (3-d) film of amorphous germanium from an experiment performed by A.H. Clarke in 1967. Figure 2-6a shows the logarithm of the

Figure 2-6

Variable range hopping between impurity states in amorphous germanium.

a)log resistivity vs 1/T: The resistivity falls off the intrinsic Ge curve indicating another conduction mechanism in addition to the intrinsic semiconducting behavior.

b)log resistivity vs $1/T^{.25}$: When the data in a) is replotted in this form one can see it is consistent with the predictions of variable range hopping in 3 dimensions (equation II.44).

Data is by A.H. Clark,Phys Rev 154,750 (1967)

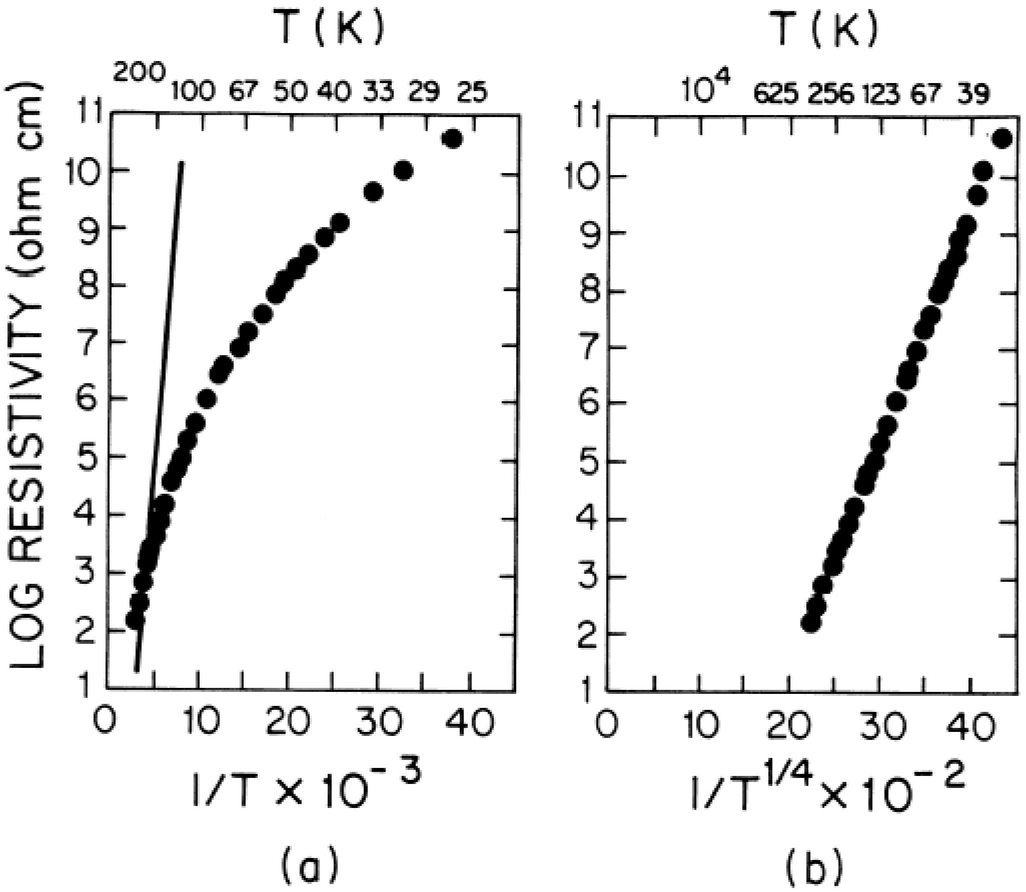

T (K)
200
100
67
50
40
33
29
25
LOG RESISTIVITY (ohm cm)
11
10
9
8
7
6
5
4
3
2
1
0
10
20
30
40
1/T × 10⁻³
(a)
T (K)
10⁴
625
256
123
67
39
0
10
20
30
40
1/T^1/4 × 10⁻²
(b)

resistivity versus 1/T which for crystalline Ge, would yield the straight line as shown. The amorphous sample has a smaller temperature dependence than crystalline Ge displaying an activation energy of about 0.15 eV at 300°K and about 0.02 eV at 30°K. When the data in figure 2-6a is replotted versus $1/T^{.25}$, as shown in figure 2-6b, one sees the data is in excellent agreement with equation II.44. An argument was advanced in 1973 by Kurkijarve which indicates that variable range hopping may not be allowed in one dimensional systems. Equation II.39 says that the hopping energy can become infinitesimally small if one has an infinite sample, since as the temperature is lowered the electron can just hop larger and larger distances to find sufficiently low energy states. This cannot happen in one dimension because the spatial resistivity alone, regardless of the excitation energy part, diverges unless the spatial concentration of states exceeds a certain density. If the spatial extent of a given localized state is $1/\alpha$, then

$$1/\rho_L = \sigma_L \propto e^{-\alpha L} \qquad \text{(II.46)}$$

is the conductivity of a hypercube of size L ($L >> 1/\alpha$). The resistivity of a conglomerate of these hypercubes is

$$\rho = \sum_{L} \rho_{L} P(L) \qquad \text{(II.47)}$$

P(L) is the probability to find a state in the hypercube at L with a specific energy, which for a random (Poisson) distribution of states is (in d dimensions)

$$P(L) \propto \exp\{ -Cr^{d} \} \qquad \text{(II.48)}$$

where C is the spatial concentration of states (regardless of their energy distribution). Equation II.47 then becomes

$$\rho \propto \int_{0}^{\infty} e^{\alpha r - Cr^{d}} \partial r \qquad \text{(II.49)}$$

which converges for any α or C if d>1 but for d=1 it diverges if $C<\alpha$, so for a given hopping energy there is a lower limit on C. Since $D(E_f)$ is the density of states (i.e. the number of states per unit energy per unit volume, equation I.14), then

$$\Delta E_{min} = C_{min}/D(E_f) = \alpha/D(E_f) \qquad \text{(II.50)}$$

which implies that at extemely low temperatures (and d=1) equation II.44 becomes

$$\sigma_{d=1}(T) = \sigma_o \exp\{ -\Delta E_{min}/[K_b T] \} \qquad (II.51)$$

which with equation II.50 is

$$\sigma_{d=1}(T) = \sigma_o \exp\{ -\alpha/[D(E_f) K_b T] \} \qquad (II.52)$$

which one can see is quite different from the variable range hopping prediction, equation II.44 .

D. Electron-Electron Interactions
in the
Near Metallic Limit

The scaling theory of localization deals only with systems of noninteracting electrons. One of the obvious questions to ask is 'What are the effects of interactions in these disordered systems ?'. In 1979 Altshuler and Aronov treated this problem of a disordered Fermi liquid in three dimensions and later with Patrick Lee extended it to two dimensions. If one performs a perturbation calculation for $k_F l >> 1$, then localization effects should be negligible and the calculation can be performed using standard diagramatic techniques (see Abirkosov, Gorkov and Dzyeloshinski).

The main feature of this interaction theory, which one must bear in mind during the calculation, is that the interaction vertex is dressed by the impurity scattering. This is illustrated by the Feynman diagram in figure 2-7, where the X with the dashed line through it denotes an interaction via an impurity. This vertex correction at finite temperatures has a diffusive form when the electron lines have frequencies of opposite sign (i.e. the electron scatters across the Fermi

Figure 2-7

The Vertex correction for impurity scattering. The dashed lines with the X denote an interaction via an impurity.

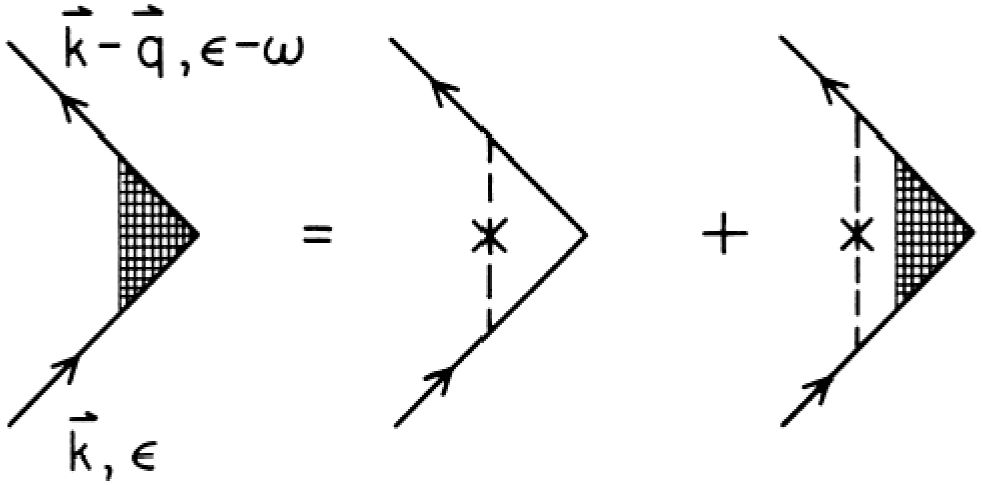
$\vec{k}-\vec{q}, \epsilon-\omega$
$\vec{k}, \epsilon$
=
+

$\Gamma(q, \omega, \epsilon)$

energy):

$$\Gamma(q,\omega_m,\varepsilon_n) = \begin{cases} (|\omega_m|+Dq^2)^{-1}\tau^{-1} , & \text{if } \varepsilon_n(\varepsilon_n-\omega_m)<0 \\ 1 , & \text{otherwise} \end{cases} \qquad \text{(II.53)}$$

where $\omega_m=2\pi m K_B T$, $\varepsilon_n=\pi(2n+1)K_B T$ are the Matsubara frequencies and we have assumed $|\omega_m|\tau, Dq^2\tau<<1$ (i.e. on time scales smaller than $\sim\hbar/K_B T$ the electron cannot tell it is in a $T\neq 0$ world). As was pointed out by Lee, this vertex correction generates an effective long range interaction regardless of how short the range of the bare interaction might be - the disorder induced diffusive motion of the electrons cause the electrons to spend a longer time in a given spatial region than they would if they were in plane wave states, thereby enhancing their mutual interactions.

The correction to the single particle density of states is

$$\delta D(\varepsilon) = (1/\pi) \sum_k \mathrm{Im}\{ G(k, \varepsilon N) \} \qquad \text{(II.54)}$$

where G(k,N) is the interaction Green's function, which is illustrated in figure 2-8 for the exchange interaction. The physical consequence of the exchange interaction is that electrons with parallel spins tend to stay apart in accordance with the Pauli exclusion principle, which results in a reduction of the Coulomb interaction between them. The free particle Green's function is

$$G_o^{\pm}(k,N) = [\ \varepsilon - \varepsilon(k) \pm i/(2\tau)\ ]^{-1} \qquad \text{(II.55)}$$

with the ± denoting whether the function is advanced or retarded, and ħ set equal to 1.

Altshuler and Aronov showed that to lowest order in the coupling, v(q), the dominant effect comes from the exchange interaction (figure 2-8) due to the two diffusion vertex corrections (equation II.53) becoming singular in the limit of small q and ω_m. The correction to the single particle density of states for this interaction then becomes

$$\delta\mathcal{D}(\varepsilon) = \frac{1}{\pi}\sum_{\vec{k}} \mathrm{Im}\left([G_o^{+}(k,\varepsilon)]^2 \sum_{\vec{q}} v(q)\int_{\varepsilon}^{1/\tau} \frac{d\omega}{2\pi}\, \Gamma(\vec{q},\omega,\varepsilon)G_o^{-}(\vec{k}-\vec{q},\varepsilon-\omega)\right) \qquad \text{(II.56)}$$

which integrating over k gives

Figure 2-8

The Exchange diagram. The exchange term is the interaction involving the ability of identical particles to trade 'identities'.

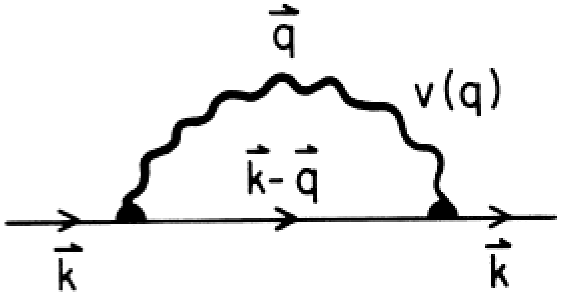
$\vec{q}$
v(q)
$\vec{k}-\vec{q}$
$\vec{k}$
$\vec{k}$

$$G(k,\epsilon)=i\sum_{q}\int_{\epsilon}^{1/\tau}\frac{d\omega}{2\pi}\left\{G_0^{+}(\vec{k},\epsilon)\,\Gamma(q,\omega,\epsilon)\,G_0^{-}(\vec{k}-\vec{q},\epsilon-\omega)\right.$$
$$\left.\Gamma(q,\omega,\epsilon)\,G_0^{+}(\vec{k},\epsilon)\,v(q)\right\}$$

$$\delta\mathcal{D}(\varepsilon) = \frac{1}{\pi}\,\mathrm{Im}\left(\mathcal{D}_o^2 \sum_{\vec{q}} v(q) \int_{\varepsilon}^{1/\tau} \frac{d\omega}{2\pi} \; \frac{1}{(Dq^2 - |\omega|^2)^2\,\tau^2} \right) \qquad \text{(II.57)}$$

Performing the X integration results in

$$\delta\mathcal{D}(\varepsilon) = \frac{1}{\pi}\;\mathrm{Im}\left(\mathcal{D}_o^2 \sum_{\vec{q}} \frac{v(q)}{2\pi\tau^2} \left[(Dq^2 - |\varepsilon|)^{-1} - (Dq^2 - |1/\tau|)^{-1} \right] \right) \qquad \text{(II.58)}$$

Now we can convert the sum over q to an integral and perform the angular integration:

$$\delta\mathcal{D}(\varepsilon) = \frac{1}{\pi}\,\mathrm{Im}\left(\mathcal{D}_o^2 \,\frac{1}{\tau^2} \int_0^{\infty} q^{d-1}\,\partial q \;\; v(q) \;\; \left[(Dq^2 - |\varepsilon|)^{-1} - (Dq^2 - |1/\tau|)^{-1} \right] \right) \qquad \text{(II.59)}$$

Since the vertex correction (equation II.53) reflects the dominance of small q interactions, we can simplify II.59 without changing the physics in any essential way by replacing v(q) with v(0), giving

$$\delta\mathcal{D}(\varepsilon) = \frac{-1}{\pi} \;\; \mathcal{D}_o^2 \;\; \frac{v(0)}{\tau^2 D} \;\; \cdot \begin{cases} (1/2)\ln|\varepsilon\tau| & , \; d=2 \\[2ex] \frac{\pi}{2}\left(\sqrt{\frac{|\varepsilon|}{D}} - \sqrt{\frac{1}{D\tau}} \right) & , \; d=3 \end{cases} \qquad \text{(II.60)}$$

for two and three dimensional systems.

The change in the single particle density of states due to the exchange interaction is reflected in the conductivity:

$$\delta\sigma_{ex} = \begin{cases} \dfrac{-e^2}{2\pi^2\hbar} \ln(T/T') & , d=2 \\ \dfrac{-e^2\, 1.3}{3\sqrt{2}\pi^2\hbar} \dfrac{1}{v_F\tau}\sqrt{\dfrac{T}{T'}} & , d=3 \end{cases} \qquad \text{(II.61)}$$

where $T'=\hbar/(4K_b\tau)$. Note that the d=2 case gives the same result as the scaling theory (equation II.36) for p=1 even though we are in a regime where localization effects should be negligible ($k_F l>>1$).

Since we obtained a correction to the density of states for even short ranged bare interactions, due to the impurity dressed vertex correction for the exchange interaction, one would expect a similar result for the Hartree interaction (figure 2-9). If the bare interactions had been delta functions in space (e.g. bulk impurity scattering) the parallel spin Hartree and exchange terms would cancel. A uniform background of electrons would also usually cancel the Hartree term, however the impurities result in a nonuniform background and so a residual interaction remains. The Hartree interaction also differs from the exchange interaction in that it is not dominated by small energy and momentum transfers. This Hartree term is reduced (and of course, opposite in sign) from the exchange term

Figure 2-9

The Hartree diagram. The Hartree term is the interaction of a given electron with the nonuniform background electron density in the ground state.

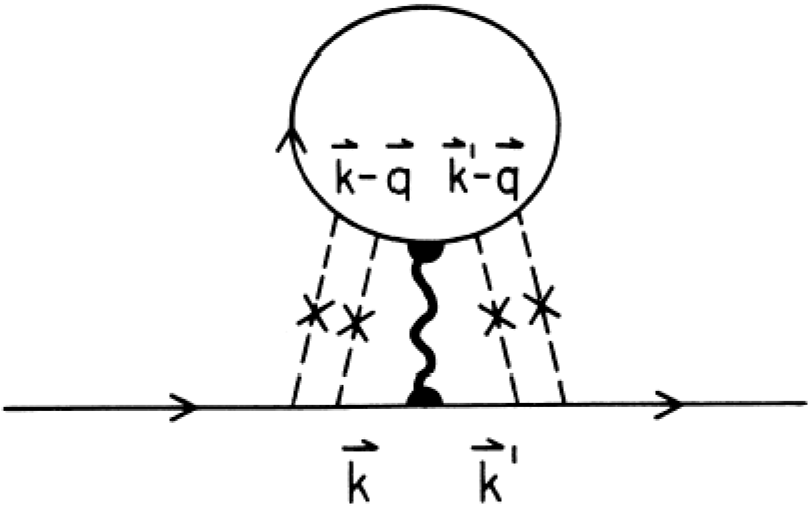
$\vec{k}-\vec{q}$
$\vec{k}'-\vec{q}$
$\vec{k}$
$\vec{k}'$

by a factor

$$F = \frac{1}{2\pi\tau\mathcal{D}_o} \sum_{\vec{k}',\vec{k}''} \frac{G_o^+(\vec{k}')G_o^-(\vec{k}')v(\vec{k}'-\vec{k}'')G_o^+(\vec{k}'')G_o^-(\vec{k}'')}{v(0)} \qquad \text{(II.62)}$$

In the limit of $1/\tau \dashrightarrow 0$, k' and $k'' = k_F$, so setting $|k'-k''| = 2k_F\sin(\theta/2)$:

$$F = \frac{\int d\hat{\Omega}\ v(2k_F\sin(\theta/2))}{\int d\hat{\Omega}} \qquad \text{(II.63)}$$

which is just the average of the interaction over the Fermi surface. The static screened Coulomb interaction is

$$v(q) = \begin{cases} \dfrac{2\pi e^2}{|q| + K_2} & , d=2 \\[2ex] \dfrac{4\ e^2}{q^2 + K_3^2} & , d=3 \end{cases} \qquad \text{(II.64)}$$

where the

$$K_d^{-1} = \begin{cases} 4\pi e^2\mathcal{D}_o & , d=2 \\[2ex] \sqrt{8\pi e^2\mathcal{D}_o} & , d=3 \end{cases} \qquad \text{(II.65)}$$

so

$$F = \begin{cases} \int_0^{2\pi} \frac{\partial\Theta}{2\pi} \; \frac{1}{1 + (2k_F/K_2)\sin(\Theta/2)} & , d=2 \\ \int_0^{2\pi} \frac{\partial\Theta}{2\pi} \; \frac{1}{1 + (2k_F/K_3)\sin^2(\Theta/2)} & , d=3 \end{cases} \qquad \text{(II.66)}$$

which for both two and three dimensions has the asymptotic forms one would intuitively expect:

$$F \text{ ----> } \begin{cases} 1 \text{ as } 2k_F/K \text{ ----> } 0 \\ \\ 0 \text{ as } 2k_F/K \text{ ----> } \infty \end{cases} \qquad \text{(II.67)}$$

which gives a total conductivity correction (Hartree + Exchange) from diagrams involving particle-hole diffusion of

$$\delta\sigma = \begin{cases} \frac{e^2}{\hbar} \; \frac{1}{4\pi^2} \; (2-2F) \; \ln(T/T') & , d=2 \\ - \frac{e^2 \; 1.3}{\hbar \; v_F \tau \sqrt{2\pi}} \; [\; 1 - (3/2)F \;] \; \sqrt{\frac{T}{T'}} & , d=3 \end{cases} \qquad \text{(II.68)}$$

where there are factors of 2 introduced for the spin. Note that now the d=2 case looks like the scaling prediction (equation II.36) with p=1 only in the limit of perfect screening, i.e. F=0.

For completeness one needs to also examine the corresponding particle-particle diffusion diagrams, which Fukuyama did in 1980. Including these diagrams only alters the above results by factors of 2.

E. Electron-Electron Interactions
in the
Insulating Regime

1. Single Particle Excitations

In 1975, A.L. Efros and B.I. Shklovskii considered the problem of electron-electron interactions in a strongly localized system which would otherwise display variable range hopping. They described the system with a hamiltonian **H**,

$$H = \sum_i \varepsilon_i n_i + \sum_{i \neq j} \frac{e^2 n_i n_j}{K|\vec{r}_i - \vec{r}_j|} \qquad \text{(II.69)}$$

where ε_i is the 'bare' energy of the i^{th} electronic state (i.e. the energy of the state if there were no electron-electron interactions), K is the dielectric constant of the medium and n_i is the occupation number of the i^{th} electronic state which (due to the Pauli exclusion principle) is either 0 or 1. The energy of the electron in the i^{th} state, when electron-electron interactions are taken into account is

$$E_i = \varepsilon_i + \sum_{j \neq i} e^2 n_j / |\vec{r}_i - \vec{r}_j| \qquad \text{(II.70)}$$

Figure 2-10

TOP

Ground state for the system. All states below the Fermi level are filled and all above are empty.

BOTTOM

One electron from a state i below the Fermi level is removed and placed in a state ℓ above the Fermi level. The change in energy is

$$\Delta E_{i \longrightarrow \ell} = \varepsilon_{\ell} - \varepsilon_{i} - e^{2}/[K|\vec{r}_{i}-\vec{r}_{\ell}|]$$

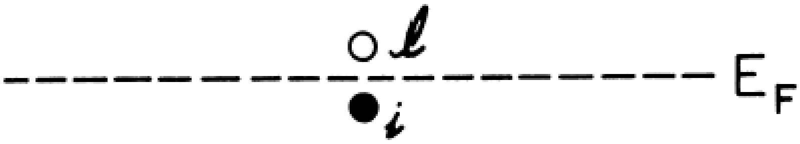
ℓ
i
E_F

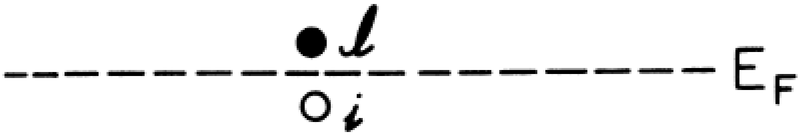
ℓ
i
E_F

Now at zero temperature there are no excitations of the system, so

$$n_i = \begin{cases} 1 \text{ for } E_i < E_f \\ 0 \text{ for } E_i > E_f \end{cases} \qquad \text{(II.71)}$$

where E_f is the Fermi energy. The ground state of the system is given by equation II.69 with a constraint given by equation II.71. There is an additional condition: suppose at T=0 we consider two states i and l where in the ground state i is occupied and l is empty. If we remove the electron from the i^{th} state and place it in the l^{th} state (see figure 2-10) the system should no longer be in the ground state, so the energy of the system should have changed to

$$\Delta E_{i\text{-->}l} = \varepsilon_l - \varepsilon_i - e^2/[K|\vec{r}_i-\vec{r}_l|] \qquad \text{(II.72)}$$

One can think of the $e^2/[K|\vec{r}_i-\vec{r}_j|]$ term as the energy of an electron-hole pair. Since the system started in its ground state, with $\varepsilon_i<E_f$ and $\varepsilon_l>E_f$, this change should represent an increase in the energy of the system, i.e.

$$\Delta E_{i\text{-->}l} = \varepsilon_l - \varepsilon_i - e^2/[K|\vec{r}_i-\vec{r}_l|] > 0 \qquad \text{(II.73)}$$

Any two states, separated by the Fermi level in the ground state, must satisfy equation II.73.

In a non-interacting d dimensional system undergoing variable range hopping, the average hopping energy is given by (equation II.39):

$$\Delta\bar{E}_{hop} = \frac{\Gamma(d/2 + 1)}{\mathcal{D}_o(E_f)\pi^{d/2}r^d} \qquad (II.74)$$

where D(Ef) is the non-interacting density of states and ` is the gamma function. Suppose we examine the excitation illustrated in figure 2-10 again. If $\Delta E_{hop}=E_h=\varepsilon l-\varepsilon_i$ is centered at the Fermi energy, the hopping distance is

$$R = \left[\frac{\Gamma(d/2 +1)}{\mathcal{D}_o\pi^{d/2} E_h}\right]^{1/d} \qquad (II.75)$$

which gives an interaction energy between the i and 1th state of

$$E_{int} = e^2/(KR) \qquad (II.76)$$

So equation II.73 can be expressed as

$$E_h - E_{int} > 0 \qquad (II.77)$$

or

$$E_h > \frac{e^2}{K} \left[\frac{\mathcal{D}_o \, \pi^{d/2} \, E_h}{\Gamma(d/2 \ +1)} \right]^{1/d} \tag{II.78}$$

$$E_h > \frac{e^{2d}}{K^d} \left[\frac{\mathcal{D}_o(E_f) \, \pi^{d/2}}{\Gamma(d/2 \ +1)} \right]^{\frac{1}{d-1}} \equiv \Delta \tag{II.79}$$

which implies (for d>1) that the effect of the electron-electron interactions is to set a minimum hopping energy of A. This just says that a hop from an occupied state below the Fermi energy to an unoccupied state above the Fermi level is only possible if the electron and hole which result from such a transition have enough energy to resist recombination.

One would expect a constant density of states would allow E_h to be arbitrarily small, which would contradict equation II.73. The minimum criteria for equation II.73 to hold is

$$| \, \varepsilon - E_f \, | = \tfrac{1}{2} E_h = \frac{1}{2} \, \frac{e^{2d}}{K^d} \left[\frac{\mathcal{D}(\varepsilon) \, \pi^{d/2}}{\Gamma(d/2 \ +1)} \right]^{\frac{1}{d-1}} \tag{II.80}$$

which results in a density of states centered about the Fermi energy (E_f) of

$$\mathcal{D}(\varepsilon) = 2^{d-1} \left(\frac{K}{e^2} \right)^d \frac{\Gamma(d/2 \ +1)}{\pi^{d/2}} \, | \, \varepsilon - E_f \, |^{d-1} \tag{II.81}$$

Comparison of equations II.79 and II.81 shows

$$\mathcal{D}(\varepsilon) = \left[\frac{2|\ \varepsilon - E_f\ |}{\Delta}\right]^{d-1} \mathcal{D}_o(\varepsilon) \qquad \text{(II.82)}$$

We may think of Δ as a Coulomb 'gap' in the density of states, in that it represents the minimum energy for a single particle-like excitation. Earlier calculations (by Pollack in 1970 and Ambegaokar, Halperin and Langer in 1971) on hopping conduction in disordered media indicated that electron-electron interactions should reduce the density of states near the Fermi energy, but not all the way to zero. It is interesting to note that if variable range hopping is applicable to a 1 dimensional system, Coulomb interactions would not alter the behavior of the system. Figure 2-11 illustrates the modifications to the single particle density of states that the electron-electron interactions introduce. If (for d>1) the average hopping energy is very much larger than Δ, i.e.

$$E_h >> \Delta \qquad \text{(II.83)}$$

then from equations II.39,II.41 and II.79

$$\left(\frac{\Gamma(d/2\ \ +1)}{\mathcal{D}_o\ \ \pi^{d/2}}\right)^{\frac{1}{d+1}} \left(\frac{2\alpha}{d}\right)^{\frac{d}{d+1}} (K_bT)^{\frac{d}{d+1}} >> \left(\frac{e^{2d}}{K^d}\ \ \frac{\mathcal{D}_o\ \pi^{d/2}}{\Gamma(d/2\ \ +1)}\right)^{\frac{1}{d-1}} \qquad \textbf{(II.84)}$$

Figure 2-11

Illustration of the effects of Coulomb interactions between electrons on the density of states in variable range hopping systems of 1,2,and 3 dimensions. The flat dashed line at $\mathcal{D}_o$ represents the density of states without interactions and the solid lines represent the density of states with the interactions. Note that in 1-d, Coulomb interactions have no effect on the density of states:

$$\mathcal{D}(\varepsilon) = \left[\frac{2|\varepsilon - E_f|}{\Delta}\right]^{d-1} \mathcal{D}_o(\varepsilon)$$

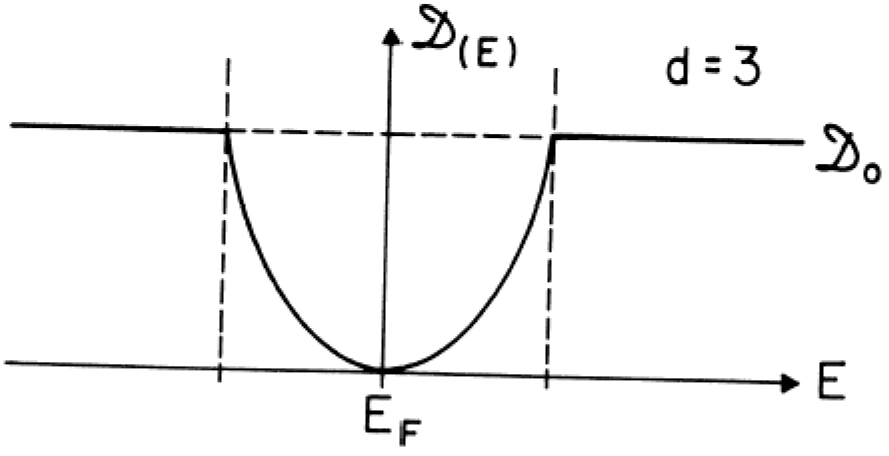
𝒟(E)
d = 3
𝒟o
E
E_F

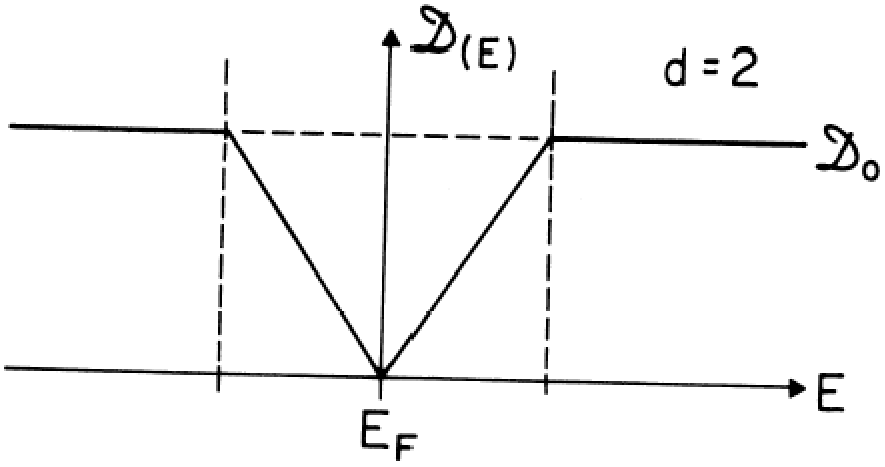
𝒟(E)
d = 2
𝒟o
E
E_F

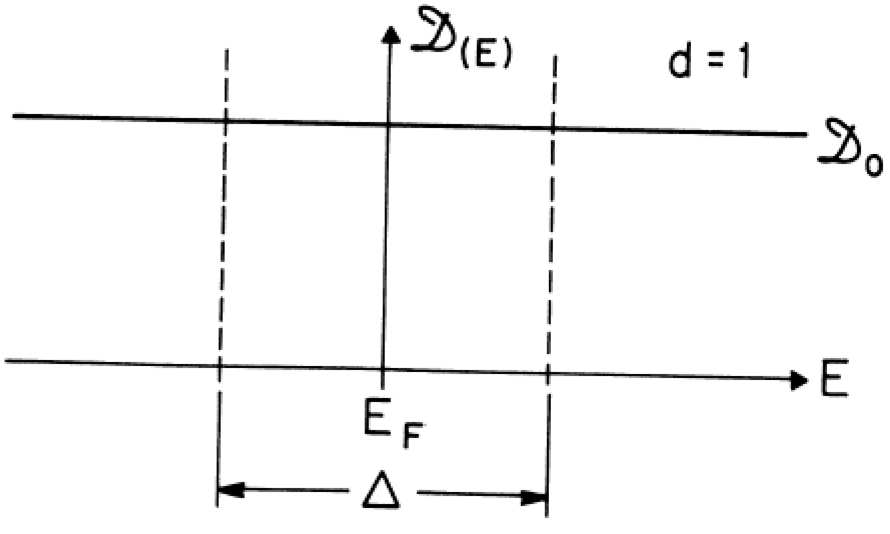
𝒟(E)
d = 1
𝒟o
E
E_F
Δ

which implies that Mott variable range hopping should be valid above some critical temperature:

$$T_c = \frac{1}{K_b}\left(\frac{e^2}{K}\right)^{\frac{d+1}{d-1}}\left(\frac{d}{2\alpha}\right)\left[\frac{\mathcal{D}_o\,\pi^{d/2}}{\Gamma(d/2\;+1)}\right]^{\frac{2}{d-1}} \qquad \text{II.85)}$$

If however, $T \ll T_c$, the states within the Coulomb gap are extremely important. Equation II.39 must be modified to take into account the nonconstant density of states, given by equation II.82, giving us

$$\overline{E}'_h = \frac{1}{\mathcal{D}_o}\left(\frac{\Delta}{\overline{E}'_h}\right)^{d-1}\frac{\Gamma(d/2\;+1)}{\pi^{d/2}\;r^d} \qquad \text{(II.86)}$$

so

$$\overline{E}'_h = \left[\frac{\Gamma(d/2\;+1)}{\mathcal{D}_o\sqrt{\pi}}\right]^{1/d}\Delta^{\frac{d-1}{d}}\;\frac{1}{r} \qquad \text{(II.87)}$$

The probability per unit time of a hop of distance r is (equation II.40):

$$P'_{hop}(r) = \omega_a \exp\{\,-2\alpha' r - E_h'/[K_b T]\,\} \qquad \text{(II.88)}$$

(the prime denotes that we are taking about an interaction picture) where as in the non-interacting case, the electrical conductivity is determined by maximizing the distance that a localized electron can hop under the opposing conditions of the exponential decrease of its wavefunction with distance and the exponential decrease of hopping probability between nearby states with large energy differences as compared to K_bT. The maximum of equation II.88 (P'_{max}) gives the optimum hopping distance for interacting electrons,

$$R' = \frac{1}{\sqrt{2\ \alpha}} \left[\frac{\Gamma(d/2\ \ +1)}{\mathcal{D}_o\ \ \sqrt{\pi}} \right]^{\frac{1}{2d}} \Delta^{\frac{d-1}{2d}} \frac{1}{\sqrt{K_bT}} \qquad \text{(II.89)}$$

which in combination with equation II.79 becomes

$$R' = [\ e^2/(2\alpha KK_bT)\ ]^{(1/2)} \qquad \text{(II.90)}$$

with

$$P'_{max}(T) = \omega_a \exp\{\ -2[2\alpha e^2/(KK_bT)]^{(1/2)}\ \} \qquad \text{(II.91)}$$

Combining this result with equations II.43 and II.7, we can see that the conductivity when $T<<T_c$ is (for d>1)

$$\sigma'(T) = e^2\ D_o(R')^2\ \exp\{\ -(T_o'/T)^{1/2}\} \qquad \text{(II.92)}$$

where

$$T'_o = 8\alpha e^2/(K_bK) \qquad \text{(II.93)}$$

A particularly interesting aspect of equation II.92 is the prediction that one of the effects of the Coulomb interaction, at extremely low temperatures, is to remove any effects of system dimensionality from the conductivity of the system, and that Coulomb interactions would not change the temperature dependence of a one dimensional variable range hopping system at all.

The effects of Coulomb interactions in a variable range hopping system have been used to explain the changeover from $\ln\sigma \propto T^{-.25}$ to $\ln\sigma \propto T^{-.5}$, reported by Shlimak and Nikulin in 1972, for impurity conduction in crystalline Ge samples which had shallow impurity states introduced into them, via nuclear transmutation produced by slow neutron bombardment of the samples. They reported a $\ln\sigma \propto T^{-.25}$ behavior for low impurity concentrations changing over to $\ln\sigma \propto T^{-.5}$ as the concentration increased, implying that as the spatial density of localized states is increased Coulomb interactions become important.

Figure 2-12 shows the conductivity of crystalline GaAs with a high impurity concentration taken by Redfield in 1973. Redfield performed high precision measurements of the conductivity of these samples and found that the data at low temperatures are consistent

Figure 2-12

The temperature dependence of the conductivity of crystalline GaAs with a high impurity concentration plotted two ways: one as $\log\sigma$ vs $T^{-.25}$ and one as $\log\sigma$ vs $T^{-.5}$.The straight lines through the lower segments are the best least square fits to the data. Best fits to the samples at low temperature gave:

$$\log\sigma = T^{-x}$$

$$x=0.509\pm0.015$$

consistent with equation II.92

Data is by D. Redfield, Phys Rev Lett 30, 1319 (1973)

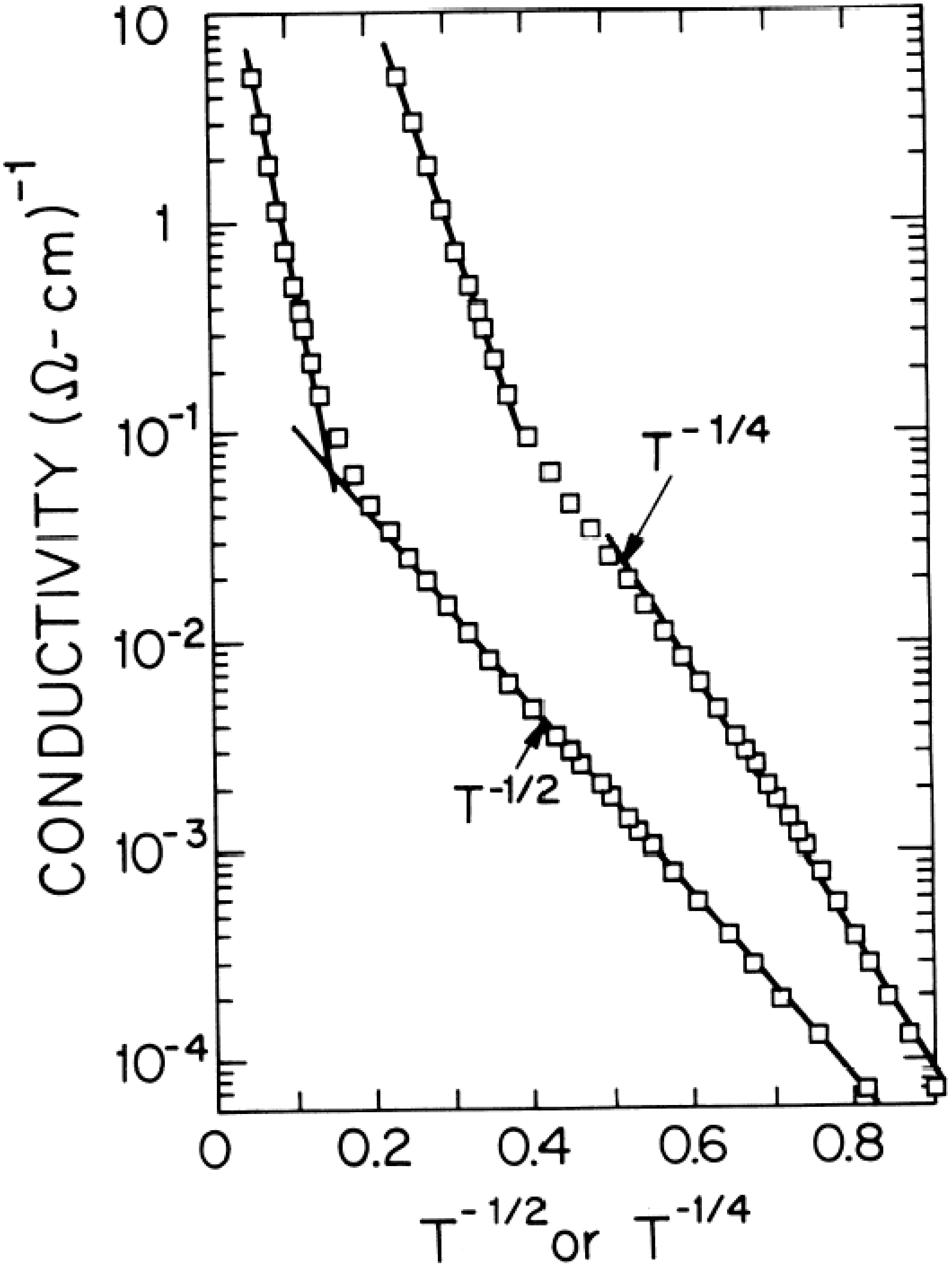
10
1
10^{-1}
10^{-2}
10^{-3}
10^{-4}
CONDUCTIVITY $(\Omega\text{-cm})^{-1}$
0
0.2
0.4
0.6
0.8
$T^{-1/2}$ or $T^{-1/4}$
$T^{-1/4}$
$T^{-1/2}$

with equation II.92, Redfield found the data following $\ln\sigma \propto T^{-x}$ within 2% where x was found to be 0.509+0.015.

E. Electron-Electron Interactions
in the
Insulating Regime

2. Polaronic Type Excitations

The treatment of Coulomb interactions by Efros and Shklovskii dealt only with the intrastate energy $e^2/K|\vec{r}_i-\vec{r}_j|$, where i and j denote the initial and final states of the hopping electron (this is the Coulomb energy between the electron in its final state and the hole which was created when the electron left its initial state). Another Coulomb interaction energy which might have an impact on the electron hopping is the Coulomb interstate energy, e^2/KR, between carriers occupying different states a distance R apart. This interaction was first discussed by Knotek and Pollack in 1972 and later by Mott in 1976. The effect of this interstate interaction is that if a given state i is occupied then the energy level of the surrounding states is raised above what they would be if the state i were not occupied, thus giving rise to an 'electronic polaron'.

Now suppose we look at an electron at the Fermi energy with its polaronic cloud about it. The electron wants to hop to states which before the hop are lower in energy than the initial state (i.e. it will try to hop to an unoccupied state of lower energy, and of course the unoccupied state will not have a polaronic cloud about it when it is empty. The electron will hop 'bare' and form a new polaron at the new site.). Since our electron is at the Fermi energy, all states with lower energies are therefore occupied... there are no states into which the electron can hop. One would then have to conclude that the Coulomb energy e^2/KR opens up a gap in the density of states. This gap would have a nonzero width in contrast to the situation described by Efros and Shklovskii. Mott went on to show that the effect of these polaronic excitations would be to alter equation II.40 to

$$P_{hop}(r) = \omega_a \exp\{ d \ln(\rho) \log_2(r/R_o) \\ -2\alpha R - \Delta E(r)/[K_b T] \} \qquad (II.94)$$

where ρ is the average probability that electrons forming the polaron cloud will also hop, and

$$R = \left(\mathcal{D}_o(E_f) \quad n^{-1/d} \quad \frac{e^2}{K\delta} \right)^{\frac{-1}{d}} \qquad (II.95)$$

where n is the number of simultaneous hops. δ is the average spatial separation between all of the states. At very low temperatures Mott showed that the effects of the extra term in the exponent of equation II.94 was negligible and equation II.44 would be recovered, although at higher temperatures deviations from equation II.44 might be expected. This prediction however, is at odds with numerical studies by Efros, Van Lien and Shklovskii in 1979, and Davies, Lee and Rice in 1982. Both groups found that both the single particle and the polaronic density of states went to zero only at the Fermi energy with the 'gap', Δ, (see Figure 2-11) narrower for the polaronic density of states. Davies, et.al. demonstrated an analogy between this system and a random field Ising spin glass with 1/r interactions, and showed that the onset of the Coulomb gap leads to an electron-glass transition with the formation of long lived metastable states for the whole system.

E. Electron-Electron Interactions in the Insulating Regime

3. Tightly Bound Electron-Hole Pairs

In the discussion of electron-electron interactions in the strongly localized regime, the Coulomb gaps in the bare (single particle) and dressed (electronic polaron) electronic density of states exist only in the spectrum of energies which correspond to the addition or removal of one electron to or from the system. Efros pointed out that there are other small energy excitations for the system - the formation of electron-hole pairs with very small spatial separation between the electron and the hole. The energy of such a pair is given by equation II.70:

$$\Delta E_{i\text{-->}l} = E_{il} = \varepsilon_l - \varepsilon_i - e^2/[K|\vec{r}_i-\vec{r}_l|] \qquad \text{(II.96)}$$

While the density of states for single particle excitations goes to zero at the Fermi energy (equation II.82, Figure 2-11), we can have $E_{il}<<\Delta$ but with N_l and N_i outside of the gap, i.e. $|N_i-E_f|>(1/2)\Delta$ and

$|N_l - E_f| > (1/2)\Delta$. This requires

$$|\vec{r}_i - \vec{r}_l| > r_o = e^2/(K\Delta) = T'_o/(8\alpha\Delta) \qquad \text{(II.97)}$$

where T'o is given by equation II.93. The density of states for electron-hole pairs which meet this requirement is nonzero as E_{il}-->0. These electron-hole pairs are rather compact, particularly at low energies. Using values for amorphous Ge taken from Knotek, et.al. (1973) of $D(E_f)=1.5\text{x}10^{18}/\text{eVcm}^3 = 9.4\text{x}10^{29}/\text{erg.cm}^3$, $\alpha^{-1}=10$ Angstroms and K=16, one gets from equations II.79 and II.85 that A=12°K, $T_c=0.15$°K, and T_o=~8400°K . Most electron-hole pairs with small excitation energies are very compact and isolated from each other (i.e. they can be considered as charge neutral and independent quantities) thereby contributing nothing to the D.C. conductivity.

F. The Effects of External Fields

1. Electric Fields in the Near Metallic Regime

The application of an electric field to any localized system with a nonzero conductivity will result in an electric current (equation I.1) and hence delocalization of the electrons (by delocalization we mean the electron propagates through a larger spatial extent of the sample than it did before application of the field). This delocalization will manifest itself as an electric field dependence of the electrical conductivity.

In 1979 Anderson, Abrahams and Ramakrishnan pointed out that an electron can absorb energy from the applied electric field and undergo Joule (I^2R) heating inbetween inelastic electron-phonon scatterings. While an electron could lose its field acquired energy in an electron-electron scattering, the electrons involved in the scattering would have just exchanged some energy but the electron gas as a whole would not have changed energy. The rate of heating of the electron gas temperature (T) is

$$\partial T/\partial t = \sigma E^2/C_{el} = [\ T - T_l\ ]/\tau_{ep} \qquad \text{(II.98)}$$

where C_{el} is the electronic specific heat, T_l is the lattice (phonon) temperature and τ_{ep} the electron-phonon scattering time. The electronic specific heat for a d dimensional electron gas is (see for example Kittel)

$$C_{el} = (\pi^2/3) K_b^2 T\ D(E_f) \qquad \text{(II.99)}$$

where $D(E_f)$ is the d dimensional density of states at the Fermi energy E_f. Combining equations II.31, II.98 and II.99 with the assumption $T >> T_l$ (i.e. we have driven the electrons out of thermal equilibrium from the Phonons by a large amount) we get

$$T \propto E^{2/(2+p')} \qquad \text{(II.100)}$$

where p' refers to the temperature exponent p in equation II.31 when only electron-phonon scattering is considered. This, in conjunction with equation II.37 implies the electric field dependent conductivity is

$$\sigma(E) = \begin{cases} \sigma_o + a_d \dfrac{e^2}{\hbar} \left(\dfrac{E}{E'}\right)^{\frac{p}{2+p'}} & , d=1 \\ \sigma_o - a_d \dfrac{e^2}{\hbar} \dfrac{p}{2+p'} \ln (E/E') & , d=2 \\ \sigma_o - a_d \dfrac{e^2}{\hbar} \left(\dfrac{E'}{E}\right)^{\frac{p}{2+p'}} & , d=3 \end{cases} \quad \text{(II.101)}$$

where p is the temperature exponent for the total inelastic scattering time and p' is the temperature exponent for the electron-phonon scattering time. This electron heating model applies to both the scaling theory of localization and the interacting electron picture. Other calculations by Tsuzaki in 1981, and also by Kaveh, Uren, Davies and Pepper in 1981, indicated that in the scaling theory the electric field changes the localization length directly, resulting in a quadratic electric field dependence at very low electric fields changing to a functional form similar to equation II.101. Altshuler, Aronov and Khmelnitzkii (1981) found that the interaction picture for the near metallic regime displayed only electron heating effects.

F. Effects of External Fields

2. Electric Fields and Hopping

The effect of an applied electric field on a hopping system is the same regardless of the details of the hopping description. The electric field inserts a directional dependence into the hopping probability through the electric field dependence the hopping energy has now acquired:

$$\frac{-e\vec{E}\bullet\vec{r}}{K_bT} \qquad \text{(II.102)}$$

where $\vec{E}$ is the electric field and -e is the electronic charge. This modifies the probability per unit time of a hop of distance r (equation II.40 or II.88) to

$$P_{hop}(\vec{E},\vec{r}) = \omega_a \exp\left[2\alpha r - \Delta E/(K_bT) - e\vec{E}\bullet\vec{r}/(K_bT)\right] \qquad \text{(II.103)}$$

$$P_{hop}(\vec{E},\vec{r}) = \omega_a \exp\left[-2\alpha + eE\cos\theta/(K_bT)\}r - \Delta E/(2K_bT)\right] \qquad \text{(II.104)}$$

where θ is the angle between $\vec{E}$ and $\vec{r}$. One can see this has the same form as the zero field expression (equation II.40 and II.88) if one makes the substitution:

$$\alpha \text{ ----> } \alpha'(\theta) = \alpha(1+eE\cos\theta/[2\alpha K_b T]) \qquad (II.105)$$

so that

$$P_{hop}(\vec{r}, \vec{E}) = P_{hop}(r,E,\theta) = \omega_a \exp\{-2\alpha'(\theta) r - \Delta E(r)/[K_b T]\} \qquad (II.106)$$

Averaging over $\cos\theta$,

$$P_{hop}(r,E) = (1/2) \int_{-1}^{1} P_{hop}(r,E,\theta) \partial(\cos\theta) \qquad (II.107)$$

gives

$$P_{hop}(r,E) = P_{hop}(r)(T/\xi)\sinh(\xi/T)$$

where $\xi = eE/(2\alpha K_b)$ and $P_{hop}(r)$ is given by II.40 for the non-interacting case and II.88 when Coulomb interactions are important. The maximum of the hopping probability is calculated the same way as for the zero electric field case, resulting in

$$P_{max}(T,E) = P_{max}(T) \ (T/\xi)\sinh(\xi/T) \qquad (II.108)$$

While both R and R' (equations II.41 and II.90) should depend on $\alpha'(\theta)$ and hence be functions of θ, one would expect on the basis of symmetry that averaging these quantities over $\cos\theta$ would result in essentially the same expressions as II.41 and II.90 for the spatial average of R and R'. Assuming the above and combining equation II.108 with II.7 and II.43 gives the conductivity to be

$$\sigma(T,E) = \sigma(T)\left[\frac{2\alpha K_b T}{eE}\right]\sinh\left[\frac{eE}{2\alpha K_b T}\right] \qquad \text{(II.109)}$$

where $\sigma(T)$ is given by either equation II.44 or II.92, depending on the importance of the Coulomb interactions.

As one can see from equation II.109, the conductivity is independent of electric field at small fields and/or high temperatures and a very strong nonlinear function at large fields and/or low temperatures. For extremely large fields ($E \gg [2\alpha K_b T/e]$) calculations by Pollack and Reiss indicate there may be large deviations from equation II.109 since then an electron can move only by hops down field, emitting a phonon at each hop. Under such conditions the electric field dependence should be the same as the zero field temperature dependence, i.e. for Mott variable range hopping, $\ln\sigma \propto (E)^{[1/d+1]}$.

F. Effects of External Fields

Magnetic Fields

Although simple free electron models for metals such as Drude's predict no change in the resistivity upon the application of a weak magnetic field ($\omega_c\tau<<1$), in reality metals do display a small positive magnetoresistance which comes about when the Lorentz Forces on the electrons cannot be completely canceled out by the Hall field. Both the scaling theory and the interaction theory predict magnetoresistance effects several orders of magnitude larger than for a simple metal, and not always positive in the near metallic regime.

In the strongly localized regime the magnetoresistance can result from a variety of effects. The magnetic field can cause the wavefunction to shrink thus reducing the spatial overlap of the states, Zeeman splitting can change the population statistics, restricting the conditions for a successful hop, resulting in a positive magnetoresistance. Or if there is a band of extended states (e.g. a conduction band as in figure 1-2) with energies only a little above the localized states the presence of the magnetic field can cause a dumping of carriers into the extended state band causing a negative magnetoresistance. Second and third order exchange scattering between extended state carriers and localized magnetic moments can also play a role in reducing the resistance in the presence of a magnetic field. In the strongly localized regime I will discuss only processes which contribute to a positive magnetoresistance.

F. Effects of External Fields

3. Magnetic Fields and the Near Metallic Regime

i) Orbital Effects and Scaling Theory

Perhaps the most obvious effect a magnetic field can have on the motion of the electron is to cause them to undergo cyclotron motion. This is also true in the localization problem and the intuitive picture of Larkin and Khmelnitskii (figure 2-3) provides a powerful but simple view of these cyclotron orbital effects. In the closed loop diffusive paths of figure 2-3a, a magnetic field will alter the phases of the subamplitudes a and b:

$$\begin{aligned} a &\longrightarrow a \cdot \exp\left(\frac{ie}{\hbar c} \oint \vec{A} \cdot \partial\vec{r} \right) \\ b &\longrightarrow b \cdot \exp\left(-\frac{ie}{\hbar c} \oint \vec{A} \cdot \partial\vec{r} \right) \end{aligned} \qquad \text{(II.110)}$$

where $\vec{A}$ is the vector potential of the magnetic field ($\vec{H} = \vec{\nabla} \times \vec{A}$) and the integral is taken around the loop. This means that the probability amplitude of the electron traversing the loop in one direction is now enhanced at the expense of the amplitude of traversing the loop in the opposite direction. This modifies equation II.25 to

$$\frac{\delta\sigma}{\sigma_o} = \int_{\tau}^{\tau_o} \frac{v\lambda^{d-1}\partial t}{(Dt)^{d/2}} \int W(S,t)\cos\left(\frac{4\pi HS}{\Phi_o}\right) \partial S \qquad \text{(II.111)}$$

where S is the projection of the area of the loop onto a plane perpendicular to the direction of the magnetic field, W(S,t) is the probability that a loop with length vt has area S, and $\Phi_\circ$ is a flux quanta $[(2\pi\hbar)/(ec)]$. In two dimensions all of the loops lie in the plane perpendicular to $\vec{H}$. While this is not true for three dimensions, we can estimate the conductivity correction by assuming all of the closed loops are flat. The angle between the magnetic field and the plane of the loop is

$$\theta = \cos^{-1}[S/(Dt)]$$

so

$$\int W(S,t)\cos\left[\frac{4\pi HS}{\Phi_o}\right]\partial S = \begin{cases} \cos\left(\dfrac{HDt}{\Phi_o}\right), & d=2 \\ \\ \dfrac{\Phi_o}{HDt}\sin\left(\dfrac{HDt}{\Phi_o}\right), & d=3 \end{cases} \qquad \text{(II.112)}$$

which gives us

$$\frac{\delta\sigma}{\sigma_o} \sim \int \frac{v\lambda^{d-1}}{(Dt)^{d/2}} \cdot \begin{cases} \cos\left(\frac{HDt}{\Phi_o}\right) \partial t & , d=2 \\ \frac{\Phi_o}{HDt} \sin\left(\frac{HDt}{\Phi_o}\right) \partial t & , d=3 \end{cases} \qquad \text{II.113)}$$

Integrating over t, we have

$$\Delta\sigma_{orb} = \sigma(H)-\sigma(0) \sim \frac{e^2}{\hbar} \cdot \begin{cases} \left.\begin{array}{ll} (H/H_o)^2 & H<<H_o \\ \ln(H/H_o) & H>>H_o \end{array}\right\} d=2 \\ \left.\begin{array}{ll} \sqrt{\frac{eH}{\hbar c}\,\frac{H}{H_o}} & H<<H_o \\ \sqrt{\frac{eH}{\hbar c}} & H>>H_o \end{array}\right\} d=3 \end{cases} \qquad \text{II.114)}$$

where $H_o=\hbar c/(4eD\tau_e)$, and τ_e is the elastic scattering time. The effect of the magnetic field is to suppress the selfinterference of the loops in figure 2-3 which are the source to the localization. As a consequence the orbital effects cause the conductivity to increase in the presence of a magnetic field in the scaling picture. In any 'real' two dimensional system, the system has a nonzero thickness and so orbital effects will make some, albeit small, contribution to the conductivity even when the field is parallel to the plane of the system.

F. The Effects of External Fields

3. Magnetic Fields and the Near Metallic Regime

ii) Spin Orbit Interaction, Zeeman Effects and Scaling

As an electron propagates through a solid it is moving past countless charged nuclei, which to the electron (which of course sees itself as stationary) looks like a current density and this current density generates a magnetic field which can interact with the electron's intrinsic magnetic moment (spin). This is the spin-orbit coupling for an electron in a metal (i.e. the interaction between the intrinsic and orbital angular momentum of the particle), which in a free atom has the effect of removing the degeneracy between some states of the same spatial wavefunction but opposite electron spin (e.g. an atomic p-state becomes two states, $p_{3/2}$ and $p_{1/2}$).

In 1980 S. Hikami, A.I. Larkin and Y. Nagaoka, and later Fukuyama and Hashino in 1981, calculated the correction to the conductivity in zero magnetic field from the spin-orbit coupling and found (for $\tau_o \gg \tau_{so}$)

$$\delta\sigma_{so} = \frac{e^2}{2\pi^2\hbar} \cdot \begin{cases} -\frac{1}{2}\ \ln(\tau/\tau_o) & , d=2 \\ \frac{\sqrt{3}}{v_F\tau}\sqrt{\frac{\tau}{\tau_{so}}}\left[3\sqrt{1+\frac{\tau_{so}}{4\tau_o}} - \sqrt{\frac{\tau_{so}}{4\tau_o}}\right] & , d=3 \end{cases} \tag{II.115}$$

where τ and τ_o are the elastic and inelastic scattering times, and $1/\tau_{so}$ is the spin relaxation rate via the spin-orbit interaction. Using equations II.2 and II.31 gives us the temperature dependence

$$\delta\sigma_{so} = \frac{e^2}{2\pi^2\hbar} \cdot \begin{cases} -\frac{p}{2}\ \ln(T/T'') & , d=2 \\ \frac{\sqrt{3}}{v_F\tau}\ \frac{\tau}{\tau_{so}}\left[3\sqrt{1+\left(\frac{T}{T''}\right)^p} - \left(\frac{T}{T''}\right)^{p/2}\right] & , d=3 \end{cases} \tag{II.116}$$

which can be approximated by (since $\tau_o >> \tau_{so}$ implies $T << T''$):

$$\delta\sigma_{so} \cong \frac{e^2}{2\pi^2\hbar} \cdot \begin{cases} -\frac{p}{2}\ \ln(T/T'') & , d=2 \\ \frac{\sqrt{3}}{v_F\tau}\sqrt{\frac{\tau}{\tau_{so}}}\left[3 - \left(\frac{T}{T''}\right)^{p/2}\right] & , d=3 \end{cases} \tag{II.117}$$

Comparing this to equation II.36, one can see that the spin-orbit coupling in zero magnetic field will change the prefactor of the temperature dependent term.

The magnetoconductivity was calculated by Maekawe and Fukuyama in two dimensions to be (for H | the plane of the system and assuming τ_o and $\tau_{so} >> C$):

$$\delta\sigma_{\perp so}(H) = \frac{-e^2}{2\pi^2\hbar}\left[\psi(\tfrac{1}{2} + c/[4DeH\tau]) - \psi(\tfrac{1}{2} + c/[4DeH\tau_1]) - \text{Real}\left\{ \frac{1}{2\delta} \left(\frac{1}{\tau_s} - \frac{1}{\tau_{so}}\right)\left[\psi(\tfrac{1}{2} + c/[4DeH\tau_2]) - \psi(\tfrac{1}{2} + c/[4DeH\tau_3])\right]\right\}\right] \tag{II.118}$$

where

$$\tau_1^{-1} = (2/\tau_s) + (4/\tau_{so}) + (1/\tau_o),$$
$$\tau_2^{-1} = (2/\tau_{so}) + (4/\tau_s) + (1/\tau_o) + 2\delta,$$
$$\tau_3^{-1} = (2/\tau_{so}) + (4/\tau_s) + (1/\tau_o) - 2\delta,$$
$$\delta = \{ [(1/\tau_s)-(1/\tau_{so})]^2 - [g\mu_B H/2]^2 \}^{1/2},$$

$\psi(x)$ is the Digamma function, and $1/\tau_s$ is the spin relaxation rate via impurity spin scattering. Note that without some mechanism for spin-flipping (e.g. spin-orbit or impurity spin scattering), the band splitting by the magnetic field (Zeeman effect) has no effect on the magnetoconductivity.

The characteristic temperature, T'', in the spin-orbit correction to the zero field conductivity is strongly material dependent, since we implied

$$\tau_{so} \propto (T'')^{-p} \tag{II.119}$$

In 1962, A.A. Abrikosov and L.P. Gorkov, while calculating the effect of the spin-orbit interaction on the Knight shift in superconductors, found the spin relaxation rate via the spin-orbit interaction to be

$$1/\tau_{so} = \{e^2Z/\hbar\}^4(1/\tau) \qquad \text{(II.120)}$$

where Z is the atomic number of the nuclei composing the material. This implies

$$T'' \propto Z^{(4/p)}\tau^{-1} \qquad \text{(II.121)}$$

indicating that the spin-orbit interaction will be negligible in the lighter elements but could play an important role in the conductivity of disordered systems composed of the heavier elements.

One would usually not expect a parallel field magnetoresistance for the spin-orbit scattering case in a two dimensional system. However, since Zeeman effects can alter the magnetoconductivity when spin-orbit coupling is present, and since the Zeeman interaction is isotropic, magnetoconductivity from a magnetic field parallel to the plane of the two dimensional system does come about:

$$\delta\sigma_{\parallel so}(H) = \frac{-e^2}{2\pi^2\hbar}\left\{\ln(\tau_1/\tau) - \mathrm{Real}\left[\frac{1}{2\delta}\left(\frac{1}{\tau_s} - \frac{1}{\tau_{so}}\right)\ln(\tau_3/\tau_2)\right]\right\} \quad \textbf{(II.122)}$$

For three dimensions Fukuyama and Hashino in 1981 found the magnetoconductivity due to the Zeeman and spin-orbit interaction to be:

$$\delta\sigma_{so}(h) = \frac{\sqrt{3}e^2}{2\pi^2\hbar v_F\tau}\sqrt{\frac{\tau}{\tau_{so}}}\left\{\sqrt{h}\,F([1+t]/h) + \frac{1}{2}\sqrt{\frac{h}{1-\gamma}}\left[F(t_+/h)-F(t_-/h)\right] - \frac{1}{\sqrt{1-\gamma}}\left(\sqrt{t_-} - \sqrt{t_+}\right) + \sqrt{t} - \sqrt{t+1}\right\} \quad \textbf{(II.123)}$$

where

$h = (v_f\tau)^2[\tau_{so}/(3\tau)eH/(ch),$

$t=\tau_{so}/(4\tau_o),$

$t_\pm = t + (1/2)(1 \pm [1-\gamma]^{1/2}),$

$\gamma = \{(g^*/2)\ \mu_B H\tau_{so}\}^2,$

$F(z) = {}_{N\neq0}\ \{\ 2([N+1+z]^{1/2}-[N+z]^{1/2}) - (N+0.5+z)^{-1/2}\ \},$

g^* is the effective electron g-factor, and μ_B the Bohr magneton ($\mu_B = e/[2m_oc]$). As in the two dimensional case, the Zeeman interaction has an effect only in the presence of spin-orbit or spin-flip interactions.

F. Effects of External Fields

3. Magnetic Fields and the Near Metallic Regime

iii) Orbital Effects and the Interaction Theory

Just as in the scaling picture of localization, orbital effects can play an important role in the magnetotransport in the interacting electron picture. The momentum of an electron in a magnetic field is the sum of two parts, the kinetic momentum

$$\vec{p}_{kin} = \hbar\vec{k} = (2m\varepsilon)^{1/2}/\hbar \qquad \text{(II.124)}$$

and the field momentum

$$\vec{p}_{field} = -e\vec{A}/c \qquad \text{(II.125)}$$

where $\vec{A}$ is the vector potential (i.e. the magnetic field is given by $\vec{H}=\vec{\nabla}\times\vec{A}$). The total momentum is just

$$\vec{p} = \hbar\vec{k} - e\vec{A}/c \qquad \text{(II.126)}$$

which implies that the total wavevector of the electron is

$$\vec{k}' = \vec{k} - e\vec{A}/(\hbar c) \qquad \text{(II.127)}$$

This modification of the electron wavevector by the magnetic field shows up in the interaction vertex correction (equation II.53 and figure 2-7) through the substitution

$$\vec{q} \dashrightarrow \vec{q} - 2e\vec{A}/(\hbar c)$$

where the factor of 2 comes from the fact that we are really dealing with particle-particle and particle-antiparticle interactions (i.e. things are in pairs). Physically, the electrons try to undergo cyclotron motion and if the inelastic scattering length ($[(D\hbar)/(K_bT)]^{1/2}$) is greater than the Landau orbit size [$2eH/(\hbar c)$], one would expect the electrons to find themselves to tend to be restricted to a spatial area the size of the Landau orbit, rather than simply diffuse all over the system - hence a positive magnetoresistance. In 1981 Altshuler, Aronov, Khmelnitskii and Larkin, and separately Fukuyama, calculated the orbital magnetoresistance in this picture arriving at similar results:

$$\Delta\sigma(H) \sim e^2/\hbar \times \begin{cases} (H/H'_o)^2 & H \ll H'_o, \quad d=2 \\ \ln(H/H'_o) & H \gg H'_o, \quad d=2 \\ & \qquad\qquad \text{(II.128)} \\ \{(eH)/(\hbar c)[H/H'_o]\}^{1/2} & H \ll H'_o, \quad d=3 \\ \{(eH)/(\hbar c)\}^{1/2} & H \gg H'_o, \quad d=3 \end{cases}$$

(II.128)

where $H'_{o}=cK_{b}T/(2eD)$ and D is the diffusion constant. As in the scaling picture there will be a small parallel field orbital contribution in two dimensions from the finite sample thickness.

F. The Effects of External Fields

3. Magnetic Fields and the Near Metallic Regime

iv) Zeeman Splitting and the Interaction Theory

In the interacting electron picture the dominant corrections to the conductivity (equation II.68) comes from the exchange interaction (figure 2-8) and the Hartree interaction (figure 2-9). One of the usual effects of a magnetic field on a system of electrons is to split the bands into spin-up and spin-down subbands producing a gap ($g\mu_B H$) between the lowest unoccupied spin-up electrons and the highest occupied spin-down electrons. Since the exchange term is the term involving the identical particles trading 'identities', the exchange interaction involves only electrons with the same spin and should be unaffected by the band splitting. Since the Hartree interaction is the interaction of the electron with the background electron density it can be separated into a Hartree term involving like-spin electrons and opposite-spin electrons. The like-spin Hartree interaction will, as in the exchange case, not be affected by the band splitting. Only the opposite-spin Hartree interaction will be affected by the band splitting. Lee and Ramakrishnan examined this problem in 1982. They found the Hartree correction to the spin-up electron conductivity due to spin-down electrons to be

$$\sigma_{\uparrow\downarrow} = F\,\frac{4De^2}{\pi\hbar}\int_0^{\infty} \partial\Omega\left[\frac{\partial}{\partial\Omega}\left(\frac{\Omega}{\exp(\Omega/K_bT)-1}\right)+\frac{1}{2}\right]f_{\uparrow\downarrow}(\Omega) \qquad \text{(II.129)}$$

where F is given by equation II.63 and

$$f_{\uparrow\downarrow}(\Omega) = \frac{1}{d}\int\frac{\partial\vec{q}}{(2\pi)^d}\;\frac{Dq^2}{[Dq^2 - i(\Omega + g\mu_BH)]^3} \qquad \text{(II.130)}$$

with d the system dimensionality. There is also a contribution from the symmetrical situation ($\sigma\uparrow\downarrow$) given by equations II.129 and II.130 but with $g\mu_BH \dashrightarrow -g\mu_BH$. This results in a magnetoconductivity given by

$$\Delta\sigma(H,T) \sim -e^2F/(4\pi^2\hbar)\;g_d(H,T)\;x\begin{cases}1, & d=2\\ [T/(2D)]^{1/2}, & d=3\end{cases} \qquad \text{(II.131)}$$

where F is given by equation II.66 and

$$g_d(H,T) = \int_0^\infty \partial\Omega \, \frac{\partial^2}{\partial\Omega^2} \left[\frac{\Omega}{e^\Omega - 1}\right] \cdot \begin{cases} \ln|1-h^2| & , d=2 \\ \sqrt{\Omega + h} + \sqrt{\Omega - h} - 2\sqrt{\Omega} & , d=3 \end{cases} \qquad \textbf{(II.132)}$$

which has the limiting behaviors

$$g_d(H,T) = \begin{cases} 0.084\ h^2 & , d=2 \\ 0.053\ h^2 & , d=3 \end{cases} \qquad \text{(II.133)}$$

where $h = g\mu_B H/[K_b T]$ and $h \ll 1$, and

$$g_d(H,T) = \begin{cases} \ln(h/1.3) & , d=2 \\ h1/2 - 1.3 & , d=3 \end{cases} \qquad \text{(II.134)}$$

when $h \gg 1$. Since this contribution to the magnetoconductivity is purely a spin effect, it is independent of the orientation of H.

F. Effects of External Fields

3. Magnetic Fields and the Near Metallic Regime

v) Spin-Orbit Coupling and the Interaction Theory

Just as in the scaling theory, the interaction of the electron spin with its orbital angular momentum has a large effect on the magnetoconductivity in the interaction picture. In 1982 Fukuyama calculated the conductivity in two dimensions for the spin-orbit interaction in zero magnetic field:

$$\Delta\sigma_{so}(0) = (e^2/[2\pi^2])\{1-(3/4)F\}\ln(4K_bT\tau/\hbar) \qquad (II.135)$$

where F is given by equation II.63, $TK_b >> \hbar/\tau o$, and τ and τ_o are the elastic and inelastic scattering times. The spin-orbit contribution to the magnetoconductivity saturates in high fields to a value which is orientation independent, but the characteristic field values do depend on the orientation:

$$\Delta\sigma_{so}(H=\infty) = -(e^2/[2\pi^2])F\ln(4K_bT\tau/\hbar) \qquad (II.136)$$

where the characteristic fields are

$$H_{||} >> cK_bT/(eD), 2\pi c\hbar/(eD\tau o)$$

$$H_\perp >> K_b/(g\mu_B), 2\pi\hbar/(g\mu_B\tau o)$$

In 1981 Altshuler, Aronov, Larkin and Khmelnitzkii calculated the spin-orbit magnetoconductivity to be the same as the orbital but reduced by a factor of 4, i.e.

$$\Delta\sigma_{so}(H) \sim e^2/(4\hbar) \text{ x } \begin{cases} (H/H'_o)^2 & H<<H'_o,\ d=2 \\ \ln(H/H'_o) & H>>H'_o,\ d=2 \\ \{(eH/(\hbar c)[H/H'_o]\}^{1/2} & H<<H'_o,\ d=3 \\ \{(eH)/(\hbar c)\}^{1/2} & H>>H'_o,\ d=3 \end{cases} \quad \text{(II.137)}$$

where $H'_o = cK_bT/(2eD)$ with diffusion constant D.

F. Effects of External Fields

4. Magnetic Fields and Hopping

i) Shrinking Wavefunctions

In 1962, N. Mikoshiba examined the problem of the behavior of the wavefunction in a magnetic field of an electron bound to an impurity atom in a semiconductor. He was interested in how the field would affect the hopping from impurity to impurity. If the wavefunction is spherically symmetric, the radial wavefunction will obey the Schrodinger equation

$$\nabla_r^2 \Psi(r) = -\frac{2m}{\hbar^2}\left(\epsilon + \frac{e^2}{Kr} - \frac{e^2H^2r^2}{8mc^2}\right)\Psi(r) \qquad \text{(II.138)}$$

where K is the dielectric constant, N the energy eigenvalue and H the magnetic field. Mikoshiba found that for an extremely strong magnetic field (H>> $[16m^2e^2c]/[\hbar^3K^2]$) the first two energy terms in II.138 can be neglected, so one can write

$$\nabla_r^2 \Psi(r) = \frac{e^2H^2r^2}{4\hbar^2c^2} \quad \Psi(r) \qquad \text{(II.139)}$$

whose solution is

$$\psi(r) \sim \beta^{-1}\exp\{ -[(eH)/(4\hbar c)]r^2 \} \qquad \text{(II.140)}$$

where

$$\beta^2 = \begin{cases} eH/(2\hbar c) & d=2 \\ (16/\pi)^{1/2}\{(eH)/(4\hbar c)\}^{3/2} & d=3 \end{cases} \qquad \text{(II.141)}$$

As one can see, this results in the wavefunction shrinking as the magnetic field increases. Since we only considered the magnetic energy in II.138 this just says that

$$a = [(\hbar c)/(eH)]^{1/2} \qquad \text{(II.142)}$$

is the spatial extent of a free electron wavefunction in a magnetic field, i.e. the arguments which follow from looking at the effect of this shrinking wavefunction on the magnetoresistance should be more general (at least qualitatively) than for just the case of impurity state hopping.

To see what this new tail-off of the wavefunction does to the magnetoconductivity we must redo the variable range hopping schemes in sections II.C and II.E.

For the noninteracting variable range hopping case (section II.C), the probability per unit time of a hop of distance r (equation II.40) becomes

$$P_{hop}(r,H) = \omega_a \exp\{ -r^2/a^2 -\Delta E(r)/[K_b T]\} \qquad \text{(II.143)}$$

where a is given by equation II.142 and $\Delta E(r)$ is given by equation II.39. The maximum of equation II.143 ($P_{max}(H,T)$) gives the new optimum hopping distance

$$R(H,T) = \left[\frac{d\hbar c \; \Gamma(d/2 +1)}{eH\mathcal{D}(E_f)\pi^{d/2}K_b T} \right]^{\frac{1}{d+2}} \qquad \text{(II.144)}$$

with

$$P_{max}(T,H) = \omega_a \exp\left[-\left\{ \left(\frac{\Gamma(d/2 +1)}{\mathcal{D}(E_f)\pi^{d/2}K_b T} \right)^2 \left[\frac{eH}{\hbar c} \right]^d \right\}^{\frac{1}{d+2}} \left(\tfrac{1}{2} d^{\frac{2}{d+2}} + d^{\frac{-d}{d+2}} \right) \right] \qquad \text{(II.145)}$$

where d is the system dimensionality. Combining this with equations II.2 and II.7 gives us

$$\sigma(H,T) = e^2 \mathcal{D}(E_f)[R(H,T)]^2 \exp\left[-A\left(\frac{H^d}{T^2} \right)^{\frac{1}{d+2}} \right] \qquad \text{(II.146)}$$

where

$$A = \left[\frac{\Gamma(d/2+1)}{\mathcal{D}(E_f)\pi^{d/2}K_b}\right]^{\frac{2}{d+2}}\left(\frac{e}{\hbar c}\right)^{\frac{d}{d+2}}\left\{\tfrac{1}{2}d^{\frac{2}{d+2}} + d^{\frac{-d}{d+2}}\right\} \qquad \text{(II.147)}$$

The effect of the magnetic field is to increase the temperature sensitivity of the conductivity and reduce it. At low fields we would expect to recover equation (II.44).

In the case of variable range hopping with Coulomb interactions (section II.E), the probability per unit time of a hop of distance r (equation II.88) becomes

$$P'_{hop}(r,H) = \omega_a \exp\{-r^2/a^2 - E'_h/[K_bT]\} \qquad \text{(II.148)}$$

where E'_h is given by equation II.87. The maximum of equation II.148 ($P'_{max}(H,T)$) gives the optimum hopping distance for the interacting electrons

$$R'(H,T) = \left[\frac{\Gamma(d/2+1)}{\mathcal{D}_o\sqrt{\pi}}\right]^{\frac{1}{d}} \Delta^{\frac{d-1}{d}} \left(\frac{\hbar c}{eHK_bT}\right)^{1/3} \qquad \text{(II.149)}$$

which in combination with equation II.79 becomes

$$R'(H,T) = \left[\frac{e\hbar c}{KK_bTH} \pi^{\frac{d-1}{2d}}\right]^{1/3} \qquad \text{(II.150)}$$

with

$$P'_{max}(H,T) = \omega_a \ \exp\left\{-\frac{1}{2}\left[\frac{e^4H^2\ \pi^{\frac{d-1}{2d}}}{KK_bT\hbar^2c^2}\right]^{\frac{1}{3}}-\left[\left(\frac{\pi^{\frac{d-1}{2d}}}{KK_bT}\right)^2\ \frac{e^5H}{\hbar c}\right]^{\frac{1}{3}}\right\} \quad \text{(II.151)}$$

where d is the system dimensionality and K is the dielectric constant for the medium. Combining this with equations II.2 and II.7 gives us

$$\sigma'(H,T) = e^2\mathcal{D}_o(R')^2\omega_a \ \exp\left\{-\frac{1}{2}\left[\frac{e^4H^2\ \pi^{\frac{d-1}{2d}}}{KK_bT\hbar^2c^2}\right]^{\frac{1}{3}}-\left[\left(\frac{\pi^{\frac{d-1}{2d}}}{KK_bT}\right)^2\ \frac{e^5H}{\hbar c}\right]^{\frac{1}{3}}\right\} \quad \text{(II.152)}$$

As in the noninteracting case the temperature sensitivity is increased and the magnetoconductivity is negative. It should be pointed out that the expressions II.146 and II.152 should not be taken too seriously. They illustrate the point that the magnetic field could shrink the localized wavefunction as one might intuitively expect, and thereby decrease the hopping probability which would lower the conductivity of the system.

F. Effects of Magnetic Fields

4. Magnetic Fields and Hopping

ii) Zeeman Effect

The effect of spin splitting on a hopping system is the same regardless of the details of the hopping description. The magnetic field inserts a spin dependence into the hopping probability through the magnetic field dependence the hopping energy has now acquired

$$\pm\mu_B gH/[K_b T] \qquad \text{(II.153)}$$

where μ_B is the Bohr magneton. This modifies the probabilty per unit time of a hop of distance r (equations II.40 or II.88) to

$$P_{hop\pm}(r) = \omega_a \exp\{ -2\alpha r - (\varepsilon \pm \mu_B gH/[K_b T]\} \qquad \text{(II.154)}$$

where ± denotes spin parallel or antiparallel to H and ε is given by equation II.39 or II.87. This can be rewritten as

$$P_{hop\pm}(r,H) = P_{hop}(r)\exp\{-(\pm\mu_B gH/[K_bT])\}$$
$$P_{hop\pm}(r,H) = P_{hop}(r)P_{\pm} \qquad \text{(II.155)}$$

In zero magnetic field an electron's hopping probability is determined by the opposing conditions of the exponential decrease of its wavefunction versus the ability to lower the energy mismatch between initial and final states by hopping farther. The magnetic field has split the electron population into two unequal subpopulations, so there is now the additional factors of being able to store (or receive) energy in the spin-field interaction by changing spin orientation, plus the fact that some states which would be unoccupied in zero field are now occupied and so no longer available to hop into (and vice versa). The average total probability per unit time of a hop of distance r is then

$$P_{hop\ Zee}(r,H) = (1/2)\{[P_{hop+} + P_{hop-}]/[P_+ + P_- + 1]\} \qquad \text{(II.156)}$$

where the normalization factor $[P_+ + P_- + 1]^{-1}$ reflects the skewing of the occupancy of the states in the system by the magnetic field. Combining equations II.155 and II.156 gives

$$P_{hop\ Zee}(r,H) = \{P_{hop}(r)\cosh(h)\}/\{2\cosh(h)-1\} \qquad (II.157)$$

where $h=\mu_B gH/[K_b T]$ and $P_{hop}(r)$ is given by equation II.40 for the noninteracting case and II.88 when Coulomb interactions are important. The maximum of the hopping probability is calculated the same way as for the zero field case, resulting in

$$P_{max\ Zee}(T,H) = \{P_{max}(T)\cosh(h)\}/\{2\cosh(h)-1\} \qquad (II.158)$$

Since this is a pure spin effect, there is no noticeable change in R and R' (equations II.41 and II.90) from the zero field case. Combining equation II.158 with II.7 and II.43 gives the conductivity to be

$$\sigma_{Zee}(T,H) = \{\sigma(T)\cosh(h)\}/\{2\cosh(h)-1\} \qquad (II.159)$$

where $\sigma(T)$ is given by either equation II.44 or II.92 depending on the importance of the Coulomb interactions. This result was calculated in 1974 by A.H. Clark, M.M. Cohen, M. Campi and H.P.D. Lanyon. As one can see from equation II.159 the conductivity is independent of magnetic field at high field and/or low temperatures after having dropped to half its zero field value. At low fields and/or high temperature the conductivity falls with the square of the magnetic field. Since this is a spin effect, one would expect it to be isotropic.

G. Thermoelectric Effects

In 1829, Thomas Seebeck observed that if two wires (A and B) composed of different conductors are joined together to form a closed loop, and if the junctions are maintained at different temperatures, a current will flow around the loop. This current is the electronic response to the temperature gradient in the loop. If the loop is open as in figure 2-13, the electrons will move until the resulting charge imbalance creates an opposing electric field which just cancels the net effect of the temperature gradient. This electric field is proportional to the temperature gradient,

$$\vec{E} = S\ \vec{\nabla} T \tag{II.160}$$

where S is the Seebeck coefficient, or thermopower. In the open loop configuration of figure 2-13, this electric field will manifest itself as a voltage difference, where for $\Delta T << T$,

$$\Delta V_{AB} = (S_B - S_A)\ \Delta T \tag{II.161}$$

In 1834, Jean Peltier noticed that if he forced a

Figure 2-13

If A and B are different conducting materials placed together to form a loop as shown, the thermoelectric potential difference generated, ΔV_{AB} will be directly proportional to ΔT if $\Delta T \ll T$.

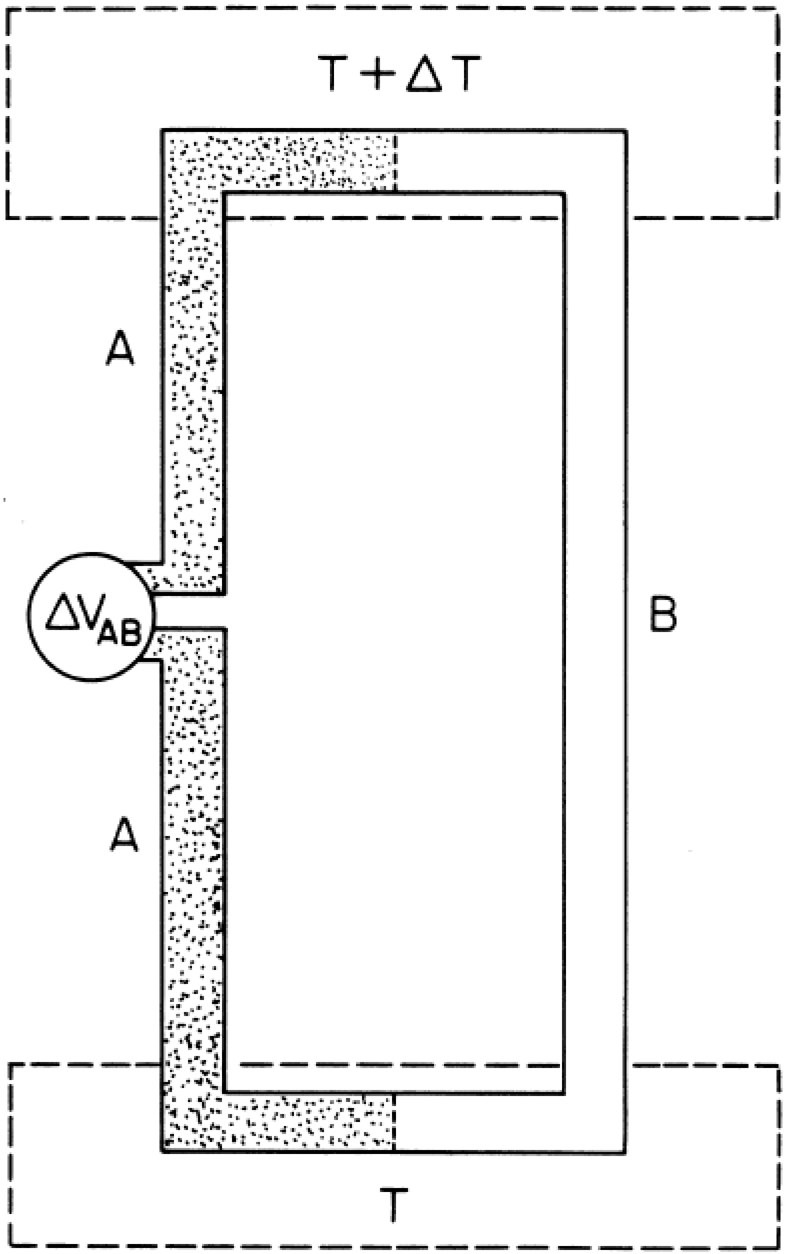
T + ΔT
A
ΔV_{AB}
B
A
T

$$\Delta V_{AB} = (S_B - S_A)\,\Delta T$$

Figure 2-14

Peltier Effect - If an electric current density ,$\vec{J}$, passes through the junction between two different conductors A and B, heat will be absorbed or generated depending on the direction of $\vec{J}$ at a rate proportional to $\vec{J}$ and also the temperature of the junction.

Thomson Effect - If a current density ,$\vec{J}$, flows in a conductor under a temperature gradient, $\vec{\nabla}T$, then heat will be absorbed or generated throughout the conductor depending on the relative directions of $\vec{J}$ and $\vec{\nabla}T$ in addition to the normal resistive heating present. The rate of production of this reversible heat is proportional to $\vec{J}\cdot\vec{\nabla}T$ and also the temperature of the conductor.

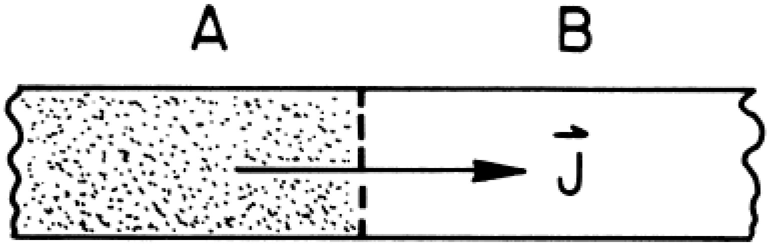

$$\dot{Q} = (\pi_B - \pi_A)\ J$$

PELTIER EFFECT

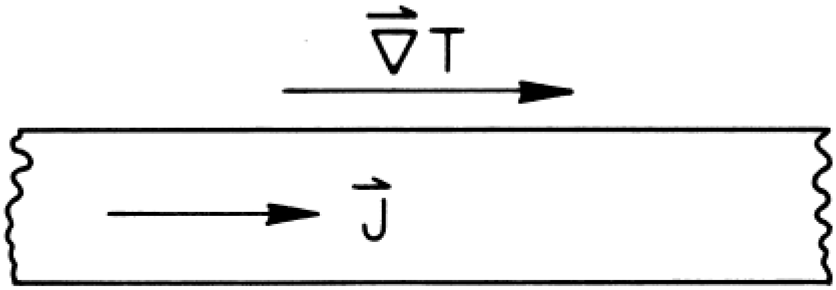
$\vec{\nabla} T$
$\vec{J}$

$$\dot{Q} = \rho\ J^2 - \mu_T \vec{J} \cdot \vec{\nabla}\ T$$

THOMSON EFFECT

current through a junction of two different conductors (see figure 2-14a) that in addition to the Joule (resistive) heating which occurred at the junction there was a certain amount of heat reversibly generated (or absorbed) at the junction, which was proportional to the amount and direction of the current:

$$Q^{\cdot} = \Pi_{AB} J \qquad \text{(II.162)}$$

where $Q^{\cdot}$ is the heat reversibly generated per unit time and cross sectional area when a current density J passes from conductor A to B, and $\Pi_{AB} = \Pi_B - \Pi_A$ with Π_i the Peltier coefficient of material i.

While the Seebeck and Peltier effects can only be observed directly when two different conductors are in contact with each other, they should not be considered contact phenomenon. The reversible heat processes involved in these phenomenon depends not on the nature of the contact between conductors but on properties intrinsic to the conductors.

In 1882, William Thomson (a.k.a. Lord Kelvin) showed that the reversible thermoelectric effects function independently of the irreversible effects arising simultaneously within the conductor (see figure 2-14b). The Thomson effect is the reversible generation (or absorption) of heat in a homogeneous conductor which carries an electric current and a heat current (i.e., has a temperature gradient imposed upon it).

$$\dot{Q} = \rho J^2 - \mu_T \vec{J} \bullet \vec{\nabla} T \qquad \text{(II.163)}$$

where ρ is the resistivity of the conductor ($\rho=1/\sigma$) and μ_T is the conductor's Thomson coefficient.

The Seebeck, Peltier and Thomson coefficients are related through the 'Kelvin Relations':

$$\mu_T = T(\partial S/\partial T) \qquad \text{(II.164)}$$

$$\Pi = TS \qquad \text{(II.165)}$$

so that the absolute Seebeck and Peltier coefficients can be calculated from the Thomson coefficient.

From equations II.163 and II.165 one can see that the Seebeck coefficient can be thought of as an indicator of the entropy per charge carrier and as a consequence of the third law of thermodynamics,

$$\lim_{T \to 0} \sigma S = 0 \qquad \text{(II.166)}$$

for any system.

G. Thermoelectric Effects

1. Boltzman Transport

The electrons in any system obey Fermi-Dirac statistics, i.e. the probability of a state of energy N being occupied is

$$f(\varepsilon) = f(\varepsilon_k) = [\exp\{ (\varepsilon-\mu)/[K_bT] \}+1]^{-1} \quad (II.167)$$

where μ is the chemical potential ($\mu \sim E_f$ = Fermi energy) and the total density of electrons in the system is

$$n = \int_0^\infty f(\varepsilon) D(\varepsilon) \partial\varepsilon \quad (II.168)$$

Now the way external fields and temperature gradients make electrons do things is to alter μ as a function of position r, so in general

$$f(\varepsilon_k) = f(\vec{k}) = f(\vec{k},\vec{r}) \quad (II.169)$$

If $f(\vec{k})$ is perturbed from its equilibrium value $f_\circ(\vec{k})$, we may write

$$f(\vec{k}) = f_{\circ}(\vec{k}) + g(\vec{k}) \qquad \text{(II.170)}$$

where we assume $g(\vec{k})$ follows the relaxation time approximation, i.e. if the perturbation is removed from the system $g(\vec{k})$, will decay as

$$g(\vec{k},t) = g(\vec{k},0)\exp\{ -t/\tau \} \qquad \text{(II.171)}$$

External fields and temperature gradients drive the electron transport processes by altering $f(\vec{k})$ spatially throughout the system, in other words, the external fields influence the probability of a given $\vec{k}$ state being occupied, with this probability now being a function of position within the system.

External fields will change the wavevector of the electron

$$(1/\hbar)m(\partial\vec{v}_{k}/\partial t) = (1/\hbar)(\partial\vec{p}_{k}/\partial t) = \partial\vec{k}/\partial t = (e/ \hbar)[E + (1/c)\ \vec{v}_{k}x\vec{H}] \qquad \text{(II.172)}$$

so

$$f(\vec{k},\vec{r},t) = f(\vec{k}-\vec{k}^{\cdot}t,\vec{r},0) \qquad \text{(II.173)}$$

and the rate of change to $f(\vec{k},\vec{r},t)$ from the fields is

$$\partial f(\vec{k},\vec{r},t)_{fields}/\partial t = -(\partial \vec{k}/\partial t)(\partial f/\partial \vec{k}) \qquad \text{(II.174)}$$

$$\partial f(\vec{k},\vec{r},t)_{fields}/\partial t = -(e/\hbar)[\ \vec{E} + (1/c)\vec{v}_k x \vec{H}\ ](\partial f/\partial \vec{k}) \qquad \text{(II.175)}$$

The electrons will also just diffuse all over the place within the sample, so

$$f(\vec{k},\vec{r},t) = f(\vec{k},\vec{r}-\vec{v}_k t,0) \qquad \text{(II.176)}$$

and the rate of change of $f(\vec{k},\vec{r},t)$ from diffusion is just

$$\partial f(\vec{k},\vec{r},t)_{diff}/\partial t = -\vec{v}_k{}^{*}(\ \partial f/\partial \vec{r}) \qquad \text{(II.177)}$$

There is one other process which will affect $f(\vec{k},\vec{r},t)$ to consider, which is the scattering of the electrons. The probability to scatter from a state $\vec{k}'$ to a state $\vec{k}$ is

$$f(\vec{k}')[1 - f(\vec{k})] \qquad \text{(II.178)}$$

and the probability to scatter from a state $\vec{k}$ to a state $\vec{k}'$ is

$$f(\vec{k})[1 - f(\vec{k}')] \qquad \text{(II.179)}$$

If $Q(\vec{k},\vec{k}')$ is the transition rate from state $\vec{k}$ to $\vec{k}'$ if $\vec{k}$ were known to be occupied and $\vec{k}'$ known to be empty, and we assume elastic scattering only (not usually a good assumption) then $Q(\vec{k},\vec{k}')=Q(\vec{k}',\vec{k})$ and

$$\partial f(\vec{k},\vec{r},t)_{scat}/\partial t = \{f(\vec{k}')[1-f(\vec{k})] - f(\vec{k})[1-f(\vec{k}')]\}Q(\vec{k},\vec{k}')\partial\vec{k}'$$

$$\partial f(\vec{k},\vec{r},t)_{scat}/\partial t = -g(\vec{k})/\tau \qquad \text{(II.180)}$$

When all these influences, electric and magnetic fields, temperature gradients and scattering, are present the system is not in equilibrium. It is however, in a steady state

$$[\partial f(\vec{k},\vec{r},t)_{scat}/\partial t] + [\partial f(\vec{k},\vec{r},t)_{fields}/\partial t] + [\partial f(\vec{k},\vec{r},t)_{diff}/\partial t] = 0 \qquad \text{(II.181)}$$

Combining equations II.174,II.177,II.180 into equation II.181 and using

$$\vec{v}_k = (1/\hbar)(\partial\varepsilon/\partial\vec{k}) \qquad \text{(II.182)}$$

while keeping only each field term to first order gives us the linearized Boltzman equation:

$$-(\partial f_{\circ}/\partial\varepsilon)\ \vec{v}_k \bullet \{ -[(\varepsilon_k-\mu)/T]\vec{\nabla}T + e\vec{E} - \vec{\nabla}\mu \} =$$
$$g(\vec{k})/\tau + \vec{v}_k \bullet (\partial g(\vec{k})/\partial r) + (e/[\hbar c])(\vec{v}_k \times \vec{H}).(\partial g(\vec{k})/\partial\vec{k}) \qquad (II.183)$$

which simply describes the out of balance of $f(\vec{k})$.

If we consider the case of a spatially independent electric field $\vec{E}$ and temperature gradient $\vec{\nabla}T$, with $\vec{H}$ and $\partial g(\vec{k})/\partial r$ both zero, then the Boltzman equation becomes

$$g(\vec{k})/\tau = -(\partial f_{\circ}/\partial\varepsilon)\vec{v}_k \bullet \{ -[(\varepsilon_k-\mu)/T]\ \vec{\nabla}T + e\vec{E} \} \qquad (II.184)$$

where we have absorbed the $\vec{\nabla}\mu$ term into the electric field , thus making $\vec{E}$ in equation II.184 the measurable electric field (instruments which purport to measure electric potentials , 'voltmeters', really can measure only the electrochemical potential, i.e. they measure only $\vec{E}-[\vec{\nabla}\mu/e]$). The electrical current density in the system is

$$\vec{J} = 2\int e\vec{v}_k g(\vec{k})\partial\vec{k}$$
$$\vec{J} = e^2\hat{\hat{K}}_0\cdot\vec{E} + (e/T)\hat{\hat{K}}_1\cdot(-\vec{\nabla}T) \qquad (II.185)$$

and the heat current density is

$$\vec{U} = 2\int \vec{v}_k g(\vec{k})[\varepsilon_k-\mu]\,\partial\vec{k}$$

$$\vec{U} = e\hat{\hat{K}}_1\cdot\vec{E} + (1/T)\hat{\hat{K}}_2\cdot(-\vec{\nabla}T) \quad .186)$$

where

$$\hat{\hat{K}}_n = 2\int \tau\vec{v}_k\vec{v}_k(-\partial f_o/\partial\varepsilon)(\varepsilon_k-\mu)^n\,\partial\vec{k} \qquad \text{(II.187)}$$

are the Boltzman transport coefficients.

One can see for example, that if $\vec{\nabla}T = 0$ the electrical conductivity (equation I.1) is just

$$\sigma = e^2K_0 \qquad \text{(II.188)}$$

and if J=0, the thermal conductivity (equation I.6) is just

$$k = (1/T)[K_2 - (K_1^2/K_0)], \qquad \text{(II.189)}$$

the thermopower (Seebeck coefficient, equation II.160) is

$$S = K_1/(eTK_0) \qquad \text{(II.190)}$$

and the Peltier coefficient is

$$\Pi = K_1/(eK_0) \qquad \text{(II.191)}$$

2. Thermopower of Metals

The integrals over k space in the Boltzman transport coefficients (equation II.187) are usually transformed into integrals over constant energy surfaces in k space:

$$\int \partial\vec{k} \;\text{-->}\; [1/(2\pi)^{d}] \int (1/|\partial\varepsilon_{k}/\partial\vec{k}|)\partial S\partial\varepsilon_{k} \qquad \text{(II.192)}$$

where S is the area of the constant energy surface in k-space. We will want to exploit a peculiar property of the Fermi-Dirac distribution function , f(k) (equation II.167), namely

$$\int_{0}^{\infty}\theta(\varepsilon)(-\partial f_{o}/\partial\varepsilon)\partial\varepsilon = \theta(\mu) + (1/6)\pi^{2}(K_{b}T)^{2}[\partial^{2}\theta/\partial\varepsilon^{2}]_{\varepsilon=\mu} + \cdots \qquad \text{(II.193)}$$

for any continuous function $\Theta(\varepsilon)$. In three dimensions this gives

$$\hat{\hat{K}}_{0} = [1/(4\pi^{3})](\tau/\hbar)\int \vec{v}\vec{v}\partial S_{f}/v \qquad \text{(II.194)}$$

$$\hat{\hat{K}}_{2} = (\pi^{2}/3)(K_{b}T)^{2}\hat{\hat{K}}_{0}(\mu) \qquad \text{(II.195)}$$

$$\hat{\hat{K}}_{1} = (\pi^{2}/3)(K_{b}T)^{2}[\partial\hat{\hat{K}}_{0}(\varepsilon)/\partial\varepsilon]_{\varepsilon=\mu} \qquad \text{(II.196)}$$

(the area integral is taken at the Fermi energy, hence ∂S_f) which implies the thermopower for a metal (equation II.190) is

$$S = (\pi^2/3)(eK_b)(K_bT)[\partial \ln K_0(\varepsilon)/\partial\varepsilon]_{\varepsilon=\mu} \qquad \text{(II.197)}$$

which illustrates an important point about the thermopower of metals:

$$S \dashrightarrow 0 \text{ as } T \dashrightarrow 0 \qquad \text{(II.198)}$$

for all metals and since it depends on the logarithmic derivative of the conductivity ($\sigma \propto K_0$) it will, in general display very different behavior than the conductivity. One can demonstrate II.198 on a very much more general basis than equation II.197. In Chapter I we pointed out that all metals conduct ($\sigma \neq 0$) at absolute zero ($T = 0^\circ$ Kelvin). On the basis of the equation II.166 which , as pointed out earlier is a direct consequence of the third law of thermodynamics, one would have to conclude that all metals obey equation II.198.

G Thermoelectric Effects

3. Thermopower of Semiconductors

When the atoms of a material are brought together in the formation of that material, the resulting density of states for the electrons in the material has energy ranges ('gaps') for which there are no allowed electron states. The difference between a metal and a semiconductor, where in this context most insulators such as quartz (SiO_2) or plastic are semiconductors with very large 'gaps', is determined by whether the Fermi energy lies inside a band of allowed states or inside a 'gap' region. If the Fermi energy lies outside of a 'gap' in a band of allowed states, then the density of states at the Fermi energy is nonzero and the material is a metal. If it lies in a gap, then for electronic transport to take place, electrons must be excited from states below the gap to states above the gap. When K_bT is much less than the energy width of the gap this cannot happen, implying that at T=0 the 'semiconductor' will not conduct at all, i.e. it is fundamentally an insulator. The difference between a common semiconductor such as Ge and an insulator such as quartz (SiO_2) is merely the size of the energy gap.

In conventional semiconductors and insulators such as Ge, Si and SiO_2, these gaps are of nonzero width, as opposed to the 'soft' gaps of zero width one may get in other systems (see section II.E for an example of a system with a 'soft' gap).

The gap in the electronic density of states means that for a semiconductor, one cannot use the integral expansion given by equation II.193 in calculating the Boltzman transport coefficients (equation II.187) since, in three dimensions for example,

$$\mathcal{D}(\varepsilon) = 2/(2\pi)^3 \int 1/|\partial\varepsilon/\partial\vec{k}| \; \partial S = 0 \text{ when } \varepsilon_v < \varepsilon < \varepsilon_c \qquad \text{(II.199)}$$

where $\varepsilon_v < \mu < \varepsilon_c$ with ε_v is the lower boundary to the energy gap and ε_c is the upper boundary. If we assume the electronic density of states is nonzero everywhere but in the gap (i.e. the bands of allowed states have infinite width), then from equation II.187:

$$\begin{aligned} \hat{\hat{K}}_0 &= \hat{\hat{K}}_{0e} \exp\{-(\varepsilon_c-\mu)/[K_bT]\} + \hat{\hat{K}}_{0h} \exp\{-(\mu-\varepsilon_v)/[K_bT]\} \\ \hat{\hat{K}}_0 &\equiv \hat{\hat{K}}_{0e}(T) + \hat{\hat{K}}_{0h}(T) \end{aligned} \qquad \text{(II.200)}$$

where $\hat{\hat{K}}_{0e}$ is the contribution to $\hat{\hat{K}}_0$ from electrons in the 'conduction' band (i.e., electrons with $\varepsilon \geq \varepsilon_c$) and $\hat{\hat{K}}_{0h}$ the contribution from 'holes' in the 'valance' band (i.e., empty states with $\varepsilon \leq \varepsilon_v$). For $\hat{\hat{K}}_1$ we get (from equation II.187)

$$\hat{\hat{K}}_1 = -(\varepsilon_c - \mu)\,\hat{\hat{K}}_{0e}(T) + (\mu - \varepsilon_v)\,\hat{\hat{K}}_{0h}(T) \qquad \text{(II.201)}$$

which combining these with equation II.190 gives us the thermopower (or Seebeck coefficient):

$$S(T) = \frac{-(\varepsilon_c - \mu)K_{0e}(T) + (\mu - \varepsilon_v)K_{0h}(T)}{eT\,[\,K_{0e}(T) + K_{0h}(T)\,]} \qquad \text{(II.202)}$$

If for example, the holes did not contribute to the conductivity, then from equation II.188 we could infer that $\hat{\hat{K}}_{0h}=0$, and the thermopower of the electron dominated semiconductor would be

$$S(T) = S_e(T) = -(\varepsilon_c - \mu)/(eT) \qquad \text{(II.203)}$$

conversely, if the semiconductor were hole dominated (so $\hat{\hat{K}}_{0e}=0$) then

$$S(T) = S_h(T) = -(\mu - \varepsilon_v)/(eT) \qquad \text{(II.204)}$$

Setting $\sigma_h = e^2\hat{\hat{K}}_{0h}$ and $\sigma_e = e^2\hat{\hat{K}}_{0e}$ we can rewrite equation II.202 as

$$S(T) = [\ \sigma_e S_e(T) + \sigma_h S_h(T)\ ]/(\ \sigma_e + \sigma_h\ ) \qquad \text{(II.205)}$$

where $\sigma=\sigma_e+\sigma V_h$ is the total conductivity of the system. This illustrates an important point about the thermopower of all semiconductors (i.e., systems whose Fermi energy sits in a nonzero width gap in the density of states)
which is

$$S \dashrightarrow \infty \text{ as } T \dashrightarrow 0 \qquad \text{(II.206)}$$

for all semiconductors which do not display perfect electron hole symmetry, which real semiconductors do not.

G. Thermoelectric Effects

4. Thermopower Definition of Metals and Insulators

As pointed out in Chapter I, the ability of a metal to conduct electricity at absolute zero requires a nonzero density of states at the Fermi energy of some finite width. The density of states behavior is generally reflected in the thermoelectric properties as illustrated in figure 2-15. In a system with a nonzero density of states at $\mu \sim E_f$, the electron can have an energy arbitrarily close to μ and so carry around an arbitrarily small amount of heat $\sim(\varepsilon-\mu)$. The heat current will be

$$\vec{Q}^{\cdot} = C_{el} T \vec{v} \tag{II.207}$$

where C_{el} is the electronic specific heat of the electrons (equation II.99) and $\vec{v}$ the electronic velocity. The electrical current is given by equation I.2,

$$\vec{J} = ne\vec{v}$$

so from equations II.99 and II.162, the Peltier coefficient for a metal generally will go something like

$$\Pi = (K_bT)^2/[e\mu] \qquad (II.208)$$

and from equation II.165 the thermopower will go as

$$S = (K_b/e)(K_bT)/\mu \qquad (II.209)$$

which has S-->0 as T-->0 consistent with equation II.166. This illustrates that any system with a nonzero density of states at the Fermi energy (i.e., metallic system), will have its thermopower go to zero as the temperature goes to zero, since the carrier distribution can collapse to zero width about the Fermi energy.

In a system whose Fermi energy lies in a gap region, the minimum energy an electron can have is ε_c so the minimum amount of heat it can carry is $\sim(\varepsilon_c-\mu)$, so the heat current would go as (for an electron dominated system)

$$\vec{Q}^{\cdot} = (\varepsilon_c-\mu)nv \sim (E_g/2)n\vec{v} \qquad (II.210)$$

where $E_g = (\varepsilon_c-\varepsilon_v)$ is the energy gap width and n the electron density. Using this equation and equations I.2 and II.162,

$$\Pi = -E_g/(2e)$$

Figure 2-15

Metals

The carriers can be arbitrarily close to the Fermi level so the entropy per carrier (~ $[\varepsilon-\mu]/[eT]$) will decrease towards zero as the temperature goes to zero since $[\varepsilon-\mu]$ will go to zero faster than T. The thermopower will therefore behave as:

$S \longrightarrow 0$ as $T \longrightarrow 0$ for metals

Insulators (Gapped)

The minimum entropy per carrier any carrier in the system can have is $\sim E_g/(eT)$, which will diverge as the temperature is lowered towards zero (E_g is a constant). The thermopower will therefore behave as:

$S \longrightarrow \infty$ as $T \longrightarrow 0$ for insulators

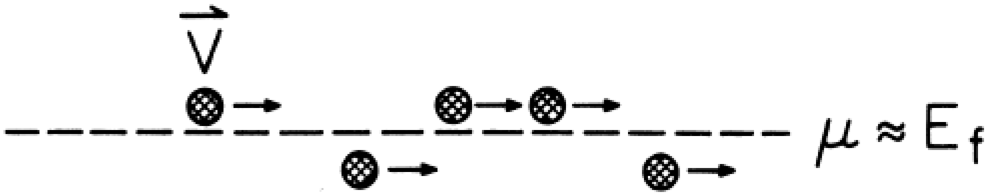
$\vec{V}$
$\mu \approx E_f$

$$\pi \simeq \frac{C_{el} T \vec{V}}{\vec{J}} \simeq \frac{(K_b T)^2}{e\mu}$$

METALS

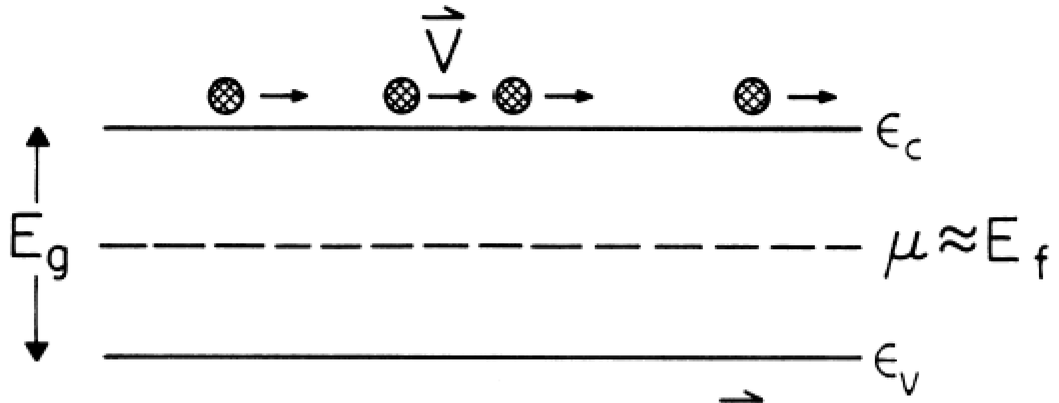
$\vec{V}$
ϵ_c
E_g
$\mu \approx E_f$
ϵ_v

$$\pi \simeq \frac{(E_g - \mu) n \vec{V}}{\vec{J}} \simeq \frac{E_g}{2e}$$

INSULATORS

which results in a thermopower which will go something like

$$S = -E_g/(2eT) \qquad \text{(II.211)}$$

which agrees well with equation II.203 and has S-->∞ as T-->0, although equation II.166 still holds since σ-->0 faster than S-->∞. If there is a gap of nonzero width in the density of states about the Fermi energy (and therefore the system will be an insulator) then the thermopower will diverge as T-->0.

This leads us to the use of the thermopower as a definition of metallic behavior. Since at T=0 all metals conduct (σ≠0) then from the third law of thermodynamics,

$$S \rightarrow 0 \text{ as } T \rightarrow 0 \text{ for all metals} \qquad \text{(II.212)}$$

Since all systems with a zero density of states at the Fermi energy do not conduct (σ=0) at T=0 then from the third law

$$S \rightarrow \text{ ANYTHING as } T \rightarrow 0 \text{ for all insulators} \qquad \text{(II.213)}$$

and if the region about the Fermi energy where the density of states is zero is of nonzero width, then

ANYTHING = ∞, otherwise it will of course be material specific.

G. Thermoelectric Effects

5. Thermopower in the Near Metallic Regime

i) Thermopower and the Scaling Theory

In 1982, C.S. Ting, A. Houghton and J.R. Senna calculated the thermopower of a two dimensional system of noninteracting weakly localized electrons and found there was no localization correction to the thermoelectric power.

We can see why this is so if we examine the simple model of Larkin and Khmelnitzkii (see section II.B). The correction to the heat current will be proportional to the probability of the diffusive paths selfintersecting, i.e. proportional to the ratio of the volume swept out by the particles to the volume it could have classically diffused through:

$$\frac{\delta \dot{Q}}{\dot{Q}} = \int_{\tau}^{\tau_0} \frac{v \lambda^{d-1} \partial t}{(D t)^{d/2}} \qquad \text{(II.214)}$$

$$\frac{\delta \dot{Q}}{\dot{Q}} = \frac{2v\lambda^{d-1}}{dD} \cdot \begin{cases} \ell_o - L & , d=1 \\ 2\ \ln(\ell_o/L) & , d=2 \\ \frac{1}{L} - \frac{1}{\ell_o} & , d=3 \end{cases} \qquad \text{(II.215)}$$

Expressing the total heat current as

$$\dot{Q} = \dot{Q}_\circ + \delta\dot{Q}$$

and realizing that $\delta\dot{Q}$ is negative since the quantum selfinterference hinders the electronic (and hence electronic heat) transport

$$\dot{Q} = \dot{Q}_\circ[1-\gamma]$$

where

$$\gamma = \frac{2v\lambda^{d-1}}{Dd} \cdot \begin{cases} \ell_o - L & , d=1 \\ 2\ \ln(\ell_o/L) & , d=2 \\ \frac{1}{L} - \frac{1}{\ell_o} & , d=3 \end{cases} \qquad \text{(II.217)}$$

From equations II.28 and II.217 we know

$$\sigma = \sigma_\circ(1-\gamma) \qquad \text{(II.218)}$$

Now the net electrical current when the thermopower (Seebeck Effect) is observed is zero (see figure 2-13), so the current equation in the presence of diffusion (equation II.1) must be

$$\vec{J} = \sigma\vec{E} - eD\vec{\nabla}n = 0 \qquad \text{(II.219)}$$

which means that the diffusive current,

$$J_{diff} = eD\vec{\nabla}n \qquad \text{(II.220)}$$

must just cancel the current driven by the electric field created by the charge imbalance arising from the temperature gradient driven diffusion of the electrons. This means we may write the Peltier coefficient as

$$\Pi = Q^{\cdot}/J_{diff} = \{Q^{\cdot}_{o}[1-\gamma]\}/(eD\vec{\nabla}n) = \{Q^{\cdot}_{o}[1-\gamma]\}/(E\sigma_{o}[1-\gamma])$$

$$\Pi = \Pi_{\circ} \qquad \text{(II.221)}$$

where $\Pi_{\circ}$ is the unperturbed Peltier coefficient. So using equation II.165,

$$S = S_{\circ} \qquad \text{(II.222)}$$

Since the corrections to the heat current and the electrical current from localization are the same, they cancel each other in the Peltier and Seebeck coefficients.

G. Thermoelectric Effects

5. Thermopower and the Near Metallic Regime

ii) Thermopower and the Interaction Theory

The thermopower in two dimensions for an interacting electron system has also been calculated by Ting, Houghton and Senna. The diagrams which give a net contribution to the heat current - electrical current correlation function (eK_1 in equation II.186) are shown in figure 2-16, where as in section II.D, the X denotes an interaction via an impurity, with the wavy line denoting the Coulomb interaction. They found the correction to K_1 to be (in two dimensions)

$$\Delta K_1 = -K_{1o}[e^2/(\sigma_o \pi 2\hbar)]\ln(T/T') \qquad (II.223)$$

where $T' = \hbar/(4K_b\tau)$ and $\sigma_o = N^2\tau/m$ with N as the areal electron concentration. Inclusion of the Hartree diagrams alters this to

$$\Delta K_{1} = -K_{1o}[e^2/(\sigma_o \pi 2\hbar)]\{1-F\}\ln(T/T') \qquad (II.224)$$

where F is given by equation II.66. Using

Figure 2-16

Diagrams which give net contributions to the heat current-electrical current correlation function K_1 for interacting electrons with weak impurity scattering.

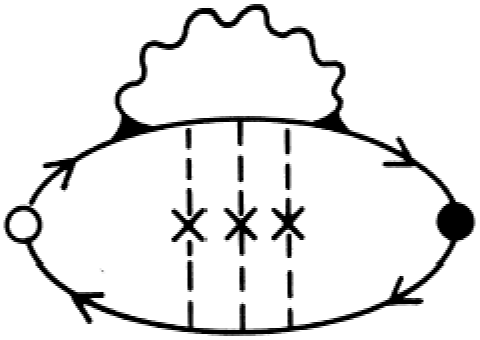

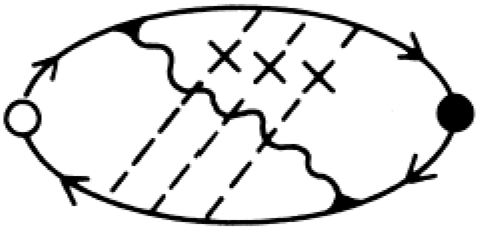

$$\delta \equiv [e^2/(\sigma_o \pi 2\hbar)]\{1-F\}\ln(T/T')$$

we have

$$K_1 = K_{1o}[1-\delta] \qquad (II.225)$$

and from equations II.68 and II.188

$$K_0 = K_{0o}[1-(1/2)\delta] \qquad (II.226)$$

where K_{1o} and K_{0o} are the unperturbed transport coefficients. Plugging these into equation II.190 gives

$$S(T) = S_o(T)\ \{[1-\delta]/[1-(1/2)\delta]\} \qquad (II.227)$$

$$S(T) \sim S_o(T)\ \{[1-\delta]/[1-(1/2)\delta]\} \qquad (II.228)$$

which, keeping only the lowest order correction, gives

$$S(T) \sim S_o(T)\{\ 1 - [e^2/(\sigma_o \pi 2\hbar)]\{1-F\}\ln(T/T')\} \qquad (II.229)$$

G. Thermoelectric Effects

6. Thermopower and Hopping

The treatment of the thermopower for variable range hopping systems is similar regardless of the importance of Coulomb interactions. The behavior of the thermopower does however, depend very much on their importance.

Using equations II.187,II.188 and II.190, we can write the thermopower as

$$S = [(2K_b)/(e\sigma)] \int -\tau v_k v_k (\partial f_o/\partial \varepsilon)[(\varepsilon_k - \mu)/(K_b T)] \partial \vec{k} \quad \text{(II.230)}$$

where

$$\sigma = 2e^2 \int -\tau v_k v_k (\partial f_o/\partial \varepsilon) \partial k \qquad \text{(II.231)}$$

is given by equation II.44 for variable range hopping in a noninteracting system, and by equation II.92 when Coulomb interactions are important.

Utilizing equations II.192 and II.199 with II.230 and II.231 results in

$$S = [(2K_b)/(e\sigma)] \int -\tau v_k v_k (\partial f_o/\partial \varepsilon)[(\varepsilon_k-\mu)/(K_bT)]\mathcal{D}(\varepsilon)\partial\varepsilon \qquad \text{(II.232)}$$

The range of energies which will contribute to the transport will be E_{hop}, where

$$E_{hop} = \begin{cases} \left[\dfrac{\Gamma(d/2+1)}{\mathcal{D}_o(\mu)\pi^{d/2}}\right]^{\frac{1}{d+1}} \left[\dfrac{2\alpha K_bT}{d}\right]^{\frac{d}{d+1}} & \text{(noninteracting)} \\ \sqrt{\dfrac{e^2}{K}}\,\sqrt{2\alpha K_bT} & \text{(interacting)} \end{cases} \qquad \textbf{(II.233)}$$

Integrating equation II.232 and using equation II.7, we have

$$S = [K_b/(2e)]\{(E_{hop})^2/(K_bT)\}[\partial \ln D_o(\varepsilon)/\partial\varepsilon]_{\varepsilon=\mu} \qquad \text{(II.234)}$$

which gives us

$$S(T)_{non} = \frac{K_b}{2e}\left[\frac{\Gamma(d/2+1)}{\mathcal{D}_o(\mu)\pi^{d/2}}\right]^{\frac{2}{d+1}}\left(\frac{2\alpha}{d}\right)^{\frac{2d}{d+1}}\left[\frac{\partial \ln \mathcal{D}_o(\varepsilon)}{\partial\varepsilon}\right]_{\varepsilon=\mu}\left(K_bT\right)^{\frac{d-1}{d+1}} \qquad \textbf{(II.235)}$$

$$S(T)_{int} = \frac{K_b e}{K}\,\alpha \left[\frac{\partial \ln \mathcal{D}_o(\varepsilon)}{\partial\varepsilon}\right]_{\varepsilon=\mu} \qquad T<<T_c \qquad \textbf{(II.236)}$$

where $D_o(\varepsilon)$ is the noninteracting density of states. In the interacting system, if $T>T_c$ where T_c is given by (equation II.85):

$$T_c = \frac{1}{K_b}\left(\frac{e^2}{K}\right)^{\frac{d+1}{d-1}}\frac{d}{2\alpha}\left[\frac{\mathcal{D}_o\pi^{d/2}}{\Gamma(d/2+1)}\right]^{\frac{2}{d-1}} ,$$

variable range hopping should be valid so the thermopower will follow equation II.235, which can be rewritten as

$$S_{non}(T) = (1/d)[T/T_c]^{\{(d-1)/(d+1)\}}S_{int} \qquad \text{(II.237)}$$

which drops towards zero with decreasing temperature, dropping below the temperature independent value given by equation II.236 when

$$T \leq d^{\{(d+1)/(d-1)\}}T_c \qquad \text{(II.238)}$$

reaching a value at $T=T_c$ of

$$S_{non}(T=T_c) = (1/d)S_{int} \qquad \text{(II.239)}$$

and then climbing so that at $T<<T_c$ the thermopower is given by equation II.236.

H. Localization, Interactions and Superconductivity

As was seen in section II.D, one of the effects of disorder in a system is to increase the Coulomb interaction between the electrons. In both the scaling and the interaction pictures, this can have a drastic effect on the superconducting properties of a two dimensional system.

In 1981, S. Maekawa and H. Fukuyama examined the problem of superconductivity in the near metallic regime in a two dimensional interaction picture. They found that the disorder enhanced Coulomb interaction between the electrons had a profound effect on the Cooper pairs in superconductivity. The vertex correction (equation II.53 and figure 2-7) itself alters the Cooper pair diagrams to resemble those in figure 2-16, only with the hole propagator replaced with an electron. As one might expect, this has the effect of reducing the total attractive interaction between the electrons forming the Cooper pair (i.e. the enhancement of the total Coulomb interaction offsets more of the phonon mediated attractive interaction). Maekawa and Fukuyama found that a mean field calculation predicts that the transition temperature (T_c) should decrease with increasing resistivity even if the BCS coupling constant is fixed (i.e. larger amounts of disorder enhance the Coulomb interaction greater amounts thereby suppressing the T_c more).

Maekawa and Fukuyama also found that the logarithmic depression in the electronic density of states (equation II.60) will also contribute to a depression in the T_c. The total correction to the critical temperature is predicted to be :

$$\ln\left[\frac{T_c}{T_{co}}\right] = -\frac{1}{2}\,\frac{g\mathcal{D}_o(\epsilon_F)R_{\#}}{\pi R_{2D}}\left\{\ln\left[5.5\,\frac{\xi_o}{L}\,\frac{T_{co}}{T_c}\right]\right\}^2 \cdot \left(1 + \frac{2}{3}\ln\left[5.5\,\frac{\xi_o}{L}\,\frac{T_{co}}{T_c}\right]\right) \qquad \text{(II.240)}$$

where T_{c0} is the transition temperature in the non-disordered system, ξ_0 is the bulk coherence length and L is the mean free path. The first term in II.240 is due to the depression of the density of states about the Fermi energy, the second is due to the vertex correction.

In 1983, P.W. Anderson, K.A. Muttalib and T.V. Ramakrishnan examined the problem of localization (a la scaling theory) and superconductivity in resistivity ranges about R_{2D}. They found that the main effect came about due to the disorder enhanced Coulomb interaction - the main effect of the localization was to increase the Coulomb pseudopotential, μ^*. They found that for resistivities ($R_\#$) where $R_\# < R_{2D}$, μ^* retains its classical value of

$$\mu_0^* = \mu / [\ 1 + \mu \ln(\varepsilon_F / \omega_D \hbar)\ ] \qquad \text{(II.241)}$$

where ω_D is the Debye frequency and ε_F is the Fermi energy. For $R_\# \geq R_{2D}$,

$$\mu^* = \mu' / [1 + \mu' \ln(\varepsilon_F / \omega_D \hbar) - (\mu' - \mu) \ln(\alpha^{1/2} \varepsilon_F / \omega_D \hbar)] \qquad \text{(II.242)}$$

where

$$\alpha = [R_\# / R_{2D}]^3$$

and

$$\mu' = \mu[1 + \{9\pi / (4|k_{F1}|^2)\} \ln\alpha\ .$$

The transition temperature can then be calculated using a formula derived by McMillan (1981):

$$T_c = [\omega_D / 1.45]\ \exp\ \{\ -\ [1.04(1+\lambda)] / [\lambda - \mu^*(1+0.62\lambda)]\} \qquad \text{(II.243)}$$

where λ is the electron-phonon coupling constant.

Anderson, et.al. assume that λ and μ do not change with disorder. To compare equation II.243 with experiments, one needs to be able to measure B and ω_D seperately.

CHAPTER III -- EXPERIMENTAL BACKGROUND

Since the renewed interest in the problem of electron localization in recent years there has been considerable experimental work reported in the literature. While experiments have been reported on systems of all three dimensions, due to the surprising and novel prediction of universal nonmetallic behavior for two dimensional systems the bulk of the experimental background presented in this chapter and all of the experiments in the chapters which follow will be concerned with two dimensional systems. The purpose of the **brief** survey of experimental results in this chapter is to illustrate the atmosphere under which the experiments in this thesis were started in late 1980. This survey will be divided between different electron systems and usually will be restricted to the studies published prior to the start of the series of experiments presented in this thesis.

A. Metal Based Systems

Soon after Thouless advanced his ideas on localization, investigations on systems constructed from 'metallic' elements were undertaken. 'Metallic' elemental systems had the advantage of being easy to measure and due to the technologies borrowed from both the semiconductor industry and inherited from years of superconductor research, were relatively easy to fabricate. Constructing systems out of 'metallic' elements also gave the experimentor the ability to simply construct a very large variety of systems with different secondary properties (e.g. magnetism, superconductivity, weak or strong spin-orbit interactions, etc.) to test the universality of the various properties observed in these systems.

Systems composed of metallic particles in an insulating matrix have been studied for a large number of years. These systems are three dimensional and their electronic transport is usually by hopping or tunneling from grain to grain. We generally will not be concerned with these systems in the survey which follows. B. Abeles wrote an excellent review article in 1976, 'Granular Metal Films' on this subject.

A. Metal Based Systems

1. One Dimensional Wires

In 1979, Giordano, Gilson and Prober fabricated ultra small wires with cross sections on the order of $10^{-11}cm^{2}$ composed of polycrystalline Pd-Au (60 percent Au, 40 percent Pd by weight). At low temperature they found the resistance to increase with decreasing temperature, with thinner wires displaying a stronger temperature dependence. The functional form for the temperature dependence of the resistivity was not in agreement with the theories, although it is possible the samples were not strictly one dimensional.

Chaudhari and Habermeier in 1980 measured amorphous W-Re wires as a function of temperature and magnetic field. For samples greater than 10 Kohms, the samples behavior was consistent with one dimensional localization.

A. Metal Based Systems

2. Two Dimensional Ultra Thin Films

In 1978 Dynes, Garno and Rowell reported resistivity measurements on ultra thin copper (Cu) and gold (Au) films. They observed very nonmetallic behavior in the temperature dependence of those films whose resistivities were above <30000 ohms/square (remember the Ioffe-Regel rule). These high resistivity films displayed an activated behavior but with a fractional temperature dependence, similar to that predicted by the various hopping theories. At the sensitivities of these measurements, the films whose resistivities were below 30000 ohms/square appeared to remain metallic.

In 1979, Dolan and Osheroff showed that two dimensional Pd-Au films whose resistivities were below 30000 ohms/square were also nonmetallic, displaying a logarithmic temperature and electric field dependence in agreement with both the scaling theory and the interaction theory (i.e. $p=1$ in equation II.36).

Van den Dries, Van Haesendonck, Bruynseraeda and Deutscher in 1981 found that two dimensional copper films in the near metallic regime (resistivities below 30000 ohms/square) displayed a logarithmic temperature dependence which was consistent only with the scaling theory (p=2 in equation II.36) and the films also displayed a negative magnetoresistance.

In 1981 McGinnis, Burns, Simon, Deutscher and Chaikin found that Pd and Pd-Au films displaying weak localization characteristics (p=1) displayed a positive magnetoresistance which becomes isotropic above <1000 ohms/square due to the strong spin-orbit coupling present in these films.

In 1982 Gerd Bergman published experiments on two dimensional magnesium (Mg) films demonstrating the interplay between pure localization and the spin-orbit interaction by altering the spin-orbit coupling in the films through the successive introduction of trace amounts of high Z atoms (e.g. Au) into a given film. By increasing the spin-orbit coupling in the films, Bergman found that the negative magnetoresistance given by pure localization could be lessened and even reversed into a positive magnetoresistance by increasing the spin-orbit coupling in the film.

A. Metal Based Systems

3. Three Dimensional Granular Metal Films

Dynes and Garno in 1981 studied granular aluminum (Al) films which were thick (3-d) and relatively low in resistance by resistivity and tunneling measurements. They observed the metal-insulator transition (in contrast to 1-d and 2-d systems which seem to always display resistivities consistent with insulating behavior) to be preceded by a zero bias anomaly indicating a square root energy dependence to the density of states about the Fermi energy in agreement with the predictions of Altshuler and Aronov.

McMillan and Mochel in 1981 conducted tunneling studies on amorphous $Ge_{1-x}Au_x$ which also showed a square root energy depression in the density of states about the Fermi energy in agreement with Altshuler and Aronov.

B. Inversion and Accumulation Layers

1. MOSFETS

It has been known for quite a while that inversion layers in Metal Oxide Semiconductor Field Effect Transistors (MOSFET) can be considered two dimensional. Handler and Eisenhouer, also Murphy and, Fang and Triebwasser examined inversion layers as early as 1964 looking for electron energy quantization in the direction perpendicular to the inversion layer as postulated by Schrieffer in 1957.

Thus inversion layers were a natural system to look for the unusual predictions of the scaling and interaction theories for two dimensional systems. With this in mind, D.J. Bishop, D.C. Tsui and R.C. Dynes in 1980 performed measurements on Si MOSFET devices as a function of temperature down to 50 milliKelvin and observed a logarithmically increasing resistivity with decreasing temperature, with the effect scaling only with the resistivity of the inversion layer as one would expect from equations II.36 or II.68. Their findings for the resistivity gave a value for p in equation II.36 of p=1 for scaling or F in equation II.68 of F=0 for the interaction picture. They also measured the electric field dependence of the resistivity and found it to vary logarithmically as predicted by equation II.101 yielding p'=2.7. Later studies of this system by Bishop, Tsui and Dynes on the Hall effect were inconsistent with predictions of the scaling theory.

In 1980 M.J. Uren, R.A. Davies and M. Pepper also examined the low temperature behavior of MOSFET inversion layers and found the temperature dependence to be similar to that observed by Bishop, Tsui and Dynes, but found the electric field exponent to be p'=1. In addition they measured the Hall effect as a function of electric and magnetic fields finding the fractional change in the Hall coefficient varied at twice the rate of the conductivity as predicted by Altshuler, Khmelnitzkii, Larkin and Lee in 1980 for the interaction picture. At very low magnetic fields however, they observed a negative magnetoresistance indicating that localization was also present and is destroyed when the magnetic field reaches a certain value leaving the electron-electron interactions dominating the transport. They could also induce a transition from localization dominated transport to interaction dominated transport by altering the electronic temperature (at constant lattice temperature) with an electric field (see section II.F.1).

In 1982, A.B. Fowler, A. Hartstein and R.A. Webb studied accumulation layers in MOSFETS which were constructed to allow them to control the accumulation layer channel width in two directions, thus allowing them to change both the thickness of the layer (its 2-dness) and its width (so 1-d <---> 2-d system transitions could be made). These samples exhibited strong localization consistent with variable range hopping rather than the near metallic behavior observed in the inversion layer systems. The dimensionality could be controlled by the gate voltage and at a well defined value the temperature dependence of the conductivity (given by equation II.44) would change from $\ln\sigma \sim T^{1/2}$ to $\ln\sigma \sim < T^{1/4}$.

B. Inversion and Accumulation Layers

2. Heterostructures

In 1979, H.L. Stormer, R. Dingle, A.C. Gossard, W. Wiegmann and M.D. Sturge found that the band bending at the interface between epitaxially grown layers of GaAs and GaAlAs creates an electron inversion layer where the electronic mobilities are quite high (in the initial studies the mobilities at 4.2°K were <5000cm^2/Vsec) and the electron gas in the layer was two dimensional as evidenced by the angular field dependence of the Shubnikov-de Haas oscillations. In 1981, D.A. Poole, M. Pepper and R.W. Glew observed localization and interaction effects in the inversion layers of GaAs-GaAlAs heterojunctions at low temperatures. The resistivity of the layer had a logarithmic temperature dependence consistent with both localization and interaction effects (p=1). Their measurements were complicated by the fact that the electron gas in their heterojunctions was split into two sub-bands with different mobilities and carrier concentrations. At low magnetic fields they observed a negative magnetoresistance indicating that localization effects were dominating but at higher fields the magnetoresistance became positive as interaction effects took over and at very high fields they observed Shubnikov-de Haas oscillations. They also measured the Hall effect in their heterojunctions and found the fractional change in the Hall coefficient with temperature to go at twice the fractional change in the resistivity with temperature consistent with the interaction theory.

CHAPTER IV -- EXPERIMENTAL TECHNIQUES

A. Sample Preparation and Characterization

1. Palladium and Palladium-Gold Films on Glass and Quartz

The films used in most of the transport studies presented in this thesis were made by electron beam evaporation of a Marz grade (99.95 percent pure with less than 10 parts per million of magnetic impurities) Palladium (Pd) ingot, or a Palladium-Gold (Pd-Au) alloy ingot (42 percent Pd, 58 percent Au by weight) which itself was formed in an ultraclean arc furnace in an ultrapure Argon (Ar) atmosphere from Marz grade Pd and 99.9999 percent purity Au. The ingot was annealed at 800°C in vacuum for over 24 hours and then quick quenched (while still under vacuum) to room temperature (quenching was estimated to be less than 3 seconds). This later procedure improved the homogeneity of the ingot. The boiling point of Pd and Au are similar (they have vapor pressures of 10^{-4}Torr at 1465°K for Pd and 1405°K for Au) so the composition of the films deposited from the condensation of the vapor of such an ingot should be within a few percent of the ingot composition.

The films were deposited on vapor degreased pyrex glass microscope slides or on fused quartz at a rate of 0.1 Angstroms per second at pressures on the order of 10^{-7}Torr during the evaporation (the base pressure of the system is 10^{-8}Torr). The choice of substrate was determined by the needs of the specific transport measurement techniques. The film characteristics were essentially independent of the substrate material.

The film deposition rate was controlled by modulating the power of an electron beam bombarding the ingot of source material. The beam power was controlled by a Sloan 9000 Deposition Controller, which senses the deposition rate by monitoring the mechanical resonance of an oscillating (~5 Megahertz) quartz crystal which is placed in close proximity to the substrate and has one face exposed to the evaporant flux so that a film is also deposited on it simultaneously with the substrate. The material deposited on the crystal face mass-loads the crystal, causing a shift in its resonance frequency. The crystal was calibrated before the deposition by depositing a very thick (~5000 Angstrom) film on the substrate and measuring its correct thickness by an optical interference technique. Based on the information sensed via the quartz crystal, the controller adjusts the electron beam power to keep the deposition rate following the controller's programmed instructions. When the proper evaporation conditions are achieved, the controller opens a shutter exposing the substrate to the molecular flux emanating from the electron bombarded ingot, thus allowing the film to condense on the substrate. After the film has reached its proper thickness, as calculated by integrating the deposition rate as sensed by the quartz crystal monitor over the time since the shutter was opened, the controller closes the shutter and implements its electron beam power-down instruction sequence.

Since the thickness of the glass and quartz substrates prevented taking transmission electron micrographs (TEM) of the actual samples used in the transport studies, electron micrographs and transmission electron diffraction (TED) patterns were taken of similarly prepared films deposited on amorphous quartz (SiO_2) and Carbon (C) film electron microscope grids (the quartz was ~500 Angstroms thick electron beam deposited on top of the carbon film grid). Identical structural results were found for both types of 'substrate'. Figure 4-1 shows transmission electron micrographs (TEM) of nominal 24 Angstrom thick Pd and 25 Angstrom thick Pd-Au films deposited on a carbon film electron microscope grid. These micrographs and others of similarly prepared Pd and Pd-Au films of nominal thicknesses of 18-30

Figure 4-1

Electron micrographs and electron diffraction pattern of (a) nominal 24-Angstrom-thick palladium film,(b) nominal 25-Angstrom-thick palladium-gold film. Both films are deposited on carbon-coated grids.

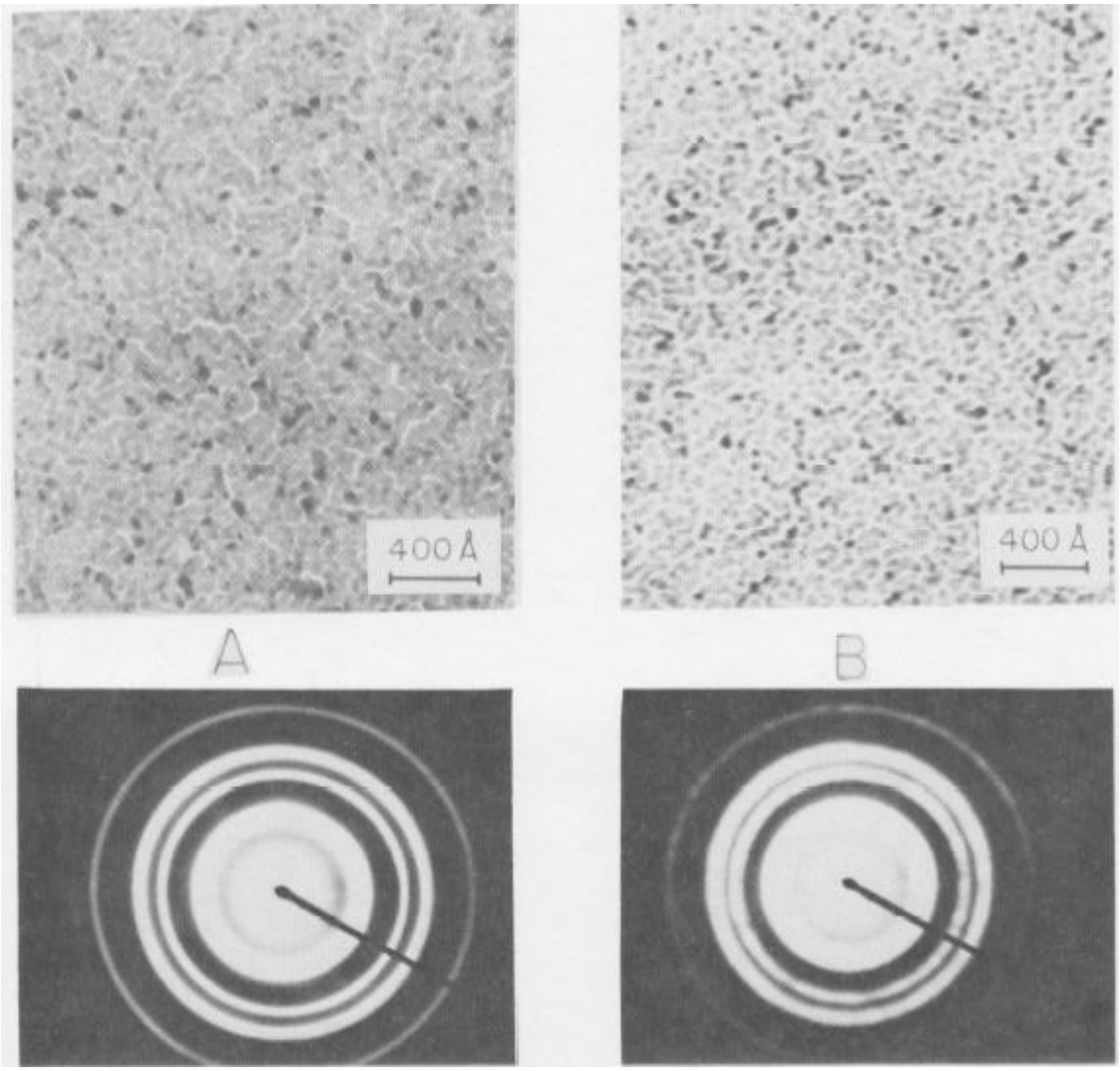
400 Å
400 Å
A
B

Angstroms show continuous films of fairly uniform thickness with a large number of nonpercolating cracks. The samples are therefore highly inhomogeneous on a scale of 100 Angstroms but appear quite homogeneous on a micron scale.

The transmission electron diffraction (TED) patterns of these Pd films (see Figure 4-1) show crystalline grains of ~50 Angstrom dimensions and face centered cubic (FCC) structure. The TED patterns for Pd-Au show similar size grains also with FCC structure, but they also indicate (by their 'fuzziness') the presence of a larger degree of disorder than in the Pd films.

Although these structural characterizations would seem to imply that the film structure is independent of the specific amorphous substrate (as long as no alloying with the substrate occurs), the electronic transport would be extremely sensitive to the distribution of barriers and traps arising from the details of the grain-grain boundaries and cracks in these films.

In Figure 4-2 is a plot of the thickness dependence of a Palladium film at room temperature. The resistivity was measured in situ during the film growth. The film was deposited onto a pyrex glass microscope slide at a rate of ~0.1 Angstrom per second. An electrometer first indicated an increased conductivity ($<10^{-12}\Omega^{-1}$) at a

Figure 4-2

Resistivity vs film thickness measured *in situ* for a palladium film deposited on glass at room temperature.

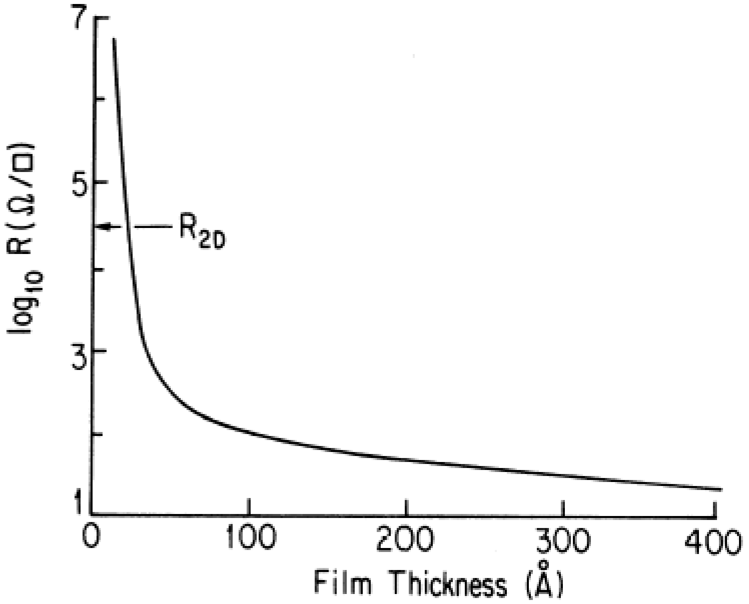
7
5
3
1
0
100
200
300
400
log₁₀ R (Ω/□)
R₂D
Film Thickness (Å)

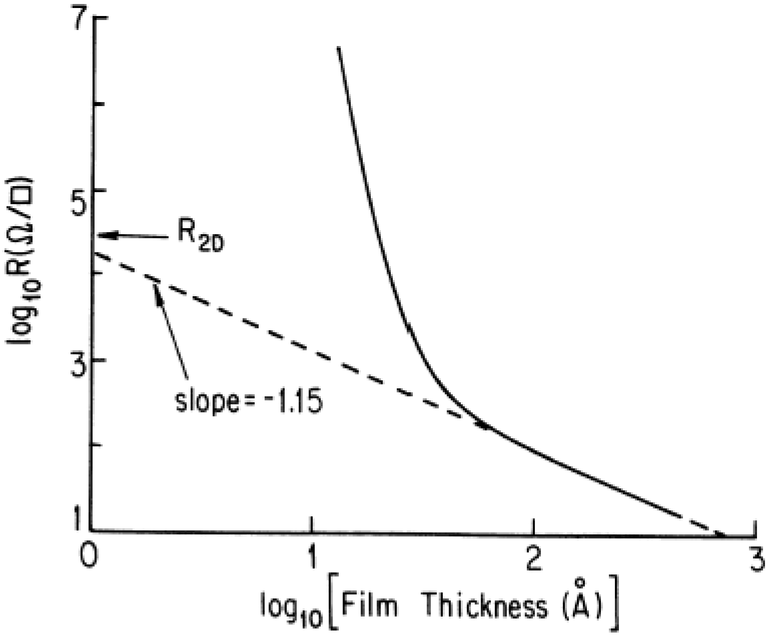
7
5
3
1
0
1
2
3
log₁₀R(Ω/□)
R₂D
slope= -1.15
log₁₀[Film Thickness (Å)]

nominal thickness of ~4 Angstroms. The resistance then fell smoothly but rapidly and crossed the interesting value of ~30kΩ per square at ~25 Angstroms. At thicknesses greater than ~80 Angstroms the resistivity decreases as the inverse of the film thickness increases, indicating a mean free path of about 80 Angstroms at room temperature. From this curve one could then make films of the desired resistivity by controlling the approximate thickness.

The film geometry was controlled by a series of masks which allowed the evaporant molecular flux though in various patterns. The masks could be changed in vacuo as could the source material ingots thus allowing quite complex patterns and multilayered structures to be fabricated (see for example, section IV.B). Various contacts (usually 3000 Angstroms of Ag) were electron beam evaporated onto the substrate after the films were fabricated to facilitate the various transport measurements.

A. Sample Preparation and Characterization

2. Ultrathin Silver Films Epitaxially Grown on (001) Ge

Some films used in the later stages of the two dimensional electron transport studies in this thesis were prepared by J.R. Lince, J.G. Nelson and R.S. Williams (1983) using single crystals of Germanium (Ge) oriented with surfaces within 0.5° of a (001) plane which had been highly polished chemomechanically, mounted in an ultrahigh vacuum chamber (base pressure < 10^{-10}Torr) and then further cleaned in vacuo by several cycles of argon (Ar) ion bombardment followed by annealing at <825°K.

The surface before, during, and after film growth was structurally characterized using low energy electron diffraction (LEED) and Auger electron spectroscopy (AES).

Silver (Ag) was deposited using a pyrolithic graphite Knudsen effusion cell operated at 1200±75°K allowing deposition rates of 2-30 Angstroms per minute. The substrate temperature was measured to be ~315°K during the deposition. The chamber pressure rose to ~2×10^{-9}Torr during the initial Ag film growth but dropped back into the 10^{-10}Torr range as the growth progressed.

The deposition rate and the film thickness were determined by using a quartz crystal oscillator similar to that used for the Pd and Pd-Au films only the calibration of this system was performed using Rutherford backscattering (RBS) analysis of the area density of similar but much thicker Ag films grown on Ge (001), rather than the optical interferometer used for the Pd and Pd-Au system calibration. This allowed the thickness of the films (for low coverages) to be determined to within ~5 percent of a Ag (001) monolayer.

The samples were then removed from the ultra high vacuum system and stored in air until they could be analyzed by scanning electron microscopy (SEM), RBS or conductivity. The samples were placed in a conventional evaporation system (the same one used to produce the Pd and Pd-Au films) and 3000 Angstrom Ag contacts were electron beam deposited onto the samples.

The LEED studies indicated that the clean Ge surface initially dimerized (reconstructed) but would relax when less than a monolayer of Ag was deposited upon it. The LEED also indicated that Ag forms a crystalline monolayer coverage of the surface, followed by the formation of three dimensional islands. Heating the substrate to ~600°K for <10 minutes destroys the monolayer leaving Ag islands (the monolayer clumps up, this temperature is too low to cause the Ag to desorb from the surface), and the

LEED indicates that the Ge surface redimerizes. This would indicate there is no interfacial alloying or interdiffusion of the Ag and Ge at room temperature. Photoemission studies of Ag on Ge (111) by Rossi, Abbati, Brairovich, Lindau and Spicer (1982) were interpreted as implying strong chemical interaction and intermixing of the first several layers. Rossi, et.al. did not perform any structural measurements however, and very complete structural studies (containing LEED, photoemsission, etc.) by Bertucci, LeLay, Manneville and Kern (1979) of Ag on Ge (111) indicated no interfacial alloying or interdiffusion of the Ag and Ge at room temperature. Studies of growth of Ag on Ge (001) by Miller, Rosenwinkel and Chaing (1984) using high energy electron diffraction (HEED) and photoemission support the contension that no alloying or interdiffusion occurs at the Ag-Ge interface and also imply that the band bending at the surface in the Ge substrate is negligible.

B. Sample Geometry and Cryogenic Systems

A variety of sample geometries and cryogenic systems were used depending on the types of transport measurements to be performed.

Figure 4-3 shows the standard contact configuration used if the transport measurements were on Pd or Pd-Au films and were to consist on D.C. or low frequency A.C. resistivity as a function of temperature, electric and magnetic fields (separately or in combination) and Hall effect. This geometry allows a 4-probe of the sample, eliminating any effects due to contact phenomenon.

Figure 4-4 shows one of the more complex geometries used for the various thermoelectric measurements. In this geometry, only thermoelectric effects arising from dimensionality differences are observed. The details of the thermoelectric geometries will be covered in section IV.C.4.

Since the Ag on GE (001) samples and the microwave conductivity of Pd samples were usually irregular in shape, their geometries varied from sample to sample.

The samples were glued to the copper sample block of the probe, all wires to the sample and any sensors were thermally shorted to the block, and the probe placed in

Figure 4-3

Geometry used for electrical measurements.

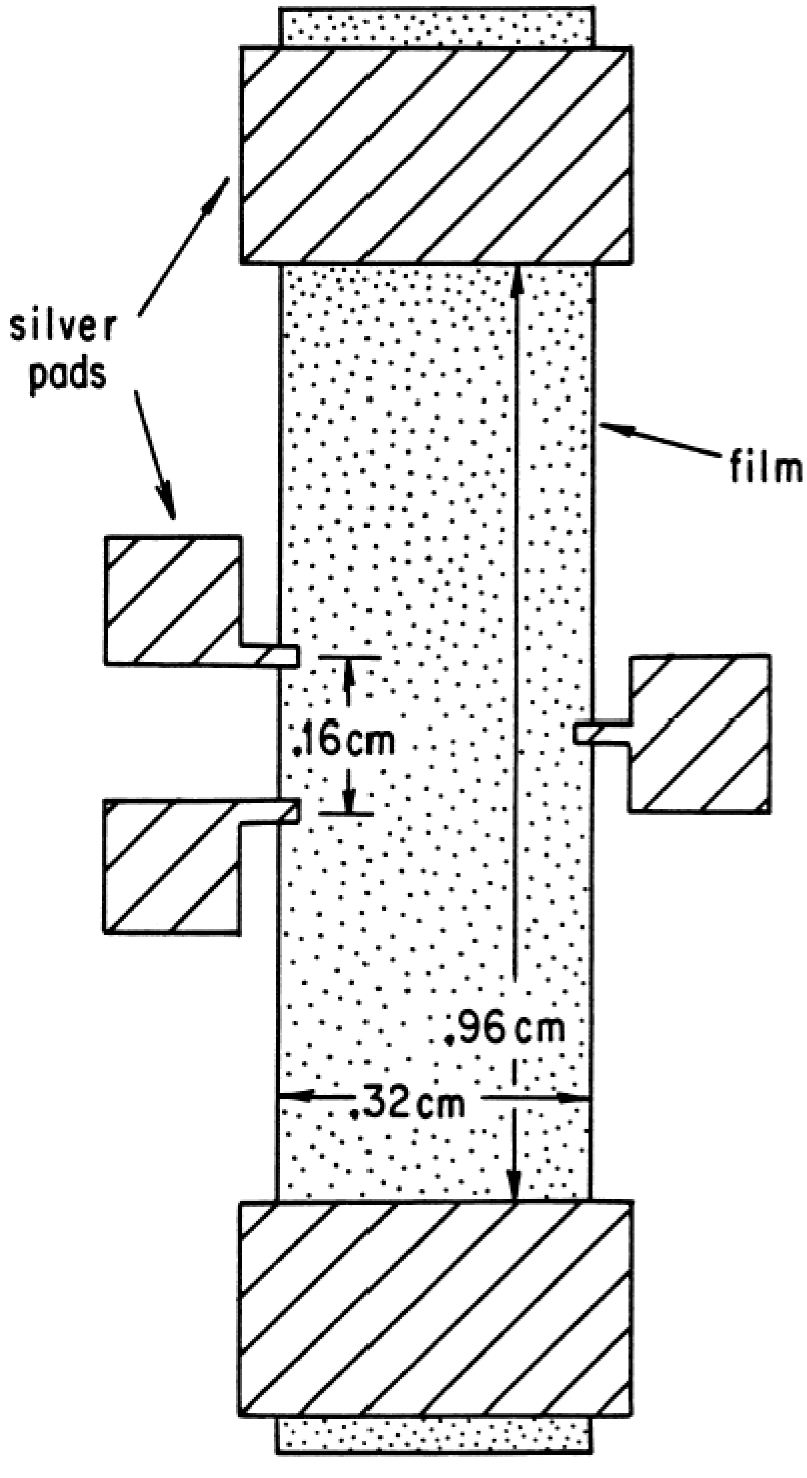
silver pads
film
.16cm
.96cm
.32cm

Figure 4-4

Geometry used for measuring very small differences between the thermopower in two dimensional and three dimensional Pd films. Structure forms ten 3d-2d-3d differential thermocouples side-by-side that are electrically in parallel.

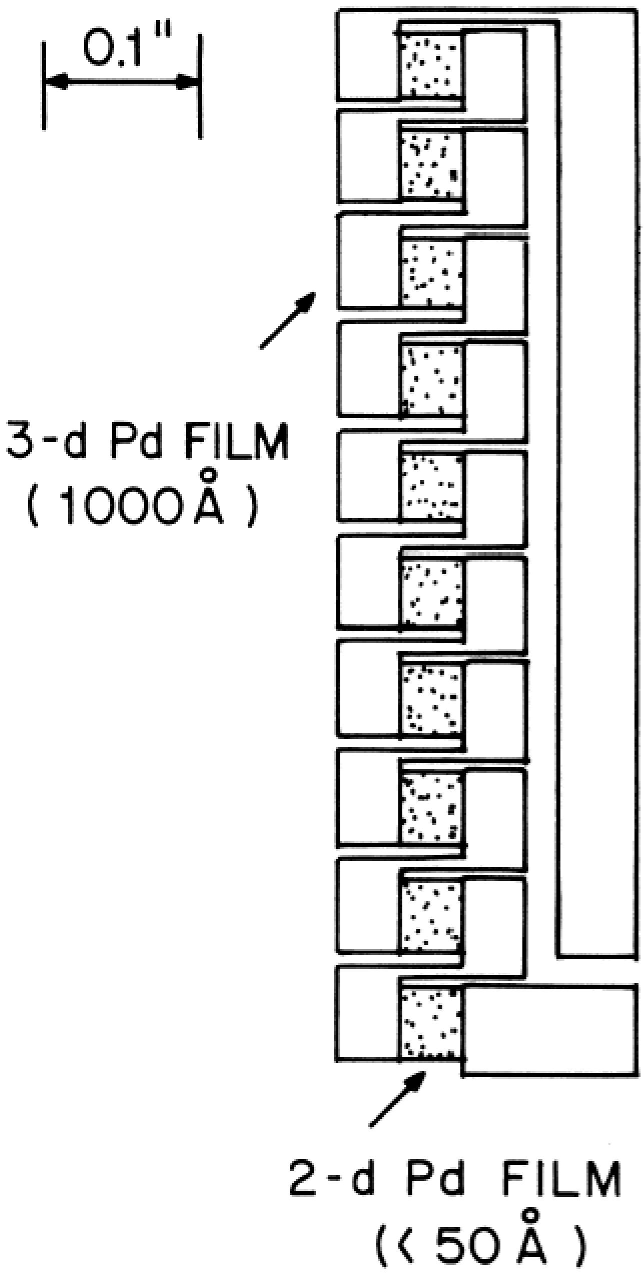
0.1"
3-d Pd FILM
(1000 Å)
2-d Pd FILM
(< 50 Å)

(or were already an integral part of) one of three types of cryogenic systems:

(1) A 'double-can' system as illustrated in figure 4-5. An outer can contained the entire probe, and was placed in the inner dewar of a double glass dewar system. The inner can surrounded the sample holder block and any associated apparatus. The inner can could be filled with He4 exchange gas to help insure isothermal conditions throughout the probe, or could be evacuated to allow the controlled creation of thermal gradients for the measurement of nonequilibrium phenomenon (such as thermoelectric effects). The outer can could also be filled with some He^4 exchange gas to allow the inner can to thermally couple to the liquid He^4 in the inner glass dewar. By evacuating the outer can, the thermal coupling between the inner can and the liquid He^4 could be reduced allowing the sample temperature to be controllably elevated up to <100°K, while the inner glass dewar was full of liquid He^4. A vacuum pump could be used to reduce the pressure in the inner glass dewar containing the liquid He^4, reducing its temperature to <1°K. This system allowed measurements over a range in temperature from 1.05°K up to 300°K.

(2) For measurements at temperatures down to ~0.5°K another 'double-can' system employing He^3 was used (see

Figure 4-5

'Double can' system used for reaching temperatures between ~1.05°K and 300°K. Thermopower measurements used this system.

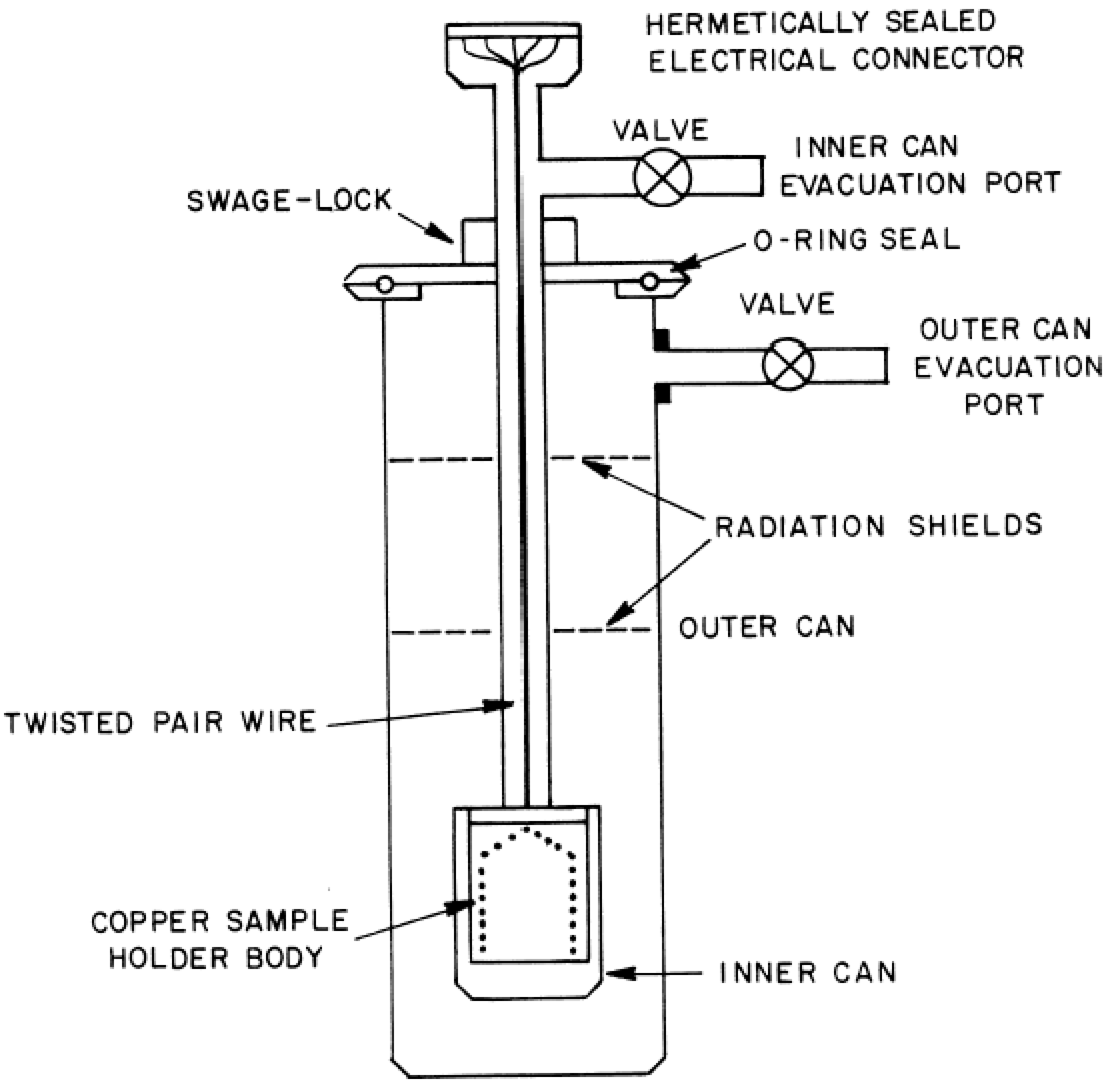
HERMETICALLY SEALED ELECTRICAL CONNECTOR
VALVE
INNER CAN EVACUATION PORT
SWAGE-LOCK
O-RING SEAL
VALVE
OUTER CAN EVACUATION PORT
RADIATION SHIELDS
OUTER CAN
TWISTED PAIR WIRE
COPPER SAMPLE HOLDER BODY
INNER CAN

Figure 4-6

'Double can' system used with He^3 in 'single-shot' mode to attain temperatures down to ~0.5°K. This system has a temperature range from ~0.5–300°K.

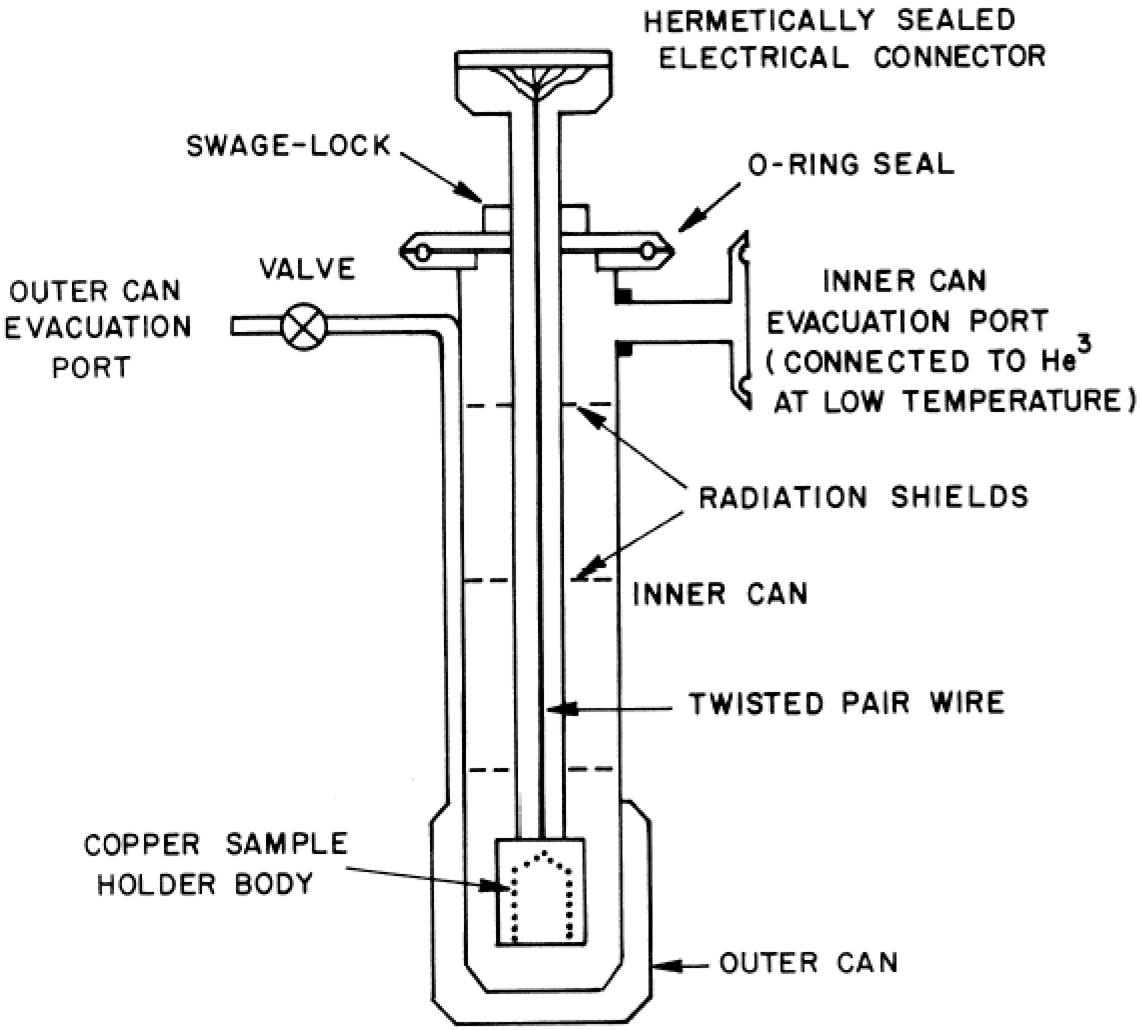
HERMETICALLY SEALED ELECTRICAL CONNECTOR
SWAGE-LOCK
O-RING SEAL
VALVE
OUTER CAN EVACUATION PORT
INNER CAN EVACUATION PORT (CONNECTED TO He^3 AT LOW TEMPERATURE)
RADIATION SHIELDS
INNER CAN
TWISTED PAIR WIRE
COPPER SAMPLE HOLDER BODY
OUTER CAN

figure 4-6). The 'double-can' is also placed in a glass dewar system. At low temperature (~1°K), He^3 is condensed into the inner can immersing the samples in liquid He^3. The outer can is evacuated to thermally decouple it from the liquid He^4 in the inner glass dewar, and a vacuum pump is used to create a partial vacuum in the inner can, thereby lowering the He^3 temperature. The He^3 is recovered from the pumping system and reused. This gives a 'single-shot' cooling (i.e. the He^3 is not continuously recirculated) effect (T<~0.5°K) which can last several hours.

(3) For temperatures below 0.5°K a He^3-He^4 dilution refrigerator was used. Temperatures down to 50mK could be reached in this way. This method was very rarely used in these studies.

The double glass dewar systems consisted of two glass vessels each with double walls (i.e. the walls were hollow), one vessel inside a much larger one. The walls of the vessels were coated with silver (Ag) and evacuated. The silvering reflected thermal radiation away from the vessel interior and evacuating the walls provided direct thermal isolation between the inside and outside of each vessel. The larger, outer vessel was filled with liquid nitrogen (N_2), cooling the inner vessel to ~77°K. The inner vessel, into which the 'double-can' probe systems were placed, was filled with liquid He^4. One of the double glass dewar systems contained a superconducting magnet allowing measurements (in one field orientation only) in fields up to 10 Tesla (100 KiloGauss). Another double glass system was inside a large rotatable magnet allowing measurements (with the field restricted to a plane) in fields up to 1 Tesla.

C. Measurement Techniques

1. Probe Temperature Measurement

i) Diode Sensors

According to the work of Sah, Noyce, and Shockley (1957), the current through a forward biased p-n semiconductor junction will follow

$$I_f = I_s \exp\{ qV_f/(2K_bT)\} \qquad \text{(IV.1)}$$

where q is the carrier charge and V_f is the bias voltage. I_s is given by

$$I_s = AK_bTn_i/(\tau E) \qquad \text{(IV.2)}$$

where A is the junction area, τ is the average carrier lifetime, E is the electric field in the depletion region, and n_i is the carrier density. n_i is given by

$$n_i = 2(mK_bT/[2\pi\hbar^2])^{3/2} \exp\{ -qE_g/(2K_bT) \} \qquad \text{(IV.3)}$$

with E_g as the intrinsic energy gap of the semiconductor.

Combining these three equations and solving for $V_f(T)$, we find

$$V_f(T) = E_g - (2K_bT/q)[\ \ln(\alpha) + (5/2)\ln(T) - \ln(I_f)] \quad \text{(IV.4)}$$

where

$$\alpha = 2(mK_b/[2\pi\hbar^2])^{3/2}[AK_b/(\tau E)]. \quad \text{(IV.5)}$$

Equation IV.4 implies that a p-n semiconductor junction, under constant current forward bias, will display a voltage that will be approximately linear with temperature (until the carriers freeze out and some type of hopping conduction dominates the transport) and independent of the specific doping. In other words, all silicon (Si) diodes should display approximately the same behavior as a function of temperature under the same constant current conditions.

Figure 4-7 illustrates the simple diode temperature sensor configuration used for measurements from 300°K down to ~1°K. The diodes were DT series silicon diodes purchased from Lakeshore Cryotronics, Inc. These diodes are specially manufactured to be repeatedly cycled between room temperature and liquid He temperature

Figure 4-7

TOP: Diode sensor schematic

BOTTOM:

Capacitor sensor setup. Controller can hold temperature constant or can output a signal proportional to the sensor capacitance for temperature measurement.

DIODE TEMPERATURE SENSOR

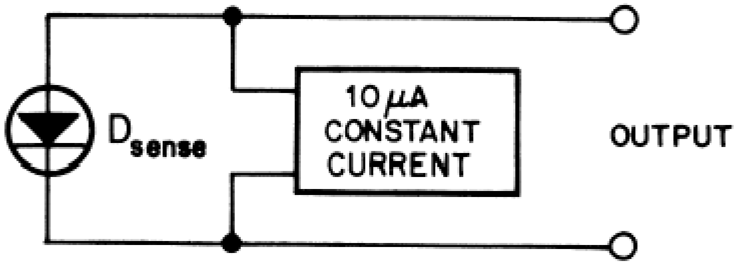
D$_{sense}$
10 μA
CONSTANT
CURRENT
OUTPUT

CAPACITOR TEMPERATURE SENSOR

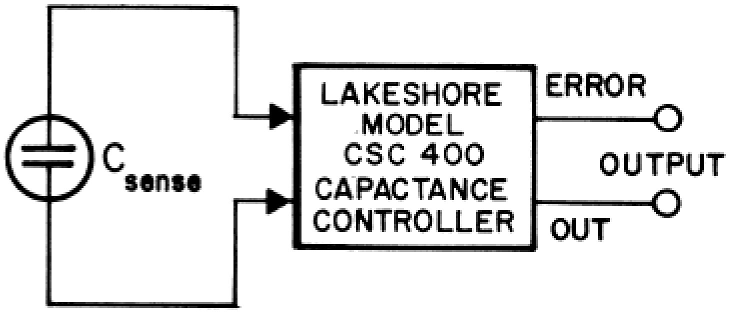
C$_{sense}$
LAKESHORE
MODEL
CSC 400
CAPACTANCE
CONTROLLER
ERROR
OUTPUT
OUT

without damage. Since all diodes fabricated using the same type of semiconductor are only approximately the same in their $V_f(T)$ curves (equation IV.4), each diode was calibrated against a sensor calibrated by Lakeshore. The calibrations are unaffected by repeated cycling of the diodes. Using one of these silicon diodes, forward biased at 10μamps+0.05%, and the forward bias voltage read using a high input impedance (> 10GΩ) digital voltmeter (DVM) with 6 digit resolution, the temperature can be determined to within 0.01°K.

ii) Capacitance Sensors

In 1971, W.H. Lawless demonstrated a glass-ceramic capacitance temperature sensor which measured the dielectric constant of $SrTiO_3$ crystallized glasses. Since only a displacement current, rather than a real current, flows through the dielectric, the sensor performance is unaffected by magnetic fields. These sensors can be used as secondary sensors to allow the temperature of the probe to be controlled while magnetic fields are applied to the samples (and hence the probe). These sensors can also be calibrated against a primary sensor in zero magnetic field (where the primary sensor functions correctly) and used to measure the temperature while the magnetic field is applied. This system is illustrated in figure 4-7. If used only to control the temperature, this system can control the temperature (independent of the magnetic field strength) to within +1milliKelvin.

iii) Resistance Sensors

For sensing temperatures below <1°K, germanium or carbon-glass resistance sensors are used. These sensors consist of a single crystal of germanium or carbon-glass is suspended by four wires inside a hermetically sealed can. The crystal is cut and mounted in a manner which minimizes the strains on it during the cool-down. The four wires are used to inject the sense current and measure the potential drop along the crystal. Figure 4-8 illustrates both the direct current (DC) and alternating current (AC) techniques used to measure the resistance of these sensors. In the DC method, a computer injects the current through the sensor and the potential drop along the crystal is measured. The computer reverses the current and the potential drop is measured again. The potential drop in both current directions is averaged and divided by the sense current to yield the sensor resistance which is compared to that sensor's calibration chart and converted by the computer to a temperature.

TOP

DC resistance sensor measurement. Computer injects current - voltage output is measured. Computer reverses current - voltage output is measured again. Both output measurements are averaged to eliminate errors due to stray thermal EMFs in the circuit.

BOTTOM

Interface box provides constant amplitude AC current at the reference frequency. Lock-in amplifier measures the sensor response at the reference frequency and reference phase. The lock-in DC output voltage is proportional to the sensor resistance.

D.C. RESISTANCE
TEMPERATURE SENSOR

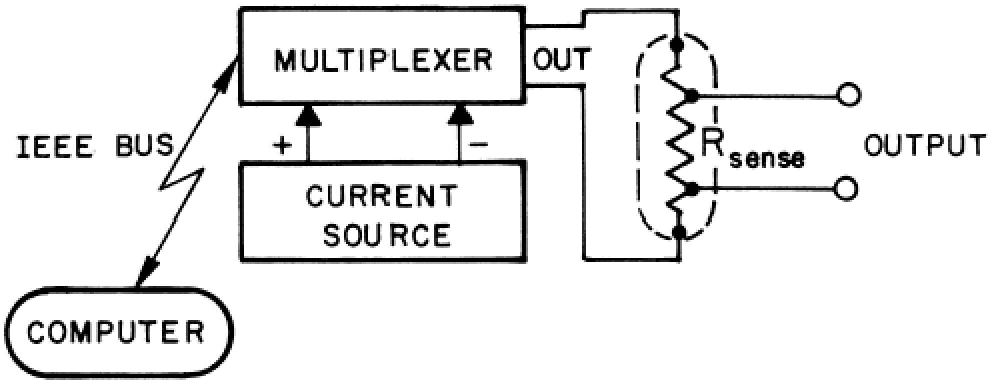
MULTIPLEXER
OUT
IEEE BUS
+
−
CURRENT SOURCE
R_{sense}
OUTPUT
COMPUTER

A.C. RESISTANCE
TEMPERATURE SENSOR

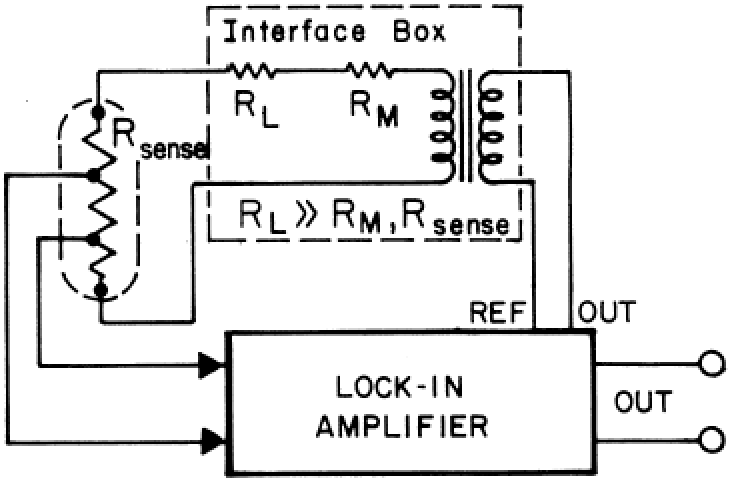
Interface Box
R_L
R_M
R_{sense}
$R_L \gg R_M, R_{sense}$
REF
OUT
LOCK-IN AMPLIFIER
OUT

Reversing the current and averaging eliminates errors due to thermally generated electromotive forces (EMFs) arising from thermal gradients in the circuit.

The AC technique (this technique is described in greater detail in section IV.C.2) utilizes an alternating current which is channeled through the sensor and a current limiting resistor, R_L ($R_L >> R_{sensor}$). A small precision resistor (R_m) is also in series with the sensor to allow a measurement of the current amplitude (by measuring the voltage amplitude across R_m). The potential drop along the sensor crystal is fed into a lock-in amplifier which measures the drop and outputs a DC voltage proportional to that potential drop. This AC technique is immune to the effects of thermal EMFs since the EMFs are DC, and since the lock-in measures only that portion of the input signal which has the same frequency and phase as the sense current, the sensor resistance can be measured extremely accurately.

Temperature measurements to within ±0.5 milliKelvin can be made using a resistance sensor and the AC technique.

C. Measurement Techniques

2. Chordal Resistance Measurements

The chordal resistance is the ratio of the voltage drop along the sample (V) to the current (I) producing that drop.

Two techniques were used for chordal resistance measurements, both capable of resolving resistance changes as small as one part in 10^5.

The first method, shown schematically in figure 4-9a, is a low frequency phase-sensitive detection technique. A reference signal, generated either by the lock-in itself or an external oscillator, is fed into a transformer which provides DC isolation between the sample and the oscillator. The output of the transformer is connected to the current contacts (for a 4-probe measurement) of the sample via two external resistors, R_L and R_m (with $R_m<R_{sample}$ and R_m known to a high precision). R_L is chosen to be at least two orders of magnitude larger than R_m and R_{sample} (the larger the better) so that R_L (known as the current limit resistor) dominates the impedance of the circuit. Thus, for a constant amplitude sine wave injected into the

Figure 4-9

Schematic diagrams for chordal resistance (V/I) measurements.

a) AC Technique: A low frequency (10hz<f<1000hz) lock-in reference signal was applied through a transformer to the current leads of the sample. The current was limited by R_L in series with the sample ($R_L >> R_m, R_{sample}$) so current is essentially of constant amplitude. The voltage across the sample is phase-sensitive detected by the lock-in which outputs a DC voltage proportional to the sample resistance (V/I).

b) DC Technique: A constant current source is connected to the current leads of the sample. The voltage across the inner leads was read by a DVM and sent to a computer. The current is reversed and the voltage read again. The computer averages the two polarity measurements to eliminate the effects of stray thermal EMFs in the circuit.

(a) RESISTANCE MEASUREMENT (A.C.)

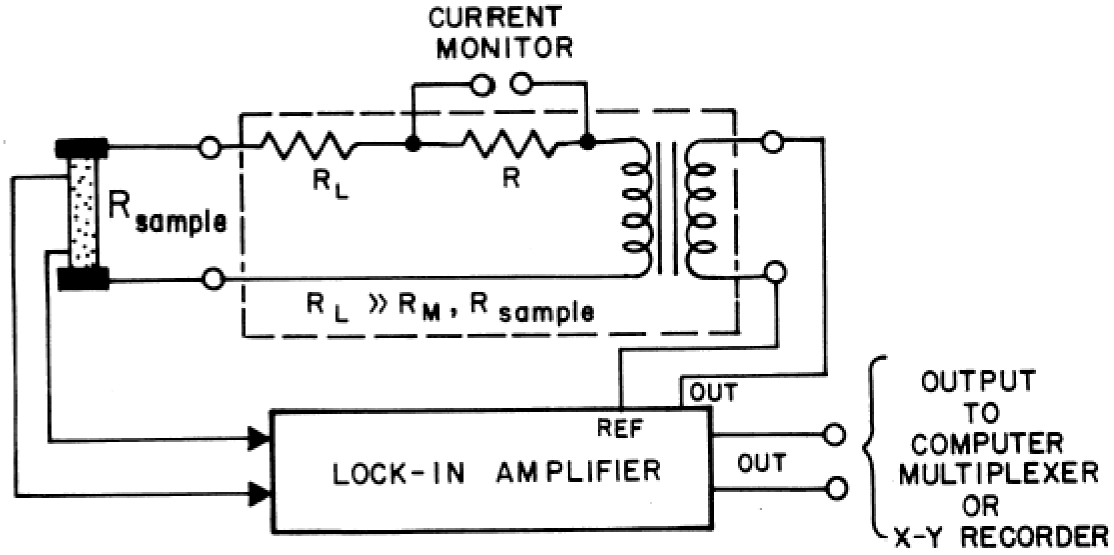
CURRENT MONITOR
R_L
R
R sample
R L » R M , R sample
OUT
REF
LOCK-IN AMPLIFIER
OUT
OUTPUT TO COMPUTER MULTIPLEXER OR X-Y RECORDER

(b) RESISTANCE MEASUREMENT (D.C.)

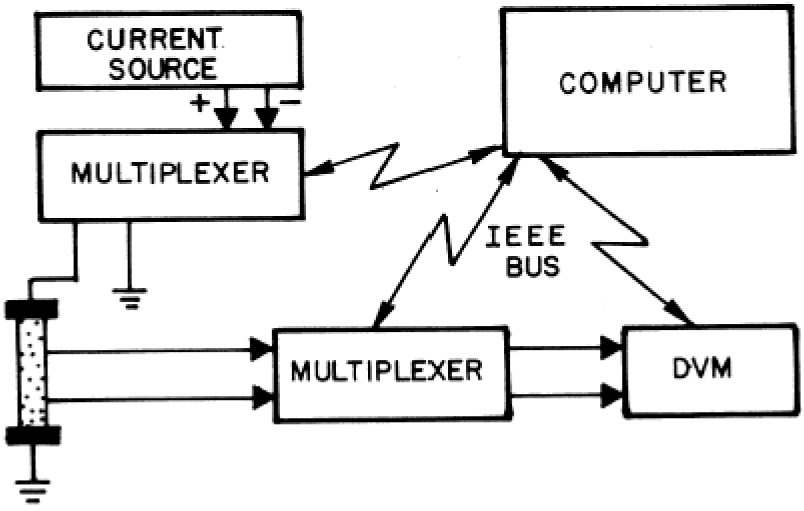
CURRENT SOURCE
+
−
MULTIPLEXER
COMPUTER
IEEE BUS
MULTIPLEXER
DVM

transformer primary, the current through Rsample will be constant to one part in $R_L/[R_m+R_{sample}]$, implying the current amplitude will be <constant as long as $R_L>>>R_{sample},R_m$. The amplitude and phase (relative to the reference) of the current through the sample is measured by monitoring the voltage drop across R_m. The voltage contacts of the sample are connected the the differential inputs of the lock-in amplifier which extracts that portion of the total input signal which has the same frequency and phase as the reference signal, and outputs a DC voltage proportional to the sample resistance. If $R_L=10^8\Omega$ and $R_m\sim R_{sample}=10^3\Omega$, then if R_{sample} changes by a factor of 2, the current through the sample will change by one part in 10^5. This would allow R_{sample} to be determined to 1 part in 10^5 assuming the sample current was constant. Correcting for the current change allows an even more precise chordal resistance determination.

The second method (figure 4-9b) utilizes a computer as an integral part of the measuring apparatus. A DC constant current source is connected to the current contacts of the sample via a computer controlled multiplexer (or 'scanner'). The multiplexer is a device which allows the computer to switch signals around from various inputs to various outputs, or to switch signals on and off. The voltage contacts of the sample are connected via a multiplexer to the input of a digital volt meter (DVM) which is controlled by the computer. The computer injects a known current through the sample and measures the voltage drop (via the DVM) along the sample, then reverses the current and measures the voltage drop again. The two measurements are averaged to eliminate any voltage offsets due to thermal EMFs in the circuit. Using this method, the computer can simultaneously measure the chordal resistance on a large number of samples. Using a sense current of ~1μamp on a ~1000Ω sample, and a DVM with 10 nanovolt resolution (such as a KEITHLEY 181), measurements can be made with a resolution of about one part in 10^5.

C. Measurement Techniques

3. Electric Field Dependent Chordal and Dynamic Resistance

Two techniques were used to study the nonlinear electric field response of the samples.

Illustrated in figure 4-10 is the technique for measuring the chordal (V/I) resistance at constant electric field. This technique was generally used to measure R vs T or R vs H (magnetic field) under different sample bias, as opposed to measuring R vs E at various T or H. One pole of the output of a constant voltage source is connected to a current lead of the sample, the other connected to the circuit ground. The other sample current lead is grounded through a precision resistor (R_I). The sense leads of the constant voltage supply are connected to the inner voltage leads of the sample, thus causing the voltage source to maintain a constant voltage between these leads. The voltage across the inner (voltage) sample leads and the voltage drop across the resistor (R_I) are fed into a multiplexer connected to a computer and a DVM. The computer measures the inner sample lead voltage and the voltage across R_I (thus measuring the

Figure 4-10

Schematic for measuring DC chordal resistance as a function of applied electric field. A current is applied to the sample by a constant voltage source in such a manner that the voltage on the voltage leads remains constant. The current is also run through R_I, the voltage drop across which can be measured to determine the current through the sample. The sample voltage and the voltage across R_I are measured, the polarity reversed and the measurements repeated. The computer averages the two polarity measurements to eliminate errors introduced by stray thermal EMFs in the circuit.

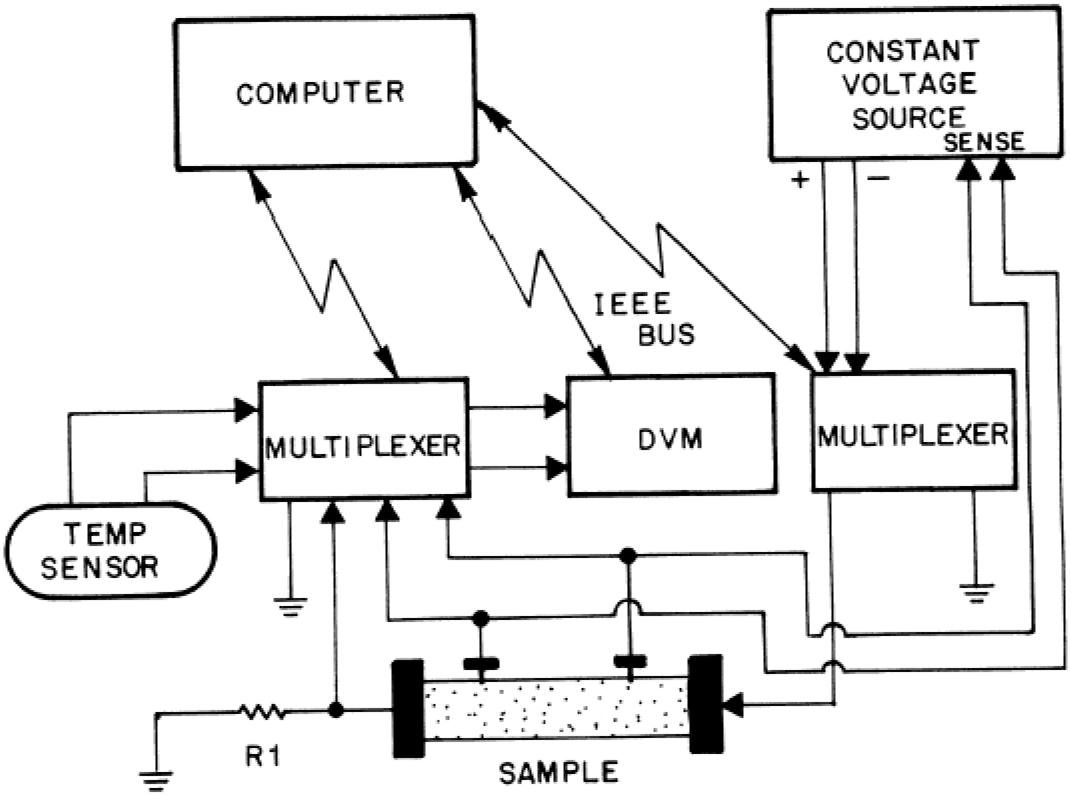
COMPUTER
CONSTANT VOLTAGE SOURCE
SENSE
+
−
IEEE BUS
MULTIPLEXER
DVM
MULTIPLEXER
TEMP SENSOR
R1
SAMPLE

current through the sample), the current is reversed and the two voltages measured again. The voltages for the two current directions are averaged to eliminate the effects of thermal EMFs in the circuit. A variation of this technique can be used to provide I-V curves (or [V/I} vs E) by replacing the constant voltage source with a voltage ramp generator.

The second technique used to study the nonlinear electric field response of the sample, illustrated in figure 4-12, measures the dynamic resistance ($\partial V/\partial I$) of the sample. The way this circuit extracts $\partial V/\partial I$ (actually it extracts $\partial I/\partial V$) from the signal is illustrated in figure 4-11. The total voltage applied to the sample is

$$V = Vo + V_1 \sin(\omega t). \qquad \text{(IV.6)}$$

The current through the sample can be expanded in a Taylor series

$$I(V) = I(V_o + V_1 \sin(\omega t))$$

$$I(V) = I(V_o) + [\partial I/\partial V] V_1 \sin(\omega t) + \ldots \qquad \text{(IV.7)}$$

so the dynamic resistance ($\partial V/\partial I$) can be extracted from the total signal at the modulation frequency, ω. As

Figure 4-11

The AC modulation voltage, $V_1\sin(\omega t)$, samples the slope of the V-I curve at V_o.

$$\partial V/\partial I \longrightarrow V/I \text{ as } V \longrightarrow 0$$

V/I = chordal resistance

$\partial V/\partial I$ = dynamic resistance

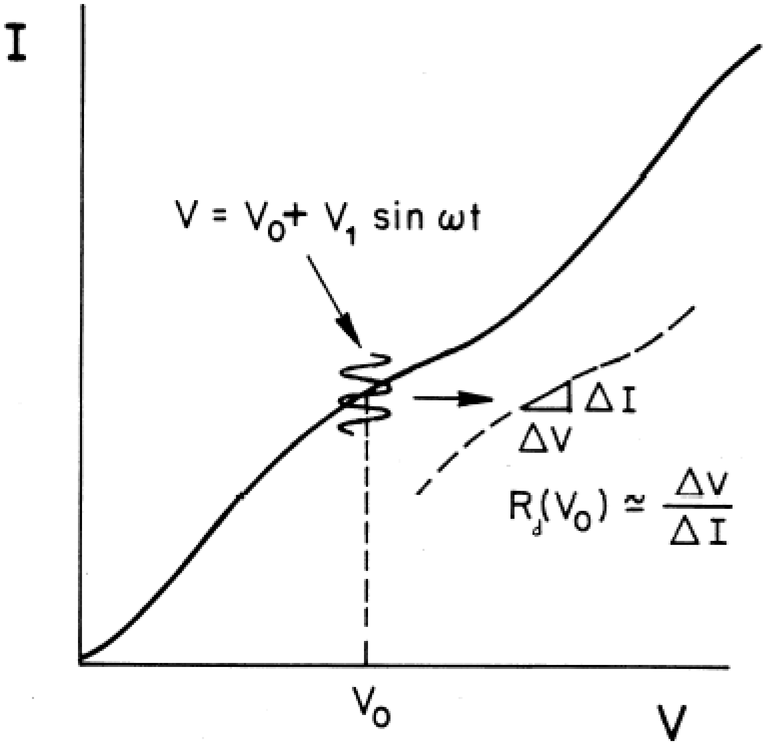
I
V = V0+ V1 sin ωt
ΔI
ΔV
Rd(V0) ≃ ΔV/ΔI
V0
V

$$R_d \equiv \frac{\partial V}{\partial I}$$

Figure 4-12

Two schematics of the bridge circuit used to measure dynamic resistance ($\partial V/\partial I$).

$R_{sample} = R_1+R_x+R_2$

R_x = resistance of portion of sample being probed.

R_1,R_2 = contact resistances.

R_A = armature resistances ($R_A \gg R_b, R_{sample}$)

R_b = variable bridge resistance

R_L = DC bias limit resistor

C_b = bridge capacitance

The optional DC bias supply is not shown in the lower illustration.

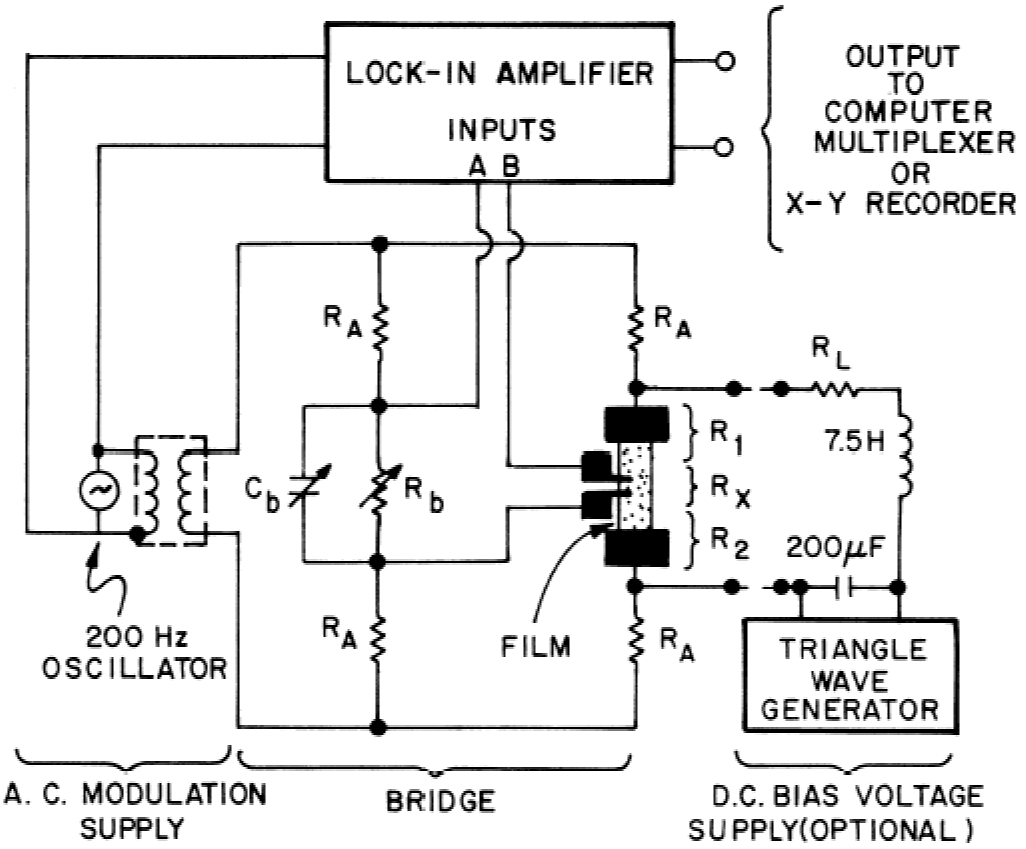

LOCK-IN AMPLIFIER
INPUTS
A B
OUTPUT TO COMPUTER MULTIPLEXER OR X-Y RECORDER
R A
R A
R L
R 1
7.5H
C b
R b
R X
R 2
200µF
R A
FILM
R A
TRIANGLE WAVE GENERATOR
200 Hz OSCILLATOR
A. C. MODULATION SUPPLY
BRIDGE
D.C. BIAS VOLTAGE SUPPLY(OPTIONAL)

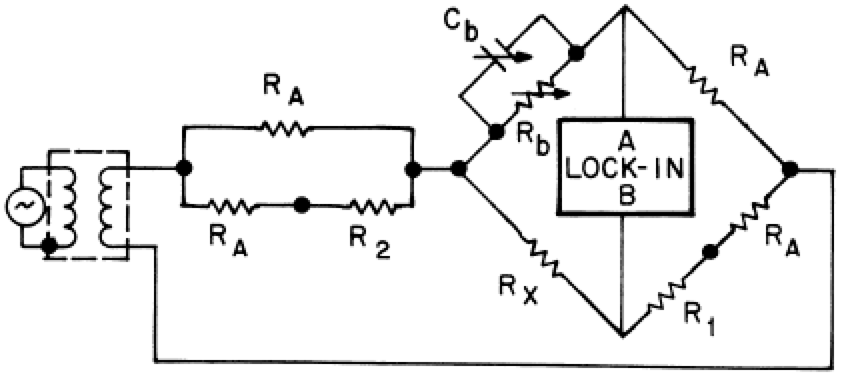

C b
R A
R b
A
LOCK-IN
B
R A
R A
R 2
R A
R X
R 1

figure 4-11 shows, the signal at frequency ω samples the slope of the V vs I curve at the DC bias voltage V_o. As V_o-->0, the chordal and dynamic resistances will be the same.

The circuit in figure 4-12 functions as a Wheatstone bridge. The modulation signal is run through an isolation transformer and then fed into two subcircuits connected in parallel to form the bridge. One subcircuit consists of two precision armature resistors (R_A) in series with and adjustable precision decade resistor block (R_b) and, in parallel to R_b, an adjustable precision capacitor block (C_b). The other subcircuit consists of two armature resistors in series with the sample, connected through the sample current leads. All four armature resistors are matched to each other within ~0.1%. The armature resistors used are several orders of magnitude larger than R_b and $R_{sample}(=R_1+R_x+R_2)$, thus dominating the circuit impedance, placing equal (within one part in $\{4R_A\}/[R_b+R_{sample}]$) current amplitudes through R_b and R_{sample}. When R_b and R_{sample} are connected to the differential inputs of a lock-in amplifier as shown, the lock-in will see the voltage imbalance (proportional to R_x-R_b) between the sample and R_b. When R_b is adjusted until the lock-in displays a null reading, then $R_x=R_b$. Fractional changes in resistance can be measured with this circuit easily to an accuracy exceeding one part in 10^6. A DC bias can be injected into the sample as shown in figure 4-12, to allow measurements of $\partial I/\partial V$ vs E.

C. Measurement Techniques

4. Thermoelectric Power (TEP)

As pointed out in Chapter II, the thermopower can supply a great deal of information on the energy distribution of the carriers in a system - more so than any transport measurement other than tunneling. TEP measurements indicate the sign of the majority carrier, indicate the presence of phonon drag or energy gaps in the density of states, and for semiconductors, can indicate whether the conduction is via carrier excitation across a gap or via hopping between localized states (e.g. impurity hopping). Since TEP is a zero current measurement, it is insensitive to the sample geometry. All these factors make TEP measurements not only an excellent supplement to conductivity measurements, but usually much more valuable.

Schematically, measuring TEP is very simple. A known temperature gradient is placed across the sample and the resulting voltage across the sample is measured. The main problems encountered in making TEP measurements are the result of stray thermal EMFs (which can reach several microvolts making measurements in the nanovolt range

Figure 4-13

Sample arrangement on copper holder, (a) cross section,(b) offset view. Sample substrate was cantilevered on step holder with heater placed on far end. Holder was sealed in copper can which was placed in an exchange gas can and submerged in liquid He^4.

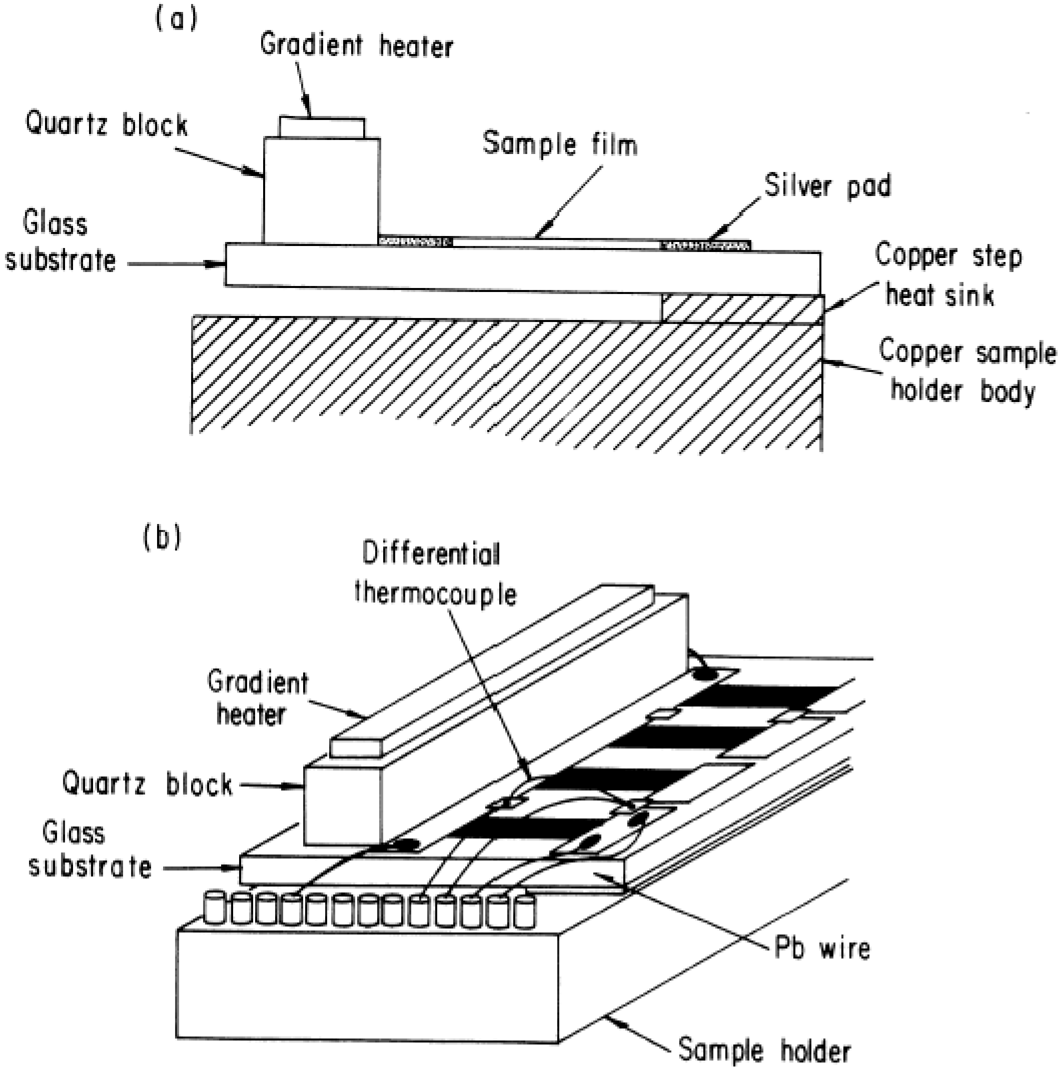
(a)
Gradient heater
Quartz block
Sample film
Silver pad
Glass substrate
Copper step heat sink
Copper sample holder body
(b)
Differential thermocouple
Gradient heater
Quartz block
Glass substrate
Pb wire
Sample holder

impossible) and high sample resistances. The stray thermal EMFs can be reduced by proper heat sinking of the wiring in every part of the measurement circuit. High sample resistance is a problem simply because until quite recently, nanovoltmeters had relatively low input impedances (<100kΩ). This complicated measurements of samples with comparable resistances. With the introduction of FET input nanovoltmeters (e.g. Keithley 181 Nanovoltmeter) these measurements have been simplified.

The setup used for measuring the TEP of Pd and Pd-Au films with resistivities ranging from 500 to 500000 Ω/square at 10°K is shown in figure 4-13. The samples were mounted so that one of the silver pads rested over a copper step heat sink to which the glass substrate was attached. The remainder of the slide was cantilevered into the vacuum. A single crystal quartz block with a heater attached was then glued on top of the other silver pad. Thus the heat flow was through the glass slide to the heat sink and the temperature gradient was established in the substrate supporting the thin metal films. Lead (Pb) wires were then indium soldered or silver painted to the silver pads and a 50-μm Chromel-Constantan differential thermocouple was placed in close proximity to the thin-film junction to monitor the

Figure 4-14

Thermopile sample arrangement.

Two thermopiles were fabricated onto each fused quartz substrate resulting in a factor of 10 increase in the sensitivity to any differences between 2-d and 3-d Pd films. Sample substrate is cantilevered on center sapphire step with thin film heaters along the outer edges. Sapphire on the underside of the heaters helps insure no gradients form sideways along pile. Sample holder was sealed in a copper can which was placed in an exchange gas can and submerged in liquid He^4.

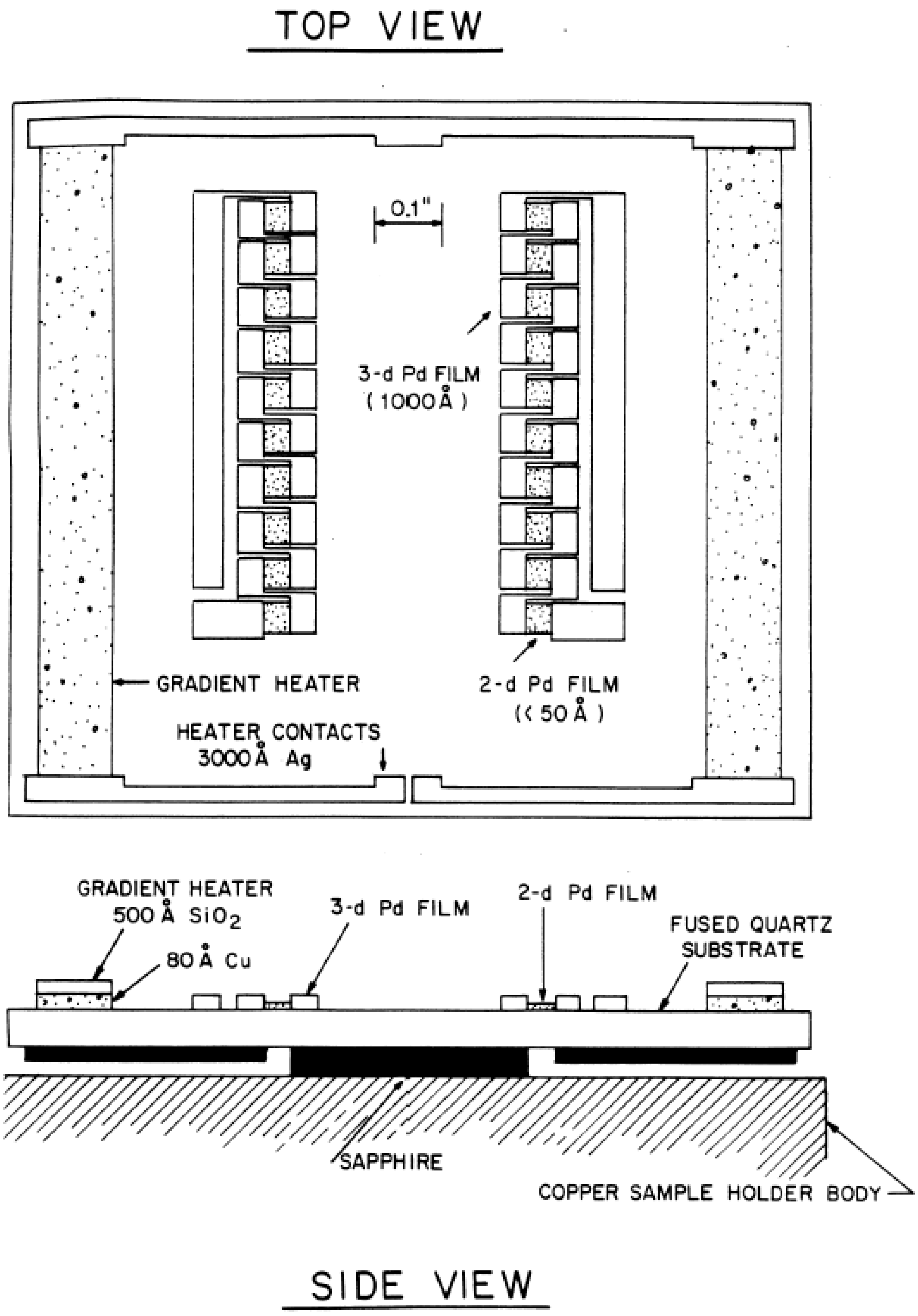
TOP VIEW
0.1"
3-d Pd FILM
(1000 Å)
GRADIENT HEATER
2-d Pd FILM
(< 50 Å)
HEATER CONTACTS
3000 Å Ag
GRADIENT HEATER
500 Å SiO2
80 Å Cu
3-d Pd FILM
2-d Pd FILM
FUSED QUARTZ
SUBSTRATE
SAPPHIRE
COPPER SAMPLE HOLDER BODY
SIDE VIEW

temperature difference.

For more sensitive measurements to check for corrections to the TEP due to the film dimensionality (see section II.G.5), a different apparatus was constructed, illustrated in figure 4-14. Thick films (3-d) and thin films (2-d) were fabricated in a geometry which created two thermopiles each consisting of 10 sample differential thermocouples. This setup should accentuate differences between 2-d and 3-d films of Pd by a factor of 10.

The samples were mounted so that the inner 3-d contacts of the piles rested over a thick single crystal sapphire step heat sink to which the fused quartz substrate was attached. The remainder of the substrate was cantilevered into the vacuum. Two thin film copper (Cu) heaters were electron beam deposited along the outer edges of the substrate and passivated with an overlayer of electron beam deposited SiO_2. Thin single crystal sapphire sheets were attached to the underside of the cantilevered substrate edges under the heaters running to under the outer 3-d contacts of the thermopiles. Thus the heat flow was through the fused quartz substrate to the thick sapphire heat sink. The sapphire sheets under the heaters insured the temperature gradient was perpendicular the the length of the heaters directed in to the center sapphire step heat sink. Lead (Pb) or gold (Au) wires were indium soldered to the two thermopile end pads (located physically next to each other) and to a few other contacts along the pile (to allow a check on the pile uniformity). Two 50-μm Chromel-Constantan differential thermocouples were placed in close proximity to the two thermopiles to monitor the temperature difference.

All sample leads and differential thermocouple leads were heat sunk to the copper sample holder to avoid additional temperature gradients from the room temperature leads. Current was supplied to the heater to establish a temperature difference of ~0.3°K and the voltage from the sample and the differential thermocouple were plotted against each other on an x-y recorder. The current was then turned off and the gradient diminished to check for temperature drifts. An alternate method was sometimes used if the thermal time constants were short enough. The data were taken by continuously applying an offset square wave to the gradient heater. The voltage from the differential thermocouple and the samples were plotted continuously on the y-axis of two separate x-y recorders with the x-axis being the output of a temperature sensor circuit. The peak-to-peak change in the thermocouple and sample voltage supply the necessary

Figure 4-15

Schematics for thermopower measurements.

a) Thermocouple (TC) voltage and sample voltage are plotted against each other as the temperature gradient is turned on and off. The slope is determined by the two steady state (this is not an equilibrium measurement) end points for heater on and heater off. From this slope the thermopower is calculated:

$$\text{SLOPE} = [S_{sample} - S_{leads}]/S_{TC}$$

b) Gradient heater is pulsed and both TC voltage and the sample voltage are plotted versus the independent variable (e.g. temperature or magnetic field). Thermal time constants of the system must be shorter than the gradient heater pulse period.

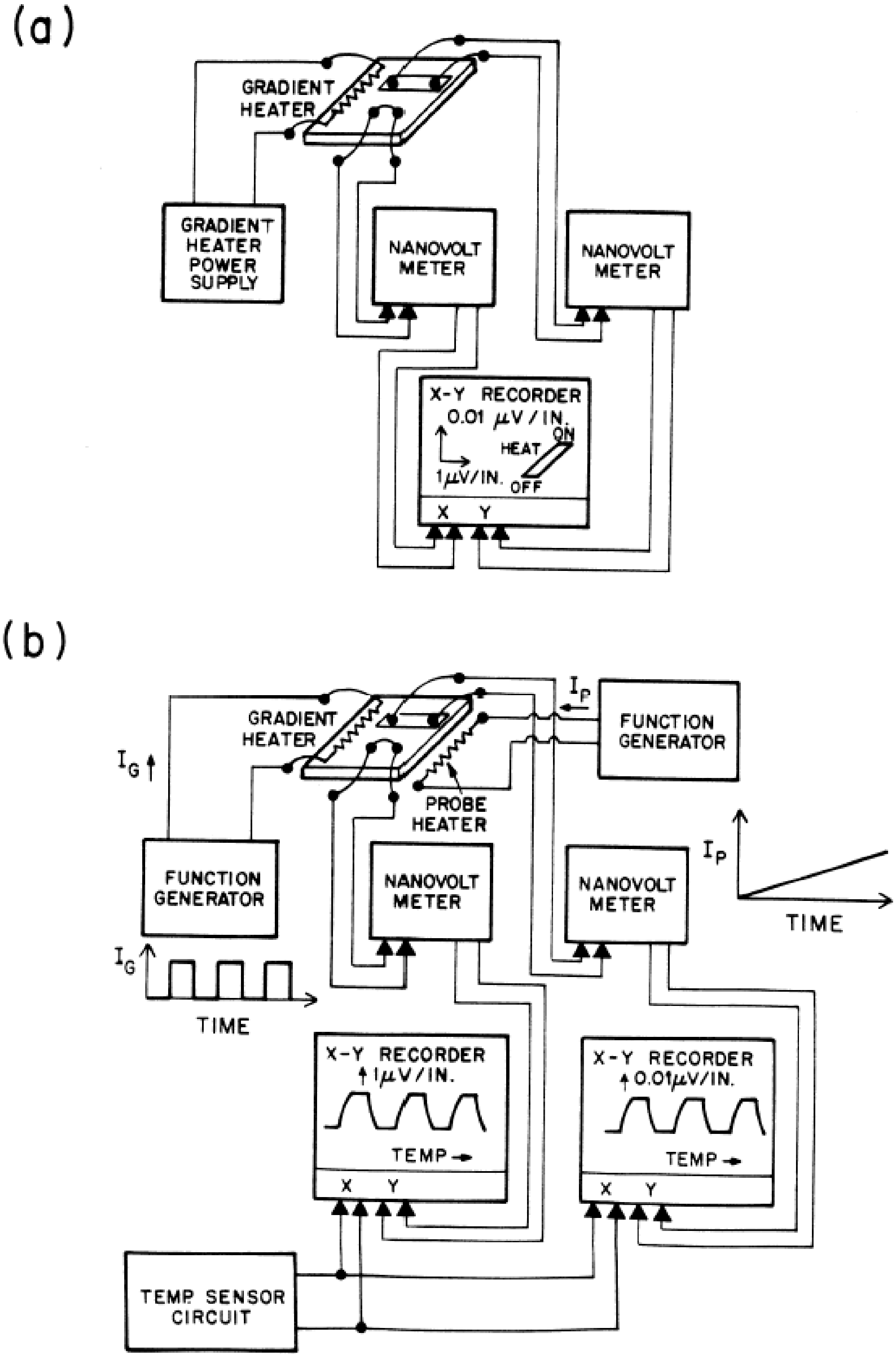
(a)
GRADIENT HEATER
GRADIENT HEATER POWER SUPPLY
NANOVOLT METER
NANOVOLT METER
X-Y RECORDER
0.01 μV / IN.
1μV/IN.
HEAT
ON
OFF
X
Y
(b)
GRADIENT HEATER
I_G
I_P
FUNCTION GENERATOR
PROBE HEATER
FUNCTION GENERATOR
NANOVOLT METER
NANOVOLT METER
I_P
TIME
I_G
TIME
X-Y RECORDER
1μV/IN.
TEMP
X
Y
X-Y RECORDER
0.01μV/IN.
TEMP
X
Y
TEMP. SENSOR CIRCUIT

information for the calculation of the TEP. It is necessary to observe the relative phase of the motion of the two pens to determine a sign change in the thermopower. These alterations can lead to more sensitive measurements of small changes as well as allowing a quasi-continuous monitoring of the TEP as a function of temperature. Both schemes are illustrated in figure 4-15.

To lift an autumn hair is no sign of great strength;
to see sun and moon is no sign of sharp sight;
to hear the noise of thunder is no sign of a quick ear.

The Art of War by
Sun Tzu
(c. 400 B.C.)

CHAPTER V -- EXPERIMENTAL RESULTS AND DISCUSSION

A. Regimes of the Theories

While the theories presented in Chapter II purport to describe the electronic transport of disordered systems, clearly the amount of disorder plays a crucial role in the systems behavior. In the near metallic regime, both the scaling theory and the interaction theory strongly utilize concepts, such as scattering times, valid only in purely metallic systems (and hence extended electronic states). The role of the disorder is to alter the electronic mean free path and hence alter $k_F l$. Both descriptions utilize $(k_F l)^{-1}$, explicitly and implicitly, in perturbation expansions in the near metallic regime, which is where the Ioffe-Regel Rule would say metallic behavior should be observed. The theories all agree that very weak non-metallic behavior should be observed in two dimensions when $k_F l>1$, gradually changing to strong localization when $k_F l<1$, with the 'boundary' between the regimes at $k_F l<1$. As we shall see, crossing this 'boundary' has a dramatic effect on some transport properties and very little on others.

Alice laughed. "There's no use trying," she said: "one *ca'n't* believe impossible things."

"I daresay you haven't had much practice," said the Queen. "When I was your age, I always did it for half-an-hour a day. Why, sometimes I've believed as many as six impossible things before breakfast."

Through the Looking-Glass by
Lewis Carroll
(Charles Lutwidge Dodgson)
(1832-1898)

B. Palladium and Palladium-Gold Films on Glass and Quartz

1. Temperature Dependence of the Resistivity

The surprising predicions of the various theories of the nonmetallic behavior for two dimensional electronic systems, even when the Ioffe-Regel criteria for metallic conduction are satisfied, has stimulated considerable interest in 2-d systems in recent years.

The various theories describing the electronic transport in these disordered systems give radically different predictions for the resistivity (or conductivity) depending upon whether the product of the Fermi wavevector (k_F) and the mean free path (l) satisfies this Ioffe-Regel criteria ($k_F l>>1$). In the regime where metallic conduction should take place (a la Ioffe-Regel), both the single particle scaling theory and the interacting electron theory predict similar behaviors for the conductivity. A logarithmically decreasing conductivity with decreasing temperature is predicted (equations II.36, II.68, II.116 and II.135) given by:

$$\sigma(T) = \sigma_{\circ} + (e^2/[2\pi^2\hbar])\alpha \ln(T) \qquad (V.1)$$

where

$$\alpha = \begin{cases} p & \text{(scaling, no spin-orbit)} \\ -(p/2) & \text{(scaling, spin-orbit)} \\ & \\ 1-F & \text{(interaction, no spin-orbit)} \\ 1-(3/4)F & \text{(interaction, spin-orbit)} \end{cases} \tag{V.2}$$

with p and F given by equations II.37 and II.66. As the disorder in the system is increased, the conductivity should, according to these theories, gradually change to a variable range hopping scheme (with or without interactions), becoming (equations II.44 and II.92):

$$\sigma(T) = \begin{cases} \sigma_{\circ}\exp\{ -(T_{\circ}/T)^{1/3} \} & \text{(noninteracting)} \\ & \\ \sigma_{\circ}\exp\{ -(T'_{\circ}/T)^{1/2} \} & \text{(interacting)} \end{cases} \tag{V.3}$$

where $T_{\circ}$ and $T'_{\circ}$ are given by equations II.45 and II.93. One must bear in mind that even the thinnest metal films in this study, while cracked, are structurally and electrically continuous (see section IV.A.1), so one would not expect grain to grain (or island to island) tunneling (see Abeles, 1976) to ever dominate the transport. Behavior along the lines of equations V.1 and V.3 has been observed in a variety of metal film systems

Figure 5-1

Resistivity as a function of temperature from a wide selection of palladium and palladium-gold films used in these studies.

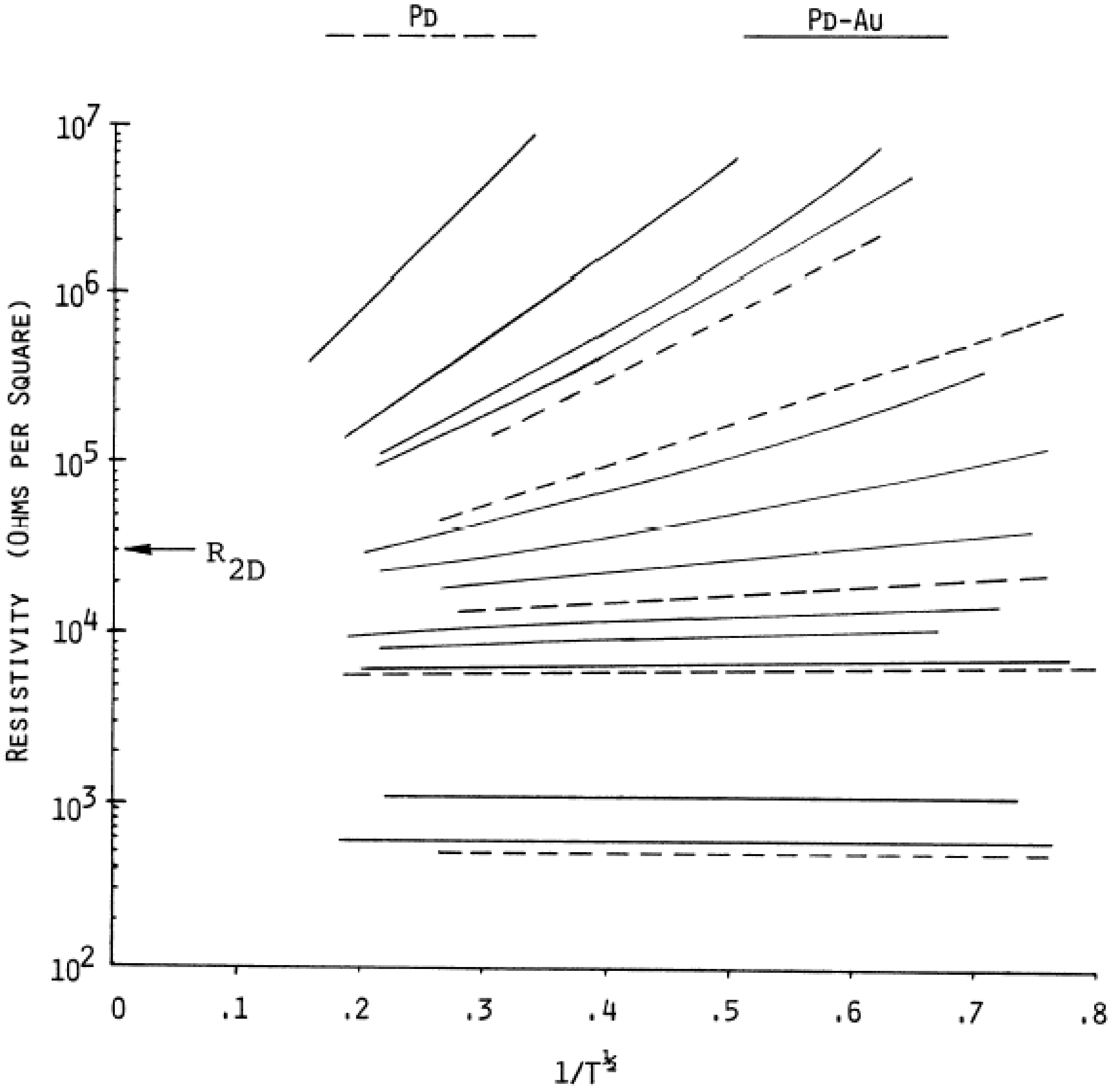
Pd
Pd-Au
10^7
10^6
10^5
10^4
10^3
10^2
Resistivity (Ohms per Square)
R_{2D}
0
.1
.2
.3
.4
.5
.6
.7
.8
$1/T^{1/3}$

Figure 5-2

Resistivity change divided by the square of the resistivity as a function of temperature. These films appear flat on figure 5-1.

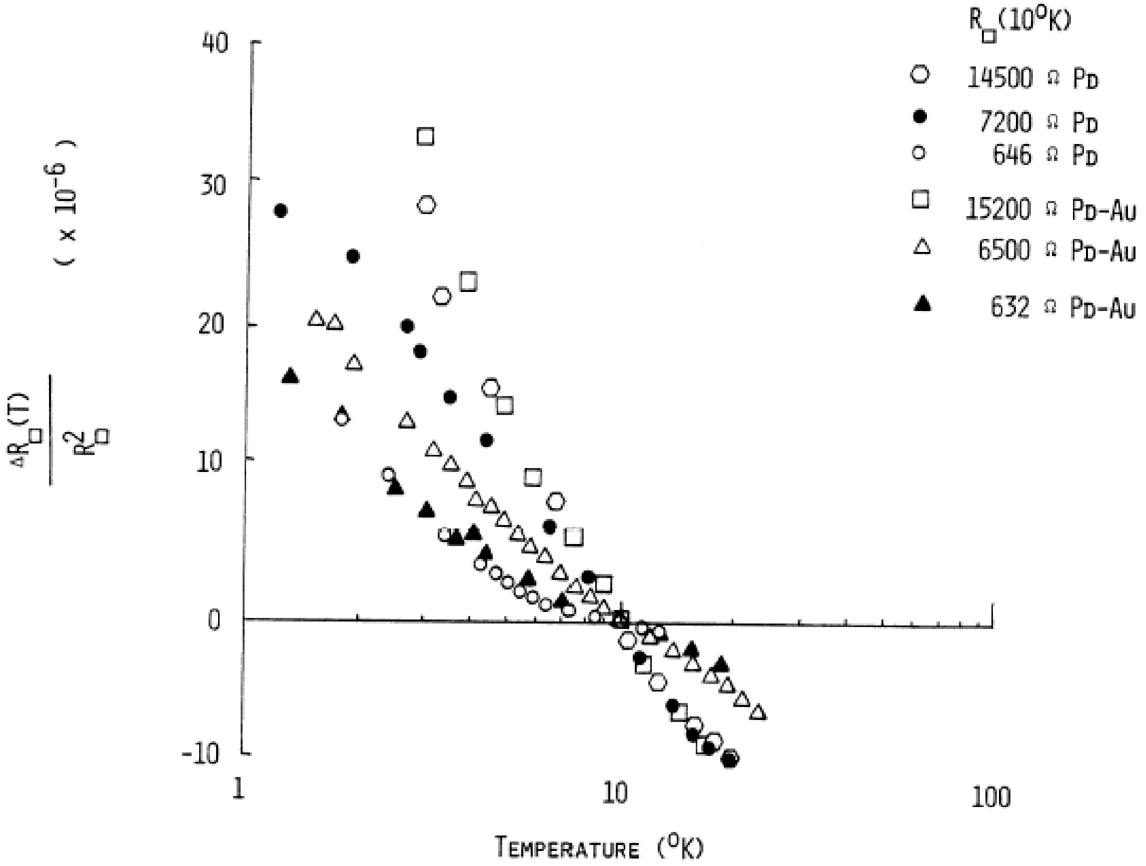
$\frac{\Delta R_{\square}(T)}{R_{\square}^2}$ (x 10^{-6})
40
30
20
10
0
-10
1
10
100
Temperature (°K)
R$_{\square}$(10°K)
○ 14500 Ω Pd
● 7200 Ω Pd
○ 646 Ω Pd
□ 15200 Ω Pd-Au
△ 6500 Ω Pd-Au
▲ 632 Ω Pd-Au

Figure 5-3

Resistivity as a function of temperature from 100 mK to 4.2^{o}K. This film would appear flat on figure 5-1.

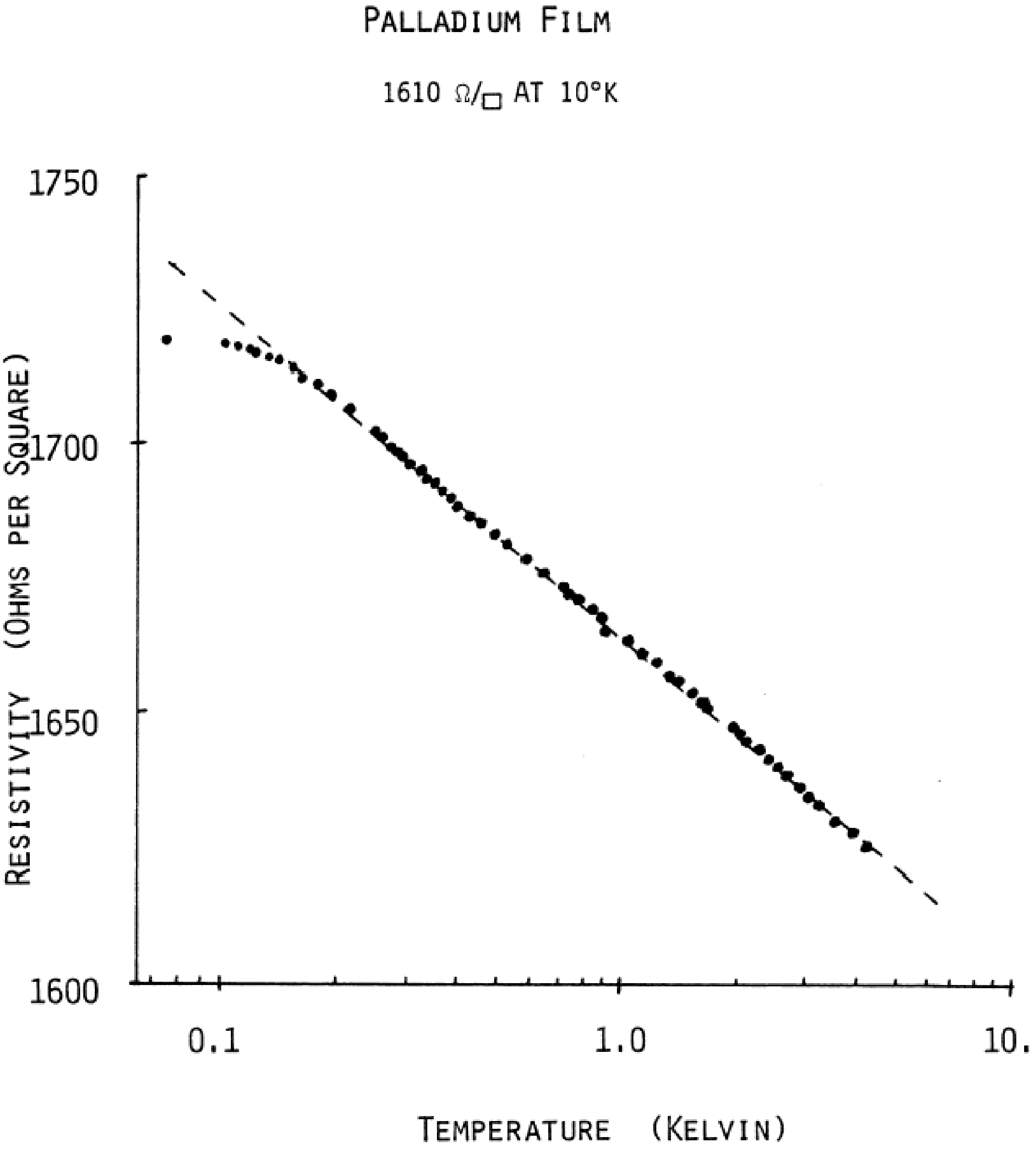

PALLADIUM FILM

1610 Ω/□ AT 10°K

(Dynes, Garno and Rowell, 1978, also Dolan and Osheroff, 1979).

Figure 5-1 shows the logarithm of the resistivity vs the inverse square root power of T of several Pd and Pd-Au films, with film thicknesses ranging from ~18 Angstroms up to ~30 Angstroms. These films were fabricated on glass substrates by the method described in section IV.A. The thicker films display a lower resistance per square ($R_\#$), which appears flat on the scale used in this figure. Films with resistivities higher than R_{2D} ($R_{2D} = [\sigma_{2D}]^{-1}$, see equation I.21) display a temperature dependence varying exponentially with an inverse root power of temperature, consistent with equation V.3. This behavior is identical to that reported by Dynes, Garno and Rowell (1978) for thin quench condensed copper and gold films. The slope of the high resistivity films is such that extrapolation of the resistivity for $T=\infty$ gives $R_\#(\infty)<R_{2D}$.

Low resistivity films ($R_\#<R_{2D}$), which appear flat on the scales used in figure 5-1, do vary logarithmically with temperature as illustrated in figure 5-2. This logarithmic behavior comes in at some finite temperature (above <4°K), with thinner films displaying this logarithmic behavior at higher temperatures, and continues down to low temperatures (see Figure 5-3).

Equation V.1 can be easily manipulated to give

$$\Delta R(T)/[R_o^2] = -e^2/[2\pi^2\hbar]\alpha\ln(T) \qquad (V.4)$$

and as figure 5-4 illustrates, the characteristic slope is relatively constant (α=1) below <10^4 ohms/square, then increases sharply with increasing resistivity, resulting in slopes neither scaling or interaction theories predict. This later behavior is not surprising, considering that the crucial assumption of the near metallic limit used to derive equation V.1, namely that $k_F l>1$, is starting to break down. These results are consistent with the results of other groups. Dolan and Osheroff (1979) found α=0.8-1.8 for Pd-Au films, Masden and Giordano found α=1 for Pd-Au films. All of these systems are in the dirty limit (see equations II.31 through II.37). Van den Dries, et. al. (1981) found for clean copper films, S=2.

In this study, the range where the characteristic logarithmic slope is relatively constant (below <5000 ohms/square), α=~1.0. This is not helpful in suggesting a mechanism for the nonmetallic behavior, i.e. choosing between the relative contributions of localization (scaling) and interaction effects. One should bear in mind that according to the theories (Chapter II), for two

Figure 5-4

Characteristic logarithmic slope of a random selection of 'flat' films in figure 5-1 as a function of resistivity. The theories claim:

$$\alpha = \begin{cases} p & \text{(scaling, no spin-orbit)} \\ -(p/2) & \text{(scaling, spin-orbit)} \\ & \\ 1-F & \text{(interaction, no spin-orbit)} \\ 1-(3/4)F & \text{(interaction, spin-orbit)} \end{cases}$$

where α appears in equation V.1 , p and F are given by equations II.37 and II.66.

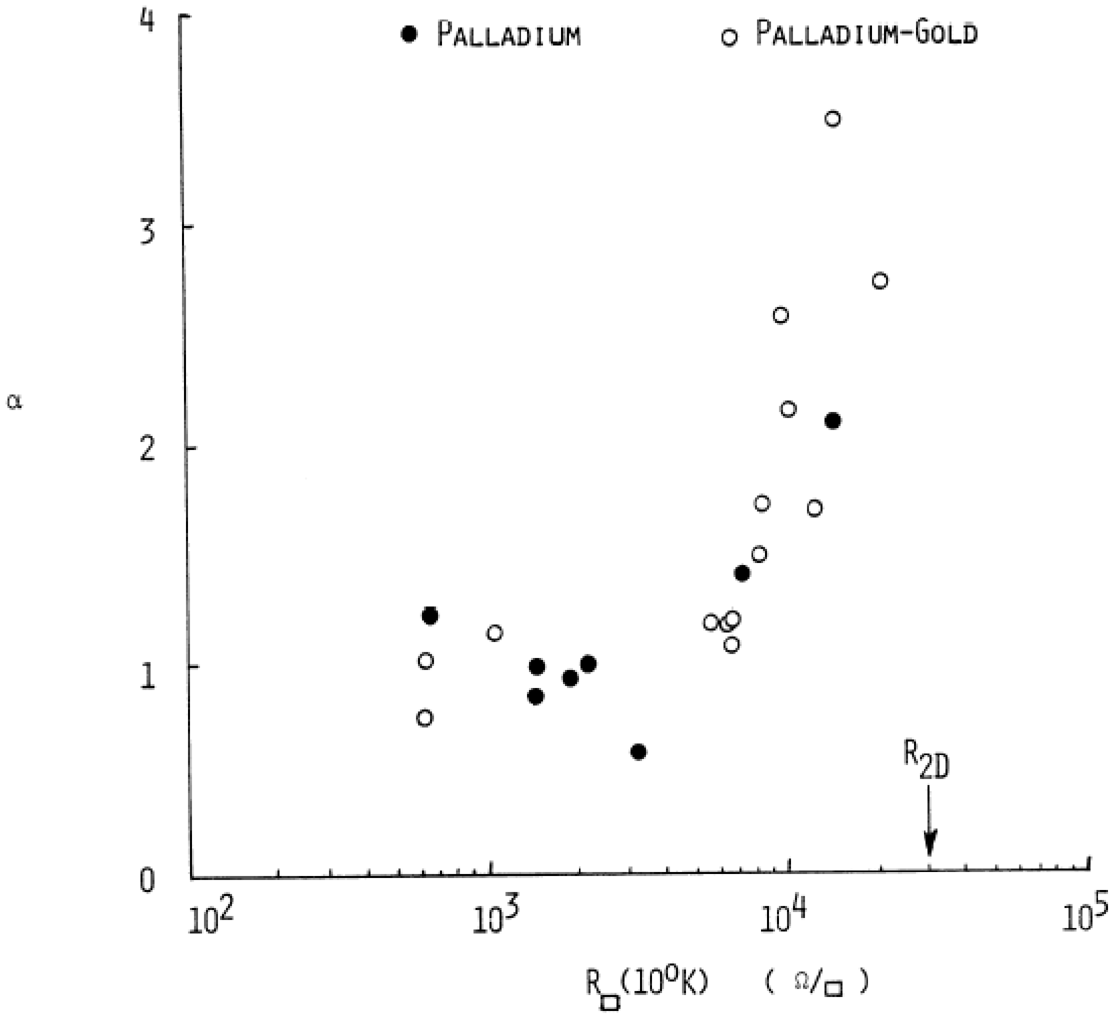
● PALLADIUM
○ PALLADIUM-GOLD
4
3
2
1
0
α
R2D
10^2
10^3
10^4
10^5
R□(10°K) (Ω/□)

dimensions p=1,2 or 3 (or possibly 4, if the phonons are three dimensional) and 0<F<1. The observed behavior for these films (in the near metallic regime) is consistent with the scaling theory alone, with p=1 or 2, depending upon the importance of the spin-orbit interaction. The behavior is consistent with the interaction picture alone, only in the limit of perfect screening (F=0) regardless of the presence of spin-orbit interactions. If both interaction and localization effects are present (and function independently), and can be combined linearly, the observed behavior is only consistent with p=F=1 and no spin-orbit interactions present.

Films with resistivities above R2D are consistent with equation V.3. Fits of the fractional power range from <.4 to <.7, however as can be seen from figure 2-12, even extremely high precision measurements, giving very good fits to a model (within 2% in the exponent), look to the casual observer to be equally well described by almost any fractional exponent. While resistivity is usually a simple measurement to produce with precision, normal ultra thin films generally are strongly nonlinear (see section V.B.2), perhaps surpassed only by granular superconducting systems, yet also of such high impedance, that attempting to distinguish between two very similar fractional powers inside an exponent yields less than optimal results. The measurements presented in figure 5-1, while generally more consistent with a 1/2 exponent than with a 1/3 exponent, are very far from conclusive.

As the above, simple analysis illustrates, the temperature dependence of the resistivity of these films, within the framework of the various theories, is incapable of distinguishing between the various possible contributions to the electronic transport. Clearly other transport measurements, particularly measurements dominated by one fundamental property of the system, such as the electronic density of states, are needed. As we shall see in the sections which follow, these other measurements answer some of our questions about two dimensional transport, and also suggest many others.

B. Palladium and Palladium-Gold Films on Glass and Quartz

2. Electric Field Dependence of the Resistivity

The application of an electric field to any electronic system with a nonzero conductivity will result in exciting some of the electrons from states just below the Fermi energy to states just above. This is done in such a way as to skew the momentum distribution of the electrons, resulting in a net nonzero velocity, and hence a current. In a localized system, this response of the electron population can alter the conductivity itself, resulting in non-ohmic behavior.

In the near metallic regime, the electric field dependence can arise from the electron and the phonon (lattice) temperatures being out of equilibrium. In the scaling theory, the electric field can also change the localization length directly (Tsuzaki, 1981). In both scaling and interaction pictures, this 'heating model' predicts, for two dimensions and high fields ,(equation II.101)

$$\sigma(E) = \sigma_o + (e^2/[2\pi^2\hbar])[2p/(2+p')]\ln(E/E_o) \qquad (V.5)$$

where p' is the electron-phonon scattering time exponent (equation II.100) and, in the scaling theory, p is the total inelastic scattering time exponent. At low fields this model predicts a quadratic electric field dependence. The interaction picture also suggests a logarithmic electric field dependence similar to equation V.5 with p=1-F (or presumably, p=1-(3/4)F in the presence of strong spin orbit coupling). The model for the scaling theory by Tsuzaki predicts a high field behavior similar to equation V.5 but with 2p/(2+p')=2/3.

In the insulating regime, the electric field inserts a direction dependence into the hopping probability, which has the same effect as distorting the shape of the wavefunction (equation II.105). The net effect is to render the conductivity independent of the electric field at low fields and/or high temperatures, and very non-linear at high fields and/or low temperatures (equation II.109):

$$\sigma(E,T) = \sigma(T)[(2\alpha K_b T)/(eE)]\sinh[(eE)/(2\alpha K_b T)] \qquad (V.6)$$

where $\sigma(T)$ is given by either equation II.44 or II.92 and α^{-1} is the characteristic length over which the localized wavefunction tails off.

If the electric field is very large, so that the probability to hop against the field is extremely low,

Figure 5-5

Dynamic resistivity of a Pd film in the near metallic regime. Resistivity is logarithmic with electric field. This film would give $p' \sim 2$ in equation V.5.

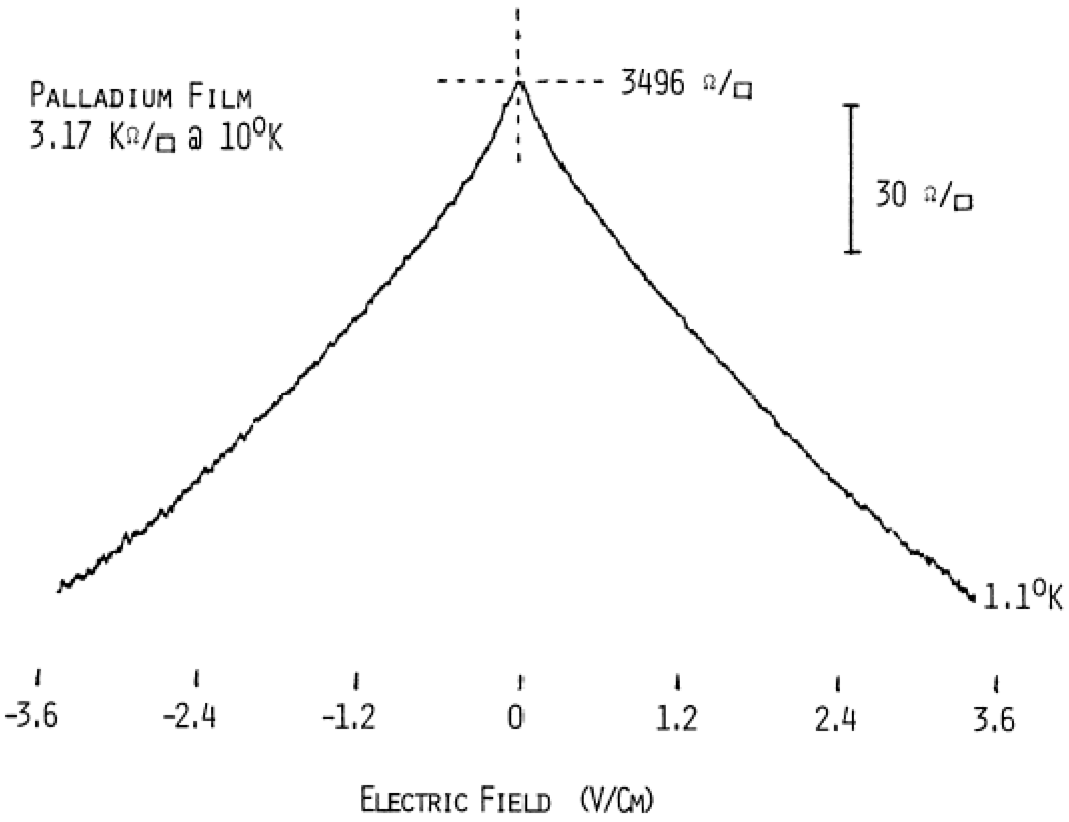
PALLADIUM FILM
3.17 KΩ/□ @ 10°K
3496 Ω/□
30 Ω/□
1.1°K
-3.6
-2.4
-1.2
0
1.2
2.4
3.6
ELECTRIC FIELD (V/CM)

Figure 5-6

J-E characteristic of a 26KΩ/square (at 10^{o}K) Pd film. Behavior is consistent with equations V.8 and V.8 with $(1/\alpha)\sim$ 5050 Angstroms. R~264 Angstroms at 1^{o}K and 123 Angstroms at 10^{o}K.

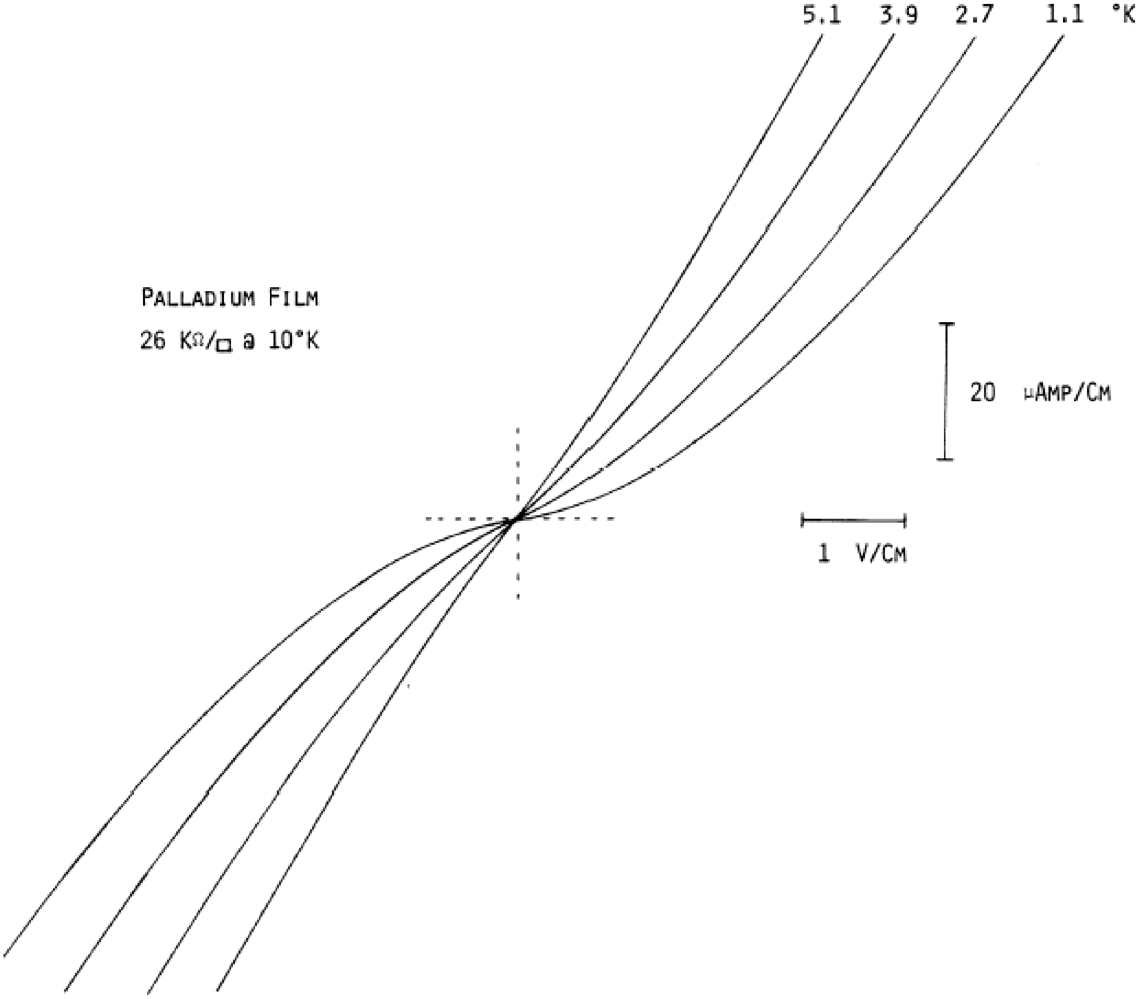
5.1
3.9
2.7
1.1
°K
Palladium Film
26 KΩ/□ @ 10°K
20 μAmp/Cm
1 V/Cm

Figure 5-7

J-E characteristic of a 480 KΩ/square (at 10°K) Pd film. Behavior is consistent with equations V.6 and V.8 with $(1/\alpha)\sim2420$ Angstroms. $R\sim206$ Angstroms at 1°K and 96 Angstroms at 10°K.

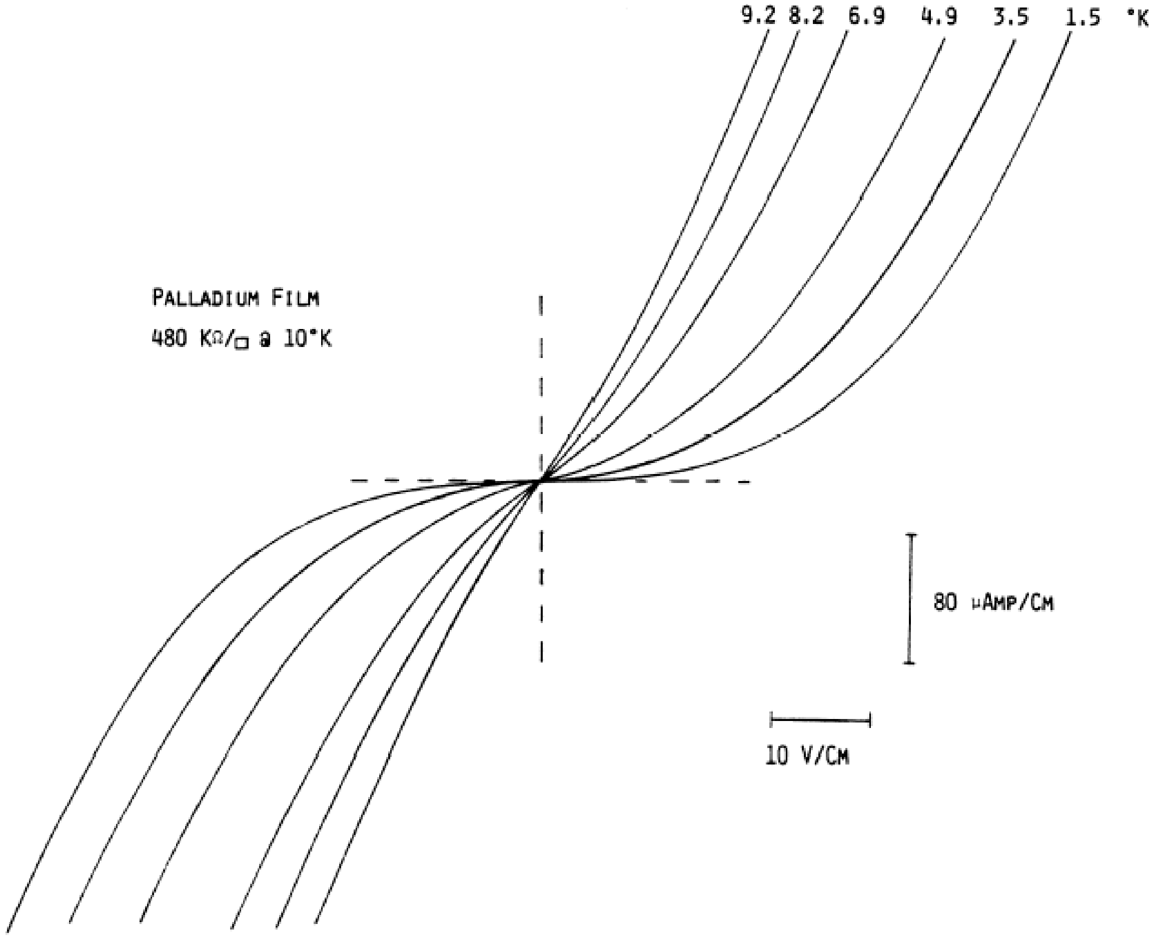
9.2 8.2 6.9 4.9 3.5 1.5 °K
PALLADIUM FILM
480 KΩ/□ @ 10°K
80 μAMP/CM
10 V/CM

then the averaging over $\cos\theta$ in section II.F.2 can be dropped (equation II.107) such that equation II.108 becomes

$$P_{max}(T,E) = P_{max}(T)\exp\{ eE/[2\alpha K_b T] \} \quad (V.7)$$

and equation II.109 becomes

$$\sigma(T,E) = V(T)\exp\{ eE/[2\alpha K_b T] \} \quad (V.8)$$

In figure 5-5 is plotted the dynamic resistance at ~1°K of a Pd film in the near metallic limit. This film displays a logarithmically decreasing resistivity with increasing electric field, consistent with p=1 and p'<2 in equation V.5. The electric field behavior of films used in these studies, in the near metallic regime, are consistent with the studies by McGinnis (1983) of similar films.

Figures 5-6 and 5-7 show the current density versus electric field characteristics of some Pd films whose resistivities (as a function of temperature) are passing through R_{2D} and are well above R_{2D}. As one can see from these plots, the films are ohmic (on the scales presented here) above 5-10°K, with the higher resistivity films deviating from ohmic behavior at higher temperatures. Although these traces are D.C., this behavior is intrinsic and not due to sample heating. The power dissipation is less than a few milliwatts/cm^2 in the films, which are in intimate contact with the substrate. These measurements were also checked against pulsed measurements which confirm that no sample heating took place.

Both equations V.6 and V.8 work well at describing the behaviors in figures 5-6 and 5-7, with V.6 working best at low resistivity and high temperatures and V.8 working best at high resistivity and lower temperatures. Fits of the data to equations V.6 and V.8 gave similar values for α, with α independent of temperature for the 480 KΩ/square (at 10°K) film in figure 5-7 and a very slight decrease in S with increasing temperature for the 26 KΩ/square (at 10°K) film in figure 5-6.

These films indicate that α has only a weak dependence on the resistivity, with the 480 KΩ/square film giving α^{-1}~2420 Angstroms and the 26 KΩ/square film giving α^{-1}~5050 Angstroms, indicating a factor of 20 in resistivity implies only a factor of 2 in the spatial extent of the wavefunctions. These values for S-1 indicate that the localized state wavefunctions are extended over very many grains, implying the detailed grain structure of the films is not important in determining the transport properties of these films (see figure 4-1). Using these values of α^{-1}, and 32.7 (states/atom)/Ry (from Anderson, 1970) for the bulk density of states at the Fermi energy for Pd, and an average film thickness of ~25 Angstroms, one finds the characteristic hopping distance (equation II.41 for the noninteracting case) to range from 264 Angstroms at 1°K for the 26KΩ/square sample down to 96 Angstroms at 10°K for the 480 KΩ/square film. All of these hopping lengths are comparable to the grain size of these films (see figure 4-1).

B. Palladium and Palladium-Gold Films on Glass and Quartz

3. Magnetic Field Dependence of the Resistivity

Previous studies of the magnetotransport of Pd and Pd-Au films identical to some of those used in this study by McGinnis, et.al. (1981,1983, and 1984) indicate, for the near metallic regime, that electronic transport in these films is dominated by localization effects with strong spin-orbit coupling present. The magnetoresistance was positive in the near metallic regime, going as H^2 in weak fields changing over to log(H) in strong fields. The magnetoresistance became less anisotropic as the film disorder increased, becoming completely isotropic for films with resistivities above ~5 Kohms per square. In this study, an examination of the magnetotransport in the transition region between the near metallic and insulating regimes was undertaken.

Magnetoresistance measurements on 'classic' variable range hopping systems usually yield a negative, rather than positive magnetoresistance. Amorphous Ge (Clark, et.al., 1974), degenerate CdS (Khosla, et.al., 1970) and Si (Roth, et.al., 1963) all display a negative

magnetoresistance, although some of these materials (such as CdS) can display a positive magnetoresistance at high fields. As was pointed out in the preface of section II.F, if the Fermi level is near a mobility edge, the presence of the magnetic field can skew the electron population statistics such that carriers are dumped into the conduction band, or high order exchange scattering between extended and localized magnetic moments can be suppressed by a magnetic field. Both effects could and have been used in attempts to explain the magnetotransport in the above systems, although neither model works very well.

An examination of the density of states for bulk palladium (see for example, Mueller, et.al., 1970) shows the Fermi level to be ~0.5 eV away from the d-band edge and even further from the s-band edge (and inside the bands), so it is not too surprising that the positive magnetoresistance these films display in the near metallic regime is continued in the insulating regime.

Figure 5-8 shows the fractional change in the resistivity with applied magnetic field (perpendicular to the film plane) for two Pd films, one of which crosses R_{2D} at ~10°K, the other at ~5°K. As can be seen, the magnetoresistance is small and positive, scaling as H/T, which strongly suggests a spin effect. While this

Figure 5-8

The fractional change in the magnetoresistance of Pd films on glass scales as H/T, essentially independent of the resistivity.

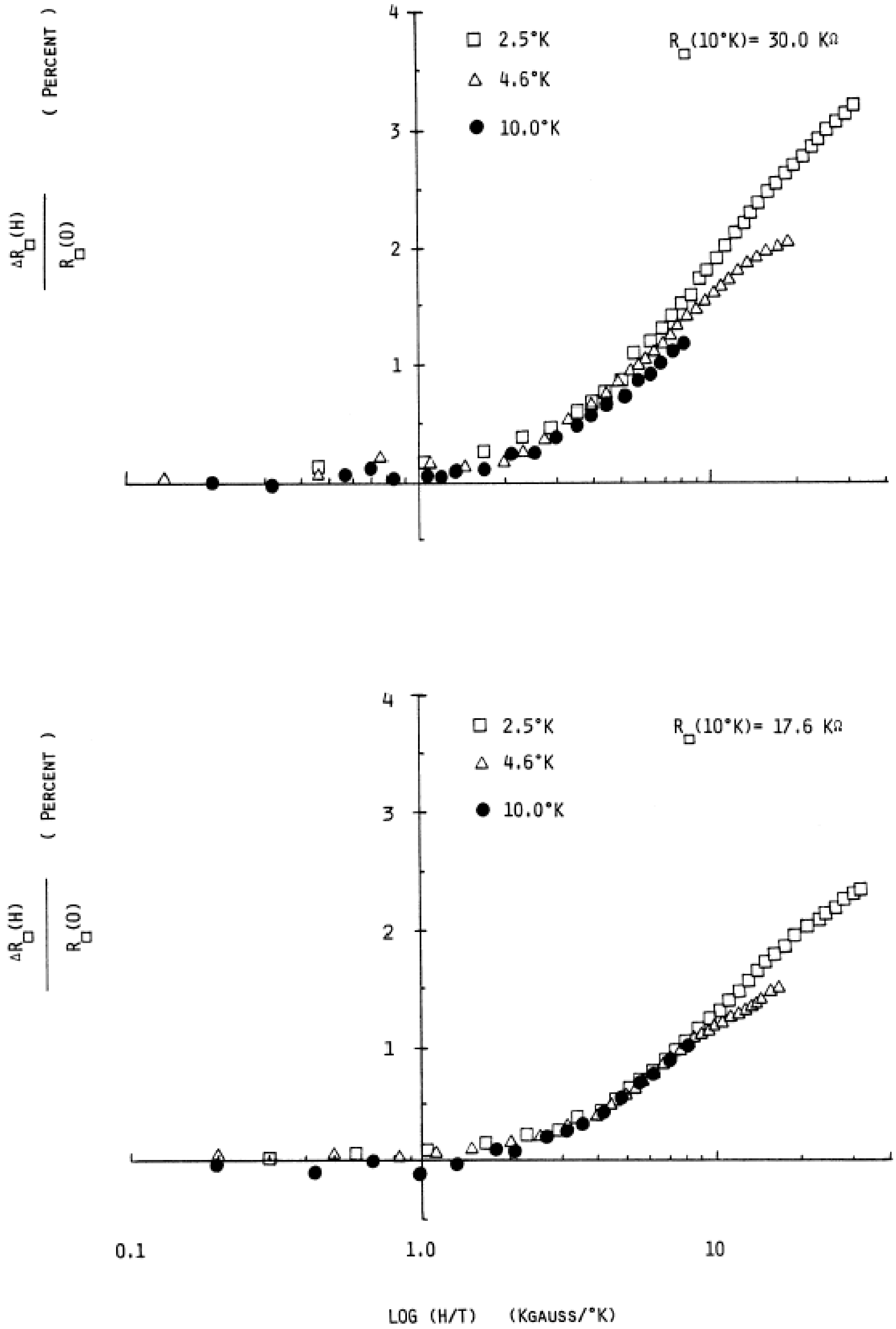
4
3
2
1
□ 2.5°K
△ 4.6°K
● 10.0°K
$R_\square(10°K) = 30.0\ K\Omega$
$R_\square(10°K) = 17.6\ K\Omega$
$\frac{\Delta R_\square(H)}{R_\square(0)}$ (PERCENT)
0.1
1.0
10
LOG (H/T) (KGAUSS/°K)

behavior is consistent with the results of McGinnis, et.al. for the near metallic regime, in view of the description of insulating regime magnetotransport (section II.F.4), the continuation of this near metallic regime behavior well into the insulating regime (for example, the 30 Kohm/square at 10°K film is <230Kohms/square at 2.5°K) is surprising.

A shrinking wavefunction explanation (section II.F.4.i) seems very inadequate in view of the fact that this mechanism predicts generally predicts magnetoresistances to scale as $\sim(H^2)/T$ and/or $\sim H/(T^2)$, and would tend to predict an effect many orders of magnitude larger than that observed.

The straightforward application of the Zeeman Effect (section II.F.4.ii) to variable range hopping yields a prediction more compatible with the behavior displayed in figure 5-8. Equation II.159 can be manipulated to give the fractional change in the resistivity,

$$(\Delta R(T,H))/R(T) = 1 - [\cosh(h)]^{-1} \qquad (V.9)$$

where $h=g\mu_B H/[K_b T]$. This predicts the data should scale as H/T, which appears to be the case. Unfortunately, equation V.9 predicts a much faster rise in $(\Delta R)/R$ with magnetic field (if $g=2$) than the data display. No adjustment of g will give a reasonable fit to the data. Equation V.9 does however, correctly predict the fractional change in the resistivity, with applied field, depending only on H/T and not on the ohms per square, as both the scaling and interaction pictures would indicate (assuming the results of sections II.F.3.ii and II.F.3.iv could be extended into the strongly localized regime).In fact, the theoretical description given in section II.F.4.ii works well if we assume only some net fraction, ξ, of the electron population dominating the transport is affected by the magnetic field. If that is so, the conductivity might be divided between a magnetic field independent part and a field dependent part:

$$\sigma(T,H) = [1-\xi]\sigma(T) + \xi\sigma_{Zee}(T,H) \qquad (V.10)$$

where $\sigma_{Zee}(T,H)$ is given by equation II.159 and $\sigma(T)$ is given by either equation II.44 or II.92, depending on the importance of the Coulomb interaction. Equation V.10 can be manipulated to give

$$(\Delta R(T,H))/R(T) = \{ ([2\cosh(h)-1]/[\xi\{\cosh(h)-1\}]) - 1 \}-1 \qquad (V.11)$$

where $h=g\mu_B H/[K_b T]$. Assuming g=2 and fitting the data in figure 5-8 to equation V.11, results in $\xi \sim 0.055 - 0.039$ for the film in the top of the figure and $\xi \sim 0.038 - 0.033$ for the film at the bottom. This would seem to imply, in view of the Einstein relation (equation II.7), that the shift in energy in the density of states due to the field induced spin splitting, eliminates only a few percent of the previously available final states.

B. Palladium and Palladium-Gold Films on Glass and Quartz

4. Thermoelectric Power

The various transport properties examined so far have been incapable of separating the contributions to the electronic transport due to changes in the carrier mobility (e.g. Mott Variable Range Hopping) from changes in the electronic density of states. Resistance (and magnetoresistance) measurements probe the carrier density and mobility but not the carrier energy distribution. The thermoelectric power (section II.G), S, is an excellent probe of the carrier energy distribution about the Fermi energy (E_f). As pointed out in section II.G.4, if the energy distribution falls to zero as T-->0 then S-->0, which is the case for metals as well as for Mott variable range hopping. If S increases as T-->0 then the conducting electrons transport more than thermal energy and there is evidence for the existence of an energy gap.

In the near metallic regime, the characteristic heat a carrier transports is K_bT, just as it is in a metal. The non-metallic behavior of the conductivity predicted by the scaling theory arises from an alteration of the carrier mobility and therefore has no effect on the thermopower (section II.G.5.i). The non-metallic conductivity behavior predicted by the interaction picture is a consequence of a logarithmic correction to the density of states (equation II.60) and therefore shows up as a logarithmic correction to the thermopower (section II.G.5.ii). The two theories predict, for the near metallic regime (equations II.222 and II.229):

$$S(T) = \begin{cases} S_\circ(T) & \text{(scaling)} \\ S_\circ(T)[\ 1 - (1/2)\xi\ ] & \text{(interaction)} \end{cases} \qquad \text{(V.12)}$$

where

$$\xi = \{(e^2)/[\sigma_\circ\pi^2\hbar]\}(1-F)\ln(T/T') \qquad \text{(V.13)}$$

In both the single particle and the interacting electron variable range hopping schemes, the characteristic heat a carrier transports is the average hopping energy, Ehop, rather than KbT. In two dimensions, this is (equation II.233)

$$\mathbf{E_{hop}} = \begin{cases} \left(\mathcal{D}_o(\mu)\pi\right)^{-\frac{1}{3}} (\alpha K_b T)^{2/3} & \text{(noninteracting)} \\ \left[\frac{e^2}{K} \quad 2\alpha K_b T\right]^{\frac{1}{2}} & \text{(interacting)} \end{cases} \qquad \text{(V.14)}$$

which results in a thermopower given by

$$\mathbf{S(T)} = \frac{K_b}{2e} \left[\frac{\mathcal{D}_o(\mu)\pi}{\alpha^2}\right]^{-\frac{2}{3}} \left[\frac{\partial \ln \mathcal{D}(\varepsilon)}{\partial \varepsilon}\right]_{\varepsilon=\mu} \left(K_b T\right)^{1/3} \qquad \text{(V.15)}$$

for the noninteracting case at all temperatures and for the interacting case when $T>T_c$, where in two dimensions

$$T_c = 1/(\alpha K_b) \ (e^2/K)^3 \ [D_o(\mu)\pi]^2$$

For $T<<T_c$, the interacting case predicts the thermopower to be a constant independent of the system dimensionality,

$$S(T)_{\mathbf{int}} = \frac{K_b e}{K} \alpha \left[\frac{\partial \ln \mathcal{D}(\varepsilon)}{\partial \varepsilon}\right]_{\varepsilon=\mu} \qquad T<<T_c \ \text{(V.16)}$$

Figure 5-9 shows a plot of the logarithm of the resistivity as a function of the square root of the reciprocal temperature for a variety of Pd and Pd-Au films fabricated on glass, using the method described in

Figure 5-9

Logarithm of the resistivity (in ohms/square) as a function of reciprocal square-root temperature for (a) palladium, (b) palladium-gold films used in the thermopower study. The same symbol for each film (within a material type) has been used in figures 5-9 through 5-12.

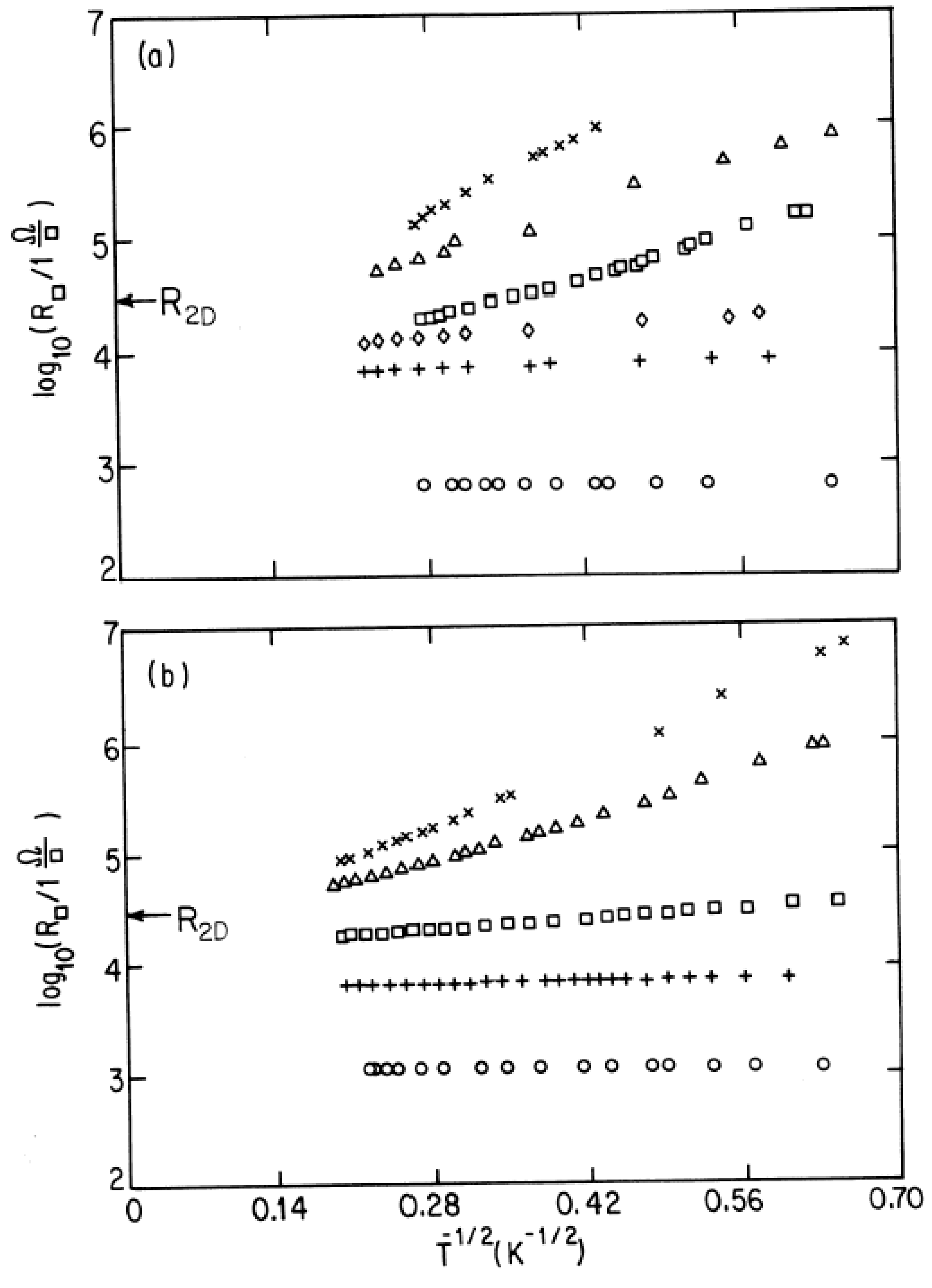
(a)
(b)
7
6
5
4
3
2
$\log_{10}(R_\square/1\frac{\Omega}{\square})$
R2D
0
0.14
0.28
0.42
0.56
0.70
$T^{-1/2}(K^{-1/2})$

Figure 5-10

Resistivity change divided by square of resistivity as a function of $\log_{10}T$ for (a) three Pd and (b) two Pd-Au film samples which show 'metallic' thermopower.

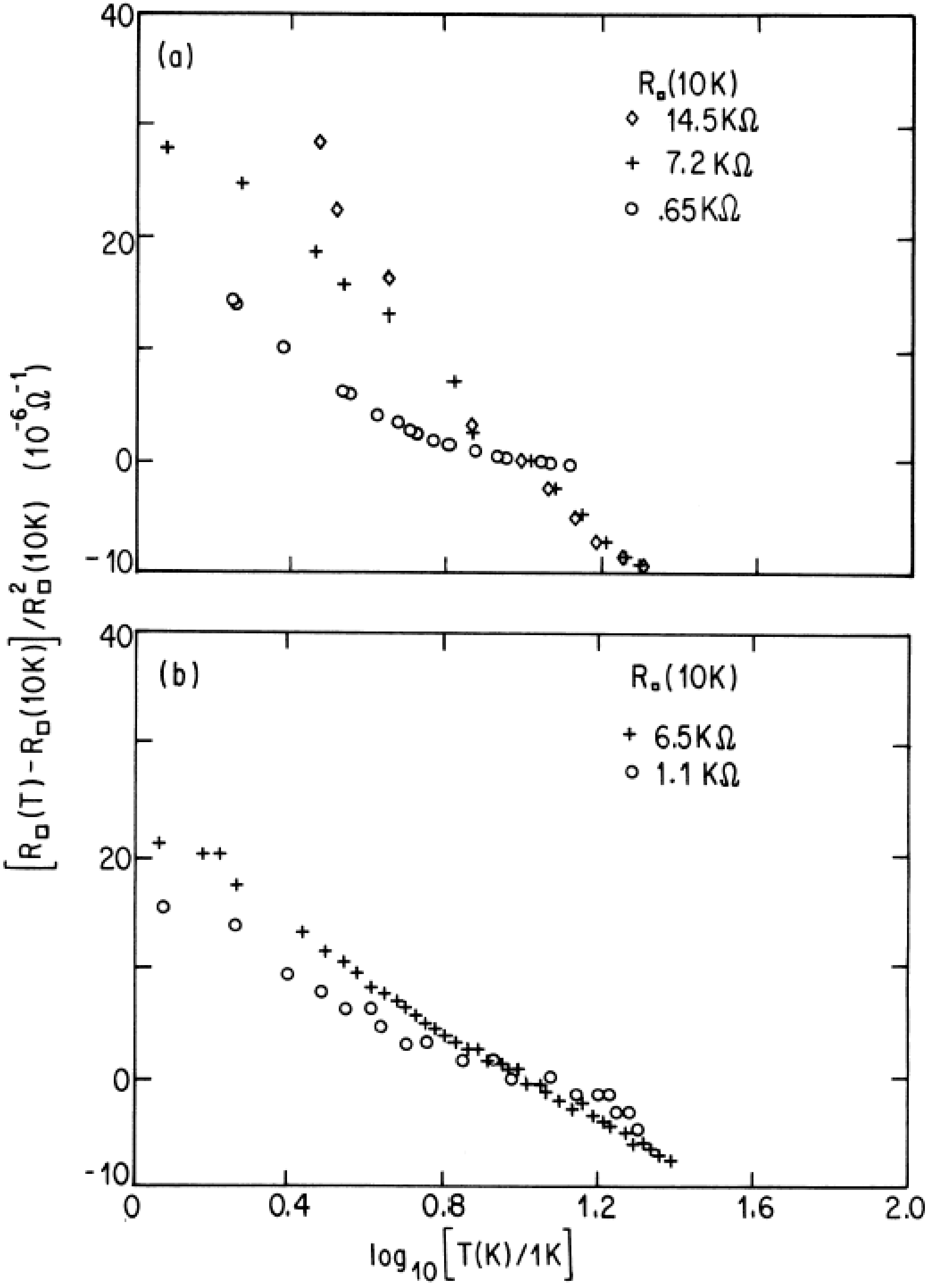(a)
R□(10K)
◇ 14.5 KΩ
+ 7.2 KΩ
○ .65 KΩ
(b)
R□(10K)
+ 6.5 KΩ
○ 1.1 KΩ
40
20
0
-10
[R□(T) - R□(10K)]/R□²(10K) (10⁻⁶Ω⁻¹)
0
0.4
0.8
1.2
1.6
2.0
log₁₀[T(K)/1K]

section IV.A.1, of nominal thicknesses of 18-25 Angstroms. Comparison of figure 5-9 and figure 5-1 shows these films to be indistinguishable. For resistivities greater than R_{2D} the temperature dependence is approximately an exponential with a square-root inverse power of temperature. For resistivities less than R_{2D} the temperature dependence of the resistivity is considerably less and the resistivities appear flat on these plots.

In figure 5-10 the films which appear flat in figure 5-9 have been plotted to show their resistivity increasing with a logarithmic decrease in temperature.

The resistivity studies show that these Pd and Pd-Au films have the same behavior, at high and low resistivity, as the films reported in section V.A.1 and the thin metal films reported by other groups where only resistivity measurements were performed (Dynes, Garno and Rowell, 1978 , Dolan and Osheroff, 1979). As shown by McGinnis, et.al. (1981,1983 and 1984), these Pd and Pd-Au films are largely indistinguishable in their temperature dependent resistivity and magnetoresistivity. As we shall see, the thermopower is of course material dependent, the low temperature behaviors are quite similar.

The absolute thermoelectric power of the series of Pd and Pd-Au films whose resistivity characterizations were shown in figure 5-9 and 5-10, is shown in figure 5-

Figure 5-11

Absolute thermopower as a function of temperature for (a) Pd and (b) Pd-Au films. Samples with resistances per square ($R_{\#}$) less than 30KΩ show 'metallic' behavior. Samples with $R_{\#}$>30KΩ show the presence of an energy gap.

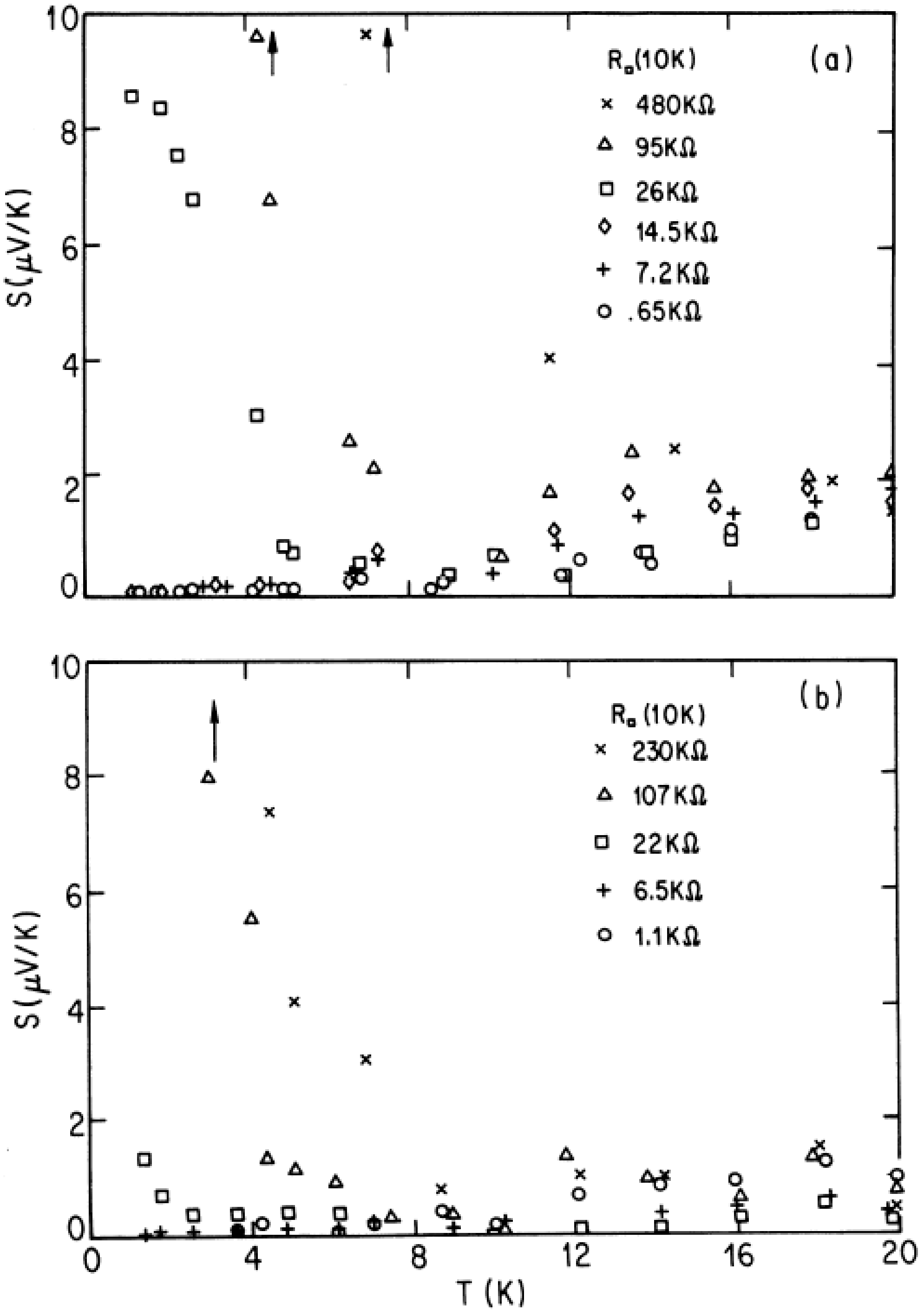
10
8
6
4
2
0
S(μV/K)
(a)
R□(10K)
× 480KΩ
△ 95KΩ
□ 26KΩ
◇ 14.5KΩ
+ 7.2KΩ
○ .65KΩ
10
8
6
4
2
0
S(μV/K)
(b)
R□(10K)
× 230KΩ
△ 107KΩ
□ 22KΩ
+ 6.5KΩ
○ 1.1KΩ
0
4
8
12
16
20
T (K)

Figure 5-12

Absolute thermopower as a function of temperature for each of two Pd and Pd-Au films. Notice at temperatures above 20°K the thermopower is quite material specific although independent of resistivity.

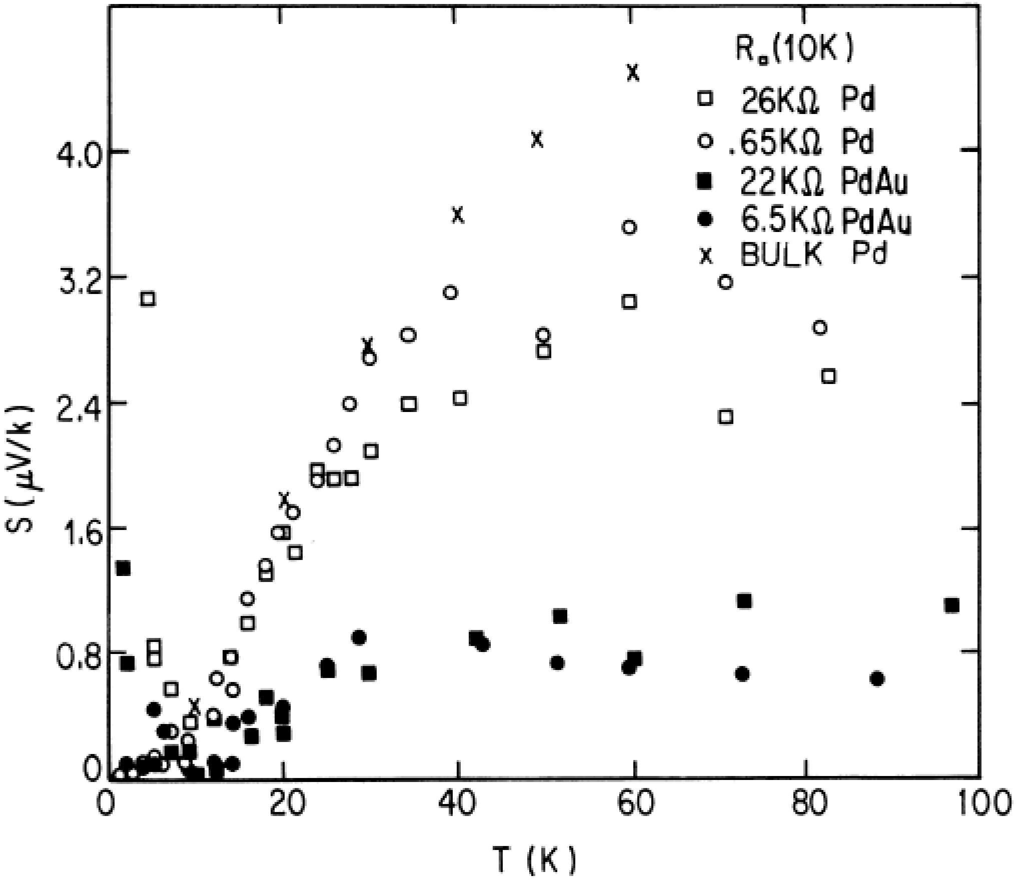

S (μV/k)
T (K)
0
0.8
1.6
2.4
3.2
4.0
0
20
40
60
80
100
R□(10K)
□ 26KΩ Pd
○ .65KΩ Pd
■ 22KΩ PdAu
● 6.5KΩ PdAu
x BULK Pd

11. Figure 5-12 shows the thermopower of several Pd and Pd-Au films up to 100°K with resistivities above and below R_{2D}. These thermopower measurements were performed using the apparatus displayed in figure 4-13.

Above ~20°K the thermopower of all the films are independent of resistivity within the accuracy of these measurements (~20%) and depend only upon the material. Note in figure 5-12 that above 20°K the Pd-Au films are quite distinct from the Pd films, which are similar to the published values for bulk palladium, but with the phonon-drag peak suppressed, probably from the large amount of structural disorder in the film.

Below ~20°K (figure 5-11) there is a qualitative difference between the exponential and logarithmic films. The films with resistances per square ($R_{\#}$) less than R_{2D} follow one specific curve (specific to each material) which is monotonically decreasing as temperature is lowered. The palladium film which has a resistivity of 26 Kohms/square at 10°K and the Pd-Au film which has a resistivity of 22 Kohms/square at 10°K follow their respective low resistivity film thermopower curves and then dramatically start increasing (the Pd film at 6°K, the Pd-Au film at 3°K) as temperature is lowered, reaching values at 1.2°K which are 1-2 orders of magnitude larger than for the logarithmic films. Films of both materials with increasing high resistivity show larger low temperature thermopowers and deviate from metallic behavior at higher temperatures.

Note in figure 5-11 that the Pd film with $R_\#(10^\circ K)=26K\Omega$ has its thermopower start climbing away from the more metallic films at $6^\circ K$ and the Pd-Au films with $R_\#(10^\circ K)=22K\Omega$ has its start at $3^\circ K$. If one examines figure 5-9, one sees that although nothing interesting is happening to the resistive behavior of any of these films, both have resistivities of approximately 30 Kohms/square at the temperature their thermopowers start deviating from metallic behavior. Note also in figure 5-11 that the Pd film with $R_\#(10^\circ K)=14.5K\Omega$ has $R_\#(1.3^\circ K)=20K\Omega$, yet its thermopower is indistinguishable (on this scale) from the more metallic films (such as the $R_\#(10^\circ K)=.65K\Omega$ film) while the $R_\#(10^\circ K)=26K\Omega$ film has $R_\#(5^\circ K)=40K\Omega$. In view of the discussion in section II.G.4, the obvious conclusion is that a metal-insulator transition, as defined by the thermopower, occurs close to R_{2D}=30Kohms/square.

The measurements in figures 5-9 through 5-12, while relatively sensitive (down to $< 0.1\mu V/^\circ K$) are incapable of probing for the small differences predicted to differentiate the scaling and interaction pictures (section II.G.5). For examining extremely small differences (down to < 1 nV/°K) in the thermopower of 2-d and 3-d films, the apparatus in figure 4-14 was used.

In figures 5-13 and 5-15 is plotted the resistivity as a function of temperature of the 3-d (1000 Angstrom) arms and 2-d sample (25-35 Angstroms) of thermopiles fabricated per section IV.A.1, in the geometry of figure 4-14.

In figures 5-13 and 5-15 is plotted the resistivity as a function of temperature of the 3-d (1000 Angstrom) arms and the 2-d (25-35 Angstrom) sample of thermopiles per figure 4-14. The thick film areas have a low resistivity which displays metallic behavior, with a resistivity decreasing monotonically with decreasing temperature. The thin film samples display resistivity minima above <10°K which proceeds to a log T dependence as the thermopower is lowered and achieves a completely logarithmic dependence for T<6°K, consistent with the film in the near metallic regime in figure 5-2.

In figures 5-14 and 5-16 is plotted the difference between the 2-d and 3-d thermopowers at low temperature, as generated by the thermopiles, normalized by the measured absolute thermopower of one of the 3-d arms. As one can see, the fractional deviation between the 2-d and 3-d thermopowers shows that the thermopower is suppressed in the 2-d film from what it would have been had the film

Figure 5-13

Top shows the low temperature resistivity of the 3-d portion of a thermopile (see figure 4-14). Bottom shows the logarithmic dependence with temperature of the resistivity of a 2-d portion.

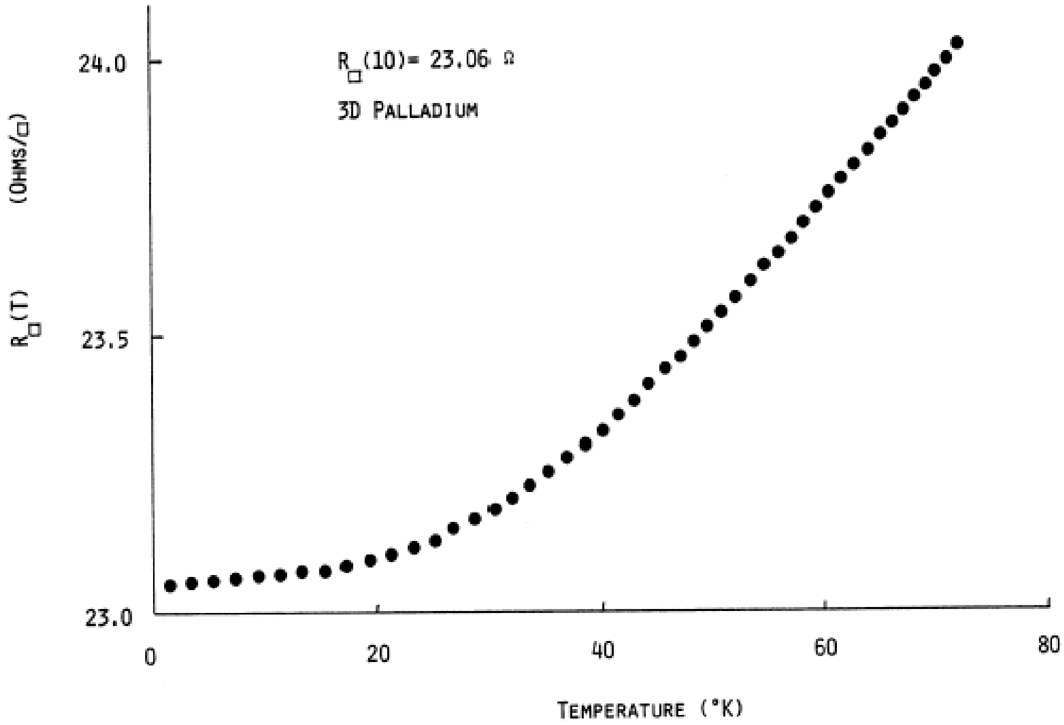

$R_\square(10)= 23.06\ \Omega$
3D PALLADIUM
$R_\square(T)$ (OHMS/□)
24.0
23.5
23.0
0
20
40
60
80
TEMPERATURE (°K)

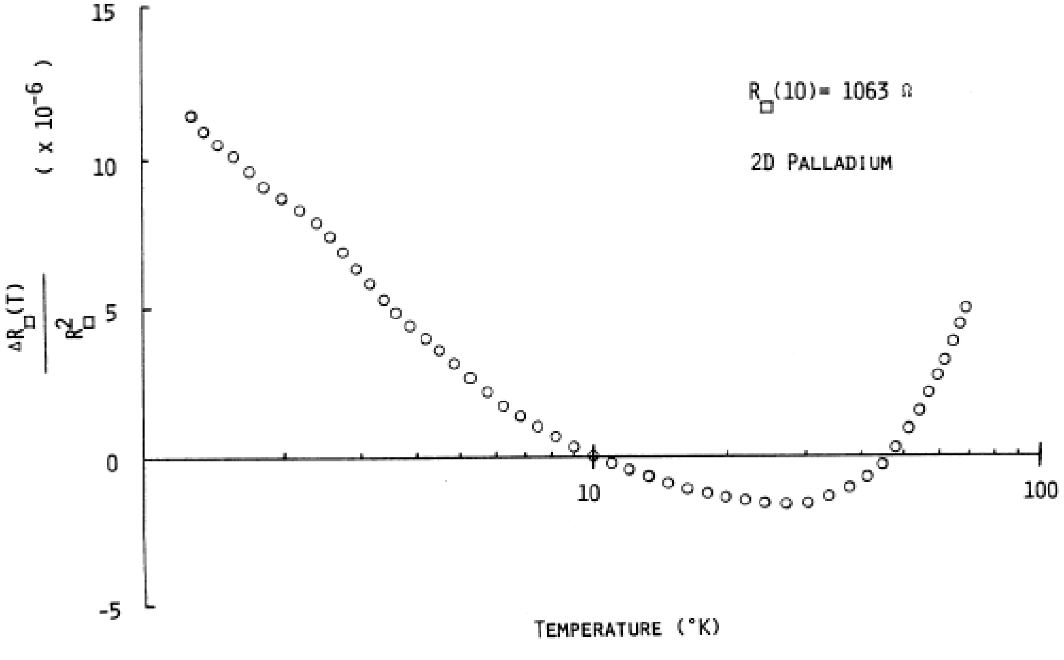

$R_\square(10)= 1063\ \Omega$
2D PALLADIUM
$\frac{\Delta R_\square(T)}{R_\square^2}$ (x 10^{-6})
15
10
5
0
-5
10
100
TEMPERATURE (°K)

Figure 5-14

Fractional difference in the thermopower between the 3-d and 2-d films comprising the thermopile whose resistivity characteristics are presented in figure 5-13.

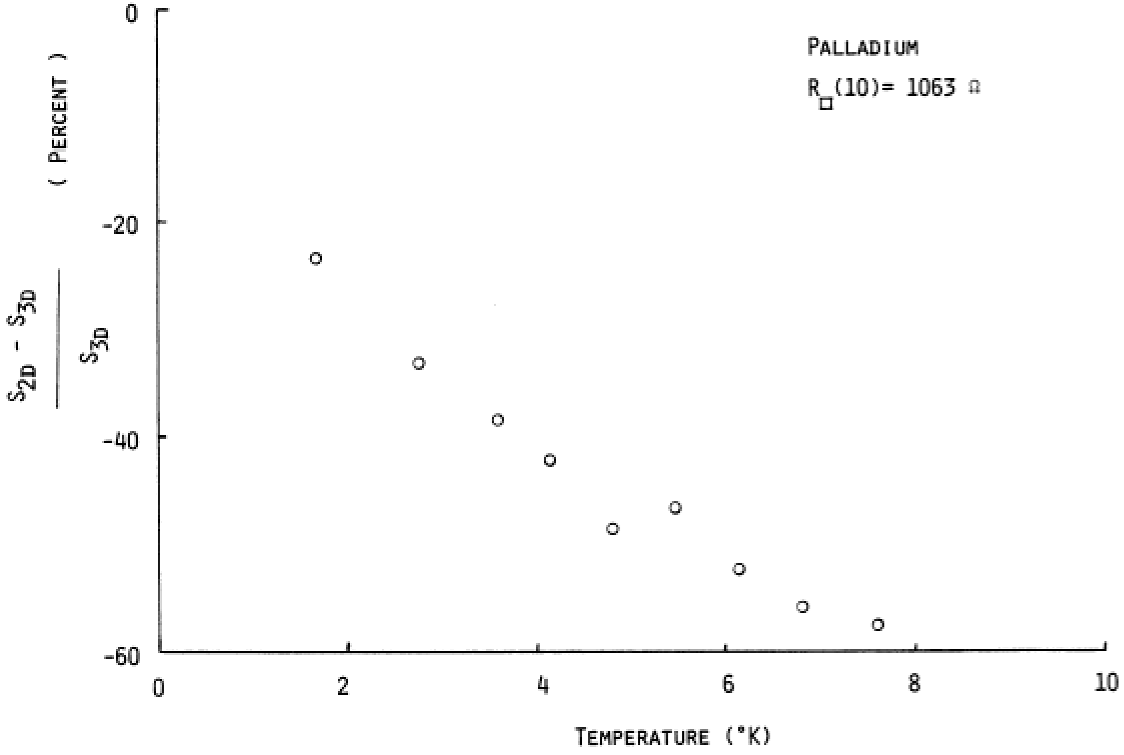
PALLADIUM
$R_{\square}(10) = 1063\ \Omega$
$\frac{S_{2D} - S_{3D}}{S_{3D}}$ (PERCENT)
0
-20
-40
-60
0
2
4
6
8
10
TEMPERATURE (°K)

Figure 5-15

Top shows the low temperature resistivity of the 3-d portion of a thermopile (see figure 4-14). Bottom shows the logarithmic dependence with temperature of the resistivity of a 2-d portion.

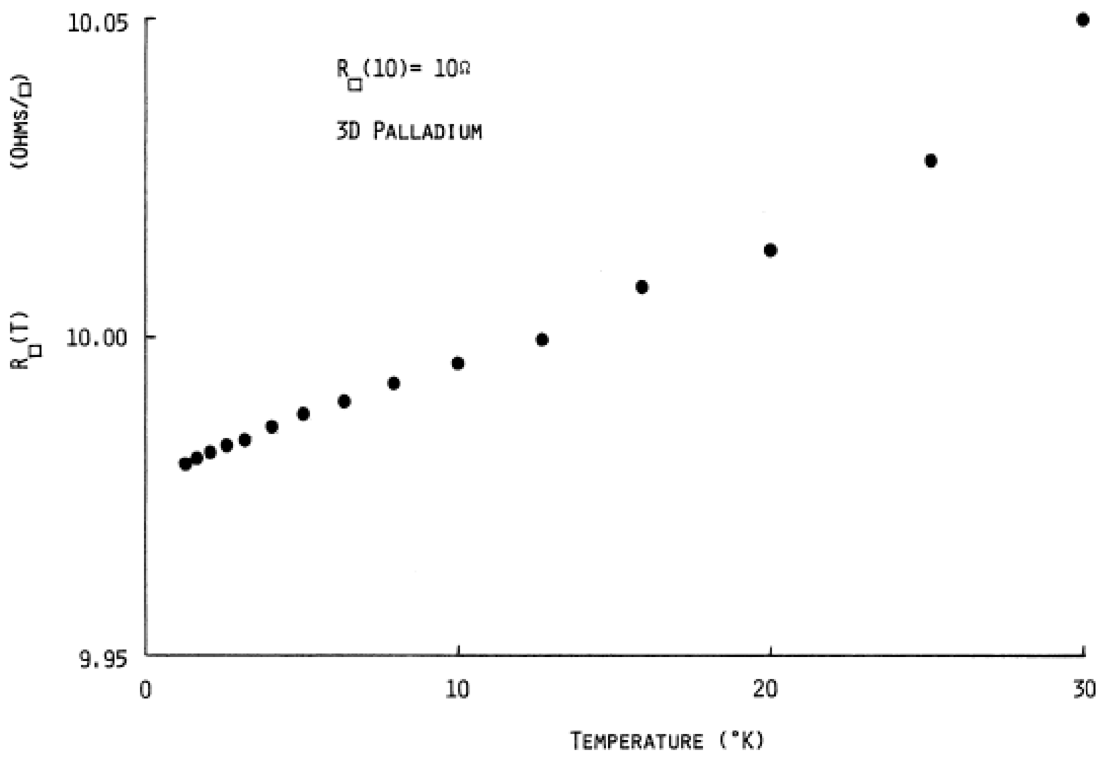
10.05
10.00
9.95
$R_\square(T)$ (OHMS/□)
$R_\square(10) = 10\Omega$
3D PALLADIUM
0
10
20
30
TEMPERATURE (°K)

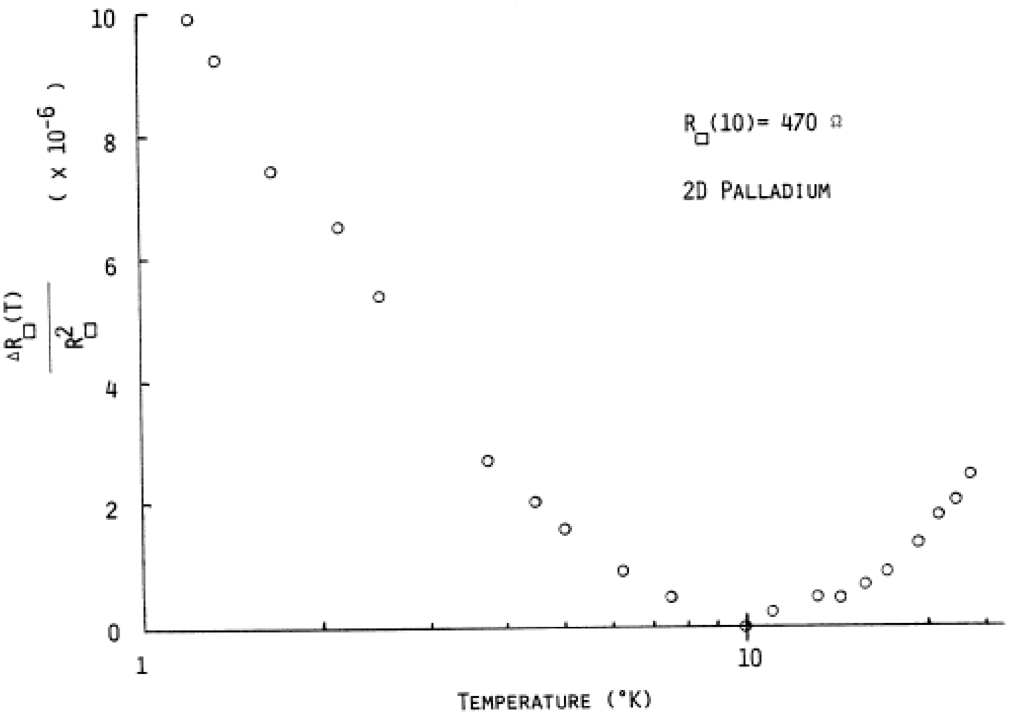
10
8
6
4
2
0
$\frac{\Delta R_\square(T)}{R_\square^2}$ (x 10^{-6})
$R_\square(10) = 470\ \Omega$
2D PALLADIUM
1
10
TEMPERATURE (°K)

Figure 5-16

Fractional difference in the thermopower between the 2-d and 3-d films comprising the thermopile whose resistivity characteristics are shown in figure 5-15.

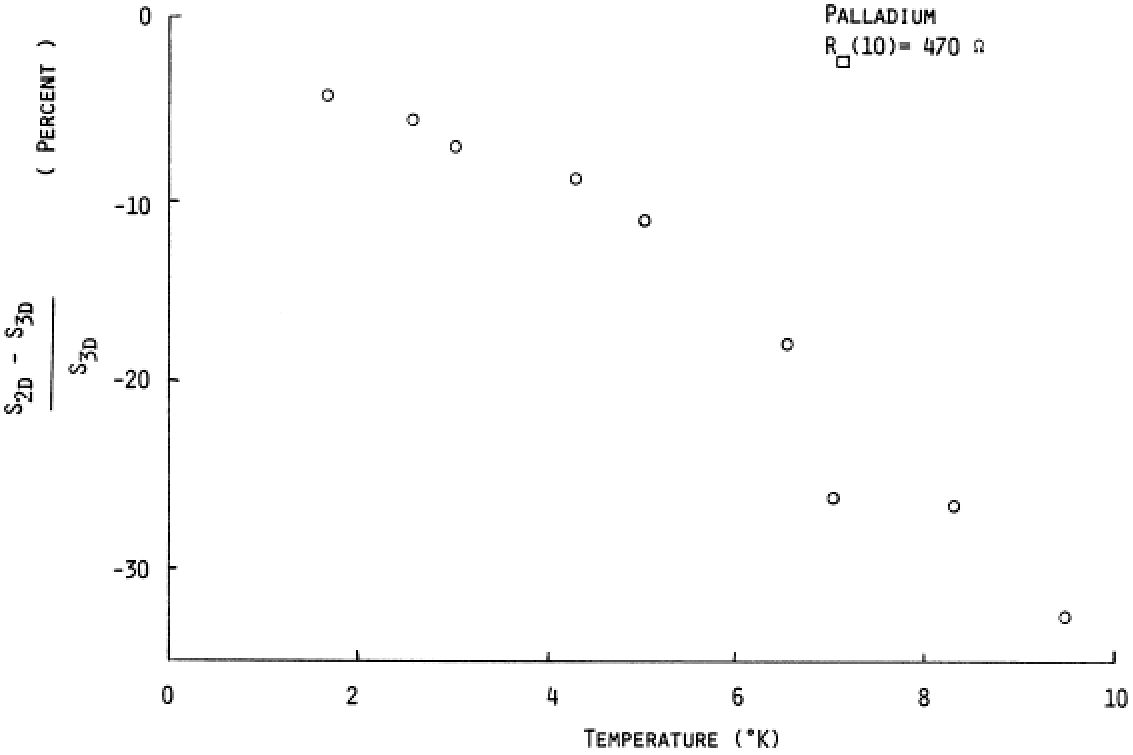
PALLADIUM
$R_{\square}(10) = 470\ \Omega$
$\frac{S_{2D} - S_{3D}}{S_{3D}}$ (PERCENT)
0
-10
-20
-30
0
2
4
6
8
10
TEMPERATURE (°K)

been 3-d, with the thermopower being suppressed a greater amount in the more highly disordered films. This fractional deviation between the 2-d and 3-d thermopower behavior decreases with decreasing temperature, rather than increasing as one might expect.

As can be seen from the resistivity curves of the 3-d sections of the thermopile (figures 5-13 and 5-15), the fact that the 3-d section has not reached a regime where the conductivity is no longer decreasing with decreasing temperature implies that electron-phonon scattering is still a dominant scattering mechanism. This assertion is supported by the thermopower curves of figures 5-14 and 5-16, which show the thermopowers of the 2-d films suppressed from that of the 3-d films. This feature can also be seen in figure 5-12 where the Pd films show the phonon drag contribution to the bulk suppressed (presumably due to the large amount of disorder in the films). The Pd-Au is suppressed even further, which is not surprising considering that Pd-Au is a substitutional alloy and therefore intrinsically disordered, even when crystalline. Since films of vastly different R# have essentially the same thermopowers at the temperatures at which the phonon drag is large, implies that the structural disorder in these films suppresses some, but not all of the phonon drag. Furthermore, while Pd-Au films also have thermopowers independent of $R_\#$ at these temperatures, the phonon drag in their thermopowers is suppressed to a greater degree than in the Pd, consistent with the higher degree of disorder implied by the Pd-Au electron diffraction patterns (Figure 4-1).

As can be seen from figures 5-9 and 5-12, any film whose resistivity crosses above R_{2D} displays a diverging thermopower. This behavior is totally inconsistent with a noninteracting variable range hopping picture.

It might be expected that the presence of a disorder induced mobility gap might explain these results in a single particle picture (see for example, figure 1-2). However, since the samples are metallic for $R_\#<R_{2D}$, the Fermi energy is far from any band edges. As pointed out in section V.B.3, the Fermi energy is ~0.5eV inside the d-band edge in bulk Pd, and even further away from the s-band edge (also the higher mobility of the s-band electrons would tend to cause them to dominate the transport). This precludes the possibility of a mobility gap opening about the Fermi energy similar to that in a semiconductor with band tailing. The density of states is continuous and nonzero at the Fermi energy when $R_\#<R_{2D}$ and the thermopower reflects this by displaying metallic behavior. If a mobility gap were to open up with decreasing temperature as $R_\#$ crosses above R_{2D}, the

mobility edges would approach the Fermi energy rather than recede from it and if the mobility edges did reach the Fermi energy then the system would be dominated by variable range hopping.

One must therefore conclude that if the single particle localization picture is to describe the behavior of these films, one should have S-->0 as T-->0, independent of the resistivity and its temperature dependence. This is the natural consequence of a theory which treats the metal-insulator transition entirely as a mobility effect.

In the interaction picture the combined effects of the elastic scattering and the electron-electron interaction is to change the density of states in the vicinity of the Fermi energy (equation II.60) as well as cause the logarithmic correction to the resistivity (equation II.68). As pointed out above, this change in the density of states should show up in in the thermopower as a logarithmic correction to the otherwise metallic behavior of the system (equation V.12). As long as there is a finite density of states at E_f, the thermopower will decrease as T-->0. This is of course, what is observed in figures 5-13 through 5-16, although any possible correction to the thermopower due to scaling vs interaction effects in the near metallic regime, is swamped by phonon drag. This problem is being eliminated from the studies currently in progress (1984).

As could be seen from the derivation of the transport properties of variable range hopping systems with electron-electron interactions present, one might expect the metal-insulator transition to occur via the reduction of the density of states at the Fermi energy (equation II.60) until a gap opens (perhaps a la Efros, equation II.82), presumably at resistivities ~R_{2D}.

The interacting electron version of variable range hopping provides a mechanism which is in qualitative agreement with the observed data. In this scheme, S-->S_{int}=constant as T-->0 after having dropped to (1/2)S_{int} at T=T_c (equations V.15 and V.16). While the data in figures 5-11 and 5-12 continue diverging well past twice its minimum value, and does not appear to level off, the details of the predicted behavior result from specific assumptions about the nature of the density of states and certainly do not account for the added complication of the phonon drag in these films.

Another possibility is that the electron-electron interactions open a real gap (nonzero width) in the density of states. As shown in section II.E.2, this could happen if the carriers are heavily dressed, i.e. 'electronic polarons'. This later explanation becomes

Figure 5-17

The thermopower plotted versus 1/T for comparable Pd and Pd-Au films with thermopowers which diverge as $T \longrightarrow 0$.

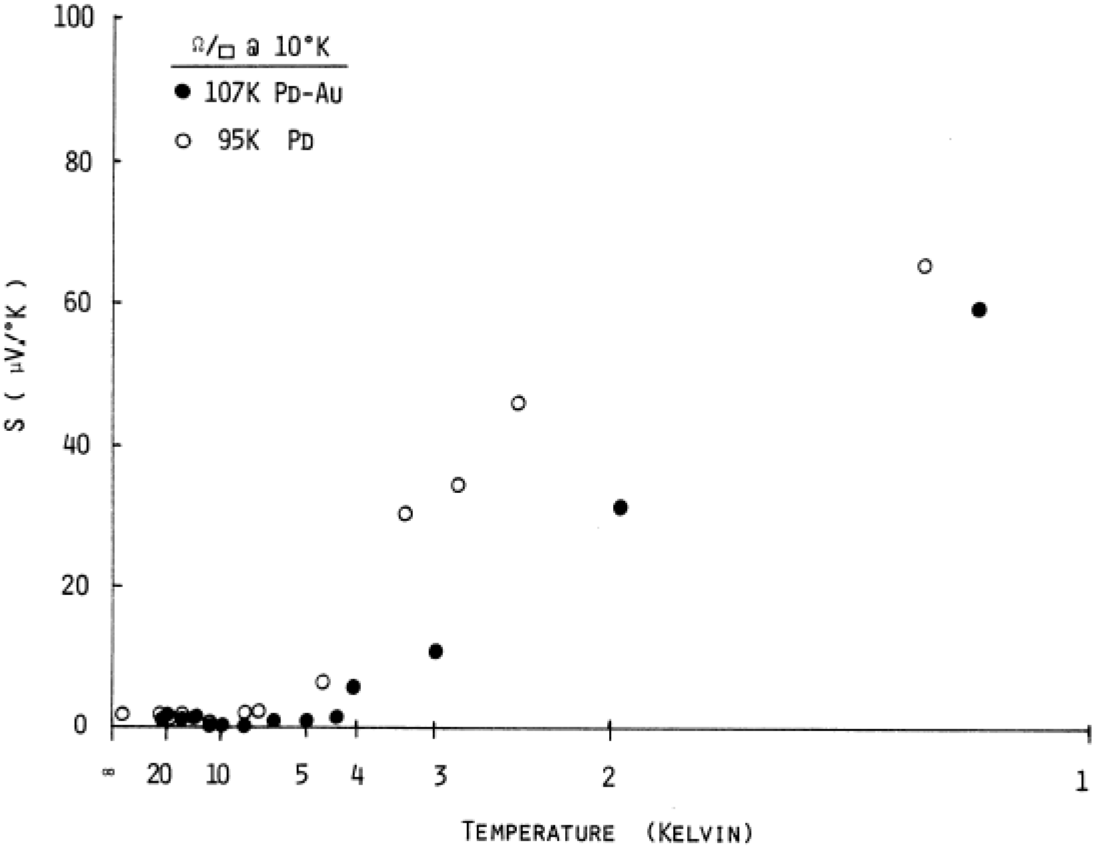
Ω/□ @ 10°K
● 107K Pd-Au
○ 95K Pd
S (μV/°K)
100
80
60
40
20
0
∞
20
10
5
4
3
2
1
Temperature (Kelvin)

more plausible if one examines figure 5-17, which shows the thermopower of a Pd and a Pd-Au film plotted vs 1/T, as one might expect for a conventional semiconductor. The thermopower of the Pd-Au film is more consistent with a 1/T dependence than is the Pd. The resistivity of these films is inconsistent with a fixed gap semiconductor model. The thermopowers of both films in figure 5-17 give a gap energy of ~0.4meV (~5°K) assuming a simple semiconducting model, which agrees with the temperature at which their thermopowers start diverging from the more metallic samples.

The increase in the thermopower in the high resistivity samples leads us to conclude that a gap is appearing, favoring the interpretation in terms of an interaction electron model. In addition to these studies [Burns and Chaikin (1983), Burns, et.al. (1981)], tunneling measurements on some three dimensional systems by Dynes and Garno (1981) and McMillian and Mochel (1981) have also shown an interaction gap. The sharpness of the transition in the thermopower as a function of film resistivity suggests that the gap is opening at a well defined value of $R_{\#}$, namely at the Ioffe-Regel minimum metallic conductivity of R_{2D}^{-1}~(30000 ohms/square)$^{-1}$.

They sought it with thimbles, they sought it with care;
    They pursued it with forks and hope;
They threatened its life with a railway-share;
    They charmed it with smiles and soap.

They shuddered to think that the chase might fail,
    And the Beaver, excited at last,
Went bounding along on the tip of its tail,
    For the daylight was nearly past.

"There is Thingumbob shouting!" the Bellman said
    "He is shouting like mad, only hark!
He is waving his hands, he is wagging his head.
    He has certainly found a Snark!"

The Hunting of the Snark by
Lewis Carroll
(Charles Lutwidge Dodgson)
(1832-1898)

C. Ultrathin Silver Films Grown Epitaxially On Germanium (001)

1. Experimental Results

i) Temperature Dependence of the Resistivity

Ultrathin silver films epitaxially grown on (001) Ge, as described in section IV.A.2, display a wide variety of interesting phenomenon. The more ordered films, which are grown on substrates which have their crystal planes well aligned (within ~0.5°) with the surface, display transport properties consistent with two dimensional electron localization. Films with larger amounts of structural disorder also display interesting behaviors. As discussed in section IV.A.2, these films consist of a crystalline Ag monolayer film with additional Ag forming three dimensional islands. The monolayer film is certainly discontinuous, resting on plateaus on the Ge surface with step heights corresponding to 1/4th the lattice spacing of Ge. These plateaus are presumably bridged by the excess 3-d Ag islands, resulting in the observed conductivity usually being dominated by the monolayers at low temperatures.

Figure 5-18

Resistivity of a sample comprising of a 2.5 monolayer thick Ag film on Ge (001) from 250-0.6^{o}K. Curve is well fit by a log(T) resistor in parallel with a semiconductor with a ~0.14eV gap.

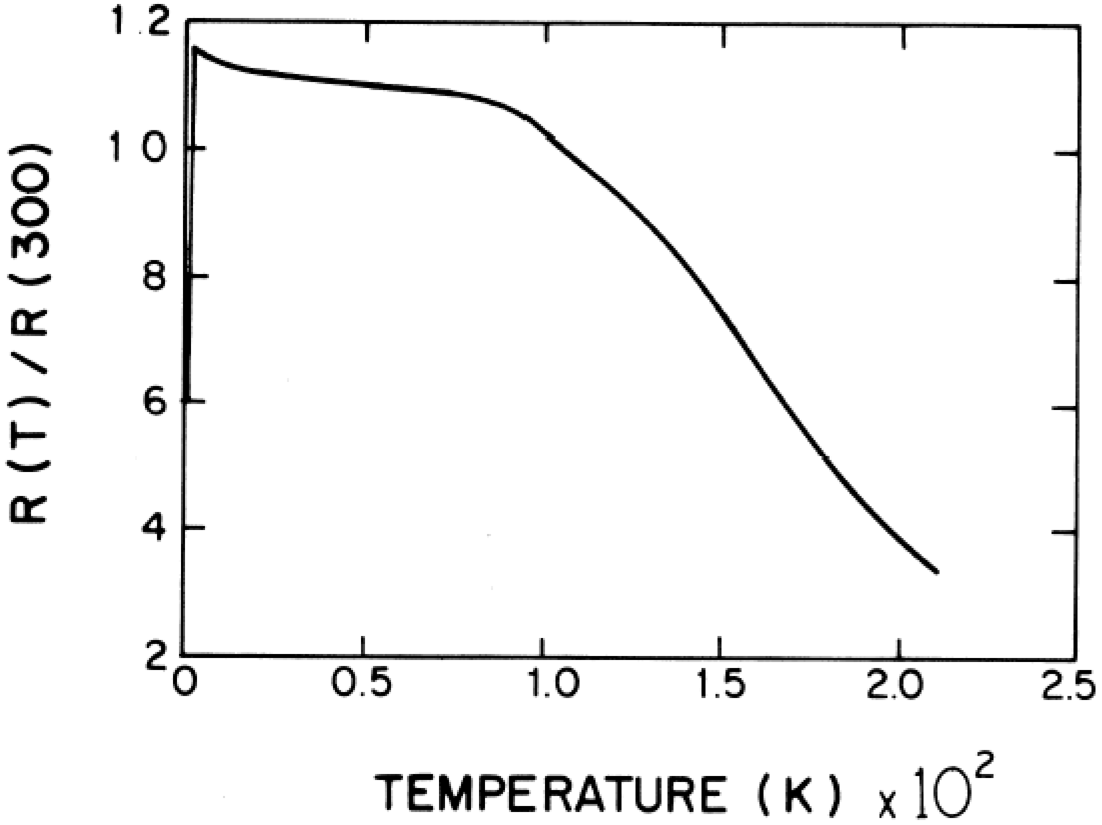
1.2
10
8
6
4
2
0
0.5
1.0
1.5
2.0
2.5
R (T) / R (300)
TEMPERATURE (K) x 10^2

Figure 5-19

Fractional change in the film resistivity at low temperature. Microscopic terraces in the substrate prevent absolute resistivity measurements, but assuming $\alpha=1$ in equation V.1, would give a resistivity of ~1.4KΩ/square.

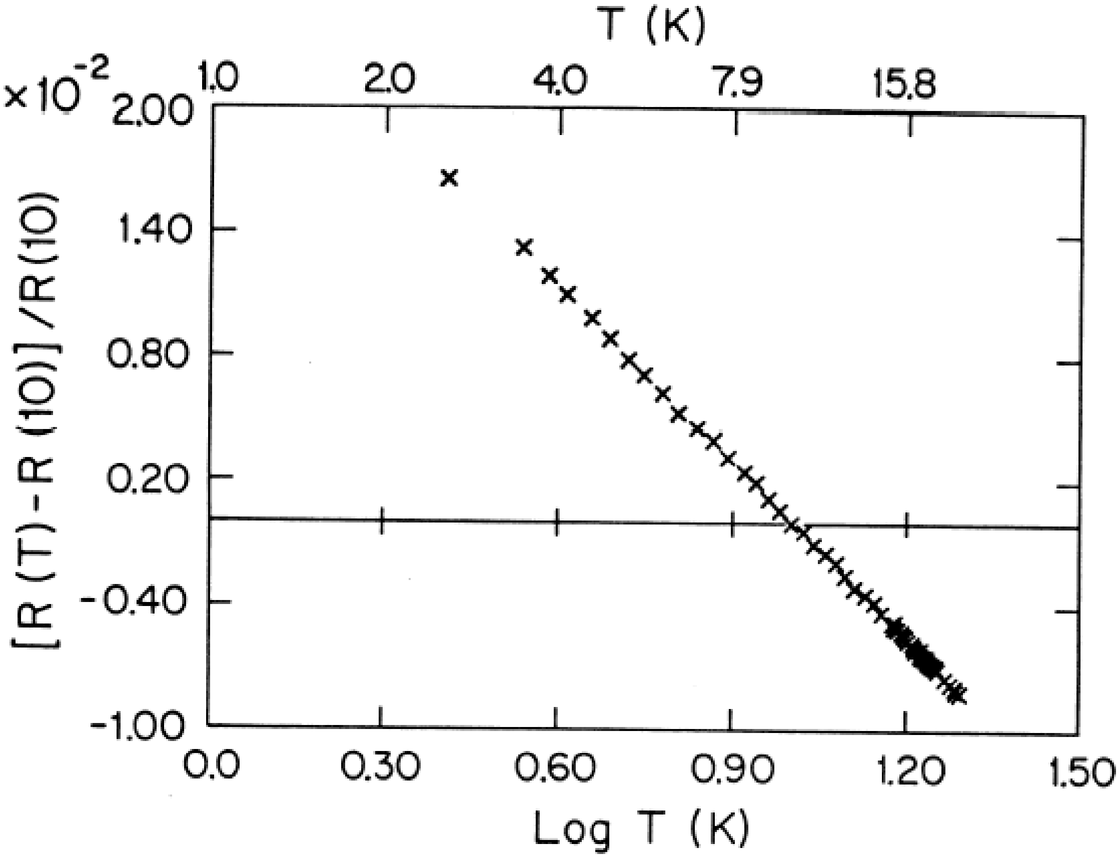
T (K)
1.0
2.0
4.0
7.9
15.8
×10^{-2}
2.00
1.40
0.80
0.20
-0.40
-1.00
[R (T) - R (10)] /R(10)
0.0
0.30
0.60
0.90
1.20
1.50
Log T (K)

In figure 5-18 is plotted the 2-probe resistance (normalized to room temperature) of a film with an average thickness of 2.5 monolayers of Ag. The substrate for this film was well aligned, the surface and the Ge (001) planes were parallel to within 0.5°. Above ~1.6°K, the resistivity is well fit by a log(T) resistor in parallel with a semiconductor with a ~0.14eV gap. A typical acceptor or donor ionization energy in Ge is 0.095-0.125 eV. Below ~1.6°K, the resistivity of these samples decreases very rapidly with decreasing temperature, consistent with an incomplete superconducting transition, as might be found in an inhomogenious sample with a variety of transition temperatures (T_c's).

In figure 5-19 is plotted the fractional change (relative to 10°K) in the 2-probe resistance of the sample in figure 5-18 as a function of the logarithm of the temperature below 20°K. The exact geometry being probed is unknown due to the discontinueties discussed above. One can see however, that the sample resistance displays a logarithmically increasing resistance with decreasing temperature, as one would expect for a two dimensional system in the near metallic regime according to both scaling and interaction pictures (sections II.B and sections II.D).

Figure 5-20

Below ~1.6°K the resistivity of this sample (same as in figures 5-18 and 5-19) shows a very rapid decrease with decreasing temperature. Insert is the same as figure 5-19.

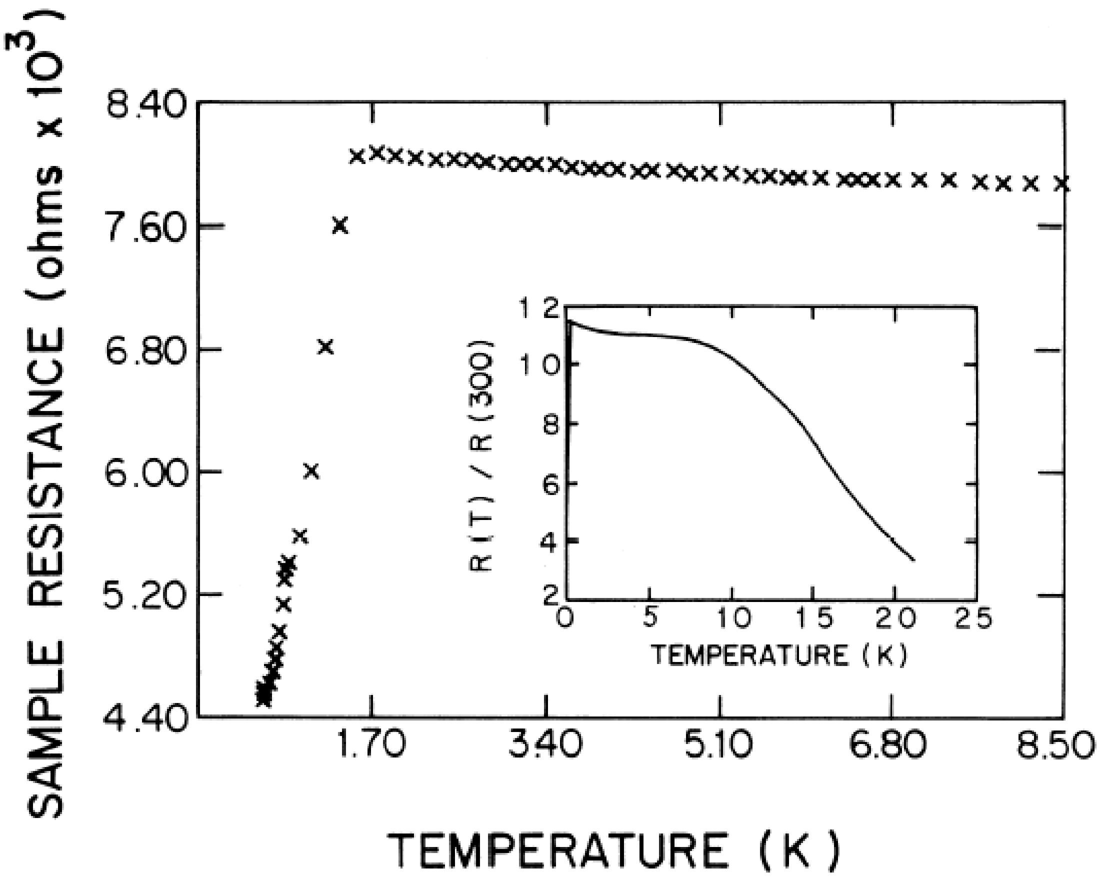
SAMPLE RESISTANCE (ohms x 10^3)
8.40
7.60
6.80
6.00
5.20
4.40
1.70
3.40
5.10
6.80
8.50
TEMPERATURE (K)
R(T) / R(300)
12
10
8
6
4
2
0
5
10
15
20
25
TEMPERATURE (K)

Figure 5-21

Temperature dependence of the resistance of a 2.5 monolayer Ag film on Ge (001) below 25°K.

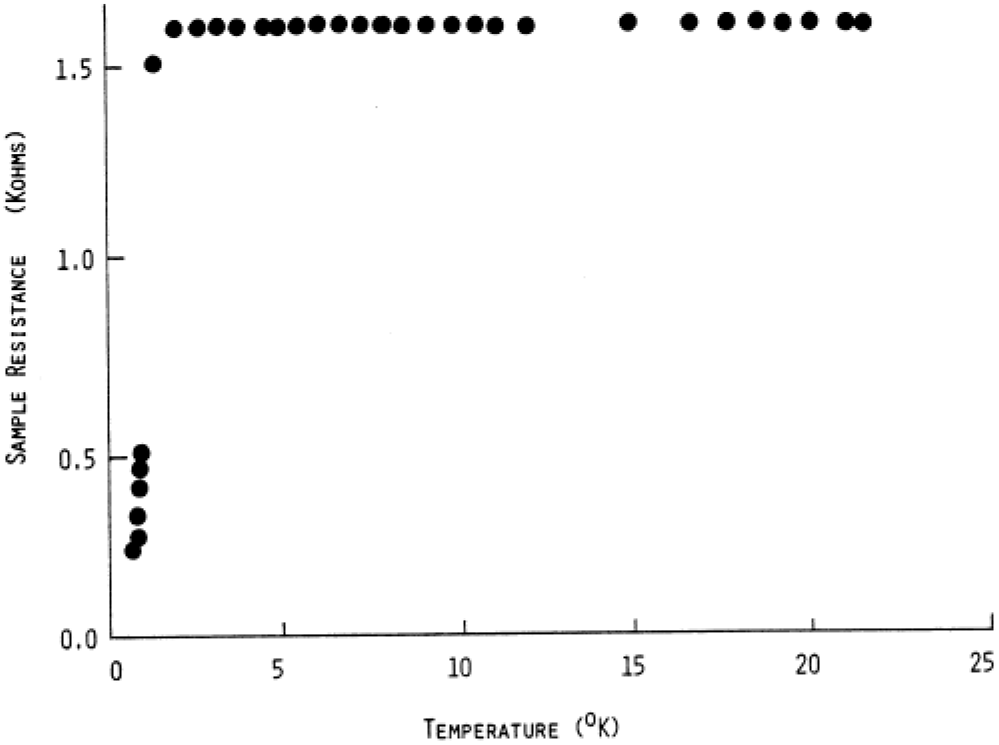
Sample Resistance (Kohms)
1.5
1.0
0.5
0.0
0
5
10
15
20
25
Temperature (°K)

Figure 5-22

Temperature dependence of the resistance of a 3.0 monolayer Ag film on Ge (001) which has a misalignment between the Ge surface and the Ge (001) plane of 5°.

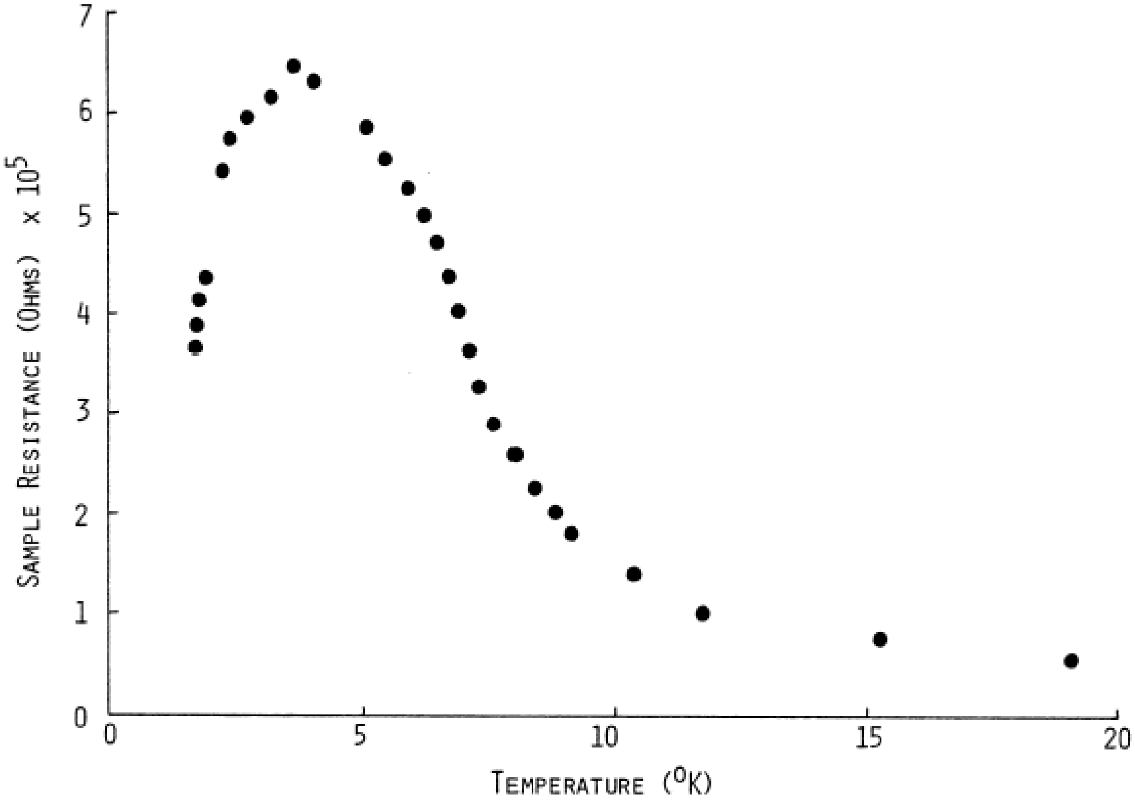

Sample Resistance (Ohms) x 10^5
0
1
2
3
4
5
6
7
0
5
10
15
20
Temperature (^oK)

In figure 5-20 we show the 2-probe resistivity of the film in figures 5-18 and 5-19 down to 0.65°K. The sample resistivity is increasing logarithmically with decreasing temperature until the temperature drops to about 1.6°K. Below this temperature the resistivity decreases rapidly. At 0.65°K its value is 55% of the resistivity at 2°K.

In figure 5-21 is plotted the 2-probe resistivity of a sample whose resistivity has been reduced at 0.55°K to 15% of its 2°K value.

In figure 5-22 is plotted the 2-probe resistance of a sample fabricated on a substrate with the surface at ~5.0° relative to a (001) plane (as opposed to the usual alignment of better than 0.5°), causing the terraces on the substrate to be ~16 Angstroms apart. As one can see, this more disrupted film displays a very rapid increase in resistance below ~10°K (presumably due to a high impurity concentration in the Ge) but the resistance starts decreasing even more rapidly below ~4°K.

C. Ultrathin Silver Films Grown Epitaxially On Germanium (001)

1. Experimental Results

ii) Electric and Magnetic Field Dependence of the Resistivity

The films which display a logarithmic temperature dependence show other characteristics consistent with two dimensional systems in the near metallic regime.

In figure 5-23 is the fractional change in the dynamic resistance at various temperatures of the sample in figures 5-18 through 5-20.At low fields the resistance behavior is consistent with a quadratic electric field dependence. At higher fields a logarithmic dependence appears which becomes more pronounced at lower temperatures.

Figure 5-24 shows the change in the fractional resistivity with applied magnetic field of the sample in figure 5-23. The magnetoresistance is isotropic, indicating that orbital effects are negligable. This isotropic behavior is similar to that found in Pd films for which the resistivities are above a few Kohms per

Figure 5-23

The dynamic resistance of this 2.5 monolayer film is consistent with a quadratic field dependence for low electric fields, changing to a logarithmic dependence at high fields. This sample gives p'=2.6 in equation V.5.

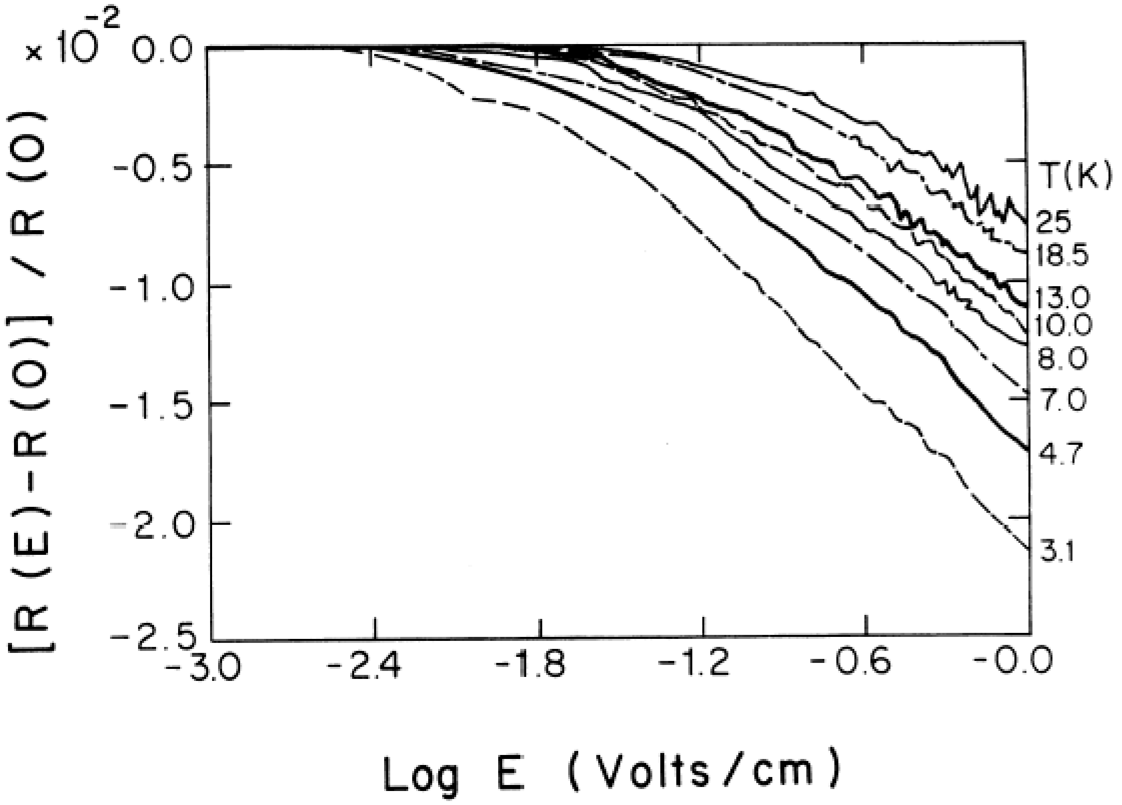

× 10⁻²
0.0
-0.5
-1.0
-1.5
-2.0
-2.5
-3.0
-2.4
-1.8
-1.2
-0.6
-0.0
[R (E) - R (O)] / R (O)
Log E (Volts/cm)
T(K)
25
18.5
13.0
10.0
8.0
7.0
4.7
3.1

Figure 5-24

The magnetoresistance of this sample (same sample as in figure 5-23) shows a positive isotropic magnetoresistance, open symbols are for H⊥ film, solid for H|| film.

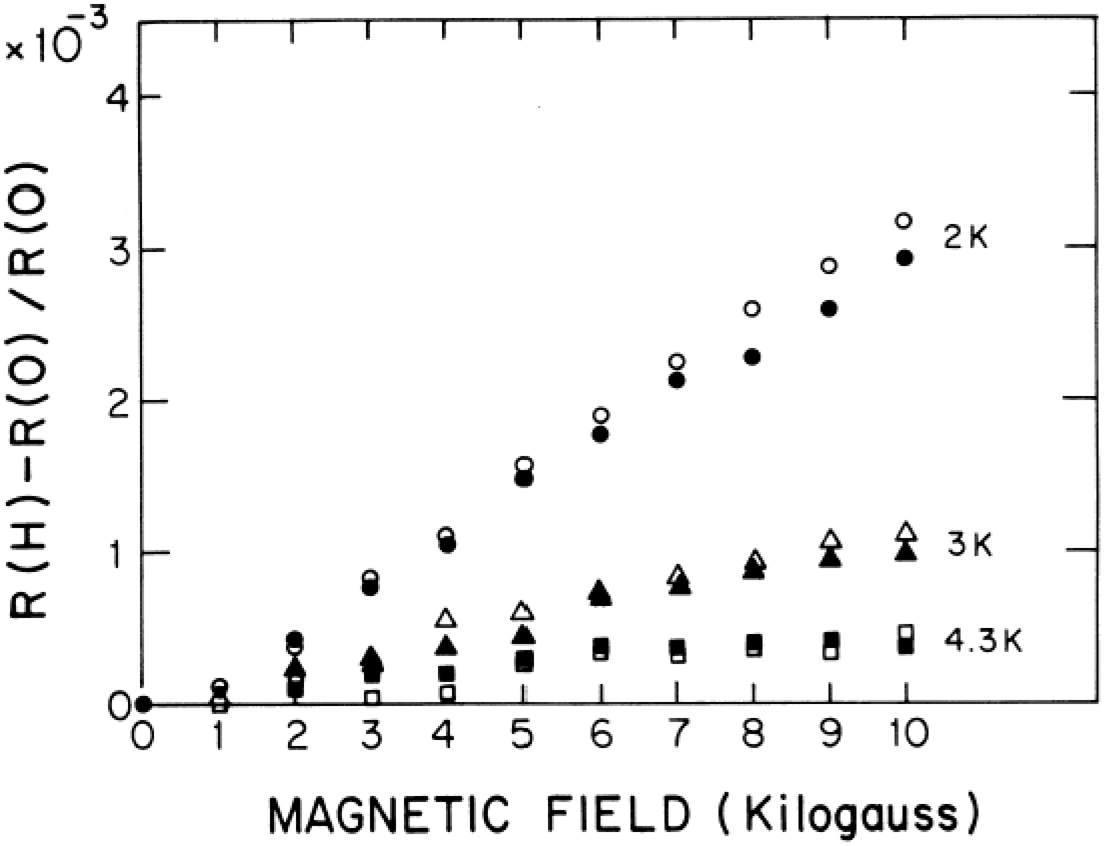
×10^{-3}
4
3
2
1
0
R(H)-R(O)/R(O)
0
1
2
3
4
5
6
7
8
9
10
MAGNETIC FIELD (Kilogauss)
2K
3K
4.3K

square (McGinnis and Chaikin, 1984, McGinnis, 1983, also see section II.B.3).

C. Ultrathin Silver Films Grown Epitaxially On Germanium (001)

1. Experimental Results

iii) Superconductivity

The previous figures in this section (V.C) show that these ultrathin crystalline films of Ag epitaxially grown on Ge (001)$\pm$0.5° exhibit electronic transport consistent with two dimensional behavior and display weak electron localization above approximately 2°K. In figures 5-20 and 5-21, we saw that the sample resistivity is increasing logarithmically with decreasing temperature until the temperature drops to about 1.6°K. The resistance then drops dramatically as the temperature is lowered further.

In figure 5-25 is plotted the resistance versus magnetic field for the film in figures 5-18 through 5-20 at various temperatures below 1.6°K. The magnetoresistance is still positive and isotropic. In figure 5-26 is plotted the perpendicular magnetic field behavior of the sample of figure 5-21 (which also appears in the insert of figure 5-26), whose resistance has been reduced at 0.55°K to 15% of its 2°K value. Above ~1.4°K,

Figure 5-25

Same film as in figure 5-24. Magnetoresistance (up to 1 Tesla) is still positive and isotropic during the transition.

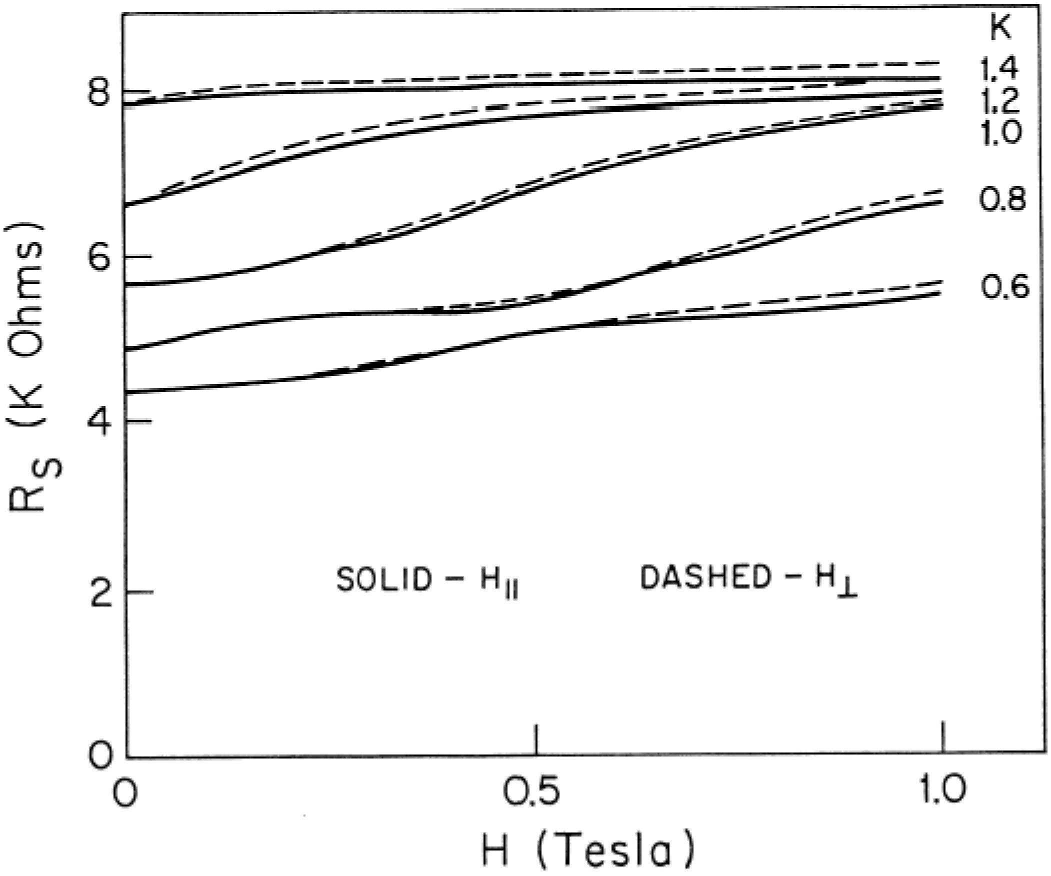
K
1.4
1.2
1.0
0.8
0.6
R_S (K Ohms)
8
6
4
2
0
0
0.5
1.0
H (Tesla)
SOLID – $H_{\parallel}$
DASHED – $H_{\perp}$

Figure 5-26

The perpendicular magnetoresistance of the sample in figure 5-21, in fields up to 10 Tesla. The insert is the same as figure 5-21.

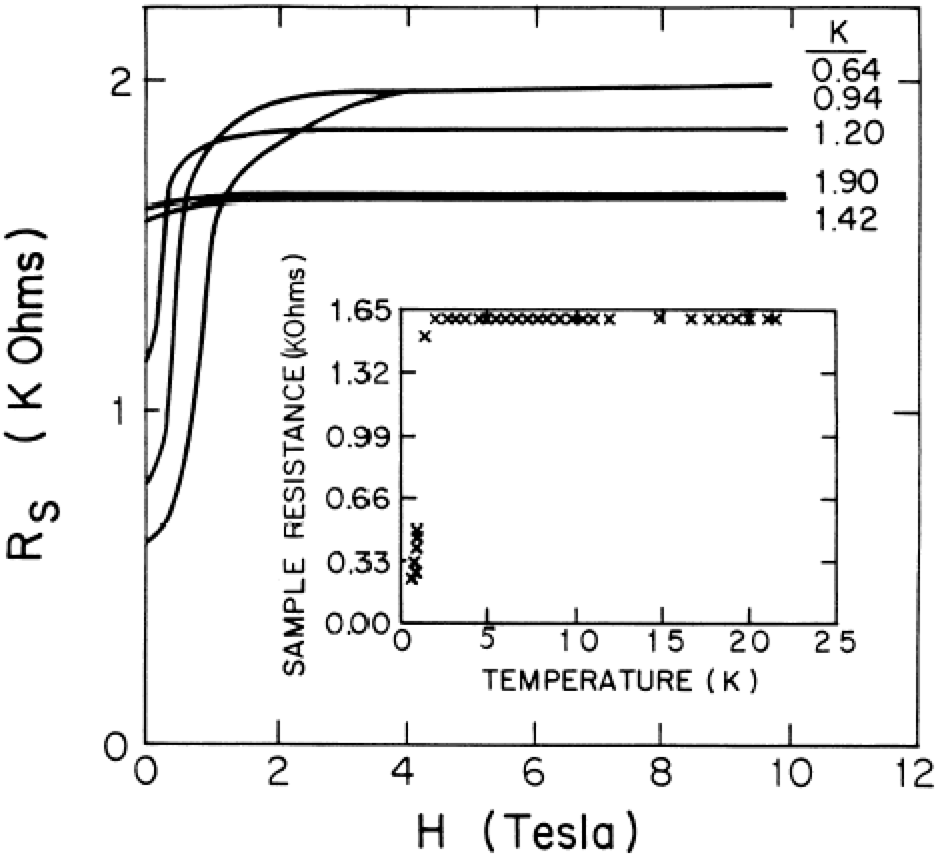

K
0.64
0.94
1.20
1.90
1.42
R_S (K Ohms)
0
1
2
0
2
4
6
8
10
12
H (Tesla)
SAMPLE RESISTANCE (KOhms)
1.65
1.32
0.99
0.66
0.33
0.00
0
5
10
15
20
25
TEMPERATURE (K)

the resistance increases immediately with the application of a magnetic field and then levels off at a value only slightly above the zero field resistance. At low temperature the magnetic field dependence is more dramatic. The resistance is flat for small fields, then increases abruptly and levels off at a resistance much higher than the zero field value.

C. Ultrathin Silver Films Grown Epitaxially On Germanium (001)

1. Experimental Results

iv) Miscellaneous Observations

In addition to the measurements presented on this system in the preceding sections, here are a few other observations which are not only interesting, but contain information critical to trying to understand the physics of this system:

(1) Critical current measurements indicate a current density of 10^5-10^6 amperes/cm^2 assuming the film is continuous and of uniform thickness.

(2) Heating a superconducting sample to ~600°K for ~10 minutes under vacuum permanently destroys all signs of 2-d electronic behavior and superconductivity, consistent with the surface studies which indicate the monolayer should be unstable against island formation at that temperature (Lince, Nelson and Williams, 1983, also see section IV.A.2). This temperature is also much too low for the Ag to desorb from the Ge surface.

(3) These monolayer films are chemically rather

inactive. We were concerned that exposure to air could damage the monolayer films. After the experiments were performed and repeated (over periods extending months) some samples were reexamined by AES. This analysis showed that although the 3000 Angstrom Ag contact pads were tarnished (sulfur contamination), the only foreign substance on the 'monolayer' film was carbon - presumably from pump oil.

C. Ultrathin Silver Films Grown Epitaxially On Germanium (001)

2. Discussion

The previous figures show that ultrathin crystalline films of Ag epitaxially grown on Ge (001) exhibit transport consistent with two dimensional behavior and display weak electron localization above approximately 2°K.

Both the scaling theory (section II.B) and the interaction theory (section II.D) predict a logarithmically increasing resistivity with decreasing temperature (equation V.1). In the scaling theory the prefactor of the logarithm depends on the exponent of the temperature dependence of the total inelastic scattering time while in the interaction picture the prefactor depends on the systems screening factor (see equation V.1 and V.2).

In between inelastic electron-phonon scatterings the electrons can absorb energy from the applied electric field and undergo Joule (I^2R) heating (section II.F.1). This results in a quadratic electric field dependence for low fields changing over at large fields to a logarithmic dependence. The prefactor for the logarithmic electric field dependence depends on the temperature log prefactor (equation V.2) and the exponent for the temperature dependence of the electron-phonon scattering time (see equation V.5). This electron heating model works in both scaling and interaction theories. There is also a possibility, in the scaling theory, that the electric field alters the localization length directly (Tsuzaki, 1981, also Kaveh et.al., 1981) giving a prefactor equal to the temperature prefactor if one set replaces [2p/(2+p')] with 2/3 in equation V.5.

From the data presented in section V.C.1, one cannot determine the exponent S (in equation V.1) for the temperature dependence since the geometry is undefined due to the terraces discussed in section V.C.1.i. Taking a value of α as 1 in equation V.1 for example, would imply that the resistance of 7700 ohms of the sample in figures 5-18 through 5-20, is equivalent to a measurement of <5.5 squares in series. As one can see from equations V.1 and V.5, the ratio of the logarithmic slopes of the temperature and electric field dependencies can be used to calculate the temperature dependence of the electron-phonon scattering time. Using the logarithmic electric field dependence in figure 5-23 at 3°K, one finds p' in equation V.5 to give p'=2.6, which compares with p'=1.8 to 4.5

found for Pd films by McGinnis, et.al. (1983,1984) and briefly discussed in section V.B.2. p'=1.3 was reported for Pt films by Hofmann, Hoffmann and Schoepe in 1982.

Both scaling theory and the interacting electron picture predict magnetoresistance effects in classically small fields ($\omega_c\tau<<1$) which are several orders of magnitude larger than the 'usual' positive magnetoresistance seen in metals. As pointed out in section II.F, electron orbital effects, Zeeman splitting, spin-orbit coupling, and impurity spin scattering can all make contributions to the magnetoresistance in both pictures. Zeeman splitting makes a contribution which while isotropic, manifests itself only in the interaction picture (section II.F.3.iv). There is a contribution from the Zeeman effect in the scaling theory only when spin-orbit coupling is included (see section II.F.3.ii). Spin-orbit coupling has a significant effect in both the interaction and scaling pictures (sections II.F.3.ii and II.F.3.v).

Considering that Ag and Pd are situated side by side in the periodic table, the similarity in their magnetoresistance behavior is not surprising. The spin-orbit interactions couple as Z^4 (see equation II.120), where Z is the nuclear charge. The results of McGinnis, et.al. (1981, 1983 and 1984) indicate spin-orbit coupling dominates the magnetoresistive behavior of Pd films. Z_{Ag}=47 and Z_{Pd}=46 which means AZ^4/Z^4 is less than 10%.

The most striking feature of these films is the rapid decrease of the resistance below 2°K which we tentatively associate with an incomplete superconducting transition, as might be found in an inhomogeneous sample with a variety of T_c's. The magnetic field dependence shown in figure 5-26 is consistent with this interpretation if the 'critical field' for the highest T_c portion of the film is taken as indicative of Pauli limiting. A critical field of ~25 Kilogauss is expected at low temperatures for a T_c of 1.6°K.

While it is not clear what is responsible for the superconductivity, it should be noted that there are no know stable AgGe compounds. Lou, Merriam and Hamilton (1964) reported Ag_4Ge (which is metastable) superconducting at 0.85°K. While each Ge atom at the interface has four Ag neighbors, so one might be tempted to explain figures 5-20 and 5-21 in terms of a broad transition involving a monolayer of quasi-Ag_4Ge, one would still have trouble explaining the much higher T_c displayed by the film in figure 5-22. Stritzker and Wuhl (1971) and also Alekseevskii, Zakosarenko and Tsebro (1971) have reported quenched condensed AgGe alloys of unknown stoichiometry, made at 4.2°K which are superconducting at up to 1.6°K. These quenched condensed films are so unstable as to decompose when temperature cycled to liquid nitrogen temperature (77°K) and fail to superconduct after such cycling. One should bear in mind that the films reported in section V.C.1 were fabricated at room temperature.

As discussed in section IV.A.2, all of the surface characterization done on the samples in section V.C.1 indicate only weak interactions (on a chemical binding scale) between the monolayer Ag and the substrate, with no compound formation occurring and a sharp interface between the Ag and Ge. Studies by Miller, Rosenwinkel and Chiang (1984) of this growth of Ag on Ge also suggest the absence of intermixing, chemical shifts or compound formation. However, the resolution of the different surface probes cannot detect regions of the surface which comprise only a few percent, and it is always possible, even if unlikely, that a small interconnected part of the surface may contain compounds that remained undetected but which short out the rest of the surface as they go superconducting. Our critical current measurements (section V.C.1.iv., item 1) would tend to argue against this. The critical current density of 10^5-10^6 amperes/cm^2 for a film is typical for a superconductor with T_c's of a few degrees (see Rose-Innes and Rhoderick, 1969, pages 106-111 for example), indicating that if any filamentary structure were responsible for our observations, it would have to have an anomalously high critical current density.

If in fact the monolayer is superconducting, while bulk Ag is known not to be, there can be several explanations. Since the observed transition temperature is low, there is no need to invoke any mechanism other than the usual electron-phonon interaction and BCS superconductivity. A monolayer of Ag has a vastly different band structure and is interacting with quite different phonons than the bulk material. If further investigations point to another mechanism, it should be remembered that the monolayer metal film on a Ge substrate is an ideal system for studying the excitonic mechanism proposed by Allender, Bray and Bardeen in 1973. This model states that if the workfunctions of a narrow gap semiconductor (Ge has in intrinsic gap of .67eV and impurity ionization levels of ~.1eV) and a thin metal film in contact with the semiconductor are well matched, then the wavefunctions of the electrons within KbT of the Fermi energy may tail into the semiconductor. If this occurs, a positive electron-electron interaction may occur in the metal mediated by virtual excitons in the semiconductor within a screening length of the interface, perhaps allowing the occurrence of exciton mediated superconductivity in the metal film. While there is nothing unique to the data presented in section V.C.1 which would suggest this process is occurring in these samples, this is an intriguing idea considering that the photoemission studies of Ag on Ge (001) by Miller, Rosenwinkel and Chiang indicate that there is negligible band bending at the Ge-Ag interface.

A question which must be addressed concerning these samples is the effect of the resistive behavior the samples show prior to the superconducting transition on the transition itself. In 1981 Maekawa and Fukuyama examined how superconductivity would be affected in a disordered system which, before the onset of the superconductivity, displayed the effects of electron-electron interactions in the near metallic regime. Coulomb electron-electron interactions are repulsive, suppressing the density of states about the Fermi energy, creating a logarithmically increasing resistivity (in 2-d) with decreasing temperature. Superconductivity requires a net attractive electron-electron interaction. In their study of the competition between the disorder enhanced electron-electron repulsion and the phonon mediated attraction, Maekawa and Fukuyama found that the superconducting T_c of a 2-d disordered system (in the interaction picture, not the scaling picture) is reduced with the reduction increasing as the resistance per square ($R_\#$) increases. This reduction in the T_c results from both the logarithmic reduction in the density of states (equation II.60) and the fact that the total electron-electron interaction (phonon + disorder enhanced Coulomb) is less attractive due to the disorder enhanced Coulomb part. Their perturbation calculation gives the ratio of the reduced transition temperature (T_c) to the 'bulk' transition temperature (T_{co}) to be (in 2-d):

(V.17)

where g is a coupling parameter (~1), ξ_o is the unperturbed bulk superconducting coherence length ($\xi_o = v_f \hbar / [1.75 \pi K_b T_{co}]$) and L is the mean free path. This result actually predicts reentrant insulating behavior. The first term in equation V.17 is due to the reduction of the density of states (equation II.60) and the second term is due directly to the vertex correction of the electron-electron interaction (equation II.53). For a typical 2-d system, these equations predict $T_c < 0$ for $R_\#$ of a few Kohms. This T_c reduction is quite a bit larger

(~1 order of magnitude) than that predicted for a Kosterlitz-Thouless transition (Beasley, Mooij and Orlando, 1979, Kosterlitz and Thouless, 1973).

Since the samples presented in section V.C.1 are superconducting yet have normal state resistivities of 1-2 Kohms/square or more, one might, in light of Maekawa and Fukuyama's assertions, claim that electron-electron interactions must be negligible in these samples. However, Graybeal and Beasley (1984) studied the effect of $R_{\#}$ on the T_c of Mo-Ge films and found, while Maekawa and Fukuyama's calculations were obeyed at low $R_{\#}$, at higher $R_{\#}$ the data showed higher T_c's than predicted. Some of their films went superconducting which had resistivities so high that the predicted T_c's were ~0 (which in their system should have occurred at ~1100 ohms). Graybeal and Beasley concluded that higher order positive interaction terms must be included into Maekawa and Fukuyama's theory.

CHAPTER VI -- CONCLUSION

The scaling theory and interacting electron theory predict a very wide variety of novel and interesting behaviors for two dimensional systems. In some regimes, the two theories can predict almost identical behaviors, such as the logarithmic variations of the resistivity with temperature and electric field. In other regimes, such as the insulating regime, other properties (such as the thermopower) are very different in the two descriptions. The two theories differ in their relationship to the superconducting transitions of two dimensional systems, with the interaction picture predicting competition between insulating and superconducting behaviors.

In Pd and Pd-Au films, the characteristic slope parameter in the prefactor of the logarithmic temperature dependence in the near metallic regime (equations V.1 and V.2) is S=1. The relative contributions to this value from the scaling and interaction pictures cannot be determined by resistivity measurements . The temperature dependence of the resistivity does not suggest that spin-orbit interactions are important, but the magnetoresistance does. The electric field dependence of the resistivity does not by itself distinguish between the two theories either, but does, in conjunction with the temperature dependence of the resistivity, eliminate the possibility that the localization length itself is electric field dependent. In the insulating regime, the electric field affects both interacting and noninteracting variable range hopping schemes in the same manner. It does however, provide a method to determine the spatial extent of the localized states. Even the states in films which are very strongly insulating (<480 K\/square at 10°K) extend over a few thousand Angstroms, while states in films at R_{2D} extend over a distance only a factor of two larger.

The magnetic field dependence of Pd films with resistivities around R_{2D} present an interesting puzzle. While the magnetoresistance behavior is isotropic, as it is for films of low resistivity, both interacting and noninteracting variable range hopping schemes predict the same behavior for the Zeeman interaction. However, the observed magnetotransport is consistent with the theories only if one assumes that a small fraction (~5%) of the carriers have their energies shifted by $g\mu H$, rather than all of the carriers.

The thermopower behavior for both Pd and Pd-Au films are totally inconsistent with a noninteracting single particle picture. The thermopower of both types of films, while slightly complicated at high temperatures by phonon drag effects, show the sharp opening of a gap in the density of states as the film resistivity crosses above R_{2D}. Such behavior is consistent with an increase in electron-electron interactions, and hence a reduction in the density of states (correlation gap), as R_{2D} is approached from below, becoming a real gap at R_{2D}. Such a gap can also come about if the transport in the insulating regime is via 'electronic polarons' as discussed in section II.E.2.

Ultrathin crystalline films of Ag grown epitaxially on Ge (001) substrates exhibit electronic transport consistent with two dimensional electron localization. In samples with surfaces well aligned to the (001) plane (within 0.5°), the samples display a logarithmically increasing resistance with decreasing temperature, which crosses over to a superconducting region below 1-2°K. Samples with a large degree of misalignment (~5°) show strongly insulating behavior and the superconducting like behavior below ~4°K. At low temperatures, in the normal state, the films displaying weak electron localization in their temperature dependence also display it in their electric field behavior. At low electric fields the normal state resistivity is consistent with a quadratic field dependence changing over to a logarithmic dependence at high electric fields. There is a small, positive isotropic magnetoresistance in the normal state, probably due to the large spin-orbit coupling one would expect in Ag films. Below ~2°K the resistivity displays a broad superconducting transition. The magnetic field behavior remains isotropic in the superconducting state and appears to be in the Pauli limit.

In conclusion, as the resistivity of 2-d Pd and Pd-Au films approach R_{2D}, the electron-electron interactions become increasingly important until at R_{2D} they open up a gap in the density of states. By use of the thermopower to define a system as metallic or insulating, one would have to conclude that in two dimensions there exists a minimum metallic conductivity of $R_{2D}^{-1} < (30000\Omega/\text{square})^{-1}$.

As the temperature is lowered below ~2°K of crystalline monolayer Ag films grown epitaxially on Ge (001), weak localization behavior converts to Pauli limited superconductivity.

"Where we goin', George ?"

The little man jerked down the brim of his hat and scowled over at Lennie. "So you forgot that awready, did you ? I gotta tell you again do I ? Jesus Christ, you're a crazy bastard !"

"I forgot," Lennie said softly. "I tried not to forget. Honest to God I did, George."

"O.K. - O.K. I'll tell ya again. I ain't got nothing to do. Might jus' as well spen' all my time tellin' you things and then you forget 'em, and I tell you again."

"Tried and tried," said Lennie, "but it did'nt do no good."

Of Mice and Men by
John Steinbeck
(1902-1968)

REFERENCES

Abeles B., 1976, Applied Solid State Science, (Academic Press, New York, vol 6)

Abraham E., Anderson P.W., Liccardello D.C., Ramakrishnan T.V., 1979, Phys Rev Lett 42, 673

Abrikosov A.A. and Gorkov L.P., 1962, Sov Phys JETP 15, 752

Abrikosov A.A., Gorkov L.P., Dzyaloshinskii I.E., 1963, Methods of Quantum Field Theory in Statistical Physics (Pergamon Press, London)

Alekseevskii N.E., Zakosarenko V.N. and Tsebro V.I., 1971, JETP Pis Red 13, 412

Allender D., Bray J. and Bardeen J., 1973, Phys Rev B7, 1020

Altshuler B.L. and Aronov A.G., 1979, Sol Stat Comm 30, 115

Altshuler B.L., Khmelnitzkii D.E., Larkin A.I. and Lee P.A., 1980, Phys Rev B22, 5142

Altshuler B.L., Aronov A.G. and Khmelnitzkii D.E., 1981, Sol Stat Comm 39, 619

Altshuler B.L., Aronov A.G. Khmelnitzkii D.E. and Larkin A.I., 1981, Sov Phys JETP 54, 411

Ambegaokar V., Halperin B.I. and Langer J.S., 1971, Phys Rev B4, 2612

Anderson O.K., 1970, Phys Rev B2, 883

Anderson P.W., 1958, Phys Rev 109, 1492

Anderson P.W., Abrahams E. and Ramakrishnan T.V., 1979, Phys Rev Lett 43, 718

Anderson P.W., Muttalib K.A. and Ramakrishnan T.V., 1983, Phys Rev B28, 117

Beasley M.R., Mooij J.E. and Orlando T.P., 1979, Phys Rev Lett 42, 1165

Bergman G., 1982, Phys Rev Lett 48, 1046: Phys Rev B25, 2937

Bertucci M., LeLay G., Manneville M. and Kern R., 1979, Surf Sci 85,471

Bishop D.J. Tsui D.C. and Dynes R.C., 1980, Phys Rev Lett 44, 1153

Burns M.J., McGinnis W.C., Simon R.W., Deutscher G. and Chaikin P.M., 1981, Phys Rev Lett 47, 1620

Burns M.J. and Chaikin P.M., 1983, Phys Rev B27, 5924

Burns M.J., Lince J.R., Williams R.S. and Chaikin P.M., 1984, Sol Stat Comm 51, 865

Chaudhari P. and Habermeier H.U., 1980, Phys Rev Lett 44, 40: Sol Stat Comm 34, 687

Clark A.H., 1967, Phys Rev 154, 750

Clark A.H., Cohen M.M., Campi M., Lanyon H.P.D., 1974, J Non Cryst Sol 16, 117

Davies J.H., Lee P.A. and Rice T.M., 1982, Phys Rev Lett 49, 758

Dolan G.J. and Osheroff D.D., 1979, Phys Rev Lett 43, 721

Drude P., 1900, Annalen der Physik 1, 566: Annelen der Physik 3, 369

Dynes R.C., Garno J.P. and Rowell J.M., 1978, Phys Rev Lett 40, 479

Dynes R.C. and Garno J.P., 1981, Phys Rev Lett 46, 137

Efros A.L. and Shklovskii B.I., 1975, J Phys C8, L49

Efros A.L., 1976, J Phys C9, 2021

Efros A.L., Nguyen Van Lien and Shklovskii B.I., 1979, Sol Stat Comm 32, 851

Fang F.F. and Triebwasser S., 1964, Appl Phys Lett 4, 145

Fowler A.B., Hartstein A. and Webb R.A., 1982, Phys Rev Lett 48, 196

Fukuyama H., 1980, J Phys Soc Jpn 48, 2169

Fukuyama H., 1981, J. Phys Soc Jpn 50, 3562

Fukuyama H. and Hoshino K., 1981, J Phys Soc Jpn 50, 2131

Fukuyama H., 1982, J Phys Soc Jpn 51, 1105

Giordano N., Gilson W. and Prober D.E., 1979, Phys Rev Lett 43, 725

Graybeal J.M. and Beasley M.R., 1984, Phys Rev B29, 4167

Hall E.A., 1897, Am J Math 2, 287

Handler P. and Eisenhour S., 1964, Surf Sci 2, 64

Hikami S., Larkin A.I. and Nagaoka Y., 1980, Prog Theor Phys 63, 707

Hofmann F., Hoffman H. and Schoepe W., 1982, Phys Rev B25, 5563

Ioffe A.F. and Regel A.R., 1960, Prog in Semiconductors 4, 237

Kaveh M., Uren M.J., Davies J.H.and Pepper M., 1981, J Phys C14, 413

Khosla R.P. and Fischer J.R., 1970, Phys Rev B2,4084

Kittel C., 1976, Introduction to Solid State Physics, 5th ed.,(John Wiley and Sons, Inc, New York)

Kosterlitz J.M. and Thouless D.J., 1973, J Phys C6, 1181

Knotek M.L. and Pollak M., 1972, J Non Cryst Sol 8-10, 505

Knotek M.L., Pollak M., Donovan T.M. and Kurtzman H., 1973, Phys Rev Lett 30, 853

Kurkijarvi J., 1973, Phys Rev B8, 922

Larkin A.I. and Khmelnitzkii D.E., 1982, Sov Phys Usp 25, 185

Lawless W.N., 1971, Rev Sci Inst 42, 561

Lee P.A. and Ramakrishnan T.V., 1982, Phys Rev B26, 4009

Lince J.R., Nelson J.G. and Williams R.S., 1983, J Vac Sci Technol B1, 553

Lou H.L., Merriam M.F. and Hamilton D.C., 1964, Science 145, 581

Maekawa S. and Fukuyama H., 1980, J Phys Soc Jpn 50, 2516

Maekawa S. and Fukuyama H., 1981, J Phys Soc Jpn 51, 1380

McGinnis W.C., Burns M.J., Simon R.W., Deutscher G. and Chaikin P.M., 1981, Physica B+C107, 5

McGinnis W.C., 1983, Thesis, (University Microfilms International, Ann Arbor, Michigan U.S.A.)

McGinnis W.C. and Chaikin P.M., 1984, (unpublished)

McMillan W.L., 1981, Phys Rev B24,2739

McMillan W.L. and Mochel J., 1981, Phys Rev Lett 46, 556

Mikoshiba N., 1962, Phys Rev 127, 1962

Miller T., Rosenwinkel E., Chiang T.-C., 1984, Phys Rev B30, 570: Sol Stat Comm 50, 327

Mott N.F., 1968, J Non Cryst Sol 1, 1

Mott N.F., 1976, Phil Mag 34, 643

Mott N.F. and Davis E.A., 1979, Electronic Processes in Non-crystalline Materials 2nd ed.,(Clarendon Press, Oxford)

Mueller F.M., Freeman A.J., Dimmock J.O. and Furdyna A.M., 1970, Phys Rev B1, 4617

Murphy N. St. J., 1964, Solid State Electron 12, 775

Peltier J., 1834, Ann Chim Phys 56, 371

Pollak M., 1970, Discuss Faraday Soc 50, 13

Poole D.A., Pepper M. and Glew R.W., 1981, J Phys C14, L995

Redfield D., 1973, Phys Rev Lett 30, 1319

Rose-Innes A.C. and Rhoderick E.H., 1969, Introduction to Superconductivity, (Pergamon Press, Oxford)

Rossi G., Abbati I., Brairovich L., Lindau I. and Spicer W.E., 1982, Phys Rev B25, 3619

Roth H., Straub W.D., Bernard W. and Mulhern J.E., 1963, Phys Rev Lett 11, 328

Sah C.-T., Noyce R.N. and Shockley W., 1957, Proc Inst Radio Engrs 45, 1228

Schrieffer J.R., 1957, Semiconductor Surface Physics, (University of Pennsylvania Press, Philadelphia)

Seebeck T., 1829, Pogg Ann 6, 133

Shlimak I.S. and Nikulin E.I., 1972, JEPT Lett 15, 20

Stritzker B. and Wuhl H., 1971, Z Physik 243, 361: Proc 12th Int Conf Low Temp Phys, 339 ,(Keigaku Pub Co., Tokyo)

Stromer H.L., Dingle R., Gossard A.C., Wiegmann W. and Sturge M.D., 1979, Sol Stat Comm 29, 705

Thomson J.J., 1897, Phil Mag 44, 293

Thomson W., 1882, Collected Papers of Lord Kelvin, (Cambridge University Press, vol 1)

Thouless D.J., 1977, Phys Rev Lett 39, 1167

Ting C.S., Houghton A. and Senna J.R., 1982, Phys Rev B25, 1439: Surf Sci 113, 244

Tsuzuki T., 1981, Physica 107B+C, 679

Uren M.J. Davies R.A. and Pepper M., 1980, J Phys C13, L985

Van den Dries L., Van Haesendonck C., Bruynseraede Y. and Deutscher G., 1981, Phys Rev Lett 46, 565

आश्चर्यवत् पश्यति कश्चिदेनम्	Marvellously, someone perceives this;
आश्चर्यवद् वदति तथैव चान्यः।	Marvellously, another declares this;
आश्चर्यवच्चैनम् अन्यः शृणोति	Marvellously, still another hears of this;
श्रुत्वाप्येनं वेद न चैव कश्चित्॥	But even having heard of this, no one knows it.

The Bhagavad-Gita, II.29